A High Froude Number Time Domain Strip Theory Applied to the Seakeeping of Semi-SWATHs

by

Damien S. Holloway

B.E.(Hons), University of Tasmania (1992)
B.Mus., University of Tasmania (1985)

Submitted in fulfilment of the requirements for the degree of

Doctor of Philosophy

at the

UNIVERSITY OF TASMANIA

November 1998

Statement of originality and authority of access

This thesis contains no material that has been accepted for a degree or diploma by the University of Tasmania or any other institution, and to the best of my knowledge and belief no material previously published or written by another person except where due acknowledgement is made in the text of the thesis.

This thesis may be made available for loan and limited copying in accordance with the *Copyright Act 1968*.

Damien Holloway

Abstract

In recent years there has been a rapid growth in the fast passenger ferry industry. Initially speed was the main selling point for designers, builders and operators, but as competition and choice have increased passengers are demanding better seakeeping performance. In addition designers and builders are starting to see the benefits of better seakeeping not only in terms of passenger comfort but in terms of structural strength and loading, allowing reduced structural weight and its many associated advantages. Two aspects of the seakeeping of fast ships are addressed in this thesis: response computation and the behaviour of semi-SWATH designs.

Motion and load prediction for the practising naval architect has traditionally been done using "strip theories", usually one closely related to the well known theory of Salvesen, Tuck and Faltinsen. This is a low Froude number theory, and although it is still being used, often successfully, for fast ships there is no rational justification for its validity in these cases. As speeds are increasing it is becoming imperative that an equivalent analysis tool suitable for higher Froude numbers be developed. This thesis proposes such a theory, based on calculation of two dimensional hydrodynamic potentials in a fixed reference frame in place of the traditional moving one. This strip theory of necessity is a time domain theory, which also allows the possibility of introducing non-linearities, random sea input, and even slamming events (although only the first of these is discussed in any detail in the thesis). Validation has involved comparison with traditional theory and tank testing. Most notably pitch and coupling effects have shown improved predictions, but heave tends to be over predicted. The main candidates for explanation of this phenomenon are argued to be wake shedding, hull entry effects, steady-unsteady interactions and three-dimensionality.

The majority of fast ferries being built at present have very conventional hull forms below the calm waterline. These have poorer seakeeping than their slower equivalents because their natural frequencies are encountered in longer waves, and traditionally designers have relied on lifting surfaces to counteract the increased motions. As these vessels get faster this approach will become less viable in terms of forces involved and appendage drag penalty. The type of hull form that will reduce motion accelerations without too much sacrifice of drag is not obvious, and a family of semi-SWATHs has been investigated as a possible alternative hull form. The investigation shows that as speed is increased the advantages of SWATH like forms become much greater if the criterion is to reduce accelerations.

Acknowledgements

This project has been undertaken under the supervision of Prof Mike Davis, who has been a great source of help over the last few years. I have needed him especially to kept the bigger picture in my focus during times when I would otherwise have been preoccupied with often minor details.

I would like to thank my fellow PhD students, in particular Jason Roberts and Nigel Watson, for their brainstorming and companionship. Jason has also taught me the majority of what I know about computers, and assisted with some of the towing tank tests.

Also, Dr David Paget, from the mathematics department of this university, started me off on the right track with some integrals in the early stages of this project.

This research has been supported by the Australian Maritime Engineering Cooperative research Centre (AMECRC) in several ways, including the following:

- Financial support, initially in the form of a supplementary scholarship, and later as an employee.
- Construction of the two semi-SWATH models and provision of towing tank resources. In particular Gregor Macfarlane, manager of the towing tank, and his team, provided much assistance with the experimental part of this project.
- Prof. Lawry Doctors (University of New South Wales) and his computer program *HYDROS* provided the "traditional strip theory" results.
- Provision of seakeeping data for the AMECRC system series hull forms, used for comparison with the semi-SWATH hull forms, and for further benchmarking of the computer program *BESTSEA*.

In addition participation in AMECRC has fostered interaction with other researchers working in related fields within Australia.

Finally, thank you to my wife Rosemary, and sons Graham and Donald, for your patience and support.

Contents

Chapter 1

Introduction

There is a rapidly growing worldwide industry in the manufacture and operation of large high speed passenger ferries. Australia in particular has become a significant participant in that industry over the last decade. The largest high speed ferries manufactured in Australia are built by Incat Tasmania, a company who have had some association with the University of Tasmania over the last several years. More recently the Australian Maritime Engineering Cooperative Research Centre (AMECRC), a company made up of participants from industrial and academic organisations, mostly from within Australia, who have an interest in research, has also been a driving force for the ship (and other maritime) related research conducted within Australia. One of its major areas of focus has been the large high speed passenger ferry industry (an area in which, as a manufacturer, Australia is regarded as a world leader). From the association of the University of Tasmania with these two companies the present research project has evolved, although it has been primarily the AMECRC through which the project has been supported (as indicated in the Acknowledgements).

Faced with competition not only from other operators, but from such things as affordable air travel, under-sea tunnels, etc., operators of high speed ferries vessels are demanding greater speeds but without wishing to sacrifice passenger comfort. As higher speeds are achieved traditional solutions to some of the unique problems of this type of vessel start to fail, particularly in less well understood aspects such as seakeeping.

On the experimental side traditional methods of investigation include regression analyses and testing of systematic series. Both of these are often treated purely as empirical approaches, in which the question of why certain trends are occurring is never asked. This is generally justified on the basis that the seakeeping problem is dependent on too many inter-related variables, and is too complex to understand at the level necessary to make useful predictions about variations in hull form without resorting to complex computer programs. A lack of willingness to explain the observed phenomena limits the ability to extrapolate information or to assess radically different designs. Furthermore the hulls investigated in these methods generally are, or are closely related

to, existing hulls. As a consequence the hull shapes often chosen for high speed vessels, while perhaps being more slender than their slower counterparts, are otherwise quite traditional in form. Of course experience is often a good substitute for physical understanding, but it does not necessarily encourage innovative design or anticipate the difficulties of a departure from the traditional domain. It might be argued that the seakeeping qualities of high Froude number fast ferries has presented a greater challenge than was anticipated from previous experience.

Often too, the differences between various models of a systematic series family are quite subtle in relation to the total spectrum of possibilities. Considering the number of hull parameters that are typically varied, the possible accuracy of the results, and the applicability to full size boats in real omnidirectional random seas (which are predictable only in terms of long term average conditions), such subtleties are likely to be overwhelmed. If some fortuitous coincidence of conditions results in a particular optimum design it is unlikely to be duplicated in reality.

Therefore one of the two main focuses of this thesis is to take a highly non-traditional design (namely the semi-SWATH form) and draw some conclusions about its seakeeping. These conclusions will be in terms of a physical understanding of the phenomena involved, in which the most important variables are identified, and will be expressed in a form enabling significant extrapolations to be easily made with some degree of confidence. It is hoped that this will help to bridge the gap between practising designers on the one hand, who are generally working within tight time and economic constraints, and therefore require the assimilated experience of many past designers and researchers in the form of simple methods of appraising preliminary designs, and researchers on the other, who are generally looking for detailed answers over longer time scales, not always sharply focused on what designers really want (or think they want), and therefore attracting criticism from them of being academic or lacking practicality.

The semi-SWATH concept and the design of the models tested as part of this project will be described in detail in chapter 5, while experimental results will be discussed in chapter 6. The latter chapter, by way of explanation of the experimental results, will introduce a simplified seakeeping model from which predictions of a broad and general nature may be made.

From the point of view of analysis of the seakeeping of a chosen hull form, the choice generally lies somewhere between a traditional strip theory, such as the one of Salvesen, Tuck and Faltinsen [84], and fully three dimensional methods. Generally for purely practical reasons, (and because it has been quite successful in the past with conventional vessels operating at conventional speeds) the former, or some variation of it, is used, and it is almost always followed up with model testing in a towing tank. Traditional strip theory is quick, robust, gives fair results, and is relatively easy to use. But it was only ever intended for low Froude numbers, and only through good fortune does it sometimes give good results at the high speeds typical of the leading edge of the fast passenger ferry industry.

Three dimensional methods on the other hand are computationally long and intensive (if they are solving the full three dimensional, time dependent problem), complex, and expensive. They

appear a long way off from replacing towing tank testing (an indictation of the inherent difficulty of the exact seakeeping problem), and most designers at present do not in general see the need for methods more sophisticated than conventional strip theory. Until three dimensional methods can consistently and easily produce sufficiently accurate results to gain the trust of designers, and until they become substantially cheaper and quicker than experimental tests, they are unlikely to enter widespread use except in very large organisations that value the research aspects and can see a future payoff. Even the most complex of three dimensional, time dependent computations are at present based on potential solutions that omit frictional, wave breaking and other non-linear phenomena. Therefore even these methods have their limitations. The question therefore emerges as to what level of computational complexity is justified and appropriate for a potential flow based solution method.

There is clearly a need for an intermediate method, capable of producing good results at reasonable computational cost (not necessarily at present, but bearing in mind likely developments in computer technology in the near future), and applicable to high Froude numbers. Such a theory must rely on a well judged assessment of which of the simplifying assumptions in traditional strip theory must be abandoned in order to obtain improved results (a factor that may vary from one type of boat to another). Chapter 4, after a description of traditional strip theory, its assumptions and limitations, and a summary of the most important existing extended theories, suggests such an intermediate high Froude number theory and its implementation in a computer program.

Results from the new high Froude number strip theory are presented in chapter 6, in which they are compared to the experimental results cited earlier, as well as to some traditional strip theory calculations. The results from the new theory were shown to be generally significantly better than those from a traditional strip theory, and positive suggestions were made as to the the source of differences remaining between these results and experimental results.

An important component of the high Froude number time domain strip theory of chapter 4 is the calculation of sectional forces. This is done using a two dimensional transient panel method. Its development and testing, as well as other related methods used for comparison, are discussed in chapters 2 and 3.

Chapter 2

An overview of panel methods relevant to the development and testing of a time domain strip theory

2.1 Panel methods

2.1.1 Introduction

Panel, or boundary element, methods were developed in the late 1950's to early 1960's by Hess and Smith [47] as a simple numerical tool for calculating potential flows about arbitrarily shaped bodies. The technique consists of discretising the boundary of the flow domain into a number of elements. (For three dimensional shapes the elements will be part of a surface, hence the name "panels".) From each element a simple flow field is considered to originate. Their strengths are determined by requiring that appropriate boundary conditions are satisfied on each panel, a process that generally involves solving a set of simultaneous equations representing each boundary condition as a function of these unknown strengths. The final flow field is the linear combination of the flow fields of now specified strength associated with each panel.

Panel methods rely on the fact that potential flows obey Laplace's equation ($\frac{\partial^2\phi}{\partial x^2} + \frac{\partial^2\phi}{\partial y^2} = 0$ in two dimensions). The two features of this equation that make it ideally suited to solution by panel methods are its linearity (allowing superposition of elemental solutions) and the fact that it is a boundary value partial differential equation, meaning that any given problem can be completely specified by its boundary conditions and does not require information about the interior of the fluid domain.

2.1.2 A derivation of the method

The usual derivation involves analytically reducing the problem to an integral equation over the boundary surface, and then discretising that equation. An equally rigorous alternative derivation is presented here without reference to integral equations, not only because of its simplicity, but because it is felt that progress in numerical techniques can be made more readily by freeing them from the constraints of their analytic origins. In support of this claim two examples will be given, one in which the sources are not placed on the boundary, and another where point sources are used.

The present derivation starts with a discrete problem, and shows that it becomes asymptotic to the continuous problem as the numerical resolution is increased. The derivation follows:

A set of elemental flows, or *sources*[1], each of which satisfies Laplace's equation but not necessarily appropriate boundary conditions, is summed to create a flow field. This set of elemental flows may also, but not necessarily, include integrals of source distributions. An infinite number of flow fields can be created in this manner from the same set of elemental flows by varying the coefficients of the linear combination, and any resulting flow field is automatically a valid potential flow because of the linearity of Laplace's equation. All that is required to obtain the *desired* flow field is to find the combination that satisfies the boundary conditions. One may specify linear or non-linear boundary conditions without loss of generality.

Boundary conditions can be written in terms of these elemental flows, and in general satisfied at a number of points equal to the number of linearly independent elemental flows by the appropriate choice of the coefficients of the linear combination. In the case of linear boundary conditions this choice is unique, but in the case of non-linear boundary conditions the existence or uniqueness of a solution can not be guaranteed. Experience shows however that the desired solution can generally be obtained for physically realistic problems, so this is not considered to be a handicap.

The coefficients, referred to as *source strengths*, are obtained by solving the system of equations representing the influence of all sources on each boundary condition. In the linear case this involves inverting an influence matrix, while for non-linear boundary conditions the process is more complex. Section 2.2.2 below deals with this in more detail.

If sufficiently many sources are used then an arbitrary flow field can accurately be represented. Taking this to the limit as the number of independent sources approaches infinity it follows that the boundary condition can be satisfied at an infinite number of points.

So far no restrictions have been placed on the location of the sources, but restrictions must apply to elemental flows containing singular points. The most basic elemental flow is the Rankine

[1] *Sources* is used here as a very general term referring to any valid elemental flow (preferably one that can be expressed analytically) and is not intended to be confined to *Rankine sources*. Valid "sources" could include for example integrated Rankine sources, Green function sources, doublets, vortices, and uniform flow fields (i.e. $\phi = const. \times x$). The latter is used implicitly in many steady flow problems, although determination of the constant is usually trivial.

source ($\phi(x,y,z) = \frac{1}{r}$ in three dimensions or $\phi(x,y) = \ln r$ in two dimensions, where r is the distance from the point at which ϕ is being evaluated to the source point.), although, as we shall see later, various Green functions have been used to satisfy particular boundary conditions, such as the radiation condition on an infinite free surface. The Rankine source and most other Green functions do not satisfy Laplace's equation at their origin, where they are singular, and this singularity must therefore be placed outside the flow domain[2] for a valid solution. Furthermore, in matching the number of equations (boundary conditions) and the number of unknowns (source strengths) it is convenient for each singularity to be paired with a boundary point at which we wish boundary conditions to be satisfied (a *collocation* point), and desirable for these points to be near each other so that the problem is well conditioned. (Well conditioned because the close proximity of the source to its corresponding collocation point causes a strong influence, and this pair defines a diagonal matrix element.) "Near" of course is a relative term, and in this case is defined in terms of typical panel dimensions.

Combining the two points above, i.e. increasing the number of panels to infinity, and noting that the panel dimensions as a consequence reduce to zero and therefore that for the problem to remain well conditioned it is desirable for the sources to approach the boundary (if they are not already distributed on the boundary), we end up with the continuous analogue of panel methods: Green's theorem applied to a field integral to convert it into a boundary path integral. In fact it is the reverse process, the discretisation of this boundary integral equation, by which the panel method is usually derived. The interested reader may read Hess and Smith's account [47]. However, as mentioned already, the present approach of starting with the discretisation is far simpler and no less rigorous.

A further refinement, bringing the technique a step closer to its continuous analogue without the need to increase the number of sources, is to distribute the sources over areas (or lines in two dimensions) rather than concentrating them at points. This has the apparent advantage that the singularity distribution, and hence the flow field at the boundary, is smoother, although it will be seen below that the advantage is sometimes minimal. The influence on the collocation point must then be determined by integrating the source over its area of distribution. The distributed source can be brought arbitrarily close to the boundary while its influence on the collocation point remains finite and bounded. The limiting value of this influence as the two are brought into coincidence depends on whether the source approaches the boundary from outside or inside the flow domain, and clearly only the former is consistent with satisfying Laplace's equation everywhere in the flow domain.

Only when the sources actually coincide with and are distributed on the boundary does the technique represent a true discretisation of the analogous boundary integral equation, and because panel methods had their origins in analytical methods this was the norm for many years. (In fact early refinements of the technique focused on higher order source distributions, such as

[2] Distributed sources may also be placed *on* the boundary, but never within it.

sources with linearly or quadratically varying strength over each panel.)

However in tackling problems with non-linear boundary conditions the iteration process becomes extremely complex when restricted to having the sources on the boundary, and Raven [82] proposed placing the sources a small distance outside the boundary so that they did not have to be moved in the iteration process. Provided that the distance was not too great the problem remained well conditioned. It was considered a significant step to free the technique from the restriction of having sources distributed on the boundary, but in the light of the present derivation there seems nothing remarkable about it.

Beck and Scorpio [6] further proposed, for the sake of making considerable savings in computational effort[3], returning to point sources rather than distributed sources. Because point sources are more concentrated than distributed sources they do not need to be quite as close to the boundary for the problem to be well conditioned. Beck argued that since the sources were some distance outside the boundary the effects at the boundary resulting from the point source discretisation could be reduced to acceptable limits. In fact it could be argued that the flow field everywhere on the boundary will be smooth, not the case for constant sources distributed over elements on the boundary.

2.1.3 Further background and brief historical development

The advantage of panel methods in calculating flows about arbitrary bodies was immediately recognised by the aeronautical industry, where it originated. The main focus in that industry since the development of panel methods has been to predict three dimensional circulating flows, hence calculation of lift forces, for the design of aircraft. Extensions have included the capability to calculate propeller flows and compressible (transonic) flows. These are summarised by Hess [46]. Other work has involved higher order methods, as mentioned above, in which constant sources are replaced with sources whose strength varies linearly (or according to some higher degree polynomial) over the panel, but Hess points out that no improvement in accuracy can be guaranteed unless the order of the approximation is made consistent by the use of curved panels. Furthermore analytic integration of the sources over curved panels does not produce a result in closed form, and experience shows that, with only two exceptions, first order methods are preferable.

As a tool in hydrodynamics panel methods were adopted somewhat more slowly than in aerodynamics, being hindered by the complication of the free surface. This complication is fourfold: there are two boundary conditions to be satisfied on the free surface, the boundary conditions are non-linear (highly so in the case of breaking waves), the boundary itself is infinite in extent, and its location is unknown. In addition, where the free surface intersects a floating body there becomes three boundary conditions to satisfy at the point of intersection, and in the

[3]He was working on three dimensional non-linear time domain flows, which are extremely computationally intensive.

vicinity of this intersection breaking waves are almost always involved (e.g. bow splash). To this day the fully non-linear problem has not been satisfactorily solved, and perhaps the most elusive of these four problems is the infinite extent of the free surface. However, just as any panel method involves the neglect of viscosity, various further simplifications may be employed to obtain successful and useful solutions to many hydrodynamics problems.

The first hydrodynamics problems to be solved involved linearising the free surface boundary condition by assuming small disturbances. One of the earliest successful examples is the solution by Giesing and Smith [33] of flow about a submerged body in steady translational motion in two dimensions. They used Green functions that automatically satisfied the linearised free surface boundary condition to avoid the need to represent an infinite free surface. Others have used a similar technique to solve problems involving oscillation about a mean position (e.g. Doctors [21] in the frequency domain, and Yeung [99] in the time domain). Three dimensional problems have also been solved (for example Newman [76]).

The Green function technique is restricted to linear problems, and other techniques had to be developed if ultimately the non-linear problem was to be solved. The first major step in this direction was Dawson [19], who used simple sources but panelled a finite portion of the free surface, although the linear free surface boundary condition was still used. This has given rise to much activity in solving non-linear problems, a considerable portion of which has been focused at such institutions as *Massachusetts Institute of Technology* ([76], [101], [71], [55], [87]), *University of Michigan* ([14], [4], [13], [5], [6]), and *Maritime Research Institute Netherlands (MARIN)* ([82]).

Unsteady hydrodynamic flows in particular incur a great computational burden over their aerodynamic equivalents. The latter (in the absence of shock waves, present in transonic flows) can be solved as a succession of steady state problems since the only boundary conditions are kinematic. Hydrodynamics problems, because of the dynamic boundary condition that gives rise to free surface waves, involve a "memory" of the flow. In the case of Green function methods this is in the form of a convolution integral, and in simple source methods it requires time stepping the free surface position in addition to solving for the flow at each time step (i.e. it becomes a combined initial value-boundary value problem). It is not surprising therefore that the only problems to be solved for some considerable time were steady state flows, either translational or oscillatory.

2.2 Mathematical formulation of the method

2.2.1 Setting up equations (linear boundary conditions)

Let the number of panels be n. Suppose that we look initially only at the flow field due to a source of unit strength distributed on the jth panel ($1 \leq j \leq n$). We will denote the potential function value at an arbitrary point (x_i, y_i) due to the jth unit source as ϕ_{ij}. Suppose further

that the actual strength of the source at j is Q_j, then taking into account all sources on all panels the total potential at (x_i, y_i) can be written as

$$\phi_i = \phi(x_i, y_i) = \sum_{j=1}^{n} Q_j \phi_{ij}.$$

Noting that the derivative is a linear operator, we can similarly write expressions for flow velocities ($u = \frac{\partial \phi}{\partial x}$, $v = \frac{\partial \phi}{\partial y}$), or any other derivative of ϕ, by differentiating ϕ_{ij} with respect to the appropriate variable. For example

$$\frac{\partial \phi_i}{\partial x} = \frac{\partial \phi(x_i, y_i)}{\partial x} = \sum_{j=1}^{n} Q_j \frac{\partial \phi_{ij}}{\partial x_i}, \text{ etc.}$$

If the point (x_i, y_i) is now taken to be the ith collocation point, we can easily set up equations for boundary conditions. Writing the ith boundary condition in the form

$$f_i(\phi) = R_i$$

where f_i is an arbitrary linear function of ϕ and/or its derivatives, and R_i is independent of ϕ, and noting therefore that $f_i(\phi) = \sum_{j=1}^{n} Q_j f_i(\phi_{ij})$, we can write the boundary condition at i in the form

$$\sum_{j=1}^{n} A_{ij} Q_j = R_i$$

where $A_{ij} = f(\phi_{ij})$. The set of equations representing all boundary conditions can therefore be written in matrix form as

$$[A]\{Q\} = \{R\} \tag{2.1}$$

and the source strengths are simply

$$\{Q\} = [A]^{-1}\{R\}.$$

2.2.2 Solving problems with non-linear boundary conditions

As will be seen in the section below on free surface problems, boundary conditions may be non-linear. There is no difficulty in formulating the equations in the same manner as above, but where a numerical solution is sought it can not be obtained by matrix inversion as above, and difficulties arise in solving the equations. A numerical solution therefore relies on linearising the solution process in one of two ways.

First, in problems where a solution is sought at a sequence of time values, the solution at the next time step may be expressed as a perturbation about the solution at the current time step. If the time step is sufficiently small the non-linear terms in the perturbation will be small compared with the linear terms, and the problem can be treated as a linear one. This can be refined by the use of standard techniques for the solution of initial value differential equations (e.g. Runge-Kutta, etc.).

Second, where a solution to a steady state problem is sought, one can use an iterative method. In such a method an approximate solution is first obtained, typically the linear solution. Next, considering the final solution to be a perturbation about the current "guess", one can proceed as above to obtain an improved solution. The improved solution then becomes the new guess, and is further improved by iteration until some convergence criterion is satisfied.

Both techniques are essentially the same in the sense that the problem is linearised by assuming the desired solution to be a perturbation of an approximate or previous solution.

The linearisation used for both above methods is achieved by considering the first two terms in the Taylor series expansion of the boundary condition equations about the current solution. Thus, if the boundary conditions are written in the form

$$f_i\left(x_1, x_2 \ldots x_n\right) = 0, \text{ for } i = 1, n \tag{2.2}$$

then the Jacobian matrix

$$[J] = \begin{bmatrix} \frac{\partial f_1}{\partial x_1} & \frac{\partial f_1}{\partial x_2} & & \\ \frac{\partial f_2}{\partial x_1} & \frac{\partial f_2}{\partial x_2} & & \\ & & \ddots & \\ & & & \frac{\partial f_n}{\partial x_n} \end{bmatrix} \tag{2.3}$$

can be formed, where the element on the ith row and jth column is $J_{ij} = \frac{\partial f_i}{\partial x_j}$. For the sake of generality x has been used rather than Q to represent the unknowns because, as will be seen below, in non-linear free surface problems the complete set of unknowns also includes the free surface elevation at each boundary point.

If the current estimate of the solution vector is $\{x\}_k$ and the true solution vector $\{x\}$ then, using the notation $\{f\}_k$ for the vector whose ith component is $f_i\left(\{x\}_k\right)$, the Taylor series for the boundary condition equations about the point $\{x\}_k$, including only up to the first derivative terms, and assuming $(\{x\} - \{x\}_k)$ is small, is

$$\{f\} = 0 = \{f\}_k + [J]\left(\{x\} - \{x\}_k\right) + \text{higher order terms.}$$

The equations have been successfully linearised, and from this we can write an approximate expression for $\{x\}$. Assuming the neglected higher order terms to be small this can be taken as an improved estimate of the solution, thus

$$\{x\}_{k+1} = \{x\}_k - [J]^{-1}\{f\}_k\,. \tag{2.4}$$

This is a generalisation of Newton-Raphson iteration to many dimensions, as is obvious from the form of equation (2.4). It is quite successful where good initial estimates of the solution can be obtained, particularly in time stepping problems where the time step can be made small so that the solution does not change dramatically from one time step to the next, but, as one would expect, problems encountered in the solution of systems of non-linear equations are many times greater than in the solution of single non-linear equations. A more complete discussion can be found for example in the *Numerical Recipes* books [79].

2.2.3 Boundary Conditions

The most common boundaries are solid boundaries, and the appropriate boundary condition requires that the fluid velocity and boundary velocity be compatible, i.e. that the components of these velocities in the direction normal to the surface are equal. For the case of flow about a fixed object this equates to

$$\nabla\phi \cdot \hat{n} = \frac{\partial\phi}{\partial n} = 0, \tag{2.5}$$

and for a body moving with velocity $\vec{V}$,

$$\nabla\phi \cdot \hat{n} = \frac{\partial\phi}{\partial n} = \vec{V} \cdot \hat{n}, \tag{2.6}$$

where n represents the normal direction and $\hat{n}$ the unit normal vector. This of course also applies to a body that is rotating, or deforming in a known manner, in which case $\vec{V}$ varies in space and is taken to be the *local* boundary velocity.

On an open boundary the normal velocity may be specified arbitrarily, i.e.

$$\nabla\phi \cdot \hat{n} = \frac{\partial\phi}{\partial n} = v, \tag{2.7}$$

where v is a user defined normal velocity. This would apply for example to flow through a duct, in which v is a function of the total flow rate.

Another class of problems involves specified pressures on a boundary that is free to move in response to that pressure. Due to its variety of manifestations and its importance to the present work this will be dealt with in detail in the following section.

It should be pointed out that in general any given problem may involve more than one of the above types of boundary.

2.3 Free surface problems

Forces acting on a free surface may include pressure (this includes constant pressures such as atmospheric pressure, and moving or time variable pressures such as produced by surface effect vehicles), inertia (this gives rise to the $\frac{\partial\phi}{\partial t} + \frac{1}{2}\nabla\phi \cdot \nabla\phi$ terms in Bernoulli's equation below), gravitational (due to a density differential between the two media separated by the free surface), surface tension, or viscous shear (such as wind forces on water).

The only free surfaces dealt with in the present work are air-water interfaces under the influence of gravity waves. It is assumed that the density of air is negligible compared with that of water, and therefore that its inertia effects are also negligible, hence its flow field does not need to be calculated. It is also assumed that any waves of interest will have a wavelength comparable to some characteristic hull dimensions (this will be defined more specifically in the derivation of a "strip theory"), and that therefore surface tension can be ignored.

Finally, since the ultimate objective is to calculate sectional forces for a strip theory, only two dimensional problems will be discussed in any detail.

2.3.1 Free surface boundary conditions

A free surface is a movable boundary, and the motion of this boundary is in general unknown. This introduces an unknown free surface elevation, which will be denoted η, in addition to the unknown source strength value, Q, at each boundary point. Therefore if a soultion is to be obtained two boundary conditions must be satisfied at each free surface point. The first of these relates to compatibility of fluid and boundary velocities, and is referred to as the kinematic boundary condition, equivalent to equation (2.6). The second relates to the interplay between pressure, gravitational, and inertial forces, and is referred to as the dynamic boundary condition.

Kinematic boundary condition

The kinematic condition requires that, as before, equation (2.6) must be satisfied, where $\vec{V}$ now refers to the local free surface velocity vector, which can be taken as $\frac{\partial \eta}{\partial t}$ in the vertical direction[4]. If n_x and n_y are respectively the horizontal and vertical components of the unit normal vector $\left(\hat{n} = n_x\hat{i} + n_y\hat{j}\right)$ then the free surface slope can be written in terms of these components as $\frac{\partial \eta}{\partial x} = -\frac{n_x}{n_y}$. We can therefore write $\nabla\phi \cdot \hat{n} = \frac{\partial \phi}{\partial x}n_x + \frac{\partial \phi}{\partial y}n_y = n_y\left(\frac{\partial \phi}{\partial y} - \frac{\partial \eta}{\partial x}\frac{\partial \phi}{\partial x}\right)$ and $\vec{V} \cdot \hat{n} = \left(\frac{\partial \eta}{\partial t}\hat{j}\right) \cdot \hat{n} = \frac{\partial \eta}{\partial t}n_y$. Substituting these into equation (2.6) yields

$$\frac{\partial \phi}{\partial y} - \frac{\partial \eta}{\partial x}\frac{\partial \phi}{\partial x} = \frac{\partial \eta}{\partial t}$$

from which the boundary condition is obtained:

$$\frac{\partial \phi}{\partial y} = \frac{\partial \eta}{\partial t} + \frac{\partial \eta}{\partial x}\frac{\partial \phi}{\partial x}. \tag{2.8}$$

One can also obtain the identical expression, $\frac{\partial \phi}{\partial y} = \frac{D\eta}{Dt}$, by noting that the free surface is a material surface[5], i.e. that a fluid particle on the free surface remains on the free surface (a consequence of irrotationality), and thus its vertical velocity component may be expressed as either $\frac{\partial \phi}{\partial y}$ or $\frac{D\eta}{Dt}$. The former approach shows more clearly however the relationship with equation (2.6).

[4] This choice is not unique; in general $\vec{V} = V_x\hat{i} + \left(\frac{\partial \eta}{\partial t} + \frac{\partial \eta}{\partial x}V_x\right)\hat{j}$ where V_x can be chosen arbitrarily, although it can easily be verified that the choice has no effect on the final expression for the boundary condition.

[5] The material derivative, $\frac{D}{Dt}$, is the time derivative observed in a Lagrangian reference frame, that is one in which we are following individual fluid particles. In addition to the $\frac{\partial}{\partial t}$ term we must include the terms $\frac{\partial}{\partial x}\frac{dx}{dt} + \frac{\partial}{\partial y}\frac{dy}{dt}$, where x and y are the particle coordinates. Noting that the fluid particles have velocity $\frac{\partial \phi}{\partial x}\hat{i} + \frac{\partial \phi}{\partial y}\hat{j}$ in a stationary reference frame we can write the material derivative as

$$\frac{D}{Dt} = \frac{\partial}{\partial t} + \frac{\partial \phi}{\partial x}\frac{\partial}{\partial x} + \frac{\partial \phi}{\partial y}\frac{\partial}{\partial y} = \frac{\partial}{\partial t} + \nabla\phi \cdot \nabla.$$

Dynamic boundary condition

The dynamic condition comes from Bernoulli's equation[6],

$$\frac{p}{\rho} + \frac{\partial \phi}{\partial t} + \frac{1}{2}\nabla\phi \cdot \nabla\phi + gy = 0. \tag{2.9}$$

This is combined with the condition that the pressure on the free surface is zero (or some other specified value). Thus, substituting the free surface elevation, $y = \eta$, and the pressure, $p = 0$, we obtain the dynamic boundary condition

$$\frac{\partial \phi}{\partial t} = -\frac{1}{2}\nabla\phi \cdot \nabla\phi - g\eta \tag{2.10}$$

Combined boundary conditions

Without linearising the boundary conditions one can not avoid the necessity for two boundary conditions. The conditions (2.8) and (2.10) can however be written in other forms that may make the solution method more efficient. For example one common simplification is to eliminate explicit reference to η from the kinematic condition, resulting in a large zero block in the Jacobian matrix. This is achieved by rewriting (2.10) to give an expression for η, differentiating the result with respect to t and x, and substituting into (2.8), giving

$$\frac{\partial^2 \phi}{\partial t^2} + g\frac{\partial \phi}{\partial y} + 2\frac{\partial \phi}{\partial x}\frac{\partial^2 \phi}{\partial x \partial t} + \frac{\partial \phi}{\partial y}\frac{\partial^2 \phi}{\partial y \partial t} + \left(\frac{\partial \phi}{\partial x}\right)^2 \frac{\partial^2 \phi}{\partial x^2} + \frac{\partial \phi}{\partial x}\frac{\partial \phi}{\partial y}\frac{\partial^2 \phi}{\partial x \partial y} = 0, \tag{2.11}$$

which can be used to replace either of equations (2.8) or (2.10). Note that an implicit reference to η still exists since the boundary condition is applied on the exact free surface.

2.3.2 Linearisation of the free surface boundary condition

One should first be reminded that for the non-linear problem all boundary conditions must be satisfied on the actual free-surface boundary, that is on $y = \eta$. If we assume that the wave height is small compared with the wavelength then several simplifications result. First, conditions at $y = \eta$ can be expressed in terms of a Taylor series about $y = 0$. If η is sufficiently small then the boundary conditions can be approximated adequately by the leading term in this series, which is identical to satisfying them on $y = 0$. Next, combining the kinematic and dynamic boundary conditions as in equation (2.11), and noting that we no longer need to know η if this equation is to be satisfied on $y = 0$, the two boundary conditions can be reduced to a single equation. Finally, since the disturbances are assumed to be small on the free surface, we note that higher order terms in (2.11) can be ignored, leaving only the first two terms. The linear free surface boundary condition then becomes

$$\frac{\partial^2 \phi}{\partial t^2} + g\frac{\partial \phi}{\partial y} = 0, \tag{2.12}$$

to be satisfied on $y = 0$.

A more comprehensive discussion of the subject is given in Wehausen [97] and Tuck [90].

[6] The right hand side may in general be an arbitrary constant, but conventionally the origin is taken to be on the undisturbed free surface, and atmospheric pressure as $p = 0$, in which case this constant is 0.

Necessary conditions for linearisation to be valid

It is clear from the above section that linearisation can be applied when free surface disturbances are small, but we seek to know what properties of the moving body under investigation bring about this condition. There are three basic categories of problems that fulfil this requirement.

- The first assumes deep submergence of the body, in which case the solution is a perturbation of the solution for the motion of that body in an infinite fluid.
- The second is the thin or slender body approximation. The body is considered to belong to a family of bodies whose geometries can be expressed in terms of a small parameter, and that as this parameter approaches zero the free surface disturbance vanishes. For example a hull surface may be defined by specifying the local transverse coordinate as a function of the longitudinal and vertical coordinates, and the family generated by multiplying this function by the small parameter.
- The third category assumes that motions of the body are small enough not to create a disturbance of the free surface. Thus an oscillating body is assumed to deviate infinitesimally from its equilibrium position.

The present investigation, being concerned with the dynamics of surface ships, and in particular the forces on two dimensional sections, falls mainly into the latter category, however aspects of the first are also relevant. The second category becomes important in the discussion of strip theory later, where the problem becomes three dimensional.

2.3.3 Complex notation

In two dimensional problems the equations can be simplified by the use of complex notation, where the coordinates (x, y) are represented by the complex number $z = x + iy$. The symbol $\Phi = \phi + i\psi$ represents the complex potential, in which $\mathrm{Re}\{\Phi\}$ is the potential function, and $\mathrm{Im}\{\Phi\}$ is the stream function. The complex velocity is $W = u - iv = \frac{\partial \phi}{\partial x} - i\frac{\partial \phi}{\partial y} = \frac{\partial \Phi}{\partial z}$.

If a panel has unit tangential vector of $e^{i\alpha}$ then $\frac{\partial \phi}{\partial t} - i\frac{\partial \phi}{\partial n} = We^{i\alpha}$, where n and t here refer to the normal and tangential directions. Thus for example $\nabla\phi \cdot \hat{n} = \mathrm{Im}\left\{\bar{W}e^{-i\alpha}\right\}$.

In addition to the simplification of notation, complex variables are convenient because all analytic functions of complex variables satisfy Laplace's equation (except at singular points), and because symmetry about the free surface is easily expressed by the use of the complex conjugate. These advantages are evident in particular in the use of Green function methods, to be discussed below.

2.3.4 Simple source (Dawson) method

The most obvious approach to treatment of the free surface is to panel it as one would any other boundary, and to apply the free surface boundary condition derived above.

An immediate complication arises, that an infinite free surface must be represented with a finite number of panels. There is little to be gained in trying to overcome this by the use of variable sized panels because, in addition to the geometric and numeric difficulties, once the panel dimensions are no longer small compared with the wavelength all useful information is lost. It is not even practical to overcome the infinite free surface problem by modelling a physically finite free surface (for example a basin or lake) because this only results in exchanging one problem for many others, including the need to represent the basin walls or lake bottom (especially near the free surface boundary edges where the two intersect), wave reflection, and the highly non-linear problem of breaking waves at the free surface edges.

The only practical solution is to truncate the panelling of the free surface at some arbitrary position that is sufficiently distant from the region of interest that negligible error results. This distance is normally determined by numerical experimentation.

Truncation of the free surface is not an entirely satisfactory solution, although its difficulties can mostly be solved well enough to obtain reasonable results. The most fundamental of these difficulties is the discontinuity between the panelled free surface and the surface beyond the truncation, preventing proper radiation of waves. No truncation boundary condition that is truly transparent to waves is known to exist.

A partial solution to the radiation problem is provided by the use of the *double body* formulation, in which the body with its associated source strength distribution is reflected about the undisturbed free surface ($y = 0$). In the absence of the sources on the free surface the undisturbed free surface becomes a line (or plane) of symmetry, and hence a streamline (or surface). In linear problems the presence of sources distributed on the free surface panels will only affect symmetry locally. Thus the far field radiation condition is satisfied exactly where no waves are present (for example ahead of a moving body) and approximately (or on average) elsewhere. In nonlinear problems the sources will not be distributed exactly on $y = 0$ so the approximation is not quite as good, but is still an improvement on single body representations. The double body formulation is almost always used, although not strictly essential.

Different classes of problem can show entirely different symptoms to the free surface truncation, but these can all be related to the fundamental absence of a proper radiation condition. In steady state investigations, for example, one experiences oscillations near the cut. These are usually confined to only a few panels, and do not in general present any difficulty. Time domain investigations on the other hand typically exhibit reflections of waves from the free surface edge. A build up of mass and energy due to the inability to control $\frac{\partial \phi}{\partial n}$ on the unpanelled free surface boundary may also cause a drift of the mean free surface elevation. In the absence of wave radiation the wave energy must be absorbed artificially by the use of a buffer zone at the edge of the free surface boundary with progressively introduced damping (referred to as a *numerical beach*). If the damping is introduced too suddenly the reflection point is only transferred from the boundary truncation point to the edge of the damped region. (See for example Liggett [59],

section 4.3.)

The first problems to be solved using simple source methods were linear steady-state problems. The technique is sometimes named after Dawson due to his pioneering work in this area [19].

A difficulty experienced only in steady state problems, and unrelated to the free surface truncation, is the fact that there is no unique solution. The cause of the problem is discussed in more detail in section 2.4.1. The desired solution only contains waves behind the body, and uniqueness can be recovered by suppressing the upstream waves. Analytic expressions for $\frac{\partial^2 \phi}{\partial x^2}$ required in the free surface boundary condition treat the upstream and downstream directions symmetrically and hence give a symmetric solution, which is not the desired solution. Part of Dawson's pioneering work involved suggesting the use of asymmetric finite difference expressions for $\frac{\partial^2}{\partial x^2}$ that numerically suppressed the upstream waves. The suppression of upstream waves has the additional advantage of preventing disturbances due to the downstream truncation from propagating upstream. The only other option is to solve the problem in the time domain, where uniqueness can be assured by the use of appropriate initial conditions.

2.3.5 Green function method

The unsatisfactory representation of infinite free surfaces in simple source based methods motivates the use of analytic solutions to the free surface radiation problem. This gives rise to Green function sources. We shall see that the technique must be restricted however to linearised problems since panel methods rely on superposition of solutions.

In place of simple sources one may choose *any* source function that satisfies Laplace's equation. If one chooses a wave function that automatically satisfies a linearised free surface boundary condition then any linear combination of such functions will also automatically satisfy that same boundary condition. It then becomes unnecessary to panel the free surface at all.

This approach offers two main advantages over the simple source approach: it removes the need to arbitrarily truncate the free surface boundary in order to solve an infinite problem with a finite number of panels, and it reduces the number of unknown source strengths (hence number of equations) considerably. The first of these is by no means trivial. However the Green function approach has two major drawbacks: that only finite order (in fact usually only linear) problems can be attempted, and the time required for the Green function evaluations is considerably larger than for simple sources. The second of these is in most cases more than compensated for by the time saved in solving a smaller set of equations, and for linear problems the Green function approach is generally the preferred method.

A list of Green functions for various types of source is given by Wehausen and Laitone [98], including stationary sources of sinusoidally pulsating strength, uniformly translating sources of constant strength, and sources of varying strength in arbitrary motion; each in both in two and three dimensions. Examples of two dimensional panel methods based on these source functions

are described respectively in Doctors [21], Giesing and Smith [33], and in this thesis (chapter 3). Three dimensional examples are described in Beck and Scorpio [6].

2.3.6 Choice of method

For problems involving non-linear boundary conditions the only option is the simple source method.

Where the linearised free surface is used both methods have certain advantages, and the choice depends greatly on the nature of the problem being solved. Some factors to be considered are listed below.

Speed

Speed is frequently an issue with free surface problems. With simple source methods the major computational cost is in matrix inversion, and the matrix may be quite large because of the free surface panels. On the other hand matrix inversion time is negligible for Green function methods, but the Green functions themselves involve considerable computational time. Yeung [101] analyses the relative speeds of the two methods, taking into account the relative costs of matrix coefficient evaluation and matrix inversion. He concludes that for two dimensional problems Green function methods are usually superior while in three dimensions the two are in some circumstances more competitive, although his analysis did not claim to be complete enough to offer more than a guideline. He did however qualitatively discuss factors such as iterative solvers and hybrid methods. More recently it has been shown (as cited for example by Newman [76], Beck and Scorpio [6], and Scorpio *et al* [88]) that using simple source methods with sufficiently many panels the use of multipole acceleration techniques allows a solution to be obtained in $O(n)$ calculations (as opposed to $O(n^2)$ for standard iterative or $O(n^3)$ for direct matrix inversion methods). This would give simple source methods a significant speed advantage over Green function methods for very large problems.

Additional factors relevant to the present work but not considered by Yeung include single vs double precision, the convolution integral in time domain Green functions, and running on vector computers. These are discussed in the following paragraphs.

- Single and double precision arithmetic operations are generally performed with comparable speed on most computers, but when double precision is required global convergence criteria for a problem must be correspondingly more severe and thus more arithmetic operations are required. Direct matrix inversion, an explicit process, will therefore not suffer significant speed loss in double precision, while iterative or relaxation methods can incur substantial speed loss. Green function evaluations on the other hand are generally evaluated using series expansions, and the use of double precision will always require additional terms and hence cause them to be slower. It may be concluded from this that the use of higher

precision will tend to favour simple source methods, at least in two dimensions where the problem is small enough for direct matrix inversion to be the preferred method of solving the equations.

- The convolution integral appearing in the time domain Green function must be evaluated numerically due to the arbitrary variation with time of the body position and source strengths. The integrand is highly oscillatory and very slowly decaying, so it is not possible to reduce it by ignoring effects exceeding a particular "age", or by integrating it with fewer points. The time required to evaluate each convolution integral is proportional to the number of integrand evaluations, which is therefore proportional to the number of time steps since motion began. The total time required to simulate n time steps is then proportional to $\sum_{k=1}^{n} k$ ($\simeq n^2/2$ for large n). The time required for the same simulation using simple source methods only increases proportionally to n (with some exceptions[7]). There will obviously then be a number of time steps, n ($n \geq 0$ but typically $\gg 0$), for most problems above which the simple source method is quicker. It can be concluded that provided simulation is for restricted time periods Green function methods may remain competitive.

- Where access to a vector computer is available special consideration must be given to Green function evaluation in order to take any advantage of the potential gain in speed. The vectorising of an algorithm relies on identical operations being able to be performed simultaneously and independently. This requires prior knowledge of the exact number and type of operations to be performed. Usual methods of evaluating many of the special mathematical functions that appear in the Green functions (e.g. exponential integrals, error functions, Bessel functions) are open ended calculations, such as series, in which terms are evaluated until a convergence criterion is achieved. These methods can not be vectorised. Suitable alternatives include polynomial or rational function approximations. Inefficiencies are inevitable because in some circumstances a series would have converged with fewer calculations, but the speed gains from vectorising far outweigh this. Also it is impractical to find one approximation that can be used over the entire computational domain. It is desirable to split the domain into various subdomains, each with its own approximation. (However each approximation must have the same form, only the coefficients differing, to vectorise successfully.) One needs to find the optimum balance between number of calculations in the approximation, number of comparisons to make in choosing the appropriate subdomain, and number of coefficients to store in memory. Newman describes the process in detail for some three dimensional Green functions [75]. In summary

[7] For example a translating body in a stationary reference frame: the length of free surface that requires panelling increases proportionally to n as the simulation time increases. Ignoring the panels on the body, the solution time for each time step then will be proportional to n^2 (matrix inversion), and the total solution time proportional to n^3.

a simple source method program can be adapted with minimal effort to take advantage of a vector computer, but the process is far more complex and may not be worth the effort for a Green function program.

Data storage

Green function methods require considerably less computer memory in almost all cases. The exception is arbitrary motion in the time domain, in which the convolution integral requires storage of the entire history of panel positions[8] and source strengths. Whether or not these requirements exceed those for the equivalent simple source method depends on the number of time steps being simulated.

In large problems where the entire problem can not be contained in the random access memory a speed penalty due to the relatively slow disk access time may result. This may occur for example when solving three dimensional problems using simple source methods, or when performing very large time simulations using Green function problems. It must be pointed out however that in Green function methods the disk access time, even if slow, will still be small compared with the Green function evaluation time. It can be concluded therefore that memory limits will only affect running times significantly when using simple source methods.

Programming difficulty

In most problems there is little to distinguish the two methods. In the Green function method the main difficulty is the evaluation of the Green functions themselves, and if a good numerical subroutine library is available it should contain the required functions (with the exception noted below). Simple source methods have the complication of two sets of boundary conditions (body and free surface), but this should pose no difficulty in programming. The banded form of the free surface equations may also allow scope for efficiencies in the matrix solver, and this can be pursued if running time is critical.

The exception is time domain problems. There are two main difficulties in using the Green function method. Firstly, the Green function for quantities such as ϕ or $\frac{\partial \phi}{\partial t}$ due to a source distributed over a panel can not be expressed explicitly in terms of known mathematical functions (see sections 3.3.1 and 3.3.2), only as the integral of known functions. This precludes the use of library subroutines, and gives the choice of either evaluating the integral numerically, which would be unnecessarily slow, or defining a new function and developing an algorithm for its evaluation. Secondly, where the body motion is arbitrary and large quantities of data associated with the convolution integral require storage, there may be "housekeeping" problems associated with moving data around in memory.

[8] Finite amplitude periodic motion requires minimal storage if the period is an integral multiple of the time step, and infinitesimal oscillation about a mean position requires only a single copy of the panel coordinates.

Accuracy

The accuracy of simple source methods, given a fixed number of body panels, is in general inferior and can only match that of Green function methods if careful consideration is given to panelling of the free surface. Green functions satisfy the linear free surface boundary condition exactly and at all points, while simple source methods do not because the free surface has been discretised. Again time domain Green function representations are an exception because the arbitrary nature of the panel positions and source strengths requires the convolution integral to be evaluated numerically, but it must be remembered that simple source methods do not necessarily offer any advantage in this regard because their solution must also be discretised in time. There is also the issue of errors due to the discretisation of the body boundary, but here there is no difference between the two methods.

The free surface panel length and extent of the panelled free surface both affect the accuracy of simple source methods. In general an accurate solution requires many more free surface panels than body panels.

Any wave that is not *long* compared with the free surface panel dimensions will be artificially damped, and waves of length comparable or shorter than the panel length can not be represented at all. In periodic oscillation or steady translation problems the wavelength can be estimated beforehand and the panel length chosen accordingly, but in time domain representations where any impulse produces waves of all frequencies this becomes of concern. However the pressure fields below short waves extend only to very shallow depths, and their omission does not cause significant error. As a consequence good accuracies may be obtained provided that the free surface panel length is small compared with the body draught and with the wavelength of any dominant frequency. This will usually be achieved if the panels on the free surface and body are similar in length.

Any wave that is not *short* compared with the extent of the panelled free surface will also not have its pressure field accurately represented. This is in addition to the radiation problem already discussed. For oscillatory problems it can reasonably be assumed that waves significantly longer than those corresponding to the resonant frequency of oscillation of the body will exert mainly hydrostatic forces, and that the latter wavelength is comparable with the body's dimensions. It can be concluded then that a free surface extent that is large compared with the body is sufficient for accurate results.

Examples of the effect of free surface panel length and extent of panelled free surface are shown in section 3.6.2.

In conclusion accuracy is strongly tied to speed. Any desired accuracy can in theory be met by panel refinement and extension of the panelled free surface, and the decision of which method to use will inevitably be in terms of the cost in speed reduction. More stringent accuracy requirements will favour Green function methods only up to the point where refinement and extension of the free surface in the corresponding simple source method reduces errors due to

the free surface truncation and discretisation to below those due to the body discretisation. Beyond this no additional accuracy can be obtained without simultaneous refinement of both the body and surface panels, at which point the additional Green function evaluations will offset the advantages of that method.

Radiation condition

This has already received much discussion in sections 2.1.3 and 2.3.4, and again Green function methods have a distinct advantage, particularly in the time domain. For this reason alone there is a strong preference among researchers for Green function methods.

2.4 Interpretation of the free surface boundary conditions for particular two-dimensional problems

2.4.1 Steady state translation and moving reference frames

Consider the problem of a body moving with constant velocity U in the $+x$ direction in an otherwise stationary fluid. Viewed in a fixed reference frame this is an unsteady flow (i.e. $\frac{\partial \phi}{\partial t} \neq 0$) but it is desirable to convert it into a steady state problem by changing to a coordinate system moving with the body, thus the boundary conditions must be rewritten in their moving reference frame form.

Consider first the more general problem of describing arbitrary motion in a moving reference frame (one might for example wish to consider periodic oscillation superimposed on steady translation). Let the subscripts $_F$ and $_M$ denote quantities in the fixed and moving reference frames respectively. We note first that ϕ represents the potential in a fixed reference frame, and that a change of reference frame is simply achieved by a change of the x variable: $\phi\left(x_F, y_F, t\right) = \phi\left(x_M + Ut, y_F, t\right)$.

From this it follows that $\frac{\partial \phi}{\partial x} = \frac{\partial \phi(x_M + Ut, y_M, t)}{\partial x_M} = \frac{\partial \phi(x_F, y_F, t)}{\partial x_F}$ = absolute x velocity of fluid (independent of the reference frame), but that $\frac{\partial \phi(x_F, y_F, t)}{\partial t} = \frac{\partial \phi(x_M, y_M, t)}{\partial t} + \frac{\partial \phi}{\partial x}\frac{dx_M}{dt}\Big|_{x_F = const} = \frac{\partial \phi(x_M, y_M, t)}{\partial t} - U\frac{\partial \phi}{\partial x}$. In fact in general we can write $\left(\frac{\partial}{\partial t}\right)_F = \left(\frac{\partial}{\partial t} - U\frac{\partial}{\partial x}\right)_M$, $\left(\frac{\partial^2}{\partial t^2}\right)_F = \left(\frac{\partial^2}{\partial t^2} - 2U\frac{\partial^2}{\partial x \partial t} + U^2\frac{\partial^2}{\partial x^2} - \frac{dU}{dt}\frac{\partial}{\partial x}\right)_M$ etc..

The boundary conditions (equations (2.10) and (2.11)) can then be rewritten as

$$\begin{aligned} \frac{\partial^2 \phi}{\partial t^2} - 2U\frac{\partial^2 \phi}{\partial x \partial t} + U^2\frac{\partial^2 \phi}{\partial x^2} - \frac{dU}{dt}\frac{\partial \phi}{\partial x} + g\frac{\partial \phi}{\partial y} \\ + \frac{1}{2}\left(\frac{\partial}{\partial t}\left|\nabla\phi^2\right| + \left(\frac{\partial \phi}{\partial x} - U\right)\frac{\partial}{\partial x}\left|\nabla\phi\right|^2\right) + \frac{\partial \phi}{\partial x}\left(\frac{\partial^2 \phi}{\partial x \partial t} - U\frac{\partial^2 \phi}{\partial x^2}\right) &= 0 \end{aligned} \tag{2.13}$$

satisfied on

$$y = \eta = \frac{1}{g}\left(U\frac{\partial \phi}{\partial x} - \frac{\partial \phi}{\partial t} - \frac{1}{2}\left|\nabla\phi\right|^2\right) \tag{2.14}$$

where a moving reference frame is now assumed. Note that equation (2.14) is an implicit equation since its right hand side must also be evaluated at $y = \eta$.

The linear form is obtained by deleting any products of ϕ or its derivatives, which gives

$$\frac{\partial^2\phi}{\partial t^2} - 2U\frac{\partial^2\phi}{\partial x \partial t} + U^2\frac{\partial^2\phi}{\partial x^2} - \frac{dU}{dt}\frac{\partial\phi}{\partial x} + g\frac{\partial\phi}{\partial y} = 0,$$

and this may be evaluated on $y = 0$.

Steady translation is represented by setting all time derivatives to zero, hence the linear form of the boundary condition becomes

$$U^2\frac{\partial^2\phi}{\partial x^2} + g\frac{\partial\phi}{\partial y} = 0, \quad \text{on} \quad y = 0. \tag{2.15}$$

Many authors view the problem of a steadily translating body as being equivalent to that of a fixed body immersed in a uniformly moving fluid with free stream velocity $-U$. One can then solve the problem in a fixed reference frame. The approach is to write the total potential ϕ_T as a sum of two component potentials: the onset flow (free stream flow) component, which we can denote $\phi_O = -Ux$, and the disturbance potential (i.e. the difference between the total potential and the onset potential, arising from the presence of the body), ϕ_D, which happens to be identical to the potential for the moving body in still water. Thus

$$\phi_T = \phi_O + \phi_D$$

One seeks a solution to ϕ_D rather than to ϕ_T.

The kinematic equivalence between ϕ_D and the potential for the moving body in still water is obvious; the body boundary condition now becomes $\frac{\partial\phi_T}{\partial n} = 0$, i.e. $\frac{\partial\phi_D}{\partial n} = -\frac{\partial\phi_O}{\partial n} = U \cdot \hat{n}$ as before. The dynamic equivalence can be verified by noting that ϕ_T must satisfy Bernoulli's equation (equation (2.9)) with the right hand side modified to account for the water velocity at $x = +\infty$, i.e.

$$\frac{p}{\rho} + \frac{\partial\phi}{\partial t} + \frac{1}{2}\nabla\phi \cdot \nabla\phi + gy = \frac{1}{2}U^2$$

hence, by putting $\phi = \phi_D - Ux$, ϕ_D satisfies

$$\frac{p}{\rho} + \frac{\partial\phi_D}{\partial t} + \frac{1}{2}\nabla\phi_D \cdot \nabla\phi_D - U\frac{\partial\phi_D}{\partial x} + gy = 0.$$

On the free surface $y = \eta$ and $p = 0$, making this condition identical to (2.14), and therefore dynamic equivalence between ϕ_D and the potential for the moving body in still water has been verified.

It is debatable whether the second approach (stationary body immersed in a uniform stream, fixed reference frame) offers any real advantage over the first (steadily translating body in an otherwise stationary fluid, moving reference frame).

It should be pointed out that the solution to the flow about a body beneath a free surface in steady translation is not unique. The desired solution is generally the time asymptotic solution for a body moving at constant speed, having started from rest beneath an initially flat free

surface, and for this problem waves are only observed behind the body[9]. The general problem may assume any initial shape for the free surface consistent with the boundary conditions, i.e. it assumes that the free surface contains initially regular waves of arbitrary amplitude but of the appropriate frequency to give a wave velocity equal to U. The general solution then is the time asymptotic solution to the problem with general initial conditions. Without resorting to the time domain it is essential to devise a method of solution that ensures that the result is both unique and that it is the desired one. Dawson's[19] use of asymmetric finite difference approximations for $\frac{\partial^2\phi}{\partial x^2}$ on the free surface to suppress upstream waves is discussed in section 2.3.4. The equivalent in the Green function method is to ensure that the wave integral in the source function is interpreted as its principal value. This is outlined by Giesing and Smith [33].

Calculation of wave height

The exact wave height is given in equation (2.14), but for problems involving a linearised free surface boundary condition the $|\nabla\phi|^2$ term must be omitted and the remaining terms evaluated on $y = 0$. For steady state ($\frac{\partial\phi}{\partial t} = 0$) the linearised wave height becomes

$$\eta = \frac{U}{g}\frac{\partial\phi}{\partial x}. \tag{2.16}$$

2.4.2 Steady state for periodically oscillating bodies

At any instant in time quantities such as position, velocity, potential etc. relating to a sinusoidal oscillation may be expressed in terms of amplitude and instantaneous phase, thus the steady state may be represented as amplitude and phase at some arbitrary time datum, or equivalently as the real and imaginary parts of a time complex amplitude. (This is not to be confused with space complex notation described in section 2.3.3. To distinguish the two the imaginary part will be indicated with i in the spatial domain and j in the temporal domain.) The desired boundary conditions may be obtained from the appropriate equations in section 2.3.1 by substituting $\frac{\partial}{\partial t}$ with $j\omega$ and $\frac{\partial^2}{\partial t^2}$ with $-\omega^2$. Thus the linear form of the free surface boundary condition, equivalent to equation (2.12), is simply

$$-\omega^2\phi + g\frac{\partial\phi}{\partial y} = 0 \quad \text{on} \quad y = 0. \tag{2.17}$$

The linearised wave heights is

$$\eta = -\frac{j\omega\phi}{g} \quad \text{evaluated at} \quad y = 0. \tag{2.18}$$

[9] Waves of all frequencies are produced but, because of dispersion, only waves stationary in phase relative to the moving body can be observed within an arbirtarily large but finite distance of the body after infinite time. Since the group velocity of any wave in deep water is always less than the phase velocity (in fact half) then, unless they are independently generated, regular waves cannot exist ahead of the body, and the regular wave train moving with the body will be observed only behind it. Further discussion of the topic can be found in Havelock [44].

It should be pointed out that, as described later in section 2.6.4, ϕ in these equations is time-complex. This means firstly that both the time-real and -imaginary parts must individually satisfy equation (2.17), and secondly that implicit in equation (2.18) is the fact that there will be an amplitude and relative phase associated with the wave height at each free surface point.

2.4.3 Arbitrary motion in a fixed reference frame

The equations in section 2.3.1 can be used without modification, but for the sake of completeness the linear versions will be repeated here. The free surface boundary condition is

$$\frac{\partial^2 \phi}{\partial t^2} + g\frac{\partial \phi}{\partial y} = 0 \quad \text{on} \quad y = 0, \tag{2.19}$$

and wave height

$$\eta = -\frac{1}{g}\frac{\partial \phi}{\partial t} \quad \text{on} \quad y = 0. \tag{2.20}$$

2.5 Calculation of pressures on the body surface in linearised problems

Calculation of body surface pressures are important in the evaluation of lift and drag forces on translating bodies, or for the evaluation of hydrodynamic coefficients for oscillating bodies.

A question arises as to whether it is consistent to calculate the exact pressure on the body boundary, given that the free surface boundary condition has been linearised, or whether the body pressure calculation should also be linearised in some sense. This is not a trivial question, and its answer can differ depending on the problem. It is also a question that has concerned various authors. Wehausen [97] (pp. 141-42) has the following to say:

> An approximation scheme in which some of the equations of the problem are satisfied to a higher order of approximation than others is said to be inconsistent...[Two examples follow.]
>
> Neither [of the two examples] is convincing and in principle each inconsistent problem is still only of first order accuracy. There is, in fact, no guarantee that the change from the consistent first order problem is in the direction of greater accuracy...
>
> One particularly misleading version of an inconsistent problem is one in which a flow is generated by a distribution of sources and sinks selected to satisfy the linearised free-surface condition and from which a "body" is generated by tracing streamlines numerically.

The problem has also been considered by Tuck [90], who says his results "show that, by a factor of at least 2 or 3 in the range of Froude numbers where wave-making is significant, it is more important to correct for non-linearity at the free surface than for the fact that the body

boundary condition is not satisfied exactly by the first approximation of the body surface." Tuck's paper however does not deal with some crucial points, and this will be discussed below after a more complete description of the problem.

Yeung [101] (p. 399) allows application of the exact body boundary condition for a deeply submerged body, but states "If the body is not deeply submerged, a consistent linearisation procedure requires that condition (2.3) [his body boundary condition] on $\mathcal{H}$ [the body surface] be satisfied in some linearised manner also."

To illustrate the difficulty let us look in particular at the calculation of pressures on a body in steady translation beneath a linearised free surface.

In section 2.3.2 it was stated that linearisation of the free surface in two dimensional flows rests on one of two assumptions: small motions, or deep submergence. It is clear that the small motions assumption can not be applied to a translating body, particularly at steady state where infinite time, hence infinitely large motions, are implicit. This leaves deep submergence as being the only valid justification for linearising the free surface boundary condition.

It is extremely important to recognise the correct form of the free surface linearisation if the body surface is also to be linearised without misleading results. The difference between the two assumptions above will be highlighted in the following discussion, and will be shown in a specific case to amount to a factor of 2.

Consider first the *small motion* assumption, applicable to some other classes of problem. We wish to calculate pressures using Bernoulli's equation. It is sufficient to consider only those terms that differ from hydrostatic pressure if we are interested in hydrodynamic forces, hence from equation (2.9) we note that dynamic pressure is

$$p = -\rho\left(\frac{\partial\phi}{\partial t} + \frac{1}{2}\nabla\phi\cdot\nabla\phi\right). \tag{2.21}$$

The flow viewed from the moving body is assumed to be at steady state, thus $\frac{\partial\phi}{\partial t} + U\frac{\partial\phi}{\partial x} = 0$ and

$$p = -\rho\left(-U\frac{\partial\phi}{\partial x} + \frac{1}{2}\nabla\phi\cdot\nabla\phi\right). \tag{2.22}$$

Ignoring second order terms in ϕ gives

$$p \simeq \rho U\frac{\partial\phi}{\partial x}. \tag{2.23}$$

Consider next the case of *deep submergence*, applicable to the present problem of a translating body. We will assume the flow to be a perturbation of the flow about a translating body in an infinite fluid (the limiting case for infinitely deep submergence). Let the potential ϕ be composed of the potential produced by the same body in an infinite fluid, ϕ_∞, and a perturbation, ϕ_P, i.e. $\phi = \phi_\infty + \phi_P$. Then $p = -\rho(\frac{\partial\phi_\infty}{\partial t} + \frac{\partial\phi_P}{\partial t} + \frac{1}{2}(\nabla\phi_\infty\cdot\nabla\phi_\infty + 2\nabla\phi_\infty\cdot\nabla\phi_P + \nabla\phi_P\cdot\nabla\phi_P)) = -\rho(-U(\frac{\partial\phi_\infty}{\partial x} + \frac{\partial\phi_P}{\partial x}) + \frac{1}{2}(\nabla\phi_\infty\cdot\nabla\phi_\infty + 2\nabla\phi_\infty\cdot\nabla\phi_P + \nabla\phi_P\cdot\nabla\phi_P))$. Noting that the non-circulating potential flow about any body in an infinite medium gives rise to no net force, then if the purpose is to calculate net forces the terms involving only ϕ_∞ can be ignored. Further,

it follows from the deep submergence assumption that the perturbation potential ϕ_P is small, therefore the second order term $\nabla\phi_P \cdot \nabla\phi_P$ can also be ignored. Thus

$$p \simeq \rho \left(U \frac{\partial \phi_P}{\partial x} - \nabla\phi_\infty \cdot \nabla\phi_P \right).$$

This expression may be simplified by noting that ϕ and ϕ_∞ satisfy on the body boundary $\nabla\phi \cdot \hat{n} = \nabla\phi_\infty \cdot \hat{n} = U n_x$, from which it follows ϕ_P satisfies $\nabla\phi_P \cdot \hat{n} = 0$. If the body boundary makes an angle θ with the x-axis in the anticlockwise direction (i.e. $n_x = -\sin\theta$, $n_y = \cos\theta$) then the boundary condition for ϕ_P gives us $\frac{\partial \phi_P}{\partial y} = \frac{\partial \phi_P}{\partial x} \tan\theta$. If we further define α such that $\frac{\partial \phi_\infty}{\partial x} = \alpha U$, then $\frac{\partial \phi_\infty}{\partial y} = U(\alpha - 1)\tan\theta$. Finally making these substitutions, and noting $\left(1 + \tan^2\theta\right) = \frac{1}{\cos^2\theta}$, we can write the deep submergence linearisation equivalent of equation (2.23),

$$p \simeq \rho U \frac{\partial \phi_P}{\partial x} \left(\frac{1 - \alpha}{\cos^2\theta} \right). \tag{2.24}$$

Returning to the small motion assumption we can assist the comparison by writing $\phi = \phi_\infty + \phi_P$, but in this case we assume only ϕ, and *not* ϕ_P, to be small. However, as in equation (2.24), we can ignore the contribution from ϕ_∞ in equation (2.23) since it makes no net contribution to the total hydrodynamic force acting on the body, hence $p \simeq \rho U \frac{\partial \phi_P}{\partial x}$. We see then that the deep submergence assumption results in an increase in hydrodynamic force by a factor of $\left(\frac{1-\alpha}{\cos^2\theta}\right)$ over the small motion assumption.

In order to illustrate how significant the factor $\left(\frac{1-\alpha}{\cos^2\theta}\right)$ is, consider now the specific case of a circular cylinder in translation. The analytic solution to ϕ_∞ is well known (e.g. Havelock [36], p82), and gives us that

$$\begin{aligned} u_\infty &= \frac{\partial \phi_\infty}{\partial x} = -U\cos 2\theta \\ v_\infty &= \frac{\partial \phi_\infty}{\partial y} = -U\sin 2\theta \end{aligned}$$

on the cylinder boundary, from which $\alpha = -\cos 2\theta$, hence

$$\left(\frac{1 - \alpha}{\cos^2\theta} \right) = 2.$$

The wrong choice of body linearisation will in this case result in a factor of 2 error. Clearly if a linearised form of the body pressure calculation is to be used care must be taken to choose its form correctly.

It is evident from the above that to evaluate *only* the first order term in the *correctly* linearised pressure for a deeply submerged body it is necessary to distinguish the contribution of ϕ_P from that of ϕ_∞. This is impractical for the general problem since it involves solving for ϕ_∞ as well as ϕ, and the question arises whether (as implied by Wehausen [97] and Tuck [90]) it is necessary.

If the problem is a valid candidate for linearisation (i.e. the body is submerged deeply enough that the linearised free surface boundary condition closely approximates the exact one) it should not matter whether non-linear terms on the body surface are included or not. Wehausen does not contradict this but does state that inclusion of the terms does not imply any improvement

in accuracy beyond first order. We want however assurance that inclusion of the terms does not result in degradation of accuracy.

To see whether inclusion of the $\nabla\phi_P \cdot \nabla\phi_P$ term adversely affects results, assume the total potential ϕ now to satisfy the nth order free surface boundary condition, and can be written as $\phi = \phi_\infty + \sum_{i=1}^{n} \phi_P^{(i)}$ where $\phi_P^{(1)}$ is identical to ϕ_P above and $\phi_P^{(i)}$ is the ith order term of the potential. The exact free surface boundary condition is satisfied as $n \to \infty$. If ε represents the linearisation parameter then we note $\phi_P^{(i)} = O\left(\varepsilon^i\right)$ on the free surface, but $O\left(\varepsilon^{i+1}\right)$ on the body surface[10], while $\phi_\infty = O\left(\varepsilon\right)$ on the free surface but $O\left(1\right)$ on the body surface. Then the leading terms in $\nabla\phi \cdot \nabla\phi$ are $\nabla\phi_\infty \cdot \nabla\phi_\infty + \nabla\phi_\infty \cdot \nabla\phi_P^{(1)} + \nabla\phi_\infty \cdot \nabla\phi_P^{(2)} + \nabla\phi_P^{(1)} \cdot \nabla\phi_P^{(1)} + \ldots$, which are of order 1, ε^2, ε^3,and ε^4 respectively on the body surface. We see that, in agreement with Tuck [90], the effect on the body of non-linearity at the free surface $\left(\nabla\phi_\infty \cdot \nabla\phi_P^{(2)}\right)$ is more significant than non-linearity in the body pressure calculation $\left(\nabla\phi_P^{(1)} \cdot \nabla\phi_P^{(1)}\right)$, but further conclude that the latter is of high enough order that its inclusion or not is irrelevant.

The crucial qualification in the previous paragraph is "if the problem is a valid candidate for linearisation". One measure of this is the wave steepness, or H/L where H is the wave height for regular waves ($2\times$ amplitude) and L is the wavelength, which can be applied to the essentially regular train of waves that appears behind any steadily translating body in two dimensions. It is well known that as $\frac{H}{L}$ increases the wave peak sharpens and the trough flattens until eventually a cusp forms at the peak and the wave breaks. Michell [68] and Havelock [40] have shown that the limiting value of $\frac{H}{L}$ is $\simeq 0.142$. Presumably then if any linear theory predicts a wave steepness approaching 0.142 or greater then it has well exceeded its range of validity.

Returning now to Tuck [90], his commentary on figure 1 of his paper (which illustrates his proposition with a particular example where the free-surface streamline bears no resemblance to the linearised free surface) includes "presumably the exact non-linear solution would involve highly non-sinusoidal or even breaking waves". His linearised free surface has a steepness $\frac{H}{L} = 0.541 = 3.8 \times \left(\frac{H}{L}\right)_{\max}$ so it is well beyond the limit where the exact solution even exists[11]. It can also be shown that the limiting value of $\frac{H}{L}$ (based on the linear estimate of H) is exceeded for the entire Froude number range in his figure 3 (in which he shows the wave resistance force for a circular cylinder whose axis is submerged by one diameter) and most of figure 4 (showing wave lift for the same body), therefore the results presented in those figures are not necessarily meaningful. In his final figure the wave steepness in the central portion of the Froude number range is now just within the limiting value, and as expected his first order, inconsistent second order, and consistent second order theories are in this case in much better agreement.

The conclusion is that Tuck's paper does demonstrate that the inconsistent second order calculation of forces on the body (i.e. without extending the free surface to second order) is

[10] The wave terms in equation (2.30) decay with depth, and the body is deeply submerged.

[11] Tuck does comment "This is a case in which we expect that the disturbance produced by the circle is too severe for the potential (3.4) to be valid as the first term in a convergent series representing the exact potential," but apparently fails to further recognise that the exact potential does not exist.

neither worse nor better that the first order calculations, but he does not demonstrate this for any physically possible flow. Also, his model, based on an asymptotic series of dipoles, differs from the present panel method solution in that only in the limiting cases of infinite order or of infinite depth does his solution satisfy the exact body boundary condition. It is perceived therefore that in the present method the effect of body non-linearity may be less.

It is without significant reservation therefore that pressures may be calculated in problems involving the deep submergence assumption in accordance with (2.22).

In problems involving the small motion assumption the more correct form is equation (2.23), but again it should not make any difference if equation (2.22) is used instead. Unlike the deep submergence problem however, it is far easier to use the linear form in this case. The linear form of pressure is also to be preferred in small motion problems because it is often the case that the motion is assumed to be of arbitrary (typically unit) amplitude, such as in the calculation of added mass and damping coefficients (see section 2.6.4), and the results scaled accordingly after the calculation. In such a case the inclusion of non-linear terms would be entirely erroneous.

2.6 Solutions for particular two dimensional problems

The following section contains details of the implementation of particular problems for which FORTRAN computer programs were written, forming a partial review of two dimensional free surface panel method techniques. This review is not intended to be complete, but rather to be for the purpose of testing the time domain Green function panel method to be discussed in the next chapter. Also, reference is made to solutions of similar problems by various authors, most notably [33], [47], [19] and [21]. The solutions presented below, although based on these works, may contain minor differences, particularly regarding notation or derivation of equations. Results and comparisons between methods will be presented in the next chapter.

2.6.1 Notation

Matrix coefficients in the following sections are generally written in terms of the variables below:

c_1, c_2	=	complex coordinate of source panel end points defined such that the direction $c_2 - c_1$ is the tangential direction on the boundary, with the normal pointing into the fluid.
z or z_i	=	complex coordinate of collocation point
α	=	slope of body boundary at collocation point (anticlockwise from $+x$ direction)
β	=	source panel slope $= \arg(c_2 - c_1)$
Q	=	strength of uniform source distributed over source panel

Other variables will be defined as required.

2.6.2 Steady translation: Green function method

The method followed here is essentially that presented in Giesing and Smith [33] and Hess and Smith [47]. The main difference is the direction of motion of the body, which is taken in this work to be from left to right.

Determination of source strengths

Source strengths are obtained by satisfying boundary conditions, which, as in equation (2.1) can be represented as a set of equations of the form

$$[A]\{Q\} = \{R\}, \tag{2.25}$$

where A_{ij} is the influence on the ith boundary condition equation due to the jth source (Q_j), and R_i represents the terms in the ith boundary condition equation independent of the sources. A solution requires interpretation of the boundary conditions to obtain the matrix coefficients A_{ij} and vector elements R_i, and these will be given, after necessary derivations, in equations (2.28), (2.34) and (2.29).

Recall from section 2.3.4 that in Green function methods the only boundary condition that $\{Q\}$ depends on is the body boundary condition (equation (2.6)), $\nabla\phi\cdot\hat{n} = \vec{V}\cdot\hat{n}$, since the Green function automatically satisfies the free surface condition. For steady translation in the positive x direction $\vec{V}$ is $U\hat{i}$ in cartesian coordinates. Using complex notation, as in section 2.3.3, this can be written as

$$\mathrm{Im}\left\{\bar{W}e^{-i\alpha}\right\} = \mathrm{Im}\left\{Ue^{-i\alpha}\right\} \tag{2.26}$$

and recall from section 2.2.1 that

$$W_i = \sum_{j=1}^{n} W_{ij}Q_j \tag{2.27}$$

thus the unknown coefficients in equation (2.25) become

$$\begin{aligned} A_{ij} &= \mathrm{Im}\left\{\bar{W}_{ij}e^{-i\alpha_i}\right\} \\ &= -\mathrm{Im}\left\{W_{ij}e^{i\alpha_i}\right\} \end{aligned} \tag{2.28}$$

and

$$R_i = -U\sin\alpha_i. \tag{2.29}$$

All that remains to be determined is W_{ij}, which will be given below as equation (2.34).

Calculation of W_{ij}

The function for the potential at z in the complex plane due to a source of constant strength Q, located at c, in uniform motion in the $+x$ direction beneath a free surface at $y = 0$, is given

by Wehausen and Laitone [98] equation (13.43) as

$$f(z) = \frac{Q}{2\pi}\left(\ln(z-c) + \ln(z-\bar{c})\right) + \frac{Q}{\pi}\,\mathrm{PV}\int_0^\infty \frac{e^{-ik(z-\bar{c})}}{k-\nu}dk + iQe^{-i\nu(z-\bar{c})}, \tag{2.30}$$

where $\nu = \frac{g}{U^2}$, and PV indicates the principal value of the integral, required to ensure uniqueness of the solution. This potential function automatically satisfies the linearised free surface boundary condition (2.15). The last term in equation (2.30) is responsible for the direction of the radiated waves, and a source moving in the $-x$ direction is represented by changing the sign of this term.

The evaluation of the integral $\mathrm{PV}\int_0^\infty \frac{e^{-ik(z-\bar{c})}}{k-\nu}dk$ is described by Giesing and Smith [33] and also by Doctors [21][12], giving

$$\mathrm{PV}\int_0^\infty \frac{e^{-ik(z-\bar{c})}}{k-\nu}dk = -e^{-i\nu(z-\bar{c})}\left[\mathrm{Ei}\left(i\nu\left(z-\bar{c}\right)\right) + \delta\pi i\right], \tag{2.31}$$

where

$$\delta = \begin{cases} 1 & \text{if} \quad \mathrm{Re}(z) > \mathrm{Re}(\bar{c}) \\ -1 & \text{if} \quad \mathrm{Re}(z) < \mathrm{Re}(\bar{c}) \end{cases}. \tag{2.32}$$

If we were to use point sources then $W_{ij} = \frac{\partial f}{\partial z}$ evaluated with $z = z_i$, $c = c_j$, $Q = Q_j$. However, distributing the sources over their respective panels we obtain

$$W_{ij} = \frac{1}{Q_j}\int_{j\text{th panel}} \frac{\partial f(z_i)}{\partial z}ds \quad \text{where} \quad ds = dc\,e^{-i\beta} = d\bar{c}\,e^{i\beta}. \tag{2.33}$$

We note that z and c (or $\bar{c}$) appear in (2.30) only as $(z-c)$ (or $(z-\bar{c})$), thus $\int \frac{\partial f}{\partial z}dc = -f$, and finally

$$\begin{aligned} W_{ij} \quad = \quad & \frac{1}{2\pi}\left(e^{-i\beta}\ln\left(\frac{z-c_1}{z-c_2}\right) + e^{i\beta}\ln\left(\frac{z-\bar{c}_1}{z-\bar{c}_2}\right)\right) \\ & + \frac{e^{i\beta}}{\pi}\left[e^{-i\nu(z-\bar{c}_k)}\left[\mathrm{Ei}\left(i\nu\left(z-\bar{c}_k\right)\right) + \left(\delta_k - 1\right)\pi i\right]\right]_{k=1}^{2} \end{aligned} \tag{2.34}$$

where $\delta_k = \delta(z, c_k)$ in equation (2.32) and $\nu = \frac{g}{U^2}$. As explained later in section 3.3.3 when $i = j$ we find $\ln\left(\frac{z-c_1}{z-c_2}\right) = \ln(-1)$, which *must* be interpreted as $-i\pi$. Note also that translation in the $-x$ direction is represented by replacing $(\delta_k - 1)$ with $(\delta_k + 1)$.

[12] It can be evaluated with the change of variable, $t = -i\left(z-\bar{c}\right)(k-\nu)$ to give $\int_0^\infty \frac{e^{-ik(z-\bar{c})}}{k-\nu}dk = -e^{-i\nu(z-\bar{c})}\,\mathrm{Ei}\left(i\nu\left(z-\bar{c}\right)\right)$, where Ei is the exponential integral, defined as $\mathrm{Ei}(z) = \int_{-\infty}^{z}\frac{e^t}{t}dt$ in the z-plane cut along the positive real axis (Abramowitz and Stegun [1] p. 228, footnote 4; this definition is chosen for consistency with the FORTRAN subroutine library used [69]). The *principal value* is taken into account by subtracting the term $\pm i\pi e^{-i\nu(z-\bar{c})}$ representing the integral half way around the singularity at $k = \nu$, included in the Exponential integral but to be omitted in the principal value integral. The sign of this term depends on the which side of the singularity the path of integration must pass to avoid the cut on the positive real axis, which in turn depends on whether $i\nu\left(z-\bar{c}\right)$ is in the first or fourth quadrant.

Calculation of free surface elevation

The free surface elevation in a translating reference frame is given in equation (2.16), which for the present method becomes

$$\begin{aligned} \eta(x) &= \frac{U}{g}\frac{\partial\phi(x,0)}{\partial x} \\ &= \frac{U}{g}\mathrm{Re}\{W\}. \end{aligned} \tag{2.35}$$

This can be calculated as in equations (2.27) and (2.34), replacing the collocation point, z, in the expression for W with $z = x + i0$, the point on the undisturbed free surface at which η is required.

Body surface pressures

As argued in section 2.5, body pressures may be calculated using equation (2.22).

The terms involved are all velocity terms, and as such may be evaluated using equations (2.27) and (2.34). Alternatively it is recognised that velocity coefficients have already been calculated in solving for source strengths (the tangential components were calculated automatically along with the normal components as the real part of equation (2.28), but were not required and therefore may not have been stored in memory), and most of the computational cost of evaluating pressures may be saved by appropriate organisation of the computer program.

2.6.3 Steady translation: simple source method

Details of this technique can be found in Dawson [19]. Dawson's most significant contribution was to devise a method, involving definition of a suitable form of the finite difference approximation for the $\frac{\partial^2\phi}{\partial x^2}$ term in the free surface boundary condition, of making the solution to the problem unique. Dawson also deals with some three dimensional problems, which will not be discussed below.

As before we can write boundary conditions in the form $[A]\{Q\} = \{R\}$, but we note that there are two sets of boundary conditions to satisfy: one on the body and one on the free surface. If we use the *double body* formulation (described is section 2.3.4) we may also distinguish between body sources and free surface sources since it is superfluous to include the image of the latter. Denoting quantities relating to the body and the free surface with the subscripts $_B$ and $_F$ respectively we can rewrite equation (2.25) as

$$\begin{bmatrix} A_{BB} & A_{BF} \\ A_{FB} & A_{FF} \end{bmatrix} \begin{Bmatrix} Q_B \\ Q_F \end{Bmatrix} = \begin{Bmatrix} R_B \\ R_F \end{Bmatrix} \tag{2.36}$$

where A_{BB}, A_{BF}, A_{FB} and A_{FF} are themselves matrices, and R_B and R_F vectors. We can then discuss separately the typical coefficients of sub-matrices A_{BB}, A_{BF}, A_{FB}, A_{FF}, R_B and R_F in terms of the relevant boundary conditions and source function. These will be given in equations (2.38), (2.39), (2.46), (2.40), (2.41), (2.47) and (2.48).

Let us further assume the body panels are numbered 1 to m, and the free surface panels $(m+1)$ to n.

Body boundary condition

The body boundary condition is identical to that in section 2.6.2, equation (2.26), and is represented in this problem as the subset of the equations in (2.36) represented by $\left[\begin{array}{cc} A_{BB} & A_{BF} \end{array}\right] \times \left\{\begin{array}{c} Q_B \\ Q_F \end{array}\right\} = \{R_B\}$. However the source function now contains just the body and image terms (these are identical for free surface sources, in which case the image term is usually omitted), and not the wave terms, i.e.

$$f(z) = \frac{Q}{2\pi}\left(\ln(z-c) + \ln(z-\bar{c})\right). \tag{2.37}$$

We obtain A_{ij} in sub-matrices $[A_{BB}]$ and $[A_{BF}]$ from equation (2.28), which, combined with equations (2.37) and (2.33) give

$$(A_{BB})_{i,j} = -\operatorname{Im}\left\{\frac{e^{i\alpha}}{2\pi}\left[e^{-i\beta}\ln\left(\frac{z-c_1}{z-c_2}\right) + e^{i\beta}\ln\left(\frac{z-\bar{c}_1}{z-\bar{c}_2}\right)\right]\right\} \tag{2.38}$$

$$(A_{BF})_{i,j} = -\operatorname{Im}\left\{\frac{e^{i\alpha}}{2\pi}\left[e^{-i\beta}\ln\left(\frac{z-c_1}{z-c_2}\right)\right]\right\}. \tag{2.39}$$

The first logarithm in equation (2.38) must be interpreted, as it was in equation (2.34), as $-i\pi$ when $i=j$.

The right hand side of the body boundary condition is identical to equation (2.29),

$$(R_B)_i = U\sin\alpha. \tag{2.40}$$

Free surface boundary condition

The remaining equations in (2.36) are $\left[\begin{array}{cc} A_{FB} & A_{FF} \end{array}\right]\left\{\begin{array}{c} Q_B \\ Q_F \end{array}\right\} = \{R_F\}$, and represent the linearised free surface boundary condition, $U^2\frac{\partial^2\phi}{\partial x^2} + g\frac{\partial\phi}{\partial y} = 0$ (equation (2.15)). We note first that this contains no terms independent of ϕ, thus

$$(R_F)_i = 0. \tag{2.41}$$

The expression $\frac{\partial^2\phi}{\partial x^2}$ may be evaluated analytically, giving terms of the type $\frac{Qe^{-i\beta}}{2\pi}\left(\frac{1}{z-c_1} + \frac{1}{z-c_2}\right)$, but this results in a symmetric solution (waves both ahead of and behind the body), which is not the desired solution. An asymmetric numerical approximation to the derivative on the other hand may well give the desired asymmetric solution.

Following the method of Dawson [19] the upstream waves may be damped out by using the upstream finite difference approximation

$$\begin{aligned}\left(\frac{\partial^2\phi}{\partial x^2}\right)_i &= \operatorname{Re}\left\{\frac{\partial W_i}{\partial z}\right\} \\ &\simeq \operatorname{Re}\left\{\frac{W_{i-3} - 6W_{i-2} + 15W_{i-1} - 10W_i}{6\,\Delta x}\right\}\end{aligned} \tag{2.42}$$

where for consistency i increases in the $-x$ direction so that the unit normal to the panels points into the fluid, and it is assumed here Δx is a constant on the free surface[13]. Dawson [19] tried several alternative finite difference operators, and found this to be the most successful. For the last three points at the upstream end ($i = (m+3)$, $(m+2)$ and $(m+1)$) other finite difference approximation must be used. The choice does not appear to be critical as errors remain localised, and in this work it was assumed

$$\left(\frac{\partial^2\phi}{\partial x^2}\right)_{m+3} \simeq \mathrm{Re}\left\{\frac{-W_{m+1}+4W_{m+2}-3W_{m+3}}{6\,\Delta x}\right\} \tag{2.43}$$

$$\left(\frac{\partial^2\phi}{\partial x^2}\right)_{m+2} \simeq \mathrm{Re}\left\{\frac{W_{m+1}+W_{m+3}}{2\,\Delta x}\right\} \tag{2.44}$$

$$\left(\frac{\partial^2\phi}{\partial x^2}\right)_{m+1} \simeq \mathrm{Re}\left\{\frac{3W_{m+1}-4W_{m+2}+W_{m+3}}{6\,\Delta x}\right\}. \tag{2.45}$$

The remaining term in the free surface boundary condition, $g\frac{\partial\phi}{\partial y}$, is very easily evaluated by noting that on the free surface, because of symmetry, the contribution to $\frac{\partial\phi}{\partial y}$ at point z_i, $(m+1<i<n)$ from any panel except panel i is zero. The only contribution is $\frac{Q}{2\pi}(-\pi)$, thus the diagonal terms of $[A_{FF}]$ must include $\frac{-g}{2}$.

Finally,

$$(A_{FB})_{ij} = (A_{FF})_{ij} = \mathrm{Re}\left\{\frac{W_{i-3,j}-6W_{i-2,j}+15W_{i-1,j}-10W_{i,j}}{6\,\Delta x}\right\} - \frac{\delta g}{2U^2} \tag{2.46}$$

if $m+4 \le i \le n$, or the analogous version of equations (2.43) to (2.45) for $m+1 \le i \le m+3$, where

$$\delta = \begin{cases} 0 & \text{if } i \neq j \\ 1 & \text{if } i = j \end{cases}$$

and

$$W_{ij} = \frac{1}{2\pi}\left[e^{-i\beta}\ln\left(\frac{z-c_1}{z-c_2}\right) + e^{i\beta}\ln\left(\frac{z-\bar{c}_1}{z-\bar{c}_2}\right)\right] \tag{2.47}$$

in (A_{FB}) $(j \le m)$ or

$$W_{ij} = \frac{e^{-i\beta}}{2\pi}\ln\left(\frac{z-c_1}{z-c_2}\right) \tag{2.48}$$

in (A_{FF}) $(j \ge m+1)$.

It may be desirable to multiply the coefficients $(A_{FB})_{ij}$ and $(A_{FF})_{ij}$ by an arbitrary constant factor (for example $\frac{U^2}{g}$) so that the diagonal elements in sub-matrices $[A_{BB}]$ and $[A_{FF}]$ are of similar order. Apart from possibly improving numerical stability (except perhaps when $\frac{\Delta x\, g}{U^2}$ is very small) this should have no effect on the solution since $(R_F)_i = 0$.

Wave height calculation

As in equation (2.35) the wave height η is given as

$$\eta(x_i) = \frac{U}{g}\frac{\partial\phi(x_i)}{\partial x} = \frac{U}{g}\,\mathrm{Re}(W_i), \tag{2.49}$$

[13] Dawson's expressions [19] are general, allowing arbitrary spacing of the free surface points, but reduce to equation (2.42) with constant spacing.

but note that it is only valid to calculate η at the free surface collocation points, unlike the Green function method where η may be evaluated at any arbitrary free surface point.

If a quicker method of calculating η is desired one can rewrite this using the free surface boundary condition $\frac{\partial^2\phi}{\partial x^2} + \frac{g}{U^2}\frac{\partial\phi}{\partial y} = 0$, and recalling $\frac{\partial\phi}{\partial y} = \frac{-Q}{2}$ due to symmetry about the line $y = 0$, to give

$$\eta(x_2) - \eta(x_1) = \int_{x_1}^{x_2} \frac{Q}{2U} dx, \tag{2.50}$$

The latter of course is subject to accumulating errors, particularly where a large number of points is desired, but apart from roundoff error it follows from the fact that the free surface boundary condition has been satisfied that the two should be identical if the numerical approximation to the integral is mathematically equivalent to the inverse of the finite difference approximation used to obtain $\frac{\partial^2\phi}{\partial x^2}$ from $\frac{\partial\phi}{\partial x}$ in the original setting up of the equations. Numerical experiments confirm that even using a crude trapezoidal integration in (2.50) gives reasonable agreement with (2.49) since the oscillatory nature of the free surface tends to cause cancellation of accumulating errors.

Body pressures

As in section 2.6.2 body pressures are calculated using equation (2.22), and again this involves only velocity terms.

2.6.4 Periodic oscillation: Green function method

A complete solution to this problem can be found in Doctors [21]. One feature of this problem encountered when modelling surface piercing bodies is the presence of irregular frequencies at which the solution becomes singular. This is discussed by Doctors, and he solves the problem by the use of a "lid", forming a closed body. Doctors also discusses the use of a *Galerkin* method, in which the satisfaction of body boundary conditions at discrete points is replaced with averaging of the boundary condition over the collocation panel, and finds that this improves convergence properties. These features are not difficult to implement, but the description below will be confined to the basic method.

Source function

For a source of sinusoidally oscillating strength in two dimensions the potential function is given by Wehausen and Laitone [98] as

$$f(z,t) = \left[\frac{1}{2\pi}\left(\ln(z-c) - \ln(z-\bar{c})\right) - \frac{1}{\pi}\,\mathrm{PV}\int_0^\infty \frac{e^{-ik(z-\bar{c})}}{k-\nu}dk\right] Q\cos\omega t - \left[e^{-i\nu(z-\bar{c})}\right] Q\sin\omega t \tag{2.51}$$

where $\nu = \omega^2/g$. The integral term is identical to that already discussed in section 2.6.2 and is given by equations (2.31) and (2.32).

In solving oscillatory problems it is convenient to eliminate the time variable by the use of complex notation, recalling that the imaginary part in the space and time domains are represented in this work respectively with i and j (section 2.4.2). Time complex (frequency domain) quantities will be distinguished from their time domain equivalents with the symbol $\tilde{}$ above the quantity, and conversion to the time domain is simply achieved by multiplying by $e^{j\omega t}$ and taking the time-real part[14]. Thus

$$\tilde{f}(z) = \tilde{Q}\left\{\frac{1}{2\pi}\left[\left(\ln(z-c) - \ln(z-\bar{c})\right) + 2e^{-i\nu(z-\bar{c})}\left(\mathrm{Ei}\left(i\nu\left(z-\bar{c}\right)\right) + \delta\pi i\right)\right] + j\left[e^{-i\nu(z-\bar{c})}\right]\right\} \tag{2.52}$$

and we recover $f(z,t) = \mathrm{Re}_j\left(\tilde{f}(z)\, e^{j\omega t}\right)$ if $\mathrm{Im}_j\left(\tilde{Q}\right) = 0$. We note that in incorporating this into a panel method we wish to allow for the possibility of arbitrary phase relationships between sources on different panels, which is achieved by allowing Q to be time complex $\left(\tilde{Q}\right)$. Note also the difference in the sign of the last terms in f and $\tilde{f}$.

Complex velocity

As before, $\tilde{W}_{i,j}$ is evaluated according to equation (2.33), replacing f and W with $\tilde{f}$ and $\tilde{W}$ since both must now be time complex. Integrating in the manner described in section 2.6.2 gives

$$\begin{aligned}\tilde{W}_{i,j} \quad = \quad & \left\{\frac{1}{2\pi}\left[e^{-i\beta}\ln\left(\frac{z-c_1}{z-c_2}\right) - e^{i\beta}\ln\left(\frac{z-\bar{c}_1}{z-\bar{c}_2}\right)\right] - \frac{e^{i\beta}}{\pi}\left[e^{-i\nu(z-\bar{c})}\left(\mathrm{Ei}\left(i\nu\left(z-\bar{c}\right)\right) + \delta\pi i\right)\right]_{\bar{c}_1}^{\bar{c}_2}\right\} \\ & -j\left\{e^{i\beta}\left[e^{-i\nu(z-\bar{c})}\right]_{\bar{c}_1}^{\bar{c}_2}\right\}\end{aligned} \tag{2.53}$$

where again the first logarithm is interpreted as $-i\pi$ when $i = j$.

$\left[\tilde{A}\right]$ matrix

As in section 2.6.2 only the kinematic boundary condition on the body boundary needs to be satisfied, giving

$$\tilde{A}_{ij} = -\,\mathrm{Im}_i\left\{\tilde{W}_{ij}e^{i\alpha}\right\}. \tag{2.54}$$

This differs from equation (2.28) only in that it is time complex.

Right hand side vector

Before proceeding we note that the source function (2.51) is for a *stationary* source of pulsating strength, thus it is not possible to represent exactly a *moving* hull, such as one oscillating with finite amplitude. The linearity of the free surface boundary condition requires small motions, at least for surface piercing bodies where the deep submergence assumption must be automatically excluded. Thus problems of this type involve the assumption of oscillations of infinitesimal amplitude.

[14] The subscripts $_i$ and $_j$ on the functions Re and Im will be used to indicate the space or time complex domains respectively.

If the body motion is given by $i\tilde{X}$ for heave, or $\tilde{X}$ for sway, and the linearity assumption allows us to solve any problem with the arbitrary choice of unit motion and zero phase, $\tilde{X} = 1 + 0j$, then the right hand side vector component $R_i = \vec{V}_i \cdot \hat{n}_i$ reduces to

$$\tilde{R}_i = \begin{cases} \mathrm{Im}_i \left\{ e^{-i\alpha_i} j\omega i\tilde{X} \right\} &= j\omega \cos(\alpha_i) \qquad \text{(for heave motion)} \\ \mathrm{Im}_i \left\{ e^{-i\alpha_i} j\omega \tilde{X} \right\} &= -j\omega \sin(\alpha_i) \qquad \text{(for sway motion)} \end{cases} . \tag{2.55}$$

Source strengths

Source strengths are obtained by solving for $\{Q\}$ in the matrix equation

$$\left[\tilde{A}\right] \left\{\tilde{Q}\right\} = \left\{\tilde{R}\right\}. \tag{2.56}$$

We notice that these are complex equations. Library subroutines are readily available to solve this type of problem. Alternatively these may be written as the set of real equations

$$\begin{bmatrix} A_R & -A_I \\ A_I & A_R \end{bmatrix} \begin{Bmatrix} Q_R \\ Q_I \end{Bmatrix} = \begin{Bmatrix} R_R \\ R_I \end{Bmatrix}$$

where subscripts $_R$ and $_I$ indicate respectively the time-real and time-imaginary parts of the matrix or vector (for example, $\left[\tilde{A}\right] = [A_R] + j\,[A_I]$).

Potentials

Potentials are next obtained from

$$\left\{\tilde{\phi}\right\} = \left[\tilde{B}\right] \left\{\tilde{Q}\right\} \tag{2.57}$$

where

$$\tilde{B}_{i,j} = \mathrm{Re}_i \left\{ \frac{1}{\tilde{Q}_j} \int_{j\text{th panel}} \tilde{f}(z_i)\, ds \right\}. \tag{2.58}$$

$\tilde{B}$-matrix

Using the fact that

$$\int_0^x e^{\pm ax}\, \mathrm{Ei}(\mp ax)\, dx = \pm\frac{1}{a}\left[e^{\pm ax}\, \mathrm{Ei}(\mp ax) - \ln ax - \gamma\right] \quad \text{where } \gamma = \text{Euler's constant}$$

(Prudnikov, Brychkov and Marichev [80], Vol. 1, equation (1.3.2.6)), and taking care that the path of integration of $\ln(z-c)$ does not cross the negative real axis (as explained in section 3.3.1) we obtain from equations (2.52) and (2.58)

$$\begin{aligned} \tilde{B}_{i,j} \;=\; & \mathrm{Re}_i \left(\left\{ \frac{-1}{2\pi} \left[e^{-i\beta}(z-c) \ln\left(e^{-i\gamma}(z-c)\right) - e^{i\beta}(z-\bar{c}) \ln(z-\bar{c}) \right]_{c_1}^{c_2} \right. \\ & \left. - \frac{-ie^{i\beta}}{\pi\nu} \left(\left[e^{-i\nu(z-\bar{c})} \left(\mathrm{Ei}\left(i\nu(z-\bar{c})\right) + \delta\pi i \right) \right]_{\bar{c}_1}^{\bar{c}_2} - \ln\left(\frac{z-\bar{c}_2}{z-\bar{c}_1}\right) \right) \right\} \\ & - j \left\{ \frac{ie^{i\beta}}{\nu} \left[e^{-i\nu(z-\bar{c})} \right]_{\bar{c}_1}^{\bar{c}_2} \right\} \Bigg) \end{aligned} \tag{2.59}$$

where $\gamma = \arg\left(z - \frac{c_1+c_2}{2}\right)$ if source and collocation panels are not identical, or $\gamma = \arg\left((c_2-c_1) + \frac{\pi}{2}\right)$ otherwise.

Forces

Total force exerted by the water on the body is the sum of forces on each panel, $\tilde{F} = \sum_{i=1}^{n} \Delta\tilde{F}_i$, where $\Delta\tilde{F}_i = -\tilde{p}_i \, ds_i \, \hat{n}_i$ and $\hat{n}_i = -\sin(\alpha_i)\ \hat{i} + \cos(\alpha_i)\ \hat{j}$. Local pressure, as described in section 2.5 and using equation (2.9), is $p_i = -\rho \frac{\partial \phi_i}{\partial t}$ in a fixed reference frame, assuming small motions and ignoring hydrostatic terms, hence $\tilde{p}_i = -\rho j\omega\tilde{\phi}_i$, and

$$\tilde{F} = \begin{cases} \rho j\omega \sum_{i=1}^{n} \tilde{\phi}_i ds_i \cos\alpha_i & \text{(heave force)} \\ -\rho j\omega \sum_{i=1}^{n} \tilde{\phi}_i ds_i \sin\alpha_i & \text{(sway force)} \end{cases} . \tag{2.60}$$

Added mass and damping

Added mass (a) represents the effective inertia of the water surrounding the oscillating body, and is therefore the component of force in phase with the body's acceleration exerted *by the body on the water* for a unit amplitude acceleration of the body. Similarly the damping coefficient (b) is defined as component of force in phase with the body's velocity exerted by the body on the water for a unit amplitude velocity of the body. Noting that $\tilde{F}$ has been defined above as the force exerted *by the water on the body*, we have $\tilde{F} + \left((j\omega)^2 a + (j\omega) b\right) \tilde{X} = 0$, giving $a = \mathrm{Re}_j \left\{ \frac{-\tilde{F}}{(j\omega)^2 \tilde{X}} \right\}$ and $b = \mathrm{Re}_j \left\{ \frac{-\tilde{F}}{(j\omega)\tilde{X}} \right\}$. Simplifying (with $\tilde{X} = 1 + 0j$),

$$a = \mathrm{Re}_j \left\{ \frac{\tilde{F}}{\omega^2} \right\} \tag{2.61}$$

$$b = \mathrm{Im}_j \left\{ \frac{-\tilde{F}}{\omega} \right\} \tag{2.62}$$

It is usual to talk of added mass and damping for a particular direction of force and mode of motion. Thus it is implied in equations (2.61) and (2.62) that the heave or sway force is indicated by the appropriate choice of $\tilde{F}$ in equation (2.60), with $\tilde{\phi}$ being the solution for heave or sway motion as determined by the appropriate choice of boundary condition represented by equation (2.55), giving a total of eight possible coefficients represented by equations (2.61) and (2.62).

2.6.5 Arbitrary motion in time domain: simple source method

The implementation of this method was restricted to fully submerged bodies. This was for two reasons: the nature of arbitrary motion excludes linearisation of the free surface based on the small motion assumption unless one wishes to restrict the possible motions to small motions about a mean position, and surface piercing bodies involve additional geometric manipulations and programming difficulties that were not justified for the applications envisaged.

The source function in this problem, as in the steady motion problem, equation (2.37), is $f(z) = \frac{Q}{2\pi} \left(\ln(z - c) + \ln(z - \bar{c}) \right)$, with the second logarithm (image term) omitted for free surface sources.

Body equations

As for all linear simple source methods there are two sets of equations, those on the body and those on the free surface, giving rise to a matrix equation identical to (2.36) in the steady motion problem. Furthermore the body boundary condition, being a kinematic condition, is identical to that for steady motion with the only exception being that the body velocity is now a function of time[15]. Sub-matrices $[A_{BB}]$, $[A_{BF}]$ and $\{R_B\}$ may therefore be evaluated using equations (2.38), (2.39) and (2.40).

Free surface equations

The linearised free surface boundary condition to be satisfied is $\frac{\partial^2\phi}{\partial t^2} + g\frac{\partial\phi}{\partial y} = 0$ (equation (2.12)), and, as in the steady motion problem, the second term in this equation is very easily evaluated using $\frac{\partial\phi}{\partial y} = \frac{-Q}{2}$.

There are two approaches to evaluating $\frac{\partial^2\phi}{\partial t^2}$: analytical or numerical. The former would at first seem preferable, but it gives rise to terms involving the derivative of the source strength, $\frac{\partial^2 Q}{\partial t^2}$, which, due to the time-discretisation and the fact that $Q(t)$ is not previously known, must be numerically evaluated anyway. Neither method has a clear advantage over the other therefore, and the numeric approach will be taken here while the analytic one will be used in the equivalent Green function solution in the next chapter.

The numerical approximation to $\frac{\partial^2\phi}{\partial t^2}$ must contain values of ϕ from past and current time steps, with the former being known explicitly and the latter being in terms of the unknown source strengths at the current time step. The three point backwards difference estimate $\frac{\partial^2\phi}{\partial t^2} \simeq \frac{\phi(t)-2\phi(t-\Delta t)+\phi(t-2\Delta t)}{\Delta t^2}$ was used. Separating terms dependent on the unknown source strengths from those independent of them, the free surface boundary condition may be written as

$$\phi(t) + \Delta t^2 g\frac{\partial\phi(t)}{\partial y} \simeq 2\phi(t-\Delta t) - \phi(t-2\Delta t). \tag{2.63}$$

This assumes at least two previous time steps have been solved. Otherwise for the first time step ($t = 0$) the condition $\phi(t) = 0$ for $t \leq 0$ substituted into (2.63) yields $\frac{\partial\phi(0)}{\partial y} = 0$ on the free surface, and for the second time step ($t = \Delta t$) $\frac{\partial^2\phi(\Delta t)}{\partial t^2} \simeq \frac{6\phi(\Delta t)}{\Delta t^2}$. The latter is based on the assumptions $\phi(0) = \frac{\partial\phi(0)}{\partial t} = \frac{\partial^2\phi(0)}{\partial t^2} = 0$ (the third of these being a consequence of the backwards difference operator applied to $\phi(t) = 0$ for $t \leq 0$), which, with the known value of $\phi(\Delta t)$, allows us to write ϕ as a cubic function of t, and the result follows by differentiation. In reality the backwards difference operator breaks down at the instant $t = 0$ because the fluid may receive a finite impulse. In fact differentiating the equivalent time domain Green function expression (equation (3.1)) analytically with respect to time, one obtains a non-zero real part in the second

[15] This assumes a rigid body. The more general case of a deforming body will be dealt with in the next chapter, but using a Green function method. The simple source equivalent may be recovered from the Green function method by omitting the wave term (convolution integral) in the Green function, leaving only the body and image terms. There is also in this case a difference in sign of the image term.

derivative of the convolution integral term at $t = 0$ of $\mathrm{Re}\left\{\frac{igQ}{\pi(z-\bar{c})}\right\} = \frac{gQ}{\pi \,\mathrm{Im}\, c}$ (unless the body accelerates from rest, in which case $Q(0) = 0$). This of course contradicts the assumption $\frac{\partial \phi}{\partial y} = 0$. However many tests were carried out using different alternatives for $\frac{\partial^2 \phi(t)}{\partial t^2}$ for the first and second time steps ($t = 0$, Δt) using both the simple source and Green function methods. It was found in all cases, even with inconsistent approximations, that as $\Delta t \to 0$ the final result was independent of the choice. This was not unexpected since the third and subsequent time steps all have consistent approximations for $\frac{\partial^2 \phi}{\partial t^2}$.

The equations equivalent to (2.63) for the first and second time steps are respectively

$$\frac{\partial \phi(0)}{\partial y} = 0 \tag{2.64}$$

$$\phi(\Delta t) + \frac{\Delta t^2 g}{6} \frac{\partial \phi(\Delta t)}{\partial y} \simeq 0 \tag{2.65}$$

The solution to (2.64) is trivial since $\frac{\partial \phi}{\partial y} = \frac{-Q}{2}$ implies that all the free surface source strengths must be zero. Only the body equations need to be solved for the first time step.

Returning to subsequent time steps, it follows from equations (2.63) and (2.65), recalling that $\left(\frac{\partial \phi}{\partial y}\right)_i = \frac{-Q_i}{2}$, that

$$(A_{FB})_{ij} = (A_{FF})_{ij} = \begin{cases} \phi_{ij} - \frac{\delta}{2}\Delta t^2 g & t \geq 2\Delta t \\ \phi_{ij} - \frac{\delta}{12}\Delta t^2 g & t = \Delta t \end{cases} \tag{2.66}$$

where

$$\delta = \begin{cases} 0 & \text{if } i \neq j \\ 1 & \text{if } i = j \end{cases},$$

and that

$$(R_F)_i = \begin{cases} 2\phi_i(t - \Delta t) - \phi_i(t - 2\Delta t) & t \geq 2\Delta t \\ \phi_i(0) & t = \Delta t \end{cases}. \tag{2.67}$$

In equation (2.66) ϕ_{ij} is analogous to $\tilde{B}_{ij}$ in equation (2.59) without the wave terms and with the body and image sources having the same sign. However we note that the collocation point, z, will always be on the free surface, and c in the lower half plane, preventing the path of integration of $\ln(z - c)$ from crossing its branch cut on the negative real axis, and making the $e^{-i\gamma}$ term unnecessary. Also the difference in sign of the image term, not to mention its absence from the free surface sources, requires the term $(c_1 - c_2)$, as described in section 3.3.1, to be retained. Thus

$$\begin{aligned} \phi_{ij} = \frac{1}{2\pi} \mathrm{Re}\big\{ & e^{-i\beta}\left((c_1 - c_2) + (z - c_1)\ln(z - c_1) - (z - c_2)\ln(z - c_2)\right) \\ & + e^{i\beta}\left((\bar{c}_1 - \bar{c}_2) + (z - \bar{c}_1)\ln(z - \bar{c}_1) - (z - \bar{c}_2)\ln(z - \bar{c}_2)\right)\big\} \end{aligned} \tag{2.68}$$

in (A_{FB}) $(j \leq m)$ or

$$\phi_{ij} = \frac{1}{2\pi} \mathrm{Re}\left\{e^{-i\beta}\left((c_1 - c_2) + (z - c_1)\ln(z - c_1) - (z - c_2)\ln(z - c_2)\right)\right\} \tag{2.69}$$

in (A_{FF}) $(j \geq m + 1)$.

Finally, $\phi_i(t-\Delta t)$ in equation (2.67) is evaluated using

$$\phi_i = \sum_{j=1}^{n} \phi_{ij} Q_j \tag{2.70}$$

where ϕ_{ij} and Q_j are the values corresponding to the previous time step, and should be known already, while $\phi_i(t-2\Delta t)$ has already been evaluated as $\phi_i(t-\Delta t)$ in the previous time step.

Non-reflecting boundary condition at the free surface edges

This difficulty has been discussed in section 2.3.4 and is particularly relevant to time domain problems.

In the present work the difficulty was eventually ignored. Some non-reflecting boundary conditions were attempted without sufficient success to justify the additional complexity to the program. Yeung [101] (p411) comments "What then is the appropriate boundary condition that will have minimal effect on the interior solution? This has always been a 'sore point' in computational fluid mechanics. There is no absolutely satisfactory answer to this nontrivial difficulty and the search still continues [references given]." while Raven [82] claims "But, particularly for 3D problems, no satisfactory non-reflective boundary conditions are known." Although various authors have worked on the problem (for example [13], [8]), it is clearly a major undertaking to deal with the problem properly, and it was therefore decided to circumvent the problem by choosing to panel a sufficiently large section of the free surface, depending on the length of time to be simulated. Nevertheless there were reflections, but, provided the simulation time was limited, not sufficient to contaminate significantly the flow around the body. Of greater concern was the general drift of the free surface observed after large time simulations. This problem appears to initiate when the first waves reach the boundary edges and are reflected, so it is presumed to be a related problem and perhaps due in part to the lack of a mechanism for the dissipation of energy. It too was minimised by matching the size of the free surface domain to the length of time being simulated.

Calculation of wave height

Wave height can very conveniently be calculated using $\frac{\partial \eta}{\partial t} = \frac{\partial \phi}{\partial y} = \frac{-Q}{2}$ on the free surface, from which (assuming an initially flat free surface) the free surface elevation at panel i is

$$\eta_i(t) = \int_0^t \frac{-Q_i(\tau)}{2} d\tau. \tag{2.71}$$

This may be evaluated given Q_i at discrete time steps, using for example a trapezoidal rule.

Alternatively, one can use

$$\eta = -\frac{1}{g}\frac{\partial \phi}{\partial t}, \tag{2.72}$$

which appears to require more computational time, but, considering that the solution requires the calculation of ϕ anyway, the difference is negligible. The results from the two methods are

virtually indistinguishable (except in the case of a very large number of small time steps, when the former may suffer from accumulated roundoff error), and the choice is usually a matter of preference.

2.6.6 Non-linear problems: arbitrary motion in the time domain

Any of the simple source methods could be extended to include non-linear terms in the free surface boundary condition, but the one described here will be that of arbitrary motion in the time domain. In addition, as in the linear solution to this problem, we will restrict ourselves to fully submerged bodies. This will be sufficient to illustrate some of the techniques and difficulties of non-linear problems.

The distinguishing feature of non-linear problems is not only the presence of non-linear terms in the free surface boundary conditions, but the fact that a moving boundary is involved (the free surface) whose motion is not known and must be ascertained as part of the solution process. One can keep track of the free surface either by an Eulerian approach, in which boundary points are fixed horizontally and the free surface elevation at that horizontal position is sought, or a Lagrangian approach, in which each boundary point is "tagged" to a fluid particle, free to move both horizontally and vertically, and the movement of that point is given by the velocity of that particle. The latter results in very simple equations, but requires two variables (three for three dimensional problems) to define the location of each point, as opposed to only one in the Eulerian method. There may be many factors involved in deciding the optimum method to use for a particular problem.

Clearly only the Lagrange approach however is capable of handling situations such as breaking waves, where the Eulerian representation would be multi-valued. It also has the advantage that points tend naturally to concentrate near regions of rapid change (such as near the crest of a wave). It is for these two reasons that it would generally be the preferred option for strongly non-linear problems. Also, a Lagrangian representation of the free surface would be almost essential for surface piercing bodies. Such a problem could certainly not be solved using an Eulerian representation without significant adaptations.

Returning to the particular problem at hand, arbitrary motion in the time domain; being of mixed boundary and initial value type, as well as involving non-linear equations, there are many approaches to its solution. Some general methods are discussed in Yeung [101] (pp.430-36) and Raven [82] (section 2), although the latter deals mainly with steady flows. To generalise somewhat, we have on the one hand methods that emphasize time stepping aspects, and on the other those emphasizing more the boundary value nature of the problem. The former approach might typically involve using a time stepping algorithm (such as Runge-Kutta) to update the free surface location, and then, with a temporarily fixed free surface, solving for source strengths, and perhaps iterating between the two. This has the advantage of a reduced set of non-linear equations to solve (slightly more than half, since the free surface update is an extrapolation

process, and does not necessitate solving a set of simultaneous equations), but the disadvantage that by separating the equations the solution process can not take into account interaction between the two sets, possibly resulting in a greater number of iterations required. The latter approach attempts to solve for both the free surface and source strengths simultaneously, and time derivatives appear in the boundary condition equations merely as finite difference functions of past and current values.

It should be apparent that where a Lagrangian approach is sought the time stepping method is more suitable, in particular since the free surface update equations are very simple and ideally suited to this approach. In addition the requirement for two unknowns to represent each free surface point would make the boundary value approach very computationally costly. Conversely the Eulerian representation is well suited to the boundary value solution.

Because of the experience gained in solving other panel method problems it was decided in this work to treat the present problem principally as a boundary value problem. The main obstacle therefore was in solving the set of non-linear equations representing the boundary conditions. Also, unlike their linear equivalents, it is easy to pose a potential flow problems with non-linear boundary conditions that has no solution (a severe case would be the re-entering jet of a breaking wave), therefore care had to be taken to select solvable problems to test the program.

The method of solution in this work was to provide an initial guess to the current time step by extrapolation from previous time steps, then to use a non-linear equation solver to refine the result until the boundary conditions were satisfied. The non-linear equation solver used was adapted from *Numerical Recipes in Fortran* [79]. The basic method was Newton's method (described briefly in section 2.2.2), with backtracking to ensure better global convergence (Section 9.7 of [79]). Backtracking was not normally required if the solution was progressing well, but provided an additional safeguard, particularly during testing and debugging, so that a solution was still obtained when minor problems were encountered.

The modifications to the non-linear equation solver included the following:

- modifying Crout's method of LU decomposition ([79] section 2.3), used to invert the Jacobian matrix, to take into account the large number of zero elements both in the matrix and its inverse. This was at the sacrifice of not pivoting, but the Jacobian matrix did not appear to be poorly conditioned (in fact, as will be seen later, many of the terms only appeared on the diagonal or one element either side), and in any case, because of the nature of the iteration procedure used, an accurate evaluation of the inverse of the Jacobian matrix was not a prerequisite for convergence to the solution.

- calculating the Jacobian matrix and its inverse only once at each time step, and assuming that if the time step is small these will not change significantly during the iteration process.

- careful ordering of equations to optimise the advantage gained from the presence of zeros

in the Jacobian matrix. The Jacobian matrix can conveniently be thought of as consisting of several sub-matrices, representing the influence of particular unknowns on particular equations, similar to the division of equations in section 2.6.2. The simplest procedure would be to order the equations so that these sub-matrices remain intact. However with this approach diagonals of sub-matrices are not necessarily diagonals of the whole Jacobian matrix, and this limits the advantage that can be gained from exploiting the presence of zero elements. By alternating kinematic and dynamic free surface equations at each successive free surface boundary point, and similarly placing source strengths and the corresponding free surface elevations adjacent to each other in the vector of unknowns, one can end up with every second column having non-zero elements only on or adjacent to the main diagonal. The resulting efficiencies possible in the matrix inversion operation represent a substantial proportion of the total solution time.

No doubt other efficiencies are possible, and because the solution of this type of problem is very time intensive they are almost always worth investigating.

The basic requirements for this method (apart from the equation solver already discussed) are to write two subroutine. One must evaluate the residuals in each boundary condition equation, equivalent to $\{f\}_k$ in equation (2.4), in which for simplicity the unknown source strengths Q_j and unknown free surface elevations η_j are collectively denoted as the vector of unknowns $\{x\}$. The other must evaluate the elements of the Jacobian matrix, defined in equation (2.3). These will be discussed in detail below.

A particular feature of the method used was to raise the free surface panels a specified distance above the actual free surface boundary, in effect desingularising the free surface. This idea is suggested by Raven [82], and used extensively by Beck and colleagues [14], [4], [5], [6]. The advantages of this will become apparent in the discussion of the Jacobian matrix below, and are particularly substantial in the present method in which the source strengths and free surface location are solved simultaneously. In this implementation the free surface *source panels* do not move during the iteration process, although the free surface itself must be adjusted. The source panels are set at a constant multiple of the free surface panel length above the initial extrapolated guess of the free surface location at each time step, and do not move thereafter until the next time step. Furthermore, to simplify calculations the panels always remain horizontal, since by removing them from the boundary there is no requirement for them to follow the boundary exactly. As described in section 2.1.2, Beck and colleagues go one step further and use point sources rather than distributing sources over panels. Finally is the question of optimising the displacement of the panels. If the displacement is too great the influence of each source becomes spread more evenly over a larger number of collocation points, and the problem becomes less well conditioned. If the source panel is too close its influence on the corresponding collocation panel may be too sensitive to movements in the latter during iteration. There is also a real danger that the collocation panel may move above its corresponding source panel, both

reversing the direction of influence and violating the requirement that the fluid domain contains no singularities[16]. Raven [82] found experimentally that between 0.5 and 2.0 panels lengths gave best results, while for the present method between 0.1 and 1.0 panel lengths was found to be optimum. The probable explanation lies in the nature of the problem being solved. The present method was applied to a time domain solution, and with time steps kept reasonably small for the sake of accuracy there is little movement of the free surface from one time step to the next, and hence minimal clearance is required. Raven on the other hand was solving a steady flow problem, and while a large clearance might superficially mean more iterations because of the poorer conditioning, it also allows larger adjustments during each iteration step. Provided there is sufficient stability there may be no net loss of performance.

The problems of reflection of waves at the free surface boundary edges are still present, but do not appear to be significantly worse than in the linear equivalent, and as in section 2.6.5 these will be ignored.

Boundary condition equations

The boundary conditions must be written in the form of equation (2.2), that is as the set of equations $f_i(x_1, x_2, \ldots x_n) = 0$. This set of equations is comprised of three subsets of equations, representing the three distinct classes of boundary condition involved in the problem. The equations within each subset all have identical form. These will be written as $F_b = 0$, representing the body boundary condition, $F_k = 0$, representing the free surface kinematic boundary condition, and $F_d = 0$, representing the free surface dynamic boundary condition. The unknowns are the source strengths, Q_j, and the free surface elevations, η_j.

The body boundary condition is identical to that for all other methods above, and written in the required form looks like

$$F_b = \frac{\partial \phi}{\partial n} - \vec{V} \cdot \hat{n} = 0, \tag{2.73}$$

where $\vec{V}$ is the body velocity, and $\hat{n}$ the local unit normal out of the body.

Recall that the kinematic boundary condition is (equation (2.8))

$$F_k = \frac{\partial \eta}{\partial t} + \frac{\partial \eta}{\partial x}\frac{\partial \phi}{\partial x} - \frac{\partial \phi}{\partial y} = 0. \tag{2.74}$$

The dynamic boundary condition on the free surface is given in equation (2.10), but this involves the term $\frac{\partial \phi}{\partial t}$, which is not straightforward to calculate since the free surface moves and time derivatives must be evaluated numerically. It is simplest to evaluate a time derivative of ϕ based on the values of ϕ at a given free surface point at different times, and taking into account the free surface movement with time, the resulting derivative, which we will denote $\frac{d\phi}{dt}$, is

$$\frac{d\phi}{dt} = \frac{\partial \phi(x, \eta(x,t), t)}{\partial t} = \frac{\partial \phi(x, y, t)}{\partial t} + \frac{\partial \phi}{\partial y}\frac{\partial \eta}{\partial t}. \tag{2.75}$$

[16] The result in this case is generally total failure of the computer program.

Modifying equation (2.10) to replace $\frac{\partial\phi}{\partial t}$ with $\frac{d\phi}{dt}$, and using the kinematic boundary condition (2.74) to simplify $\frac{\partial\eta}{\partial t}$, gives a more useful form of the dynamic boundary condition as

$$F_d = g\eta + \frac{d\phi}{dt} + \frac{1}{2}\left(\left(\frac{\partial\phi}{\partial x}\right)^2 - \left(\frac{\partial\phi}{\partial y}\right)^2\right) + \frac{\partial\eta}{\partial x}\frac{\partial\phi}{\partial x}\frac{\partial\phi}{\partial y} = 0. \tag{2.76}$$

All the required derivatives of ϕ (including those that will be required later for the Jacobian matrix) can be evaluated with the set of coefficients CP_{ij}, CX_{ij}, CY_{ij}, CN_{ij}, CXX_{ij}, and CXY_{ij}, defined such that

$$\begin{aligned}
\phi_i &= \sum_{j=1}^{n} CP_{ij}Q_j \\
\frac{\partial\phi_i}{\partial x} &= \sum_{j=1}^{n} CX_{ij}Q_j \\
\frac{\partial\phi_i}{\partial y} &= \sum_{j=1}^{n} CY_{ij}Q_j \\
\frac{\partial\phi_i}{\partial n} &= \sum_{j=1}^{n} CN_{ij}Q_j \\
\frac{\partial^2\phi_i}{\partial x^2} &= -\frac{\partial^2\phi}{\partial y^2} = \sum_{j=1}^{n} CXX_{ij}Q_j \\
\frac{\partial^2\phi_i}{\partial xy} &= \sum_{j=1}^{n} CXY_{ij}Q_j.
\end{aligned} \tag{2.77}$$

(In this notation 'C' stands for 'coefficient', the qualifier 'P' refers to ϕ, 'X', 'Y' and 'N' to its x, y, and normal derivatives, and double qualifiers to its second derivatives. The subscripts $_{ij}$ refer to the influence on the ith collocation point due to a unit strength source distributed over the jth panel.) Note that since Laplace's equation is satisfied there is no need to define CYY_{ij}. In terms of quantities defined earlier we have $CP_{ij} = \phi_{ij}$, given in equation (2.68) or (2.69)[17], and $CX_{ij} - CY_{ij}i = W_{ij}$, $CN_{ij} = -\operatorname{Im}\left(e^{i\alpha}W_{ij}\right)$ and $CXX_{ij} - CXY_{ij}i = \frac{\partial W_{ij}}{\partial z_i}$, where W_{ij} is given in equation (2.47) or (2.48).

The remaining terms that need to be expressed in terms of the unknowns are $\frac{d\phi}{dt}$, $\frac{\partial\eta}{\partial t}$ and $\frac{\partial\eta}{\partial x}$. These must all be evaluated numerically, the first two using backward differences (since future values are unknown) and the last using a central difference (except at the free surface edges where asymmetric differences must be used).

Jacobian matrix

The Jacobian matrix then must contain the typical coefficients $\frac{\partial F_b}{\partial Q}$, $\frac{\partial F_b}{\partial \eta}$, $\frac{\partial F_k}{\partial Q}$, $\frac{\partial F_k}{\partial \eta}$, $\frac{\partial F_d}{\partial Q}$ and $\frac{\partial F_d}{\partial \eta}$. Those containing $\frac{\partial}{\partial Q}$ follow directly from substituting equations (2.77) into equations (2.73),

[17] These are the forms of the equations with the $e^{i\gamma}$ term described in section 3.3.1 omitted, and should normally be adequate for submerged bodies where horizontal free surface panels are used. However for shallow bodies or large amplitude waves where the free surface may be lower at points that the highest point on the submerged body the $e^{i\gamma}$ term must be included to avoid integrating over the branch cut of the logarithm function. Furthermore, unlike in section 3.3.1, the image contribution is added, not subtracted, so the $|c_2 - c_1|$ term described in that section must also be retained.

(2.74) and (2.76), and are

$$\frac{\partial (F_b)_i}{\partial Q_j} = CN_{ij} \tag{2.78}$$

$$\frac{\partial (F_k)_i}{\partial Q_j} = \alpha CP_{ij} + CX_{ij}\left(\frac{\partial \phi_i}{\partial x} + \frac{\partial \eta_i}{\partial x}\frac{\partial \phi_i}{\partial y}\right) + CY_{ij}\left(\frac{\partial \phi_i}{\partial x}\frac{\partial \eta_i}{\partial x} - \frac{\partial \phi_i}{\partial y}\right) \tag{2.79}$$

$$\frac{\partial (F_d)_i}{\partial Q_j} = \frac{\partial \eta_i}{\partial x} CX_{ij} - CY_{ij} \tag{2.80}$$

where α is the coefficient of $\phi_i(t)$ in the finite difference estimate of $\left(\frac{d\phi}{dt}\right)_i$. (For example, using the second order approximation $\frac{d\phi}{dt} = \frac{3\phi(t) - 4\phi(t-\Delta t) + \phi(t-2\Delta t)}{2\Delta t}$ then $\alpha = \frac{3}{2\Delta t}$. Different approximations must be used for the first two time steps, and these can be derived in a similar manner to equations (2.64) and (2.65), although the results may differ depending on the assumptions made.) These terms produce full sub-matrices. Clearly also

$$\frac{\partial (F_b)_i}{\partial \eta_j} = 0. \tag{2.81}$$

The form of the remaining Jacobian elements containing $\frac{\partial}{\partial \eta}$ is not so obvious, since the coefficients CP, CX, etc. depend on η. The process has been vastly simplified however by desingularising the free surface boundary[18]. In doing so, varying η only affects collocation points during the iteration process at each time step, and not source points. The result is the y derivative of the quantity, and is only required on diagonal elements of the Jacobian sub-matrices represented by $\frac{\partial F_k}{\partial \eta}$ and $\frac{\partial F_d}{\partial \eta}$. Thus its effect on ϕ is

$$\frac{\partial \phi_i}{\partial \eta_j} = \begin{cases} \left(\frac{\partial \phi}{\partial y}\right)_i & \text{if } i = j \\ 0 & \text{if } i \neq j \end{cases}$$

and similarly for $\frac{\partial \phi}{\partial x}$ and $\frac{\partial \phi}{\partial y}$. Recall also that $\frac{d\phi}{dt}$ is evaluated in terms of a finite difference operation on ϕ, thus $\frac{\partial}{\partial \eta_j}\left(\frac{d\phi}{dt}\right)_i = \alpha\left(\frac{\partial \phi_i}{\partial \eta_j}\right)$ with α defined as above.

The only $\frac{\partial}{\partial \eta}$ terms requiring special treatment are those involving $\frac{\partial}{\partial \eta_j}\left(\frac{\partial \eta}{\partial x}\right)_i$. Again, because of the spatial discretisation of the free surface $\left(\frac{\partial \eta}{\partial x}\right)_i$ is represented as a finite difference, and denoting β_{ij} as the coefficient of η_j in the approximation of $\left(\frac{\partial \eta}{\partial x}\right)_i$ (in the manner that α was defined above) we obtain $\frac{\partial}{\partial \eta_j}\left(\frac{\partial \eta}{\partial x}\right)_i = \beta_{ij}$. Using a second order central difference approximation $\left(\frac{\partial \eta}{\partial x}\right)_i$ gives a non-zero β_{ij} only for $j = i \pm 1$, while at the free surface edges the points $j = i, i+1, i+2$ or $j = i, i-1, i-2$ are required since a forward or backward difference must be

[18] With panels distributed on the boundary the solution process would involve first determining the height, slope and length of each free surface panel (a major task in itself to determine in particular the slope, involving probably a spline fit to the points). Next the derivative of each of these three parameters for each panel with respect to each η value must be determined. Finally, these effects must be related to the Jacobian element through the effects of translation, rotation and elongation of the source panel on each of the terms of the equations (the latter effects are discussed in the next chapter, but for $\frac{\partial \phi}{\partial t}$ only). This is in addition to the effect of η on the collocation points, discussed in the main text. As well as increasing programming complexity this introduces substantial costs in computation time, both in the evaluation of the Jacobian elements and in inverting a now full Jacobian matrix.

used. Regardless of the approximation used the terms will be confined to a limited band either side of the diagonal of the sub-matrix.

The remaining Jacobian matrix elements may now be constructed, and are

$$\frac{\partial\left(F_k\right)_i}{\partial\eta_j} = \begin{cases} \alpha - \frac{\partial^2\phi_i}{\partial y^2} + \frac{\partial^2\phi_i}{\partial xy}\frac{\partial\eta_i}{\partial x} + \beta_{ij}\frac{\partial\phi_i}{\partial x} & (i=j) \\ \beta_{ij}\frac{\partial\phi}{\partial x} & (i\neq j) \end{cases} \tag{2.82}$$

$$\frac{\partial\left(F_d\right)_i}{\partial\eta_j} = \begin{cases} g + \alpha\frac{\partial\phi_i}{\partial y} + \frac{\partial\phi_i}{\partial x}\frac{\partial^2\phi_i}{\partial xy} - \frac{\partial\phi_i}{\partial y}\frac{\partial^2\phi_i}{\partial y^2} + \frac{\partial\eta_i}{\partial x}\left(\frac{\partial^2\phi_i}{\partial xy}\frac{\partial\phi_i}{\partial y} + \frac{\partial\phi_i}{\partial x}\frac{\partial^2\phi_i}{\partial y^2}\right) + \beta_{ij}\frac{\partial\phi_i}{\partial y} & (i=j) \\ \beta_{ij}\frac{\partial\phi_i}{\partial y} & (i\neq j) \end{cases} \tag{2.83}$$

Wave height and body pressures

Wave heights at the free surface collocation points are generated automatically as part of the solution process, and require no further discussion.

In calculating pressures on the body special consideration must be given to the $\frac{\partial\phi}{\partial t}$ term, as it was in the free surface dynamic boundary condition. If this term is to be evaluated numerically we need to define a quantity $\frac{d\phi}{dt}$ in the manner of equation (2.75), but this time allowing arbitrary motion $\vec{V}$ of the body. This gives

$$\begin{aligned} \frac{d\phi}{dt} &= \frac{\partial\phi}{\partial t} + \frac{\partial\phi}{\partial x}\frac{dx}{dt} + \frac{\partial\phi}{\partial y}\frac{dy}{dt} \\ &= \frac{\partial\phi}{\partial t} + \nabla\phi\cdot\vec{V} \end{aligned}$$

and Bernoulli's equation (2.9) becomes

$$\frac{p}{\rho} + \left(\frac{d\phi}{dt} - \nabla\phi\cdot\vec{V}\right) + \frac{1}{2}\nabla\phi\cdot\nabla\phi + gy = 0,$$

from which (ignoring the hydrostatic term)

$$p = -\rho\left\{\frac{d\phi}{dt} + \nabla\phi\cdot\left(\frac{\nabla\phi}{2} - \vec{V}\right)\right\}.$$

2.6.7 Other panel methods

The Green function transient solution will be discussed in detail in the next chapter, and results compared with the other methods described above.

Periodic motion using simple sources was not solved, but could be adapted using features of both the time domain solution and the steady state solution. It has the additional complication of radiation of waves in two directions.

Another possibility is the time domain solution in a moving reference frame using simple sources. This requires inclusion of reference frame velocity terms in the free surface boundary condition as described in section 2.4.1. It has a clear advantage in large simulation times of translation problems where less free surface is required than fixed reference frame representations, and no convolution integrals are required as they would be in Green function methods.

Chapter 3

Two dimensional time domain panel method: development and testing

3.1 Introduction

The strip theory to be described in the next chapter requires a two dimensional time domain panel method suitable for evaluating hydrodynamic forces on arbitrary hull sections. The previous chapter has already presented several options that fulfil this requirement, leaving two critical questions to be answered before coming to a decision regarding the final choice of method: should the method be a linear or a non-linear one, and if linear, a simple source or a Green function method.

Regarding the first, the question of linearity of the free surface boundary condition, a more complete discussion will be presented in the next chapter, but a crucial point is that in any strip theory formulation the radiated and diffracted waves exist in a plane perpendicular to the longitudinal axis of the boat, while the incoming waves may be in any plane (for example in head seas the incoming waves are in a plane parallel to the longitudinal axis of the boat). Introduction of non-linearities in the free surface is pointless without requiring simultaneous consideration of all wave systems. Without resorting to a three dimensional solution (obviously not the point of a strip theory) this is not possible. Of course other non-linear effects, such as the changing wetted hull surface, can still be considered. This is related to the weak-scatter hypothesis, used for example by Sclavounos et al. [87], in which it is assumed that radiated and diffracted waves are small compared with the incoming waves and vessel motions.

The second question requires a matching of the strengths of the two proposed methods with the requirements of the strip theory. The main points are as follows:

- The simple source method poses additional problems for surface piercing bodies because of the requirement of flexibility of the free surface panels where they intersect the body panels in cases where movement of the latter occurs (not addressed in the previous chapter), while for the Green function method the absence of free surface panels removes this problem altogether.

- The Green function method becomes slow for large simulation times, as will be described in section 3.5. This is the greatest weakness of the method, but is not a problem in this case since simulation is only performed for the length of time required for the hull to completely pass through the strip of water, i.e. $t_{\max} = \frac{L}{U}$ where L is the boat length and U is its speed.

- Reflection of waves at the free surface edges is a problem that was not satisfactorily resolved, although this is not a problem again for short simulation times.

- The Green function method is superior to the simple source method in its representation of the free surface in the sense that no discretisation is required and no truncation error exists.

Considering the above points the Green function panel method was chosen as the preferred complement to the proposed strip theory, and it will be described in detail below.

3.2 Elementary source function

The first step in obtaining a panel method solution is to define an elementary source function that satisfies Laplace's equation and the relevant boundary or radiation conditions. In the case where the free surface is not panelled the latter includes the free surface boundary condition, which must also be linear. (A non-linear free surface boundary condition can in general only be satisfied if free surface panels are included, and in this case the elementary source function will be required to satisfy only Laplace's equation.) The linearity of Laplace's equation and of the chosen automatically satisfied boundary condition allows us to integrate and sum the source function, a necessary feature for a panel method.

In the present study we seek a source function suitable for a time domain strip theory solution with linearised free surface. Such a function is given by Wehausen and Laitone [98], equation (13.54), as the complex potential in two dimensions due to a *source of variable strength, starting from rest and following an arbitrary path*, which is

$$\begin{aligned} f(z,t) &= \frac{Q(t)}{2\pi}\ln\left(z-c(t)\right) - \frac{Q(t)}{2\pi}\ln\left(z-\bar{c}(t)\right) \\ &\quad -\frac{g}{\pi}\int_0^t Q(\tau)\int_0^\infty \frac{1}{\sqrt{gk}} e^{-ik(z-\bar{c}(\tau))}\sin\left[\sqrt{gk}\,(t-\tau)\right]dk\,d\tau \end{aligned} \tag{3.1}$$

where the complex number $c(t) = a + ib$, $(b < 0)$ is the source position, $z = x + iy$ is the field position, the real number $Q(t)$ is the source strength and g is the gravitational acceleration.

This expression contains the usual double body source found in free surface problems (first two terms) and a convolution integral, which generates the required waves.

Note that the sign of the second term does not agree with Wehausen and Laitone [98]. Substitution of the expression into the boundary conditions confirms (3.1) to be the correct form[1].

The compete strip theory solution requires evaluation of ϕ, $\frac{\partial \phi}{\partial t}$ and $\frac{\partial(\phi+i\psi)}{\partial z}$ from the panel method solutions for each strip [2], where ϕ is the sum over all panels of the source function f integrated over each panel. i.e.

$$\phi(z,t) = \mathrm{Re}\left\{\sum_{j=1}^{n} \int_{\text{panel } j} f\, ds\right\}.$$

Similarly $\frac{\partial \phi}{\partial t}$ and $\frac{\partial(\phi+i\psi)}{\partial z}$ are the integrated and summed versions of $\frac{\partial f}{\partial t}$ and $\frac{\partial f}{\partial z}$ except that in the latter we must retain both the real and imaginary parts.

Let us introduce the notation

$$\begin{aligned} z_i &= \text{collocation point of panel } i \\ \phi_i(t) &= \phi(z_i,t) = \sum_{j=1}^{n} \phi_{i,j} \\ \phi_{i,j}(t) &= \mathrm{Re}\left\{\int_{\text{panel } j} f(z_i,t)\, ds\right\} \end{aligned}$$

The subscripts i and j can similarly be used for derivatives of ϕ.

Also let

$$f_c = -\frac{g}{\pi}\int_0^\infty \frac{1}{\sqrt{gk}} e^{-ik(z-\bar{c})} \sin\left[\sqrt{gk}\,(t-\tau)\right] dk \tag{3.2}$$

$$= \begin{cases} i\sqrt{\frac{g}{\pi}}\frac{1}{\sqrt{a}} e^{w^2} \operatorname{erf} w \\ \sqrt{\frac{g}{\pi}}\frac{2}{b} w e^{w^2} \operatorname{erf} w \end{cases} \tag{3.3}$$

(the reduction of equation (3.2) to (3.3) is given in Prudnikov, Brychkov and Marichev [80], equation (2.5.36.1)[3]) where $a = i(z-\bar{c})$, $b = \sqrt{g}\,(t-\tau)$, $w = \frac{ib}{2\sqrt{a}}$, and $\operatorname{erf} w$ is the complex

[1] In particular the free surface boundary condition is $\mathrm{Re}\left\{\frac{\partial^2 f}{\partial t^2} + ig\frac{\partial f}{\partial z}\right\} = 0$ on $\mathrm{Im}\, z = 0$. Clearly only the two source terms will contain $\frac{\partial Q}{\partial t}$ and $\frac{\partial^2 Q}{\partial t^2}$ when substituted into this boundary condition, therefore their real parts must cancel. Noting that $\ln(z-\bar{c}) = \overline{\ln(z-c)}$ when $\mathrm{Im}\, z = 0$ the second term must be *subtracted*.

The remaining contribution of the two source terms to the free surface boundary condition, $\frac{gQ}{\pi \,\mathrm{Im}\, c}$, then cancels with the contribution from the convolution integral.

[2] Strictly speaking we do not require both ϕ and $\frac{\partial \phi}{\partial t}$ in a fixed reference frame fomulation, however it is useful to have both for checking purposes.

[3] This can be derived as folows:

The desired integral is $\frac{-\sqrt{g}}{\pi} I$, where

$$I = \int_0^\infty \frac{e^{-ax}\sin\left(b\sqrt{x}\right)}{\sqrt{x}} dx.$$

We can substitute $\sin\left(b\sqrt{x}\right) = \frac{e^{ib\sqrt{x}} - e^{-ib\sqrt{x}}}{2i}$, hence split I into two integrals, which, by completing the square in the exponent of e, can be written in the form $\frac{e^{\frac{-b^2}{4a}}}{2i}\int_0^\infty \frac{e^{-a\left(\sqrt{x}\mp\frac{ib}{2a}\right)^2}}{\sqrt{x}} dx$. With the changes of variable $t =$

error function defined as

$$\operatorname{erf} w = \frac{2}{\sqrt{\pi}} \int_0^w e^{-t^2} dt$$

(Abramowitz and Stegun [1], equation (7.1.1); the related complementary error function erfc $z = \frac{2}{\sqrt{\pi}} \int_z^\infty e^{-t^2} dt = 1 - \operatorname{erf} z$ ([1], equation (7.1.2)) will also be used later). The convolution integral may therefore more simply be represented as

$$\int_0^t f_c \, Q(\tau) \, d\tau.$$

3.3 Integration and differentiation of the elementary source function

3.3.1 Complex potential

As seen above the source function and its derivatives must be integrated along each panel. This process is described by Giesing and Smith [33] and requires the change of variable $ds = dc\, e^{-i\beta} = d\bar{c}\, e^{i\beta}$ where β is the slope of the source panel. This can easily be shown since $ds = |dc|$ where $\frac{dc}{|dc|} = e^{i\beta}$, and similarly for the reflection $d\bar{c}$.

It is convenient to look separately at the terms which make up the source function, and to denote these with the superscripts $^{(1)}$, $^{(2)}$ and $^{(3)}$ representing respectively the source, image and convolution terms.

If we denote the end points of the source panel (panel j) c_1 and c_2 we have after integrating the first term

$$\phi_{i,j}^{(1)} = \operatorname{Re}\left\{ e^{-i\beta} \int_{c_1}^{c_2} f^{(1)} dc \right\} = \operatorname{Re}\left\{ \frac{Q}{2\pi} e^{-i\beta} \left[(z-c)\left(1 - \ln(z-c)\right) \right]_{c_1}^{c_2} \right\}.$$

Unfortunately the logarithm function has a discontinuity at the negative real axis, and if the path of integration (i.e. the straight line joining $(z - c_1)$ to $(z - c_2)$) crosses this an error of $\operatorname{Re}\left\{ \pm \frac{Q}{2\pi} e^{-i\beta} 2\pi i \left(z - \frac{c_1 + c_2}{2} \right) \right\}$ will result. This will only be zero if $z = \frac{c_1+c_2}{2}$ or (since $\operatorname{Im}\left\{ e^{-i\beta}(c_2 - c_1) \right\} = 0$) z is colinear with the source panel, and this will not generally be the case.

The logarithmic branch cut can be avoided by rewriting

$$\int \ln(z-c)\, dc = \int \left[\ln\left(e^{-i\gamma}(z-c) \right) + i\gamma \right] dc$$

$\sqrt{a}\left(\sqrt{x} \mp \frac{ib}{2a}\right)$ and $w = \frac{ib}{2\sqrt{a}}$ we can reduce I to $\frac{-ie^{w^2}}{\sqrt{a}} \left\{ \int_{-w}^{\sqrt{a}\infty - w} e^{-t^2} dt - \int_{w}^{\sqrt{a}\infty + w} e^{-t^2} dt \right\}$. Since e^{-t^2} contains no singularities we note that any closed path integral is zero, i.e. $\int_{-w}^{\sqrt{a}\infty - w} + \int_{\sqrt{a}\infty - w}^{\sqrt{a}\infty + w} + \int_{\sqrt{a}\infty + w}^{w} + \int_{w}^{-w} = 0$. The second of these integrals vanishes for $\operatorname{Re}\{a\} > 0$. The first and third are the desired integrals, which can therefore be replaced with $-\int_w^{-w}$, and the latter can be reduced (by symmetry of the integrand) to $2\int_0^w$. Hence,

$$I = \frac{-2ie^{w^2}}{\sqrt{a}} \int_0^w e^{-t^2} dt = -i\sqrt{\frac{\pi}{a}} e^{w^2} \operatorname{erf} w$$

where γ is chosen so that the path of integration of the logarithm function crosses the positive real axis. The appropriate choice of γ is not unique but if $\gamma = \arg\left(z - \frac{c_1+c_2}{2}\right)$ the discontinuity will always be avoided unless the collocation point is on the source panel ($z = \frac{c_1+c_2}{2}$ and the expression above for γ becomes undefined), in which case it is most convenient to make $e^{i\gamma}$ equal to the unit normal to the panel out of the body (i.e. $\gamma = \arg(c_2 - c_1) + \frac{\pi}{2}$, which is the value that would result in the limit as the collocation point approaches the panel from the fluid in the normal direction). These choices of γ are equivalent to rotating the system clockwise by the angle γ so that the midpoint of the path of integration with respect to $(z - c)$ is on the positive real axis.

Adopting this correction we find after putting $e^{-i\beta}(c_2 - c_1) = |c_2 - c_1|$ that

$$\phi_{i,j}^{(1)} = \frac{Q}{2\pi} \operatorname{Re}\left\{ |c_2 - c_1| (i\gamma - 1) - e^{-i\beta} \left[(z - c) \ln\left(e^{-i\gamma}(z - c)\right) \right]_{c_1}^{c_2} \right\}. \tag{3.4}$$

Obviously the term $|c_2 - c_1| i\gamma$ will always be imaginary and can be ignored, as one would expect since ϕ *must* be independent of the choice of γ. It also turns out that the $-1.|c_2 - c_1|$ term exactly cancels with the equivalent term $1.|\bar{c}_2 - \bar{c}_1|$ from $\phi_{i,j}^{(2)}$ and can also be ignored, leaving only the logarithm term[4].

In evaluating $\phi_{i,j}^{(2)}$ it is not necessary to introduce the $e^{-i\gamma}$ factor since $\operatorname{Im}\{z\} < 0$ and $\operatorname{Im}\{c\} \leq 0$ (z and c are points under the free surface but c, being a panel end point, may be at the free surface) and $(z - \bar{c})$ will therefore always be in the third or fourth quadrant of the complex plane. The path of integration can therefore never cross the negative real axis. In all other respects the integration of the second term is the same as for the first term. The first two terms then are

$$\phi_{i,j}^{(1)} + \phi_{i,j}^{(2)} = \frac{-Q}{2\pi} \operatorname{Re}\left\{ e^{-i\beta} \left[(z - c) \ln\left(e^{-i\gamma}(z - c)\right) \right]_{c_1}^{c_2} - e^{i\beta} \left[(z - \bar{c}) \ln(z - \bar{c}) \right]_{\bar{c}_1}^{\bar{c}_2} \right\}. \tag{3.5}$$

In integrating the convolution term we can integrate equation (3.3) with respect to w provided we choose the second representation in which all terms not involving w are independent of $\bar{c}$. We must also introduce the Jacobian $\frac{dw}{d\bar{c}} = \frac{-2iw^3}{b^2}$ as a denominator because of this change of variable, giving

$$\int_{\bar{c}_1}^{\bar{c}_2} f_c d\bar{c} = ib\sqrt{\frac{g}{\pi}} \int_{w(\bar{c}_1)}^{w(\bar{c}_2)} \frac{1}{w^2} e^{w^2} \operatorname{erf} w \, dw$$

hence

$$\phi_{i,j}^{(3)} = \operatorname{Re}\left\{ \int_o^t Q(\tau)\, e^{i\beta(\tau)} \frac{ig}{\sqrt{\pi}} (t - \tau) \int_{w_1}^{w_2} \frac{1}{w^2} e^{w^2} \operatorname{erf} w \, dw \, d\tau \right\} \tag{3.6}$$

where $w_i = w(\bar{c}_i(\tau))$, $e^{-\beta(\tau)} = \frac{\bar{c}_2(\tau) - \bar{c}_1(\tau)}{|\bar{c}_2(\tau) - \bar{c}_1(\tau)|}$.

Since $Q(t)$ may be an arbitrary function of time and the panel method is solved for discrete time steps the convolution integral must be integrated numerically. There is also no advantage in performing this integration using fast Fourier transforms. The panel integration

[4]This cancellation only occurs where the signs of the body and image logarithm terms are opposite. There are some cases described in the previous chapter where this condition is not met, and the term $-|c_2 - c_1|$ must be retained.

$\left(\int_{w_1}^{w_2} \frac{1}{w^2} e^{w^2} \operatorname{erf} w \, dw\right)$ on the other hand can be evaluated analytically in spite of the fact that it cannot be represented in finite form in terms of either elementary or special mathematical functions. The process will be described in section 3.4.

3.3.2 Time derivative of the complex potential

In taking the time derivative it must be recognised that the potential is a function of z and t only, and that other variables appearing in the expression (i.e. c, β, Q) are in fact all functions of t. Thus

$$\frac{\partial \phi(z,t)}{\partial t} = \frac{\partial \phi(z, c_1, c_2, \beta, Q, t)}{\partial t} + \frac{\partial \phi}{\partial \beta}\frac{d\beta}{dt} + \frac{\partial \phi}{\partial c_1}\frac{dc_1}{dt} + \frac{\partial \phi}{\partial c_2}\frac{dc_2}{dt} + \frac{\partial \phi}{\partial Q}\frac{dQ}{dt}.$$

The first of these derivatives affects the convolution integral only since t does not appear directly in the logarithm terms, while the remaining four derivatives affect the logarithm terms only since Q, c and β appear as functions of τ and not t in the convolution integral.

Using the same technique as earlier to avoid the discontinuity in the logarithm function, the contribution of the body source to the time derivative can be shown to be

$$\begin{aligned}\frac{\partial \phi_{i,j}^{(1)}}{\partial t} &= \operatorname{Re}\left\{\frac{e^{-i\beta}}{2\pi}\left[\left(\frac{dQ}{dt} - iQ\frac{d\beta}{dt}\right)\left((c_2-c_1)(i\gamma-1) - \left[(z-c)\ln\left(e^{-i\gamma}(z-c)\right)\right]_{c_1}^{c_2}\right)\right.\right. \\ &\quad \left.\left. + Q\left[\frac{dc}{dt}\left(\ln\left(e^{-i\gamma}(z-c)\right) + i\gamma\right)\right]_{c_1}^{c_2}\right]\right\}.\end{aligned}$$

One can eliminate some imaginary terms by noting that $(c_2 - c_1) = e^{i\beta}|c_2 - c_1|$, and thus making the substitution

$$\frac{d}{dt}(c_2 - c_1) = e^{i\beta}\frac{d}{dt}|c_2 - c_1| + i(c_2 - c_1)\frac{d\beta}{dt},$$

in which the derivative, taking into account the $Q\frac{e^{-i\beta}}{2\pi}$ factor, is written in terms of real and imaginary parts. Ignoring also the real term $-\frac{1}{2\pi}\frac{dQ}{dt}|c_2 - c_1|$, which as in equation (3.4) cancels with an equivalent term from the image, one obtains

$$\begin{aligned}\frac{\partial\left(\phi_{i,j}^{(1)} + \phi_{i,j}^{(2)}\right)}{\partial t} &= \operatorname{Re}\left\{\frac{e^{-i\beta}}{2\pi}\left[(A_i + (z-c_i)B)\ln\left(e^{-i\gamma}(z-c_i)\right)\right]_{i=1}^{2}\right. \\ &\quad \left. - \frac{e^{i\beta}}{2\pi}\left[\left(\bar{A}_i + (z-\bar{c}_i)\bar{B}\right)\ln(z-\bar{c}_i)\right]_{i=1}^{2}\right\} \qquad (3.7)\end{aligned}$$

where $A_i = Q\frac{dc_i}{dt}$, $B = -\frac{dQ}{dt} + iQ\frac{d\beta}{dt}$ and γ is as defined earlier. Note that $\frac{d\beta}{dt}$ is most easily evaluated as $\operatorname{Im}\left\{\frac{\frac{d}{dt}(c_2-c_1)}{c_2-c_1}\right\}$.

In evaluating the contribution from the convolution term it is easiest to start with the elementary function. Thus

$$\frac{\partial}{\partial t}\int_0^t Q(\tau)\, f_c(t,\tau)\, d\tau = Q(t)\, f_c(t,t) + \int_0^t Q(\tau)\, \frac{\partial}{\partial t} f_c(t,\tau)\, d\tau. \qquad (3.8)$$

Inspection of the form of f_c in equation (3.2) clearly shows (because of the sine term) that the first term on the right of equation (3.8) ($f_c(t,t)$) is zero, and the problem reduces to one of

evaluating

$$e^{i\beta}\int_{\bar{c}_1}^{\bar{c}_2}\frac{\partial}{\partial t}f_c\left(t,\tau\right)\,d\bar{c}.$$

First the time derivative can be performed by expressing f_c in terms of w and a (equation (3.3)) and differentiating with respect to w, where $\frac{\partial}{\partial w}\operatorname{erf} w=\frac{2}{\sqrt{\pi}}e^{-w^2}$. The result multiplied by $\frac{dw}{dt}$ must then be integrated with respect to c by expressing it as a function of w and b using the substitution $\sqrt{a}=\frac{ib}{2w}$, dividing by the Jacobian $\frac{dw}{d\bar{c}}$ (as described in the previous section) and integrating with respect to w. This gives

$$\frac{2ig}{\sqrt{\pi}}\int_{w_1}^{w_2}\left(e^{w^2}\operatorname{erf} w+\frac{1}{w\sqrt{\pi}}\right)dw,$$

and finally

$$\frac{\partial\phi_{i,j}^{(3)}}{\partial t}=\operatorname{Re}\left\{\frac{2ig}{\sqrt{\pi}}\int_0^t e^{i\beta(\tau)}Q\left(\tau\right)\int_{w_1}^{w_2}\left(e^{w^2}\operatorname{erf} w+\frac{1}{w\sqrt{\pi}}\right)dw\,d\tau\right\}. \tag{3.9}$$

Again this error function integral can be evaluated analytically and this process will be described in section 3.4.

3.3.3 Complex velocity

If we retain both the real and imaginary parts of the complex potential $(\phi+i\psi)$ and differentiate with respect to z we obtain by definition the complex velocity

$$W=u-iv=\frac{\partial\left(\phi+i\psi\right)}{\partial z}$$

where u and v are respectively the horizontal and vertical fluid velocities (i.e. $u=\frac{\partial\phi}{\partial x}$, and $v=\frac{\partial\phi}{\partial y}$).

Noting that z and c always appear in our elementary potential function in the context $(z-c)$ or $(z-\bar{c})$ the complex velocity after integrating with respect to c (or $\bar{c}$ as appropriate) is simply the original source function with a change of sign.

After applying the limits of integration and the $e^{\pm i\beta}$ factor we have

$$\begin{aligned}W_{i,j} &= \frac{Q}{2\pi}\left(e^{-i\beta}\ln\left(\frac{z-c_1\left(t\right)}{z-c_2\left(t\right)}\right)-e^{i\beta}\ln\left(\frac{z-\bar{c}_1\left(t\right)}{z-\bar{c}_2\left(t\right)}\right)\right)\\ &\quad -i\sqrt{\frac{g}{\pi}}\int_0^t e^{i\beta(\tau)}Q\left(\tau\right)\left[\frac{e^{w^2}\operatorname{erf} w}{\sqrt{i\left(z-\bar{c}\left(\tau\right)\right)}}\right]_{w_1}^{w_2}d\tau.\end{aligned} \tag{3.10}$$

As has already been done it is possible in this case to avoid the logarithmic discontinuity by expressing the difference of two logarithms as the logarithm of a quotient, both making the $e^{-i\gamma}$ factor superfluous and improving computational efficiency. However when $i=j$ (the collocation point is on the source panel) we note that $z=\frac{c_1+c_2}{2}$ and hence $\ln\left(\frac{z-c_1}{z-c_2}\right)=\ln\left(-1\right)=\pm i\pi$. In order to interpret this consistently we recall that the fluid domain may not contain any singularities. This is equivalent to taking the limit as z approaches $\frac{c_1+c_2}{2}$ from the outward

(fluid) side of the panel. Noting that the outward unit normal vector is $i\frac{c_2-c_1}{|c_2-c_1|}$ we can write $z = \frac{c_1+c_2}{2} + \lim_{\epsilon\to 0^+} \frac{i\epsilon(c_2-c_1)}{2}$, then

$$\begin{aligned}\ln\left(\frac{z-c_1}{z-c_2}\right) &= \lim_{\epsilon\to 0^+} \ln\frac{(c_2-c_1)(1+i\epsilon)}{(c_2-c_1)(-1+i\epsilon)} \\ &= \lim_{\epsilon\to 0^+} \ln(-1-2i\epsilon) \\ &= -i\pi\end{aligned}$$

Generally one wishes to calculate the velocity in order to satisfy the kinematic boundary condition on the body surface. In particular we require only the normal component if velocity on the ith (or collocation) panel. This is given by

$$(u\hat{x} + v\hat{y}) \cdot \hat{n}_i = \mathrm{Im}\left\{e^{-i\alpha}\bar{W}\right\}$$

where $\hat{x}$, $\hat{y}$ and $\hat{n}_i$ are the unit vectors in respectively the x and y directions and the normal direction on the ith panel, and α is the slope of the ith panel (direction of the tangential vector).

3.3.4 Summary of equations

Summarising, the relevant functions are:

$$\begin{aligned}\phi_{i,j} &= \mathrm{Re}\left\{\frac{-Q}{2\pi}\left(e^{-i\beta}\left[(z-c)\ln\left(e^{-i\gamma}(z-c)\right)\right]_{c_1}^{c_2} - e^{i\beta}\left[(z-\overline{c})\ln(z-\overline{c})\right]_{\overline{c}_1}^{\overline{c}_2}\right)\right. \\ &\quad \left. + \frac{ig}{\sqrt{\pi}}\int_0^t e^{i\beta(\tau)}Q(\tau)\,(t-\tau)\int_{w_1}^{w_2}\left(\frac{1}{w^2}e^{w^2}\,\mathrm{erf}\,w\right)dw\,d\tau\right\} \qquad (3.11)\end{aligned}$$

$$\begin{aligned}\frac{\partial\phi_{i,j}}{\partial t} &= \mathrm{Re}\left\{\frac{e^{-i\beta}}{2\pi}\left[(A_k + (z-c_k)B)\ln\left(e^{-i\gamma}(z-c_k)\right)\right]_{k=1}^{2}\right. \\ &\quad -\frac{e^{i\beta}}{2\pi}\left[\left(\bar{A}_k + (z-\overline{c}_k)\bar{B}\right)\ln(z-\overline{c}_k)\right]_{k=1}^{2} \\ &\quad \left. + \frac{2ig}{\sqrt{\pi}}\int_0^t e^{i\beta(\tau)}Q(\tau)\int_{w_1}^{w_2}\left(e^{w^2}\,\mathrm{erf}\,w + \frac{1}{w\sqrt{\pi}}\right)dw\,d\tau\right\} \qquad (3.12)\end{aligned}$$

$$\begin{aligned}W_{i,j} &= \frac{Q}{2\pi}\left(e^{-i\beta}\ln\left(\frac{z-c_1}{z-c_2}\right) - e^{i\beta}\ln\left(\frac{z-\overline{c}_1}{z-\overline{c}_2}\right)\right) \\ &\quad -i\sqrt{\frac{g}{\pi}}\int_0^t e^{i\beta(\tau)}Q(\tau)\left[\frac{e^{w^2}\,\mathrm{erf}\,w}{\sqrt{i(z-\overline{c})}}\right]_{w_1}^{w_2}d\tau \qquad (3.13)\end{aligned}$$

where $w = \frac{i(t-\tau)}{2}\sqrt{\frac{-ig}{z-\overline{c}(\tau)}}$, $w_k = w(c_k(\tau))$, $\gamma = \arg\left(z - \frac{c_1(t)+c_2(t)}{2}\right)$ if $z \neq \frac{c_1(t)+c_2(t)}{2}$ or $\arg\left((c_2-c_1) + \frac{\pi}{2}\right)$ otherwise, $A_k = Q\frac{dc_k(t)}{dt}$, and $B = -\frac{dQ}{dt} + iQ\frac{d\beta}{dt}$.

3.4 Evaluation of convolution integrands

Evaluation of the first two terms (body and image) in each of the above expressions is straightforward, and even the convolution term in the expression for W requires no particular effort since library subroutines for the error functions are readily available (for example NSWC [69]). The

other two convolution integrals do however contain functions for which methods of evaluation had to be devised, namely

$$\int \left(e^{w^2} \operatorname{erf} w + \frac{1}{w\sqrt{\pi}} \right) dw \tag{3.14}$$

and

$$\int \left(\frac{1}{w^2} e^{w^2} \operatorname{erf} w \right) dw. \tag{3.15}$$

These will subsequently be referred to as *Green functions*.

It can be shown, by integrating (3.14) by parts, that the two Green function are related by

$$2 \int \left(e^{w^2} \operatorname{erf} w + \frac{1}{w\sqrt{\pi}} \right) dw = \frac{1}{w} e^{w^2} \operatorname{erf} w + \int \left(\frac{1}{w^2} e^{w^2} \operatorname{erf} w \right) dw,$$

however for the sake of both speed and accuracy it is desirable to derive algorithms for the evaluation of both of these integrals.

Problems encountered include devising algorithms, testing accuracy (particularly since no tables of these functions are available) and assuring maximum precision. Each of these aspects will be dealt with below.

3.4.1 Preliminary accuracy considerations

A decision was made to work to the accuracy limits of single precision arithmetic. The program was developed on an IBM compatible PC and a Silicon Graphics Indigo workstation, both of which represent single precision floating point numbers with a mantissa containing 24 base 2 digits, thus a tolerance of ± 0.5 in the last significant binary digit is achieved if a relative error of ± 1 part in 2^{24} (or $10^{7.2}$) is met or exceeded. Factors governing this choice fell into two main categories.

First was the issue of a suitable compromise between speed and accuracy. On one hand single precision was deemed satisfactory because of the stable nature of the convolution integral and because the numerical integration of the latter negated any benefits of higher precision. On the other hand the Green function evaluations account for most of the computation time of the entire program. The computations are very slow and a choice of single precision accuracy keeps the running time of the program to within reasonable limits.

Second was the issue of being able to guarantee the specified accuracy. To achieve single precision accuracy for the function evaluations externally it was necessary to use double precision arithmetic internally. (This does not significantly affect speed since single and double precision arithmetic operations are performed with comparable speed with the computers and compilers used. Speed is therefore mainly a function of the number of terms evaluated in the series approximations, which in turn is dictated by external accuracy requirements. An exception to this is transcendental functions (e.g. log, sin, exp) which are slower in double precision. These however constitute only a minor part of the Green function evaluations.) Presumably then a double precision result would require internal calculations at greater than double precision.

Thus double precision accuracy may be very difficult to achieve and would certainly require the development of more algorithms. Even if it could be achieved there would also be the problem of testing the results without some means of evaluating the functions more accurately.

Another more subtle choice affecting accuracy was that of the lower limit of integration (or effectively the integration constant). Since these functions had to be added and subtracted it was desirable that their magnitudes be kept as small as possible to avoid roundoff error. This was achieved for most of the function domain by choosing the lower limit of integration to be $i\infty$, so that in the region of interest (i.e. second and third octants of the complex plane) the function values oscillate about zero and also approach zero as $|z| \to \infty$. This choice also gave symmetry about the imaginary axis.

Finally, although at first sight it would seem logical to separate the term $\frac{1}{w\sqrt{\pi}}$ from the integrand of the first Green function (expression (3.14)) on the grounds that it can easily be integrated, this term was retained in the definition of the first integral. This saves separate evaluation but the benefits go far beyond this. For large $|z|$ we find that $\lim_{|z|\to\infty} e^{z^2} \operatorname{erf} z = \frac{-1}{z\sqrt{\pi}}$, $\left(\frac{\pi}{4} < \arg(z) < \frac{3\pi}{4}\right)$ so that to evaluate the integral in two separate parts one would again lose accuracy in the roundoff resulting from adding two similar sized terms of opposite sign. Furthermore as one might expect $\frac{-1}{z\sqrt{\pi}}$ is the leading term in the asymptotic expansion for $e^{z^2} \operatorname{erf} z$ (see section 3.4.2) and the term cancels out altogether. It does not need to be evaluated at all, improving both speed and accuracy.

For small $|z|$ no such cancellation can be made (a Taylor series is used: see section 3.4.2) but if the $\frac{1}{\sqrt{\pi}} \ln z$ part of the integral is evaluated first and in the same subroutine the convergence test for the Taylor series would be based on the final result rather than on only the Taylor series part of it. This improves both speed and accuracy.

3.4.2 Algorithms

A search of the literature of tables of integrals revealed (in Prudnikov, Brychkov and Marichev [80], vol. 2, equation (1.5.3.2)) only a solution to the first Green function (expression (3.14)), namely

$$\int_0^x x^\lambda e^{x^2} \operatorname{erf} x \, dx = \frac{2x^{\lambda+2}}{\sqrt{\pi}\,(\lambda+2)} {}_2F_2\left(1, \frac{\lambda}{2}+1; \frac{3}{2}, \frac{\lambda}{2}+2; x^2\right), \quad \operatorname{Re}\{\lambda\} > -2 \tag{3.16}$$

where ${}_pF_q(a_1 \ldots a_p; b_1 \ldots b_q; x) \equiv \sum_{k=0}^{\infty} \frac{(a_1)_k (a_2)_k \ldots (a_p)_k}{(b_1)_k (b_2)_k \ldots (b_q)_k} \frac{z^k}{k!}$, $(a)_k = a(a+1)\ldots(a+k-1)$, $(a)_0 = 1$ is the generalised hypergeometric series. From this and the definition of the hypergeometric series we obtain

$$\int_0^x e^{x^2} \operatorname{erf} x \, dx = \frac{1}{\sqrt{\pi}} \sum_{n=1}^{\infty} \frac{2^{2n-1} x^{2n}}{n.\,(n+1)\ldots(2n)}. \tag{3.17}$$

Although this series is always convergent it is of limited use for computer evaluation since for $|x| \gg 1$ the individual terms become very large before getting smaller and roundoff error may be much greater than the actual function value.

The problem was solved by investigating methods suitable for numerical evaluation of $e^{z^2}\operatorname{erf} z$, and integrating these term by term. These methods included Taylor series, asymptotic expansions, continued fractions and rational polynomial function. These were obtained from Abramowitz and Stegun [1] and from the *NSWC Library of Mathematics Subroutines* [69] as described in the following sections.

Taylor series about the origin

From Abramowitz and Stegun (equation 7.1.6) [1]

$$e^{z^2}\operatorname{erf} z = \frac{2}{\sqrt{\pi}}\sum_{n=0}^{\infty}\frac{2^n}{1.3.5\ldots(2n+1)}z^{2n+1}. \tag{3.18}$$

Integrating this gives

$$\int_{i\infty}^{z}\left(e^{w^2}\operatorname{erf} w+\frac{1}{w\sqrt{\pi}}\right)dw = \frac{2}{\sqrt{\pi}}\left[\sum_{n=0}^{\infty}\frac{2^n}{1.3\ldots(2n+1)}\frac{z^{2n+2}}{(2n+2)}+\frac{1}{2}\ln z\right]+const \tag{3.19}$$

and

$$\int_{i\infty}^{z}\frac{1}{w^2}e^{w^2}\operatorname{erf} w\,dw = \frac{2}{\sqrt{\pi}}\left(\sum_{n=1}^{\infty}\frac{2^n}{1.3\ldots(2n+1)}\frac{z^{2n}}{2n}+\ln z\right)+const. \tag{3.20}$$

The first of these is nothing but the hypergeometric series described earlier (equation (3.17)).

The constant in each case represents the integral from $i\infty$ to 0, and had to be determined empirically.

Asymptotic expansion

Abramowitz and Stegun (3.6.15) [1] define a series $\sum_{k=0}^{\infty}a_k x^{-k}$ to be an asymptotic expansion of a function $f(x)$ if

$$f(x)-\sum_{k=0}^{n-1}a_k x^{-k} = O\left(x^{-n}\right)\ \text{ as } x\to\infty$$

for every positive integer n. This is written as

$$f(x)\sim\sum_{k=0}^{\infty}a_k x^{-k}$$

where the symbol $\sim$ means *asymptotically equal to*. The series is usually, but not necessarily, divergent, and it is unique. However, as we will see in this case, the series is still useful in spite of its divergence. Asymptotic expansions can also be integrated term by term [62].

The asymptotic expansion for $\operatorname{erf} z$ is given by Abramowitz and Stegun (7.1.23, 7.1.24) [1] in the form

$$\sqrt{\pi}z\,e^{z^2}\operatorname{erfc} z\sim 1+\sum_{m=1}^{\infty}(-1)^m\frac{1.3.5\ldots(2m-1)}{(2z^2)^m}\qquad\left(z\to\infty,|\arg z|<\frac{3\pi}{4}\right) \tag{3.21}$$

with a remainder after n terms of

$$R_n(z)=(-1)^n\frac{1.3.5\ldots(2n-1)}{(2z^2)^n}\theta, \tag{3.22}$$

where

$$\theta = \int_0^\infty e^{-t^2} \left(1 + \frac{t}{z^2}\right)^{-n-\frac{1}{2}} dt \quad \left(|\arg z| < \frac{\pi}{2}\right) \tag{3.23}$$

$$|\theta| < 1 \quad \left(|\arg z| < \frac{\pi}{4}\right). \tag{3.24}$$

This means that in the first octant of the complex plane the remainder is less in magnitude than the first neglected term. In the second octant (which is the one that we are interested in) the remainder is of comparable magnitude to the first neglected term. If $|z|$ is sufficiently large the series will begin to converge for a number of terms before diverging. Thus if we truncate the series at the point at which it just starts to diverge (which will be a function of $|z|$) then the first neglected term (hence also the remainder) is a minimum and we obtain approximately the maximum accuracy. Furthermore if $|z|$ exceeds a given value the error will be within a definable maximum tolerance. These aspects will be discussed in more detail later.

From the above asymptotic expansion we can obtain

$$e^{z^2} \operatorname{erf} z \sim e^{z^2} - \frac{1}{z\sqrt{\pi}} \left\{1 + \sum_{m=1}^{\infty} (-1)^m \frac{1.3 \ldots (2m-1)}{(2z^2)^m}\right\}$$

from which, after integrating

$$\int_{i\infty}^{z} \left(e^{w^2} \operatorname{erf} w + \frac{1}{w\sqrt{\pi}}\right) dw \sim \int_{i\infty}^{z} e^{w^2} dw + \frac{1}{\sqrt{\pi}} \sum_{m=1}^{\infty} (-1)^m \frac{1.3 \ldots (2m-1)}{2m\,(2z^2)^m} \tag{3.25}$$

and

$$\int_{i\infty}^{z} \frac{1}{w^2} e^{w^2} \operatorname{erf} w\, dw \sim \int_{i\infty}^{z} \frac{e^{w^2}}{w^2} dw + \frac{1}{\sqrt{\pi}} \left(\frac{1}{2z^2} + \sum_{m=1}^{\infty} (-1)^m \frac{1.3 \ldots (2m-1)}{(2m+2)\,.2^m z^{2m+2}}\right) \tag{3.26}$$

where

$$\int_{i\infty}^{z} e^{w^2} dw = \frac{-i\sqrt{\pi}}{2} \operatorname{erfc}(-iz) \tag{3.27}$$

and

$$\int_{i\infty}^{z} \frac{e^{w^2}}{w^2} dw = -i\sqrt{\pi} \operatorname{erfc}(-iz) - \frac{e^{z^2}}{z}. \tag{3.28}$$

These last two terms can be evaluated using equation (3.21) (or other forms where appropriate).

We recall that the asymptotic expansion is not a convergent series, but note that the remainder after n terms is some factor θ, given in equation (3.23), of the first neglected term. This gives rise to two issues in determining whether a result obtained from an asymptotic expansion is useful. The first is the question of how big the remainder is so that accuracy may be assessed (of particular relevance, given that the region of interest is the second octant where we can not assume $|\theta| < 1$). The second involves finding when the terms in the series start to increase in magnitude, thus defining the maximum attainable accuracy of the function for a particular argument, and assessing whether the result meets required tolerances.

An analytical solution to the integral for θ was not found[5], and extensive numerical experimentation was required to determine the error. However it was possible to deduce some facts

[5]In fact the remainder after integration becomes $\int_{i\infty}^{z} \frac{1}{\sqrt{\pi}z} (-1)^n \frac{1.3.5 \ldots (2n-1)}{(2z^2)^n} \int_0^\infty e^{-t^2} \left(1 + \frac{t}{z^2}\right)^{-n-\frac{1}{2}} dt\, dz$ for the first function, and similarly for the second.

about the error in the asymptotic expansion as one approached the imaginary axis, and it was assumed (and confirmed by numerical experiments) that the error between the line $\arg z = \frac{\pi}{4}$ and the imaginary axis was well behaved.

It is to be noted first that $e^{z^2} \operatorname{erf} z$ is an odd function, evident from its Taylor series (3.18), and therefore the two Green function integrals (3.14) and (3.15) are both even functions. This means that the imaginary parts of these functions should be zero when evaluated for any value of z on the imaginary axis. The asymptotic expansions for these integrals, (3.25) and (3.26), have an even part (the summation) and an odd part (represented in equations (3.27) and (3.28)). Obviously for z on the imaginary axis, and therefore also a finite (but small) distance from it, the terms (3.27) and (3.28) are not correct and must be ignored. Numerical tests confirm that these terms are the greatest source of error in this region. However in the first octant, and also in part of the second octant near the line $\arg z = \frac{\pi}{4}$, these are the dominant terms and must be retained. Some criterion must be devised for deciding whether to discard or retain these terms. Fortunately this is a relatively simple decision to make. It is related to the other problem of determining when the asymptotic expansion diverges and whether sufficient accuracy exists at that point to use the results, and it is convenient to return to that problem first.

The process of determining accuracy limits is the same for both functions, but will be illustrated here using only the first. Equation (3.25) can be written in the form $\int_{i\infty}^{z} \left(e^{w^2} \operatorname{erf} w + \frac{1}{w\sqrt{\pi}}\right) dw \simeq t_0 + \sum_{m=1}^{n} t_m$ where $t_0 = \frac{\sqrt{\pi}}{2} \operatorname{erfc}(-iz)$ and $t_m = \frac{(-1)^m 1.3 \ldots (2m-1)}{\sqrt{\pi} 2m (2z^2)^m}$. The series has been truncated to n terms, and therefore the "$\sim$" has been replaced with "$\simeq$". It turns out that the leading term is $t_1 = \frac{1}{4\sqrt{\pi} z^2}$ since t_0 is small in the second octant. Therefore given a requirement for maximum relative error, ϵ, (for example if single precision arithmetic is represented by 24 binary digits in the mantissa we may require $\epsilon = 2^{-24} \simeq 10^{-7.2}$) we need to find the smallest n ($n_{\min}$ say) for which

$$\left| \theta \frac{t_n}{t_1} \right| < \epsilon.$$

There are two difficulties. First, θ is unknown, and the best that can be done is to assume a value, say $\theta = 1$, and check the results numerically. Second, if z is not sufficiently large the inequality may have no solution since the series is divergent. We solve the latter by determining the point of divergence, defined by the largest n ($n_{\max}$ say) for which

$$\left| \frac{t_n}{t_{n-1}} \right| > 1.$$

Since t_m is a function of z and m the values $n_{\min}$ and $n_{\max}$ will both be functions of $|z|$, and solving the equation $n_{\min} = n_{\max}$ gives us the minimum radius, $|z|_{\min}$, for which the asymptotic expansion gives a useful (i.e. within the required tolerance) result. Performing this analysis we find that for $\epsilon = 2^{-24}$ we obtain $|z|_{\min} \simeq 4.3$ for both Green functions, that $n_{\min}$ decreases as z increases, and (as implied by the definition of an asymptotic expansion) that $|z|_{\min}$ increases as ϵ decreases.

We return now to the question of t_0 near the imaginary axis. It can be shown that $|t_0|$ is insignificant almost everywhere in the second octant except in a continuous region below a curve asymptotic to the imaginary axis and to the line $\arg z = \frac{\pi}{4}$, shown diagrammatically as $\left|\frac{t_o}{t_1}\right| = \epsilon$ in figure 3-1. Near the imaginary axis (*region A* in figure 3-1) t_0 must be discarded, while in the first octant and part of the second near $\arg z = \frac{\pi}{4}$ (*region B* in figure 3-1) it must be included, and because these two regions are parts of the continuous region where $\left|\frac{t_o}{t_1}\right| > \epsilon$ there is no obvious boundary that distinguishes them. However if we further recognise that only the domain $|z| > |z|_{\min}$ is of interest we see that *region A* and *region B* have been clearly separated. The boundary between the two can be placed anywhere in *region C*, in which t_0 is insignificant and it is immaterial whether or not it is included. The exact location of the boundary that determines whether or not t_0 should be included is not critical, and a very simple criterion (if $\frac{\operatorname{Im} z}{\operatorname{Re} z} > 8$ then t_0 was included) could be used without compromising accuracy.

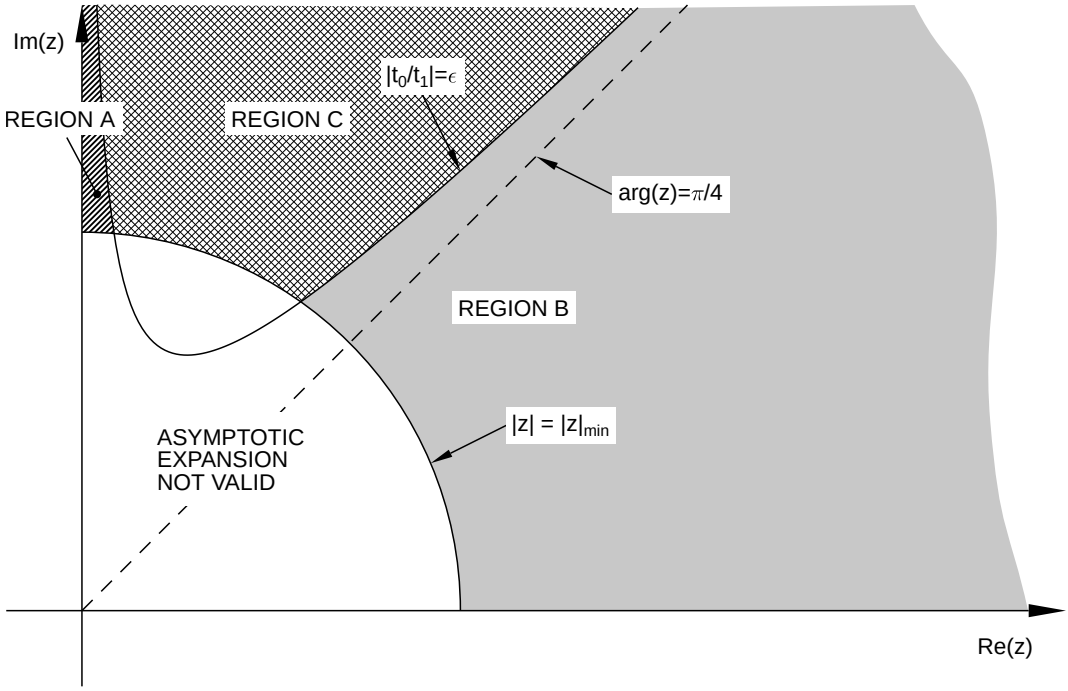

Figure 3-1: Showing the region of the complex plane where t_0 is significant.

Rational function

The error function can also be represented as a continued fraction (Abramowitz and Stegun, equations (7.1.3), (7.1.4) and (7.1.15) [1])

$$e^{-z^2}\operatorname{erfc}(-iz) = w(z) = \frac{i}{\pi}\int_{-\infty}^{\infty}\frac{e^{-t^2}dt}{z-t} \tag{3.29}$$

$$= \frac{i}{\sqrt{\pi}}\left(\frac{1}{z-}\frac{1/2}{z-}\frac{1}{z-}\frac{3/2}{z-}\frac{2}{z-}\cdots\right)$$

$$= \frac{i}{\pi}\lim_{n\to\infty}\sum_{k=1}^{n}\frac{H_k^{(n)}}{z-x_k^{(n)}} \tag{3.30}$$

where $x_k^{(n)}$ and $H_k^{(n)}$ are the zeros and weight factors (defined in [1] (25.4.46)) of the Hermite polynomial of order n, some values of which are given in [1] table 25.10.

The Hermite polynomial is a class of orthogonal polynomials defined as (see Abramowitz and Stegun (22.3.10) [1])

$$H_n(x) = n! \sum_{m=0}^{n/2} (-1)^m \frac{1}{m!\,(n-2m)!} (2x)^{n-2m}. \tag{3.31}$$

The last line of equation (3.30) can be derived by truncating the continued fraction to n terms and simplifying the denominator. One obtains a rational polynomial expression in which the numerator is a polynomial of degree $(n-1)$ and the denominator is the nth Hermite polynomial. Since the Hermite polynomial factorises as $H_n(z) = \prod_{k=1}^{n} \left(z - x_k^{(n)}\right)$ one can express the rational polynomial function as a linear combination of the reciprocals of the factors as above. Only this final form can be integrated. This unfortunately means one must choose a sufficiently large value of n and obtain the coefficients $x_k^{(n)}$ and $H_k^{(n)}$ beforehand.

From the continued fraction form it is evident that to obtain a particular accuracy the number of terms required decreases as $|z|$ increases, (and $= 1$ as $|z| \to \infty$). Thus given a particular choice of n and a required accuracy there will be a minimum value of $|z|$ for which the rational function approximation is valid.

On the other hand, provided that z is not in the vicinity of one of the $x_k^{(n)}$'s where the approximation is singular, there is no upper limit on the value of $|z|$ for which the approximation meets a given accuracy limit. However since the value of n is predetermined one finds that the asymptotic expansion form (which can be truncated once the last term is smaller than the required tolerance) is quicker for large $|z|$. The rational function form is therefore a useful bridge between the Taylor series about the origin and the asymptotic expansion.

One can improve on equation (3.30) by recognising that the Hermite polynomials contain either only odd or only even powers of z. Thus (except for a factor of z in the case of odd Hermite polynomials) the factors come in conjugate pairs, hence we can combine pairs of terms as follows

$$\frac{H_k^{(n)}}{z - x_k^{(n)}} + \frac{H_k^{(n)}}{z + x_k^{(n)}} = \frac{2zH_k^{(n)}}{z^2 - \left(x_k^{(n)}\right)^2}$$

reducing substantially the number of calculations required. Abramowitz and Stegun (Table 25.10) [1] give numerical values of $x_k^{(n)}$ and $H_k^{(n)}$ for selected values of n up to $n = 20$. This does not give a sufficiently useful domain for the function, but the appropriate coefficients ($\left(x_k^{(n)}\right)^2$ and $2H_k^{(n)}$) are given for the case $n = 35$ in the subroutines for calculating erf, erfc etc. included in *NSWC Library of Mathematics Subroutines* [69], providing a good compromise between domain coverage and computational speed, thus

$$e^{z^2} \operatorname{erf} z \simeq e^{z^2} - \frac{z}{\sqrt{\pi}} \sum_{k=1}^{18} \frac{r_k}{z^2 + \lambda_k} = e^{z^2} - \frac{1}{\sqrt{\pi}} \left(\frac{r_1}{z} + \sum_{k=2}^{18} \frac{r_k z}{z^2 + \lambda_k} \right)$$

where the new coefficients are related to the previous by $\lambda_1 = 0$, $\lambda_k = \left(x_k^{(35)}\right)^2$, $r_{1=}\frac{1}{\sqrt{\pi}}H_1^{(35)}$ and $r_k = \frac{2}{\sqrt{\pi}}H_k^{(35)}$ for $k \geq 2$. Note that here we have $+\lambda_k$ not $-\lambda_k$ since $-iz$ has been replaced with z in equation (3.30).

Integrating gives

$$\int_{i\infty}^{z}\left(e^{w^2}\operatorname{erf} w + \frac{1}{w\sqrt{\pi}}\right)dw \simeq \int_{i\infty}^{z} e^{w^2}dw - \frac{1}{\sqrt{\pi}}\left[(r_1-1)\ln z + \sum_{k=2}^{18}\frac{r_k}{2}\ln\left(z^2+\lambda_k\right)\right] \quad (3.32)$$

$$\int_{i\infty}^{z}\frac{1}{w^2}e^{w^2}\operatorname{erf} w\,dw \simeq \int_{i\infty}^{z}\frac{e^{w^2}}{w^2}dw + \frac{1}{\sqrt{\pi}}\left[\frac{r_1}{2z^2} + \sum_{k=2}^{18}\frac{r_k}{2\lambda_k}\ln\left(1+\frac{\lambda_k}{z^2}\right)\right] \quad (3.33)$$

In the second expression $\ln\left(\frac{z^2}{z^2+\lambda}\right)$ has been replaced with $-\ln\left(1+\lambda/z^2\right)$ giving a gain in computational speed.

Note that the $x_k^{(n)}$'s are real so the λ_k's are real and positive. Thus the expression is not valid for values of z near any value of $i\sqrt{\lambda_k}$ on the imaginary axis where it becomes singular.

The integrals $\int e^{z^2}dz$ and $\int \frac{e^{z^2}}{z^2}dz$ are evaluated as for the asymptotic expansion form (equations (3.27) and (3.28)). The same problem of whether or not to include these terms arises. However the rational function approximation should never be used near the imaginary axis because of singularities at $z = \pm i\sqrt{\lambda_k}$. Beyond the largest of these singularities the asymptotic expansion is far quicker computationally because it is able to use fewer terms as $|z|$ increases, and also because the rational function approximation involves logarithms, which are slower to compute that the power terms in the asymptotic expansion. It is therefore never necessary nor desirable to use the rational function approximation near the imaginary axis, and the question of discarding the terms (3.27) and (3.28) can be avoided. It turns out that the Taylor series about the origin remains accurate to a surprisingly large radius near the imaginary axis, and there is only a small gap between this and the asymptotic expansion for which another algorithm is required.

General Taylor series

The Taylor series about the origin is suitable for numerical computations for small values of $|z|$, and the asymptotic expansion for large values. The rational function approximation is suitable for intermediate values (and large, but the asymptotic expansion is quicker) except near the imaginary axis. This leaves a region in the vicinity of $z = 4.0i$ for which no algorithm so far can be applied with confidence. This also coincides with the transition between the regions where the term $\int e^{z^2}dz$ in the asymptotic expansion and rational function representations should and should not be included (in fact the uncertainty that exists here in whether or not to include the latter term arises mainly because the algorithms are near their accuracy limits). The obvious solution is to derive the Taylor series coefficients for an expansion about say $4.0i$. This was found to be necessary only for the first Green function (expression (3.14)).

Let the Taylor series about the point $i\alpha$ on the imaginary axis (i.e., α is real) be of the form

$$\int_{i\infty}^{z}\left(e^{w^2}\operatorname{erf} w+\frac{1}{w\sqrt{\pi}}\right)dw=\sum_{n=0}^{\infty}\lambda_n h^n$$

where $h=(iz+\alpha)$ and λ_0 is obviously the integration constant or $\int_{i\infty}^{i\alpha}\left(e^{w^2}\operatorname{erf} w+\frac{1}{w\sqrt{\pi}}\right)dw$.

In this form it turns out that the coefficients λ_n are real. It is also convenient to treat separately the contribution to λ_n from $\int\frac{1}{w\sqrt{\pi}}dw$ and the contribution from $\int e^{w^2}\operatorname{erf} w\,dw$.

Looking first at the Taylor series for $\ln z$

$$\int_a^z\frac{1}{w\sqrt{\pi}}dw=\frac{1}{\sqrt{\pi}}\ln\left(\frac{z}{a}\right)=-\frac{1}{\sqrt{\pi}}\sum_{n=1}^{\infty}(-1)^n\frac{(z-a)^n}{n.a^n}$$

and putting $a=i\alpha$ one obtains the contribution to λ_n as $\frac{-1}{\alpha^n n\sqrt{\pi}}$ $(n\geq 1)$.

The remaining (error function) term must be expressed as the product of two Taylor series:

$$e^{z^2}=\sum_{m=0}^{\infty}\frac{(z-a)^m}{m!}\frac{d^m}{da^m}\left(e^{a^2}\right)$$

$$\operatorname{erf} z=\operatorname{erf} a+\sum_{n=1}^{\infty}\frac{(z-a)^n}{n!}\frac{d^n}{da^n}(\operatorname{erf} a)$$

(In the case of $\operatorname{erf} z$ the first term must be separated for reasons that will be apparent below.)

From Abramowitz and Stegun [1], equations (7.1.19)

$$\frac{d^n}{da^n}\operatorname{erf} a=(-1)^{n-1}\frac{2}{\sqrt{\pi}}H_{n-1}(a)\;e^{-a^2},\quad n\geq 1$$

and (22.11.7)

$$H_m(x)=\frac{1}{(-1)^m e^{-x^2}}\frac{d^m}{dx^m}e^{-x^2},\quad m\geq 0$$

(recall that $H_n(x)$ is the Hermite polynomial, defined in equation (3.31)), from which, putting $x=ia$

$$\frac{d^m}{da^m}e^{a^2}=i^{-m}e^{a^2}H_m(ia)$$

thus

$$\begin{aligned}\int_a^z e^{w^2}\operatorname{erf} w\,dw &= \int_a^z\left(\sum_{m=0}^{\infty}\frac{(w-a)^m}{m!}i^{-m}e^{a^2}H_m(ia)\right)\\ &\quad\times\left(\operatorname{erf} a+\sum_{n=1}^{\infty}\frac{(w-a)^n}{n!}(-1)^{n-1}\frac{2}{\sqrt{\pi}}H_{n-1}(a)\;e^{-a^2}\right)dw.\end{aligned}$$

Note that only the powers of $(w-a)$ require integration, therefore by collecting the powers of $(w-a)$ we can convert the product of sums into a double sum and replace $\frac{1}{k!(n-k)!}$ with the binomial coefficient $\frac{1}{n!}{}^nC_k$ giving after integration

$$\begin{aligned}\int_a^z e^{w^2}\operatorname{erf} w\,dw &= \operatorname{erf} a\sum_{n=0}^{\infty}\frac{(z-a)^{n+1}}{(n+1)!}i^{-n}e^{a^2}H_n(ia)\\ &\quad+\frac{2}{\sqrt{\pi}}\sum_{n=1}^{\infty}\frac{(z-a)^{n+1}}{(n+1)!}\left\{\sum_{k=1}^{n}{}^nC_k(-1)^{k-1}i^{k-n}H_{k-1}(a)H_{n-k}(ia)\right\}.\end{aligned}$$

Finally changing the summation index to give the nth power of $(z-a)$ and replacing a with $i\alpha$ (where $H_n(-\alpha) = (-1)^n H_n(\alpha)$) we have (including the logarithm term and the constant of integration)

$$\int_{i\infty}^{z} \left(e^{w^2} \operatorname{erf} w + \frac{1}{w\sqrt{\pi}} \right) dw = \int_{i\infty}^{i\alpha} \left(e^{w^2} \operatorname{erf} w + \frac{1}{w\sqrt{\pi}} \right) dw + \sum_{n=1}^{\infty} \lambda_n (iz+\alpha)^n \tag{3.34}$$

where

$$\begin{aligned} \lambda_n &= \frac{1}{n!} \left\{ \frac{2}{\sqrt{\pi}} \sum_{k=1}^{n-1} \left[(-1)^{k\, n-1} C_k \left(\frac{H_{k-1}(i\alpha)}{i^{k-1}} \right) H_{n-k-1}(\alpha) \right] - i e^{-\alpha^2} \operatorname{erf}(i\alpha)\, H_{n-1}(\alpha) \right\} \\ &\quad + \frac{-1}{\alpha^n n\sqrt{\pi}}. \end{aligned} \tag{3.35}$$

Note also that the terms in $\left(\frac{H_n(i\alpha)}{i^n}\right)$ are identical to those in $H_n(\alpha)$ except that all powers of α are positive instead of alternating positive and negative, since the Hermite polynomial contains only even or odd powers. Also erf $i\alpha$ will be purely imaginary, hence λ_n will be purely real.

The coefficients λ_n are difficult to evaluate accurately since they involve small differences between larger numbers. It turns out that as n increases the value of λ_n is dominated by the Hermite polynomial (first and second) terms. These are similar in magnitude but opposite in sign, although their difference is still greater than the third term. Furthermore the first term itself comprises terms whose sum is much smaller than the largest individual component term. Thus for large n many digits of accuracy were lost in the coefficients λ_n. This does not matter when evaluating the series for small $|z - i\alpha|$ which converges with only a few terms, but it does introduce significant errors when evaluating the series for larger $|z - i\alpha|$.

A computer program was written to evaluate the coefficients λ_n, but even working to 15 digits of accuracy left no digits of accuracy in λ_n for $n \geq 23$ and $\alpha = 4$. It was necessary to evaluate the component terms of λ_n using arbitrary precision to achieve finite accuracy for arbitrarily large values of n. To achieve this the program *Mathematica* (Wolfram Research inc.) was used. The necessary *Mathematica* commands were:

```
hi[n_,a_]:=HermiteH[n,I a]/I^n
cf1[n_,a_]:=-(a^n n Sqrt[Pi])^(-1)
hermprod[n_,a_,k_]:=(Binomial[n-1,k] hi[k-1,a] HermiteH[n-k-1,a] (-1)^k)/n!
cf2[n_,a_]:=Sum[(hermprod[n,a,k],{k,1,n-1}]
cf3[n_,a_]:=(I Exp[-a a] Erf[I a] HermiteH[n-1,a])/n!
coeff[n_,a_]:=cf1[n,a]+(cf2[n,a] 2)/Sqrt[Pi]-cf3[n,a]
Table[N[coeff[n,4],40],{n,1,20}]>>>outfile
!!outfile
```

The first six commands create user defined functions, while the seventh command uses the defined function `coeff` to numerically evaluate to 40 digits of accuracy the coefficients λ_n for

$\alpha = 4$ and $n = 1$ to 20, and appends them to the file "outfile". The last command just displays the file "outfile".

In practice single precision accuracy (about 7 significant digits) was obtainable for $|z - i\alpha| \leq 1.46$ when expanding about the point $i\alpha = 4.0i$ (requiring 23 terms) but in the final implementation $|z - i\alpha|$ was restricted to a maximum of 1.3.

3.4.3 Choice of algorithm

In deciding which algorithm to use for a given subdomain accuracy is always a priority. The accuracy decision is a strictly binary decision: either an algorithm is considered sufficiently accurate in a given subdomain or it is not, and the margin by which the required tolerance is exceeded is irrelevant. If two or more algorithms meet the minimum requirements then a decision is based on speed, and only the relative speed of the competing methods matters. If the speed difference is small then the location of the boundary between the regions where different algorithms are used is not critical and can be chosen for simplicity. If the speed difference is great then clearly the faster algorithm is used up to its accuracy limit. Therefore speed boundaries may often be less sharply defined than accuracy ones.

The issues of speed and accuracy are discussed in detail below.

Analytical estimates of accuracy limits

This topic has already received some discussion in section 3.4.2 in connection with the asymptotic expansion. Many of those comments can be applied to the Taylor series, but there are a few differences.

Theoretically arbitrary accuracy is possible with the Taylor series because it is a convergent series. However due to the finite precision of the computer there is an upper limit to accuracy obtainable (using standard arithmetic operations), and further accuracy may be lost in roundoff errors associated with intermediate calculations. To illustrate the latter point, if the internal arithmetic is performed with p binary digits of precision, and the leading binary digit in the largest single term in the Taylor series is 2^m, then at best an error in that term of order 2^{m-p} may be assumed. If the final result (the complete Taylor sum) has leading digit 2^n (obviously $m \geq n$) then the relative error is $2^{(m-p)-n}$. In other words at best $m - n$ binary digits of accuracy have been lost and can not be retrieved. If $m - n$ is large the effect of accumulation of roundoff errors may be insignificant.

If we confine the use of the Taylor series to values for which $m - n = 0$, i.e. demand that the result is accurate to the precision of the individual calculations, the radius of applicability of the series is unnecessarily restricted. In practice it was found that the Taylor series remained competitive in terms of speed if double precision was used internally ($p = 48$ on a PC) while single precision was required in the output (24 binary digits[6]). In fact the speed penalty for

[6]This equates to 7.2 decimal digits, or a relative error of $10^{-7.2}$.

performing internal calculations with double rather than single precision is almost negligible, and the series only becomes slow for large $|z|$ because more terms are required.

The following discussion will concentrate on the function (3.14), and (3.15) can be analysed in a similar fashion.

The first step is to obtain a simple first order approximation to the function. The Taylor series does not provide a suitable estimate, but because we are dealing with reasonably large radii the first term in the asymptotic expansion gives a good estimate. For $|z| \geq 2.74$ this estimate is within 10%. If we call this estimate E we can write

$$\int_{i\infty}^{z} e^{w^2} \operatorname{erf} w + \frac{1}{w\sqrt{\pi}} dw \simeq E = \frac{1}{4\sqrt{\pi} z^2}.$$

Next we need to identify and estimate the magnitude of the largest term. Let this be t_L where L is the largest n for which $\left|\frac{t_n}{t_{n-1}}\right| > 1$. From the Taylor series (3.19) we have $t_L = \frac{\left(4z^2\right)^{L+1} L!}{2\sqrt{\pi}(2L+2)!}$. Also $\left|\frac{t_n}{t_{n-1}}\right| = \frac{n\left|z^2\right|}{(n+1/2)(n+1)}$, from which L is the solution to $L + \frac{3}{2} + \frac{1}{2L} = \left|z^2\right|$ rounded down to the next lowest integer.

Finally the number of lost binary digits of accuracy is $(m-n) = \log_2 \left|\frac{t_L}{E}\right|$, and by solving the above equations and plotting the result against $\left|z^2\right|$ it was found that an excellent empirical fit[7] to the theoretical accuracy limit was given by the relation

$$(m-n) = 1.440\left|z^2\right| + 0.582.$$

With a maximum loss of 24 binary digits being tolerated we obtain $|z|_{\max} = 4.03$ as the accuracy limit for the Taylor series (3.19). This agreed well with numerical accuracy experiments, with the exception that it was somewhat conservative in the first octant where the leading term in the asymptotic expansion becomes (3.27), and not E.

Testing of accuracy

The analytical accuracy limits were used as a guideline, particularly in making decisions about reasonable tolerances to seek, and in identifying where to focus the numerical experimentation effort. All final decisions regarding accuracy limits were based on numerical comparisons between methods.

In section 3.4.2 four different methods of evaluation of the Green functions were derived. It was assumed that each method, being quite distinct from the others, would have an error unrelated to those of the other methods. Therefore in comparing the results of the different algorithms if any two (or more) were consistently in agreement to a specified tolerance in a given region of the computational domain then both (or all of) those methods could be considered accurate to at least that tolerance in that region.

For this to work the regions of accuracy for each algorithm must overlap, which of course is desirable anyway. There will however inevitably be regions where only one method is of sufficient

[7] Accurate to less than 1% for $|z| > 2.5$.

accuracy. Most notably near the origin only the Taylor series is of sufficient accuracy, but its accuracy can not be verified by comparison with other methods. It is obvious though from the form of the Taylor series that if it meets accuracy requirements at large radii it will also meet these requirements at small radii.

In testing accuracy the relevant region of the complex domain was divided into a fine grid of points, so that local minima of the function could be identified. Accuracy was based on relative error, so that near local minima of the functions correspondingly smaller absolute errors were demanded. Also tolerances were applied separately to real and imaginary parts of the function values.

Contour plots of digits of agreement between algorithms were produced to assist in choosing suitable subdomains for the use of each algorithm.

Speed considerations

General comments can be made about the typical speed characteristics of each algorithm. The rational function approximation, which involves a fixed number of operations, always of the same type, has approximately constant speed regardless of where it is evaluated. The main purpose of the rational function approximation was to fill in the middle ground between the asymptotic expansion and the Taylor series where neither of the latter were of sufficient accuracy. To achieve this a large number of terms were required, and hence it is often the slower of the three methods. The computational time for the Taylor series and asymptotic expansion depend mainly on the number of terms requiring evaluation, since the evaluation time for each term is approximately constant. Both series are truncated as soon as convergence to the specified tolerance is achieved, and since the magnitudes of the terms in both series are functions of the radius $|z|$ it is not surprising to find that the computational speed for each series is essentially also a function of $|z|$. The Taylor series becomes slower as $|z|$ increases, while the asymptotic expansion becomes quicker.

This information is helpful in giving guidelines for testing speed. For example the boundary between the Taylor series and the rational function approximation is an example of a boundary based on speed. Because double precision is used for internal calculations the range of accuracy of the Taylor series is quite large, but at the same time it converges very slowly at larger radii, until it is no longer competitive for speed compared with the rational function approximation.

Decisions involving speed were made on the basis of testing on a PC. It was assumed that the relative performance of the various algorithms would be similar on different computers.

The Green function evaluations accounted for most of the running time of the panel method program, so optimising them for speed was considered to be of utmost importance. Various other factors were considered in seeking to reduce the calculation times, some of which will be listed here.

- The ordering of the calculations so that larger terms are calculated first can have a sig-

nificant effect on speed. In particular both the rational function approximation and the asymptotic expansion involve the evaluation of two sums. Using the asymptotic expansion as an example we have the sum indicated in equation (3.25) or (3.26), and another sum implicit in the additional term (3.27) or (3.28). In the first octant the second of these sums is dominant, so if it is calculated first the absolute error used to determine convergence of the first sum will be larger and fewer terms will be needed.

- In general it was found that evaluating the real and imaginary parts of the functions separately using real arithmetic was quicker than using complex arithmetic. In view of the priority given to speed this was done at the expense of conciseness and readability of the program.

- Numerous "tricks" in setting out calculations can be used to improve speed, such as the recursive evaluation of powers of z and series coefficients (particularly as the latter involves factorials), or the use of multiplication by z^{-2} in the asymptotic expansion instead of division by z^2.

3.5 Numerical implementation

As in all panel methods, the problem basically involves writing a set of equations that represent the body boundary conditions in terms of the unknown source strengths. By writing these equations in matrix form, and inverting the resulting matrix, the unknown source strengths can be obtained. Once these are known all other quantities of interest can be explicitly calculated. In this sense it is no different from any of the methods described in the previous chapter.

In this case we seek a solution at a discrete sequence of time steps, $t = 0$, Δt, $2\Delta t$, $3\Delta t \ldots n\Delta t$ for example (although one is not necessarily restricted to equal time increments). The body boundary condition, as for other panel methods, is generally one prescribing the normal velocity component, and this may be written in terms of equation 3.13. We note that this contains the usual body and image Rankine source contributions found in most free surface problems, both of which are functions of the unknown source strength at the current time step, and the wave term, a convolution integral involving the source strength history. At any given time step it can be assumed that the source strengths for all previous time steps are known, and so we can approximate this convolution integral using our known sequence of previous source strength values, using for example a trapezoidal rule. The last time step of the convolution integral poses no problem since the integrand at $t = \tau$ is zero, thus the convolution integral may be evaluated completely without knowing the source strength at the current time step. It can then be subtracted from the prescribed normal velocity at that panel to form a vector element for the right hand side of the set of equations. The body and image terms, being dependent on the unknown source strength at the current time step, form the matrix of influence coefficients.

The resulting equations have the form $[A]\{Q\} = \{R\}$ where

$$A_{ij} = -\operatorname{Im}\left\{\frac{e^{i\alpha}}{2\pi}\left[e^{-i\beta}\ln\left(\frac{z-c_1}{z-c_2}\right) - e^{i\beta}\ln\left(\frac{z-\bar{c}_1}{z-\bar{c}_2}\right)\right]\right\} \tag{3.36}$$

and

$$R_i = \vec{V}\cdot\hat{n} - \operatorname{Im}\left\{e^{i\alpha}\left[i\sqrt{\frac{g}{\pi}}\sum_{j=1}^{n}\sum_{k=0}^{n_t-1} C\Delta t\, e^{i\beta(\tau)} Q_j(\tau)\left[\frac{e^{w^2}\operatorname{erf} w}{\sqrt{i(z-\bar{c})}}\right]_{w_1}^{w_2}\right]\right\}, \tag{3.37}$$

where $\tau = k\Delta t$, $n_t = \left(\frac{t}{\Delta t}\right)$, α =slope of ith panel, and β =slope of jth panel, C is a trapezoidal integration coefficient ($= \frac{1}{2}$ for $k = 0$, or 1 otherwise) and other quantities are as defined previously.

Once the source strengths have been obtained other quantities of interest can be calculated in the usual fashion, noting again that the convolution integral must be evaluated numerically. The integrand of this integral is very slowly decaying, and in all the tests performed on this method it was not possible to ignore contributions from early time steps. As a consequence the total computational time varied approximately with the square of the number of time steps, and the method became very slow for very large simulation times.

3.6 Validation and comparisons

Any validation process must take into account a number of factors, depending on the desired purpose, and these may broadly be regarded as seeking to answer one of two fundamental, but entirely distinct, questions.

There is first the question of whether the underlying mathematics of a particular solution method adequately represent the physics involved. For example potential flow methods completely neglect viscous effects, and one may wish to determine whether this is justified. This question only arises because it is invariably necessary to simplify most problems in some way in order to make their solution feasible, or sometimes in order to obtain a solution at all. The answer to this question determines how far compromise can be taken.

The applicability and limitations of potential flow theory are fairly well understood, and will not be discussed at length here. Such phenomena as boundary layers, flow separation and turbulence play a part. These points will be explained in more detail in the chapters dealing with strip theory, the intended end product of the present time domain panel method. One can also argue over whether one should be predicting boat motions in two or three dimensions. The other main simplification in this category is the linearised free surface boundary condition.

The second question is whether a particular numerical implementation correctly represents the mathematics involved. It is concerned not only with issues such as convergence, accuracy, numerical stability and robustness, but also seeks to establish as far as possible the absence of errors or "bugs" in the computer program. That is, a method may successfully converge to a plausible solution as some parameter (such as panel length) is refined, but this is no guarantee

that it is correctly representing the intended mathematics. To that end it is essential to have a benchmark, preferably in the form of an analytical solution to the problem, but at least another solution developed independently, or one that relies on a fundamentally different approach to represent the same mathematics (for example one may compare a boundary element method and a finite element method). Obviously if the analytical benchmark is chosen we are restricted to validation for special cases, usually involving simple geometry, and the applicability to arbitrary geometry must be inferred.

In the present field of study several possible analytical solutions exist that could be used as benchmarks. The main ones involve a translating submerged circular cylinder (Lamb [57] pp 412-413, Havelock [35]) and sinusoidally oscillating floating semi-circular cylinders (Ursell [92]). However in the validation process one must be careful to recognise that the analytical solution does not always represent exactly the same flow situation as the equivalent numerical solution being validated. For example the shape described by the body streamline in Lamb's solution for a translating cylinder is only exactly circular when the body is at infinite depth, while the equivalent panel method solution will always have boundary streamline points that lie on a circle.

In order to perform validation of a numerical technique it is only necessary that the solution being tested and its corresponding benchmark solution exist, not that they be physically realistic. Thus for example linearised solutions to highly non-linear problems may be used. The remainder of this chapter deals primarily with *numerical* validation of the various panel methods discussed so far, and is not concerned therefore with whether physically realistic flows are being represented. However a small number of non-linear solutions will also be presented, merely for comparison, and as a reminder of the limitations of the techniques we are dealing with.

3.6.1 The validation process

Ideally validation of the time domain panel method presented in this chapter would involve comparisons in which the panelling and time step size were systematically refined while, if comparing with a steady state solution, the total time simulated was extended until convergence to a benchmark, such as an analytical solution, was demonstrated. Clearly this has the potential to escalate into an unmanageably large problem, and it is desirable somehow to investigate refinements of parameters one at a time.

This could be achieved by successively verifying intermediate solutions and then using them as the benchmark solution at the next level of complexity.

Figure 3-2 shows how the various panel methods described so far are related. (Note that "steady state" on the second row can refer to either translation or periodic oscillation as appropriate.) Clearly the steady Green function method can be validated by increasing the number of body panels (n). Having verified this solution one can choose an arbitrary finite value of n and demonstrate for example that the simple source solution converges to the Green function

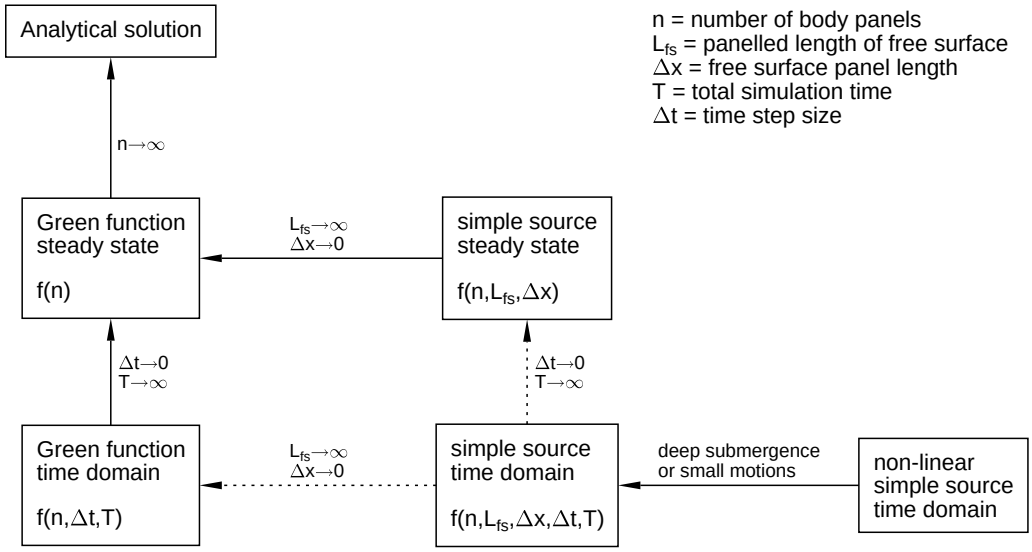

Figure 3-2: Showing the relationship between various panel methods investigated and the corresponding analytical solution

equivalent as the panelled length of the free surface (L_{fs}) is increased and the free surface panel length (Δx) is reduced in the former. Provided the two solutions have exactly the same body panelling (number and arrangement) this convergence should be demonstrable regardless of how small n is, and thus the simple source solution can be validated without needing to consider the limit as $n \to \infty$. Alternatively one could validate the transient Green function solution against the steady one by increasing T and reducing Δt. Similarly one may validate the simple source time domain solution either against the simple source steady state solution using only moderate values of n, L_{fs} and Δx, or against the Green function time domain solution using small values of n and Δt. Unfortunately with the latter a small value of Δt must still be used since the two methods handle the time stepping in entirely different ways: the simple source method by any standard integration technique suitable for initial value differential equations, and the Green function method by evaluation of a convolution integral that forms part of the body boundary condition at each time step. It will be shown later that the dependence on Δx differs also between the two methods.

Comparisons will be given below for three main categories of test case: translatory motion, oscillatory motion, and surface piercing bodies in transient motion. The results presented will not constitute the complete validation, but will serve to illustrate typical examples of tests performed. In addition a selection of results will be presented for problems solved with non-linear free surface boundary conditions.

3.6.2 Translatory motion

Steady state: Green function method

An analytical solution to the case of wave motion due to a steadily translating submerged circular cylinder was first presented by Lamb [57] (pp.410-412). Lamb (pp412-413) also extends this solution to elliptical cylinders. This solution assumes a perturbation of the flow past a cylinder in an infinite fluid, hence is applicable for a deeply submerged cylinder (that is the cylinder radius is small compared with its depth) and linearised free surface boundary condition. As such the validation of a panel method solution using this as a benchmark would require the establishment of convergence as both the depth and the number of panels are increased.

Lamb's solution is extended to a much more general form in a series of papers by Havelock. A paper of 1917 [42] approaches the problem in a different manner, and shows that the new technique can be used to solve the case of a sphere. In 1926 [39] Havelock showed that the technique presented in the 1917 paper formed the theoretical basis for extending the order of approximation of the body boundary condition to arbitrary degree, and proceeded to solve the second order problem for a circular cylinder. In 1928 [43] he considered pressures on the cylinder body boundary, and calculated vertical and horizontal forces. The latter of these forces is the wave resistance, which had previously been inferred from wave heights far behind the body through energy considerations. This calculation again assumed only a first order body boundary condition, but was extended to arbitrary order in 1936 [38], in which numerical results for lift and drag were presented for the case of fifth order. Finally in 1948 [44] and 1949 [41] wave resistance is considered respectively for cylinders started from rest and in accelerated motion, but reverting to the first order body boundary condition.

The solution chosen for validation of the steady Green function panel method was that of [38] since it has the potential to represent the body boundary condition exactly, and should therefore be identical to the Green function panel method as the number of panels $n \to \infty$ regardless of the depth of submergence of the translating body. In particular the drag and lift forces are given respectively by equations (29) and (30) in [38], with the required coefficients given in equation (22) of that work.

Figure 3-3 shows a comparison between the Havelock solution and panel method for two different body submergences, where f is the depth of submergence of the cylinder centre, a is the cylinder radius, U is the speed of translation, "order" refers to the order of approximation of the body boundary condition according to Havelock's solution, and n is the number of panels used to represent the body.

Looking first at the analytical solution, we note that the first order solution is identical in form for the two cases considered. In fact it is the exact deep submergence solution, and if the unit force is taken as $\pi\rho g a^2 \left(\frac{a}{f}\right)^2$ then the first order solution is independent of f or a. As expected therefore figure 3-3 shows much more rapid convergence for the larger ratio of $\frac{f}{a}$,

and the 3rd and 4th order approximations, being indistinguishable from the 5th order, are not shown.

The panel method solution on the other hand shows a convergence as n is increased that appears to be only very weakly influenced by depth. Again this is to be expected since in this case the approximation made to the body boundary condition due to a finite number of panels is present regardless of the depth of submergence.

In both the numerical and analytical results it is reasonable to assume that the error in the best approximation is of comparable magnitude to the difference between this and the next best approximation. The lower two graphs of figure 3-3 show the discrepancy between the analytical and numerical solutions to be consistent with this expectation.

One may wish also to look at wave profiles, and in particular the *amplitudes* of the trailing waves. Unfortunately Havelock does not present a complete solution for the wave profile with the exact (or higher order) body boundary condition. His 1926 paper [39] presents a second order solution, but this is not of sufficient accuracy for validation purposes in general. It is possible on the other hand to compare wave resistance, based on asymptotic wave height downstream, with the drag force, based on a body pressure integration as above. This however gives little information about wave elevations in the near field of the cylinder.

The *wavelength* of the trailing regular wave system may also be investigated, but it is obvious from a comparison of the forms of the Green function integrals in the numerical and analytical solutions that the two methods must always produce identical results. All validation tests performed confirmed this to be the case.

Figure 3-4 shows the convergence of the wave profile as the number of panels is increased for a case of steady translation at a Froude number based on radius of 0.8, solved using a Green function panel method. In addition the asymptotic value of wave height behind the cylinder, inferred from drag force calculations, is indicated in the figure. At a distance of approximately 11 radii behind the cylinder, as shown in figure 3-4, it can be estimated from the first order analytical solution [57] that the effect of the local component of the free surface disturbance in the vicinity of the cylinder is reduced to about 1% of the amplitude of the regular waves observed far behind the cylinder, and this is sufficient to account for the very small difference observable between the wave height here and the asymptotic values based on drag. The first order analytical solution of Lamb [57] is also included merely as a guide to the expected general form of the free surface in the near field of the cylinder.

The difference between the solutions with 96 panels and 384 panels is about 1.4%, which is barely detectable by eye at the scale of figure 3-4. The solution with 384 panels may be considered effectively converged.

One point to note is that for the solution with 6 panels the computed free surface penetrates the cylinder body. This is merely a consequence of the linearisation of the free surface, in particular that the wave height is calculated from the pressure on the line $y = 0$. It is an

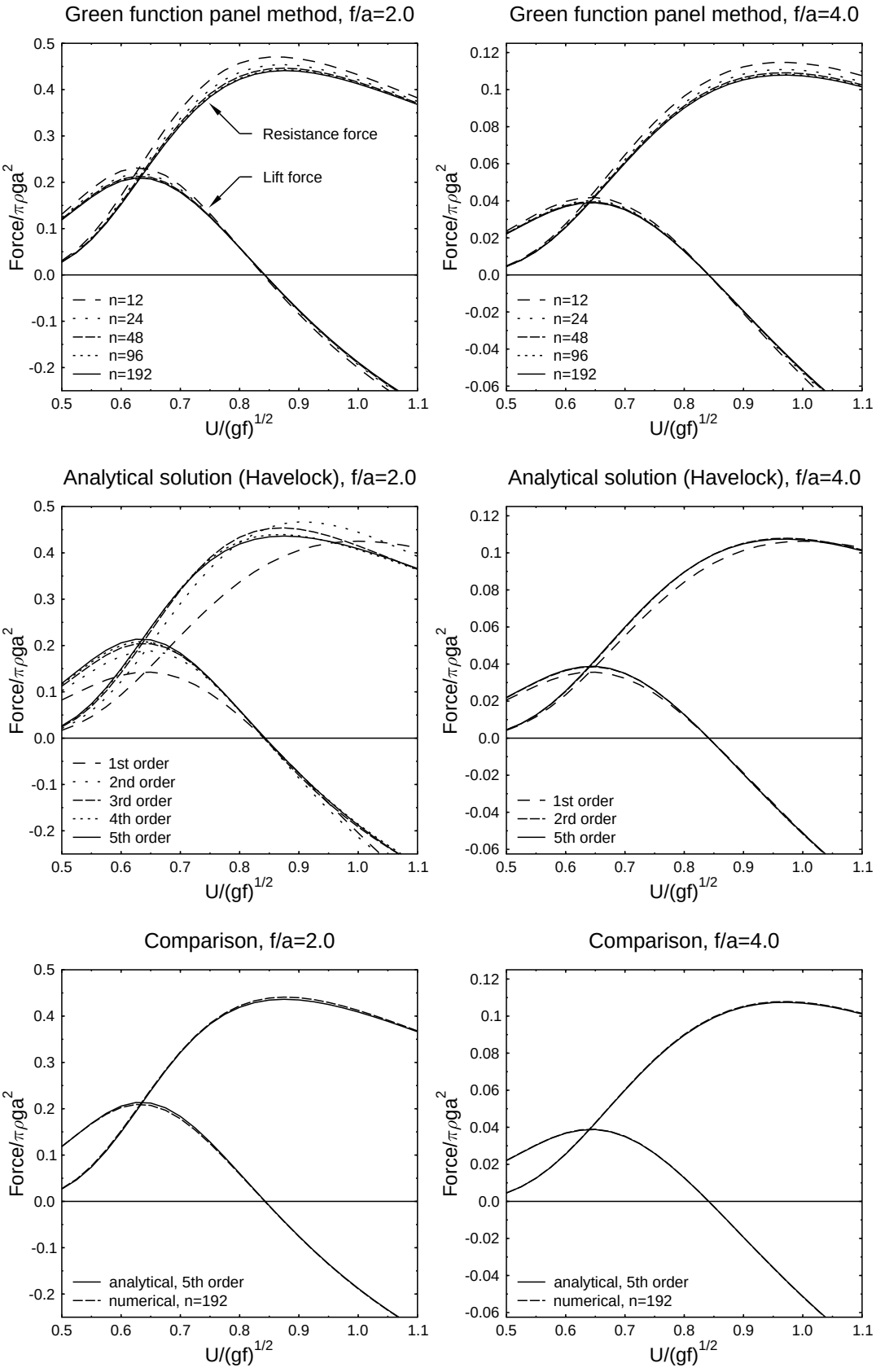

Figure 3-3: Comparisons of steady panel method and analytical equivalent (Havelock [38]).

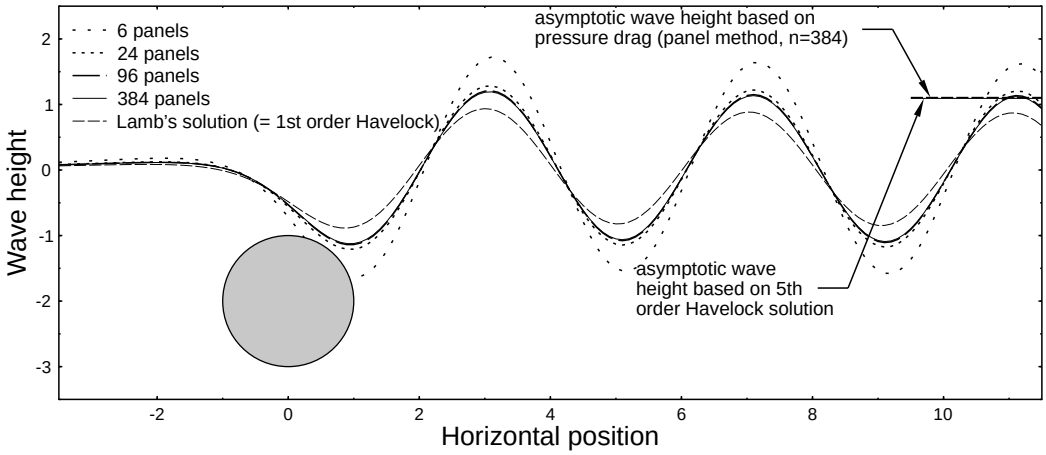

Figure 3-4: Wave profile for circular cylinder translating from right to left: Green function panel method and Lamb [57].

indication that linearisation of the flow past a cylinder at that depth and speed is not physically valid, even though the numerical solution may be mathematically valid.

All non-circulating flow cases presented by Giesing and Smith[8] [33], including a cylinder above a channel floor of finite depth and tandem cylinders, were reproduced. As far as was possible to tell from the figures in [33] the present implementation of the method gave identical wave profiles, with only one exception (the same case as illustrates in figure 3-4) in which it is believed the Giesing and Smith's version was inadvertently published upside-down.

Obviously investigating wave profiles is a far less concise method of validating a method over a wide range of depths and Froude numbers than looking at net body forces, but it does give a means of looking at a small number of cases in greater detail. Furthermore the absence of an exactly equivalent analytical solution for the near field wave profiles for shallow cylinders limits the use of such comparisons.

Steady state: simple source method

In this section some convergence properties of the simple source method will briefly be illustrated. Then the results of validation of a single case against the equivalent Green function solution will be presented.

Recall that the requirement is to show convergence to the Green function method as the extent of the panelled free surface is increased and the free surface panel length is decreased, subject to the restriction of identical body panelling. Assuming the Green function method has been validated this is sufficient to validate the simple source method.

Figure 3-5 shows the effect of the extent of the panelled free surface on the wave profile. The theoretical wavelength for this case is $\lambda = 4.02$ radii ($= 2\pi Fr^2 a$, where a is the cylinder radius

[8]The authors of the method on which the present Green function panel method is based.

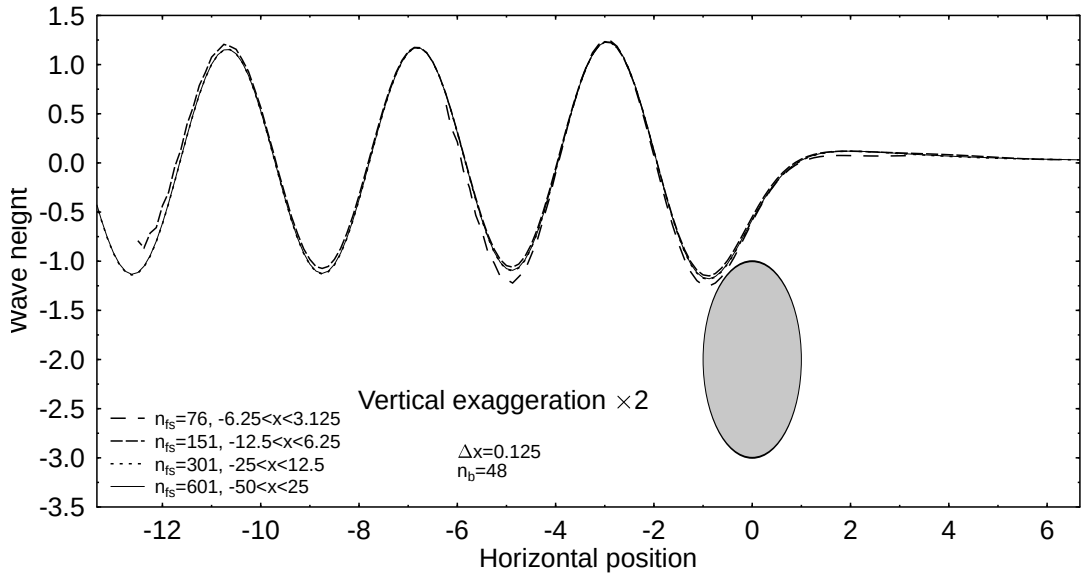

Figure 3-5: Showing the effect of extent of panelled free surface on simple source panel method solution: $Fr = 0.8$

and the Froude number is based on a). We see that the shortest free surface used, extending only 1.3λ behind and 0.53λ ahead of the cylinder, gives already quite acceptable results. The principal effect of truncating the free surface is to alter the amplitude of the waves behind the cylinder. There is some irregularity in the free surface near the downstream truncation in all solutions, observed also by Dawson [19] (on which the present method is based), but this is generally confined to within about half a wavelength and does not appear to affect the solution in the near field of the cylinder.

Free surface panel length, on the other hand, seems to have a far more dramatic effect on the wave profile. In figure 3-6 we see that the general effect of representing the free surface numerically is to cause damping of the waves behind the cylinder and to reduce the wavelength. There appears to be negligible effect on the wave amplitude in the near field of the cylinder, indicating that the effect is cumulative and is convected downstream by the asymmetry of the finite difference operator used for the free surface derivatives (the same asymmetry that is responsible for ensuring waves appear only behind the cylinder). The effect is quite severe for $\Delta x = 0.5 \simeq \frac{\lambda}{8}$, while even for $\Delta x = 0.3125 \simeq \frac{\lambda}{128}$ the wavelength is too short by 1.0%, although it does appear quite clearly to be converging to the correct value as Δx is reduced. Dawson [19] states "The wave length will be too short by about 5%," which is not as good as present results indicate, although (given that his results were published in 1977) his panel refinement would may been limited by the computer resources available to him at the time. It is perhaps possible to relax the requirement for small free surface panels by developing a higher order finite difference operator to represent the derivatives in the free surface boundary condition, although

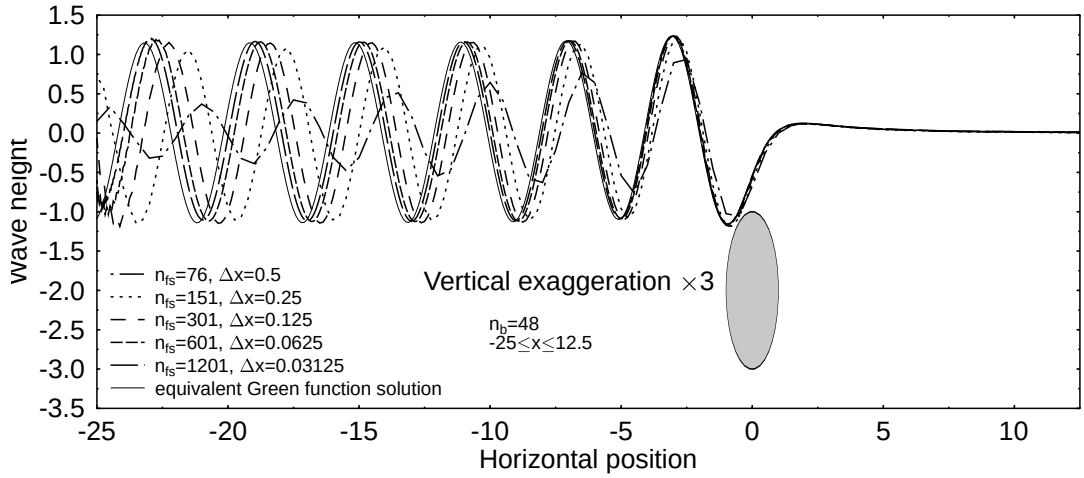

Figure 3-6: Showing the effect of free surface panel length on simple source panel method solution

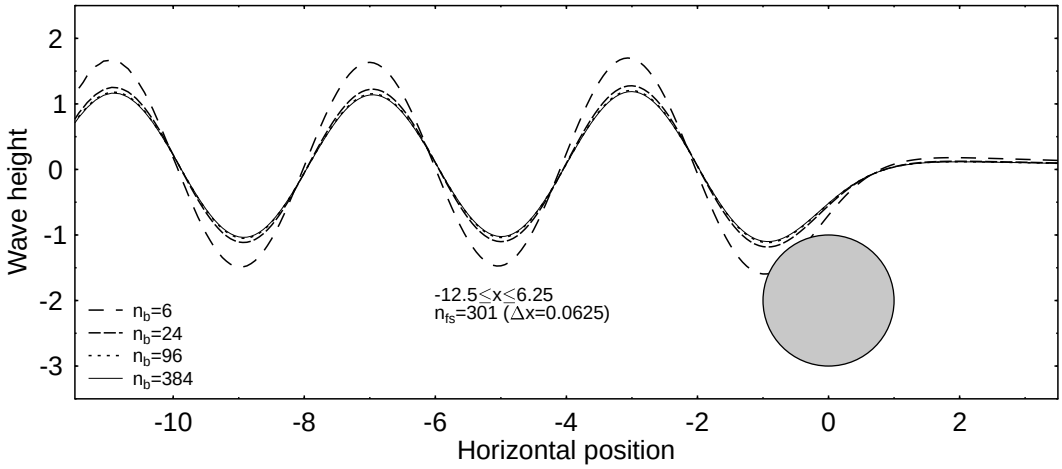

Figure 3-7: Showing the effect of body panel density on simple source panel method solution

this was not attempted.

Finally, as shown in figure 3-7, varying the body panel density in a simple source panel method, while keeping the free surface representation fixed, has the same effect that it does in the Green function method (figure 3-4). This is to be expected, provided the free surface is represented in reasonable detail, since the two methods become identical as the free surface is refined and extended.

As was done in comparing the Green function method with the analytical solutions, *net body forces* may also be investigated in validating the simple source method against the Green function method. Figure 3-8 shows for one case the convergence of the simple source solution to the Green function solution as the free surface is refined and extended[9]. As expected the

[9]The free surface was panelled in all cases in this figure for one third of its total length ahead of the cylinder centre, and two thirds behind.

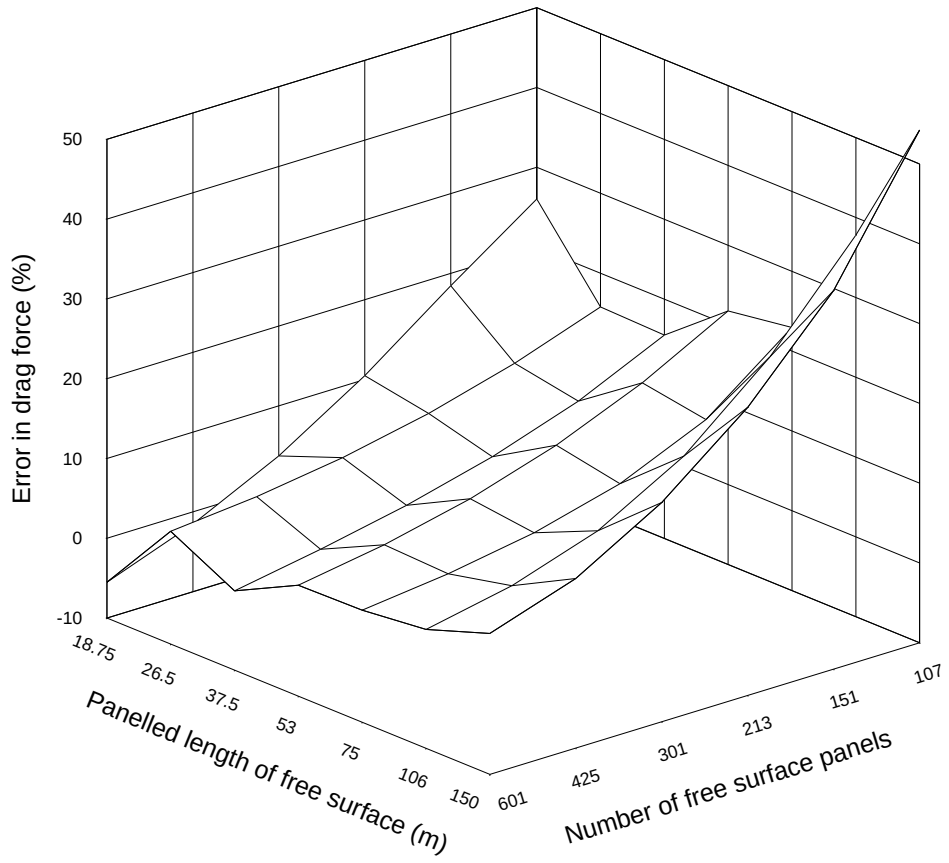

Figure 3-8: Error in drag force on translating submerged circular cylinder (Fr=0.8) for simple source method with various free surface configurations, as compared with Green function solution with identical body panelling

agreement is improved by increasing the number of free surface points, while the extent of the panelled free surface has two effects: if the panelled length of the free surface (L_{fs}) is too long then individual free surface panel lengths (Δx) will also be too long, and the quality of the solution deteriorates just as it did in figure 3-6. On the other hand if L_{fs} is too short the solution suffers from insufficient extent of free surface represented in solution. Figure 3-8 shows that this has the effect of introducing an increasing but fluctuating error on a solution that is, on average, improving due to the benefit of shorter Δx. Ideally one needs to increase the number of free surface panels while maintaining a minimum representation of the free surface extent.

In conclusion it is evident that, given finite computing resources, the priority should be to refine the panel size on both the free surface and the body, provided minimum requirements for extent of panelled free surface are met.

Transient response: Green function method

A complete validation of this method against the steady Green function method requires a large total time simulation but small time step. "Large" and "small" are of course relative, and the question arises as to what time scale characteristic to the problem can be used as a measure of these quantities.

One might conjecture that if only the steady state solution were sought then the time step size would not be critical. This follows from the assumption that if the source strengths are set at their correct steady state value then the value of the convolution integral in the Green function, when evaluated numerically, is independent of the time step size. This of course ignores the variation of the function being convolved with the source strengths, and is erroneous, as will be clearly evident in the results presented later.

Ideally it would be desirable to investigate the behaviour of the Green function convolution integral in search of a suitable time scale, but the approach taken was to seek something more physically meaningful.

Returning to Havelock's analytical solution of the transient response of a cylinder in uniform motion started from rest [44], we see that the time asymptotic behaviour of both the wave profile observed relative to the cylinder and the resistance is that of a decaying (not exponential) oscillation superimposed on the steady state value. The period of oscillation of this unsteady component of force is an obvious choice of time scale, and, denoting it T_1, is $T_1 = 8\pi Fr\sqrt{\frac{a}{g}} = 8\pi\frac{U}{g}$ where the Froude number (as will be the case for all subsequent examples) is based on the cylinder radius, a. Other possible time scales include the time required to travel a distance of one wavelength, $T_2 = 2\pi Fr\sqrt{\frac{a}{g}} = 2\pi\frac{U}{g}$, or the time required to travel one cylinder diameter, $T_3 = \frac{2}{Fr}\sqrt{\frac{a}{g}} = \frac{2a}{U}$. The most severe restriction would be to require that time step Δt satisfies

$$\begin{aligned} \Delta t &\ll \min\left(T_1, T_2, T_3\right) \\ &= \begin{cases} 2\pi Fr\sqrt{\frac{a}{g}} & \text{if} \quad Fr \leq \frac{1}{\sqrt{\pi}} \\ \frac{2}{Fr}\sqrt{\frac{a}{g}} & \text{if} \quad Fr \geq \frac{1}{\sqrt{\pi}} \end{cases}, \end{aligned}$$

and we seek to determine by numerical experimentation whether this may be relaxed at all. Similarly steady state could be assumed when $t \gg \max\left(T_1, T_2, T_3\right)$.

Figure 3-9 shows impulsive lift and drag forces on translating cylinders at three different Froude numbers, starting from rest. In both the time domain solution and the steady state solution (indicated as a horizontal line in each graph) 12 panels were used to represent the body.The vertical axis has the same scale in all cases, facilitating comparisons of convergence properties for the three speeds. Furthermore, in terms of the characteristic time scales, the time steps in figure 3-9 are shown in table 3.1.

Although steady state has not been reached in figure 3-9 the unsteady component of force is obviously decaying, and the rate of decay can be shown to be consistent with the predictions of Havelock [44]. It is also clear where the steady state value lies for each solution, and that

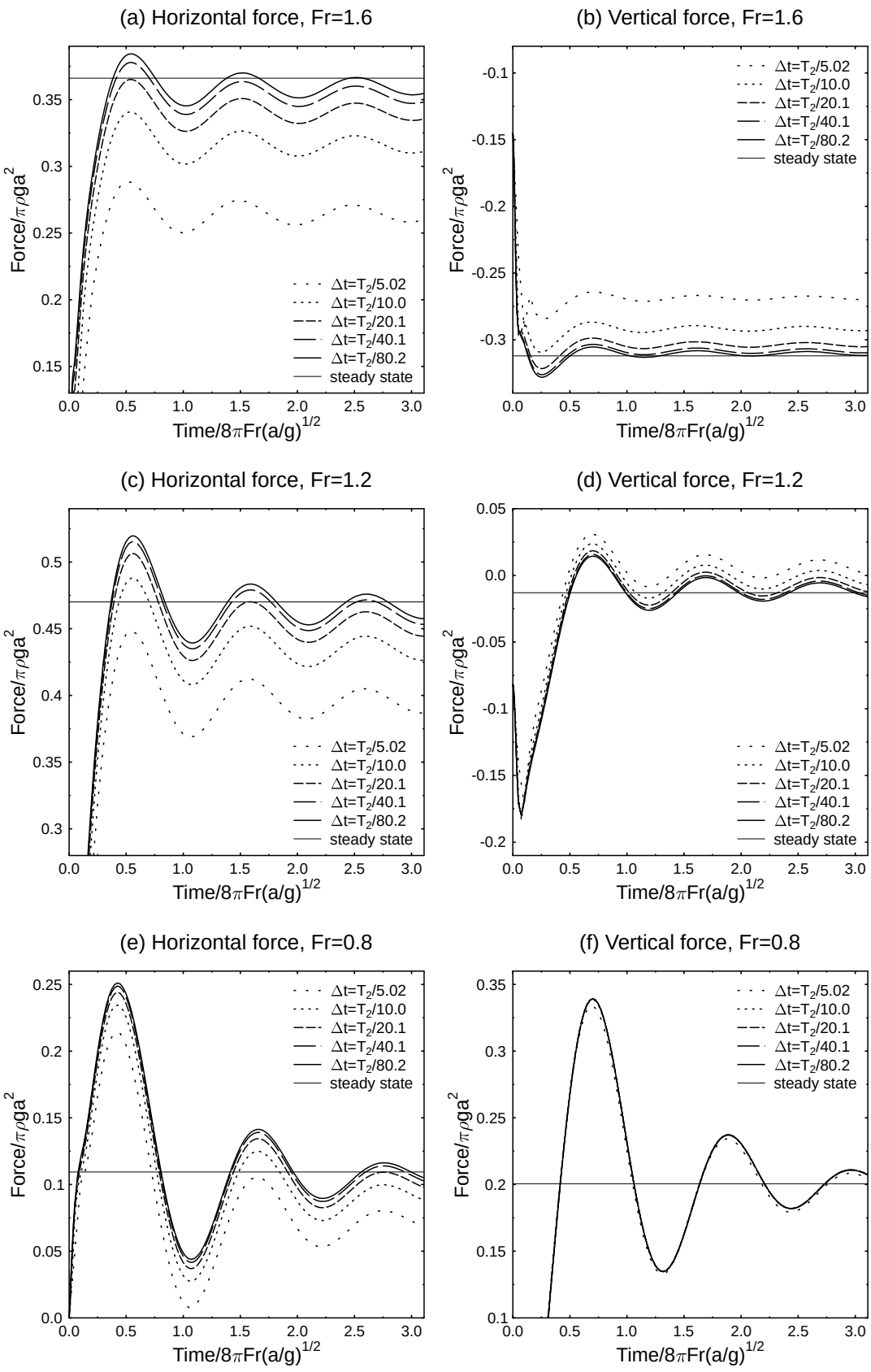

Figure 3-9: Effect of time step size on time domain Green function panel method.

	$\frac{T_2}{5}$	$\frac{T_2}{10}$	$\frac{T_2}{20}$	$\frac{T_2}{40}$	$\frac{T_2}{80}$
$Fr = 1.6$	$\frac{T_3}{0.625}$	$\frac{T_3}{1.25}$	$\frac{T_3}{2.5}$	$\frac{T_3}{5}$	$\frac{T_3}{10}$
$Fr = 1.2$	$\frac{T_3}{1.1}$	$\frac{T_3}{2.2}$	$\frac{T_3}{4.4}$	$\frac{T_3}{8.8}$	$\frac{T_3}{17.7}$
$Fr = 0.8$	$\frac{T_3}{2.5}$	$\frac{T_3}{5}$	$\frac{T_3}{10}$	$\frac{T_3}{20}$	$\frac{T_3}{40}$

Table 3.1: Relation between time step in terms of T_2 and in terms of T_3 for various Froude numbers

as Δt is reduced the mean values of the forces are approaching the correct steady state values. However despite the time step size being significantly smaller than the period of oscillation of the unsteady component of force ($\Delta t \simeq \frac{T_1}{20}$ even for the coarsest time steps) the convergence as Δt is reduced is very slow, particularly for the higher speeds. This is attributed to the fact that the cylinder travels a substantial proportion of its diameter during each time step, losing adequate resolution in the convolution integral of the Green function. It confirms the suggestion that $\Delta t \ll \min(T_1, T_2, T_3)$ is required, and hence that T_3 can not be ignored. Improved convergence is observed as the speed is decreased, where T_3 becomes longer while T_1 and T_2 become shorter. However, the magnitude of the oscillatory component of force as a proportion of the steady state value increases for lower Froude numbers, so if the steady solution is sought a longer simulation time would be required for the lower Froude numbers, negating any advantage of being able to use a larger time step size.

The rate of convergence of the mean component of force is higher for the lift force, and in fact in figure 3-9(f) the solution appears to have converged after only the second refinement of the time step.

Finally, the relative magnitude of the oscillatory component of force increases for lower Froude number. This means that if a steady solution is sought a longer simulation time would be required for the lower Froude numbers, negating any advantage of being able to use a larger time step.

Transient response: simple source method

The main features of the validation of this method are illustrated in figure 3-10, which shows an example of the waves behind a cylinder of 1m radius (shown in the figure), tranlsating at a Froude number based on radius of 0.8, at an instant of time 12.5s after motion began.

It is immediately evident that the chosen panel lengths on both the body and the free surface

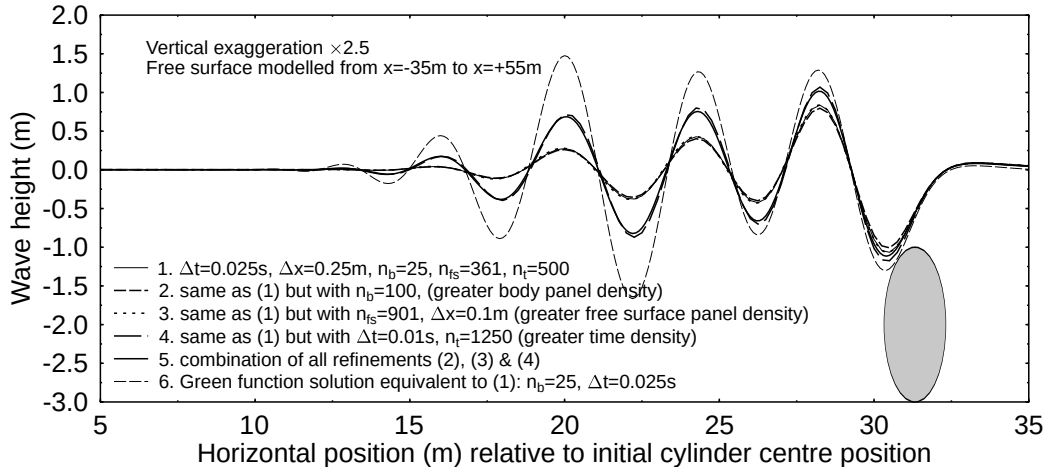

Figure 3-10: Wave profile behind steadily translating cylinder after 12.5 seconds: time domain simple source method in fixed reference frame, $Fr = 0.8$

were sufficiently small to achieve good results, but that the time step sizes[10] were much to large. Based on the results of figure 3-9, which closely approached convergence using larger time step sizes than in figure 3-10, one would have expected better results. The extent of the wave system following the cylinder is well predicted, including a similar but smaller system of waves that travelled in the opposite direction from the initial disturbance (not visible in figure 3-10 because these waves are in the vicinity of $x = -30$m), but the wave amplitude is not well predicted. The newly created waves immediately behind the cylinder have their amplitude well predicted, but progressing further away from the cylinder there is clearly an attenuation of the waves. Unlike the steady simple source solution this attenuation is present without a corresponding degree of shortening of the wavelength, and additionally it appears not to be significantly affected by the free surface panel length. Recall that in the steady solution the same free surface panel lengths would have caused significant shortening of the wavelength, but little attenuation of the amplitude (figure 3-6).

The explanation lies in the fact that the free surface boundary condition for the two cases are quite different: in the case of steady motion it is a statement about the spatial derivative of the wave height ($U^2 \frac{\partial^2 \phi}{\partial x^2} + g \frac{\partial \phi}{\partial y} = 0$), while in the present transient response solution it is one about the temporal derivative ($\frac{\partial^2 \phi}{\partial t^2} + g \frac{\partial \phi}{\partial y} = 0$). It is not surprising then that in the former the waves are attenuated in space progressing in the direction away from the cylinder if the free surface panel length is not sufficiently refined, while in the latter the waves are attenuated in time.

For a given free surface panel in one of the solutions represented in figure 3-10, fixed in space, observing a wave passing over it, the period of oscillation is equivalent to approximately 64 of the larger time steps (or 160 of the smaller), and thus one would expect that the derivatives

[10] $\Delta t = 0.025$s and 0.01s correspond to $\Delta t \simeq \frac{T_2}{64}$ and $\frac{T_2}{160}$ respectively, where T_2 is defined as in the previous section.

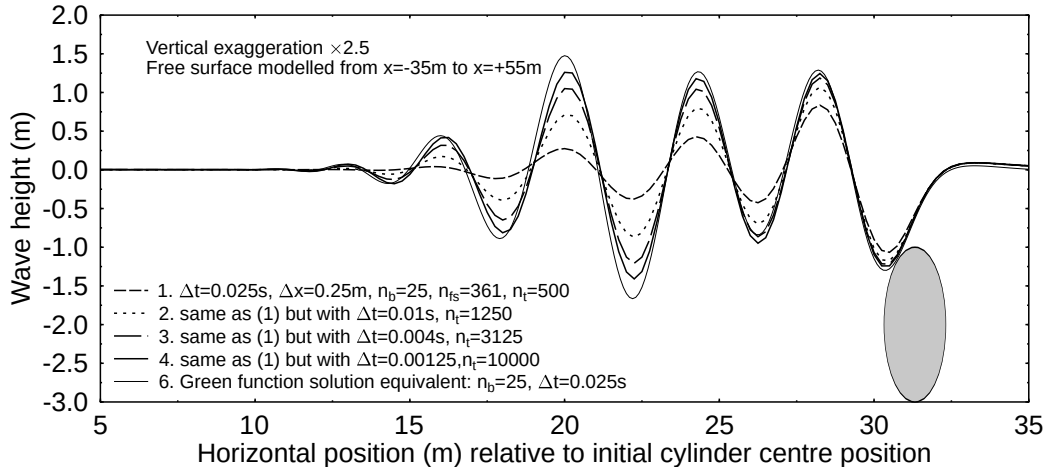

Figure 3-11: Comparison of time domain simple source panel method solution with various time step sizes, and equivalent Green function solution: $Fr = 0.8$, $t = 12.5$s.

in the free surface boundary condition were calculated with sufficient accuracy. The problem is that after a large number of oscillations the effects accumulate and the amplitude is attenuated despite small time steps.

Figure 3-11 shows solutions to the same problem as illustrated in figure 3-10, but with further refinement of the time step. The Green function equivalent used for comparison has a larger time step, but this seemed sufficient for convergence of the solution. All profiles were generated using 25 body panels ($n_b = 25$).

The wave amplitude appears to be approaching that given by the Green function solution as the time step size is decreased, however the degree of refinement required to achieve this was considered excessive, and for the solution with $\Delta t = 0.00125$ the changes from one time step to the next were so small that double precision had to be used to obtain a meaningful result. The problem almost certainly is that only a first order approximation to the $\frac{\partial^2 \phi}{\partial t^2}$ term in the free surface boundary condition was used, and it is recommended that higher order approximations to this derivative be investigated by anyone seriously considering this method. It should be noted that Dawson [19] used a third order approximation to the equivalent term, $\frac{\partial^2 \phi}{\partial x^2}$, in his steady state solution.

Although the wave amplitude seems to be improving as the time step size is reduced the wavelength in figure 3-11 appears to remain consistently slightly short. This is most likely due to the free surface discretisation, which was kept constant at approximately 16 panels per wavelength.

In light of this discussion it is clear that the connection between the two methods implied in figure 3-2 is not strictly correct (hence the dotted line), and that validation of the simple source time domain method against the simple source steady state solution requires, in addition to the indicated requirements ($\Delta t \to 0$, $T \to \infty$), either a time domain solution in a reference frame moving with the cylinder or $\Delta x \to 0$, as well as some form of absorbing the waves as they reach

the edges of the panelled free surface so that the requirement that $T \to \infty$ can be realistically achieved.

There is, by a similar argument, not a clearly defined relationship between the simple source time domain and the Green function time domain solutions, also suggested in figure 3-2. Again the two methods have completely unrelated dependencies on the time step size, so that one can not infer from the behaviour of one method as Δt is varied how the other method will behave. On the other hand we have seen that the dependence on Δx (and also on L_{fs} provided the total simulation time is restricted) is far less important than the dependence on Δt. Figure 3-10 bears this out. Validation is perhaps best carried out then for small total time, with a very limited free surface, but with very small time steps.

Finally, although not necessarily evident from the figures, both the Green function and simple source solutions to the transient problem of a translating cylinder initially at rest exhibit all the features described by Havelock [44] in his analytical solution to the problem; namely a local symmetrical disturbance travelling with the cylinder, a regular train of waves behind the cylinder and a disturbance spreading out in both directions but diminishing in magnitude as time passes. As observed by Havelock, the trailing end of the regular wave train travels at the wave group velocity (half the cylinder velocity) while the leading end, being continually created by the moving cylinder, travels at the wave phase velocity (equal to the cylinder velocity). The disturbance spreading out in both directions contains waves of various wavelength, which can be clearly seen in the numerical results, and through the effects of dispersion these eventually becomes insignificant.

3.6.3 Oscillatory motion

As in the translatory motion problems (section 3.6.2) one may choose to validate the various methods in this category by looking at either wave elevations or forces, but in either case the steady state solutions involve both amplitude and phase of these quantities. Alternatively, as is more usual for this type of problem, one may look at the forces in terms of added mass and damping coefficients. On the other hand it makes no sense to refer to added mass and damping for transient problems, and in that case it is far simpler to look directly at the time history of forces or wave profiles.

Steady state: Green function method

The added mass and damping coefficients for a heaving floating semi-circular cylinder using a steady periodic Green function panel method are presented in figure 3-12. Added mass and damping for heave are indicated respectively as a_{33} and b_{33}, and here the cylinder radius is denoted R to avoid confusion with added mass.

Comparison with similar figures in Doctors [21] shows excellent agreement (as far as can be ascertained by scaling values from Doctors' figures). As noted also by Doctors, the present

method exhibited an irregular frequency at $\omega\sqrt{\frac{R}{g}} \simeq 1.349$, where the numerical solution becomes nearly singular[11]. This was remedied in both the present work and in Doctors [21] by panelling a "lid" on the floating body.

Figure 3-12 also shows the analytical solution to the same problem, described by Ursell [92] in terms an infinite number of equations in an infinite number of unknowns[12]. Approximate numerical values were obtained for a discrete set of frequencies by replacing the set of equations with a finite set, the coefficients of which were obtained by least squares. The resulting finite set of equations was then solved using a relaxation method. His results for the damping coefficient are included in figure 3-12 for comparison, and agree well with those of the present method. Ursell's numerical results for added mass however do not agree with the present method, and in fact do not appear to be approaching the theoretical limit (mentioned in [21] and [72]) of $\frac{\pi}{2}$ at infinite frequency. However if one assumes there to be a missing $\frac{2}{\pi}$ factor[13] then his results are in excellent agreement, and these results, with the included $\frac{2}{\pi}$ factor, are also shown in figure 3-12.

It was found that only one lid panel was sufficient to completely remove the near singular behaviour at the irregular frequency at $\omega\sqrt{\frac{R}{g}} = 1.349$, and at low to moderate frequencies the solution was independent of the number of lid panels. However, it appears that the irregular frequencies arise from internal waves within the cylinder, and at higher frequencies (where such internal waves could be considered deep water waves) the lowest irregular frequency was found by numerical experimentation to approach $\omega\sqrt{\frac{R}{g}} = \sqrt{\frac{\pi}{2} n_{\text{lid}}}$, which is easily shown to be the frequency of the wave whose node spacing in deep water is equal to the lid panel length. For $n_{\text{lid}} \geq 4$ this estimate is within 3%. The only exception to this was found to be with a single lid panel, where there were no clearly definable irregular frequencies, but merely a general deterioration of the solution, as shown most clearly in the damping force on the right hand side of figure 3-13. Note that the vertical scale has been changed for the higher frequencies to exaggerate the behaviour. Thus in general increasing the number of lids merely shifts the onset of irregular behaviour to a higher frequency.

As the number of body panels was increased (with a fixed n_{lid}) behaviour of the solution near the irregular frequencies improved, although the frequency at which irregular behaviour occurred did not change. Figure 3-13 shows that with 640 panels (including 1 lid panel) no discernable irregular behaviour was observed, and this solution was also used in figure 3-12.

Doctors' paper [21] focused in particular on the problem of the first irregular frequency, and he did not present any results for frequencies greater that $\omega\sqrt{\frac{R}{g}} = 1.5$. He also appeared to

[11] The curve is actually smooth and continuous at the irregular frequencies, although very steep, but this behaviour is strongly affected by the panelling of the body, and is not correct.

[12] To this day an explicit solution to the problem remains elusive [94].

[13] Possibly his results were accidentally multiplied by $\frac{\pi}{2}$ twice instead of once. A later paper by Yu and Ursell [103] includes a $\frac{2}{\pi}$ factor in the expression for the added mass, while the results (in this case graphical) appear to differ from those in [92] by $\left(\frac{2}{\pi}\right)^2$.

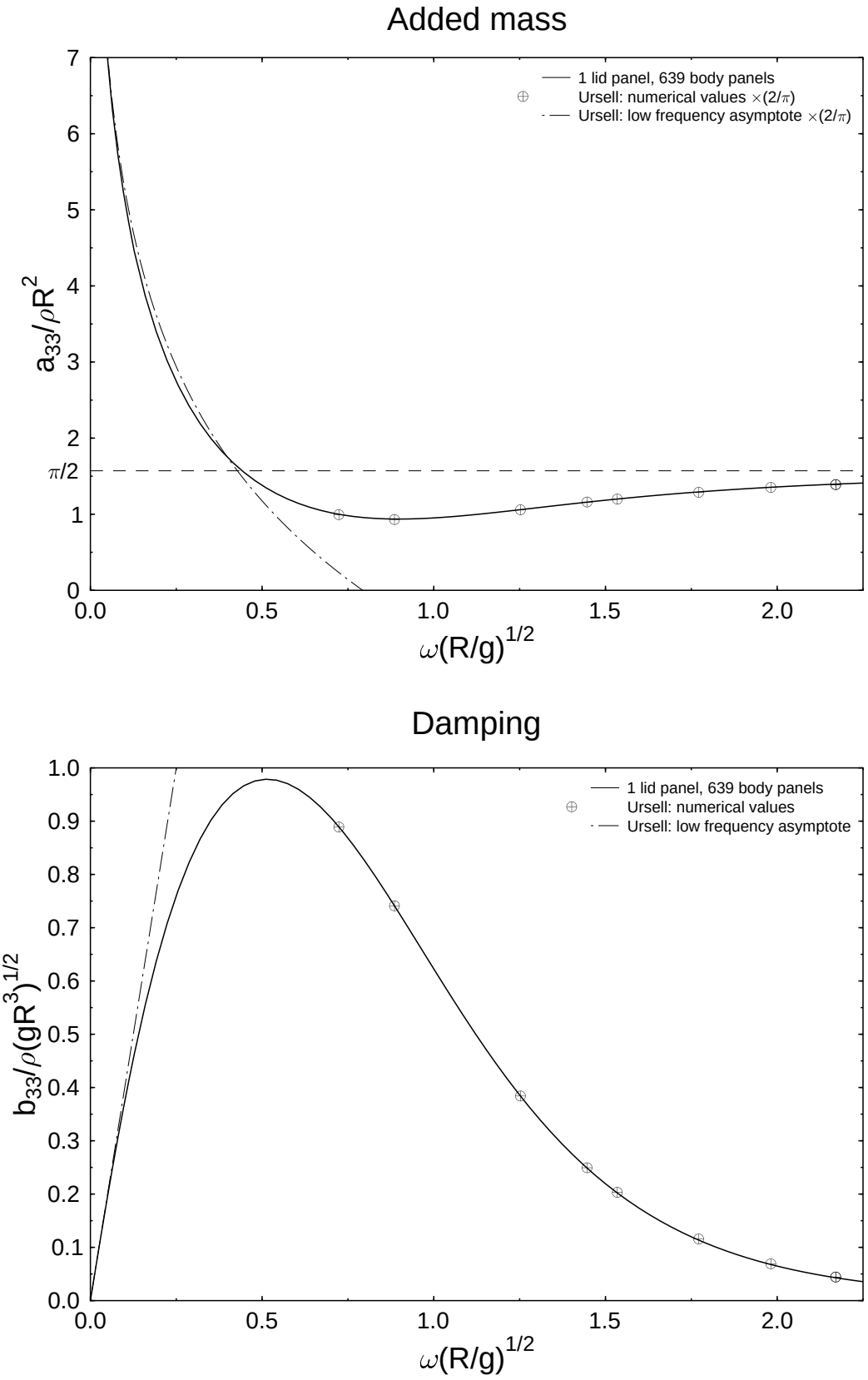

Figure 3-12: Heave added mass and damping for floating semi-circular cylinder: comparison between periodic Green function panel method and analytical solution (Ursell)

use only a large number of lid panels (generally $\frac{1}{3}$ of the total number). It is probably for these reasons that he did not comment on the presence of irregular behaviour at higher frequencies when using a lid. In addition to the lid Doctors introduced other refinements, including the use of a *Galerkin* method (in which an averaged form of the body boundary condition was satisfied over each boundary panel, rather than the simpler, more common approach of satisfying it at a set of boundary points) and extrapolation of the solution to that for an infinite number of body panels, based on solutions with 24, 48 and 96 body panels. Both of these would significantly improve the results, and help account for Doctors not observing anomalous behaviour at high frequencies when the lid was used. Doctors also placed the source panels a small distance outside the flow boundary, while in the present work they were placed exactly on the boundary. This small panel offset was tried in the present work for the lid only, but the result was worse, and it also introduced substantial errors at very low frequencies.

Transient response: Green function method

The validation and testing of the transient Green function method for oscillatory motion represents perhaps the most important part of section 3.6 for two reasons. The first is that it is this method is the one to be used in the time domain strip theory to be described in later chapters, and oscillatory motion most closely simulates the use that the method will be put to in practice. The second is that, unlike many of the other methods, no suitable published results for such a method were found for comparison purposes. In particular the algorithms for the evaluation of the required Green functions were developed without any known results to compare with, allowing opportunity for bugs in the computer program to pass undetected. Although the Green function algorithms were thoroughly tested it is reassuring that they stood up to their intended use in practice.

As in the equivalent method applied to translatory motion, there are at least two time scales of relevance, and a time step size must be chosen that is significantly smaller than both. The most obvious is the period of oscillation, while the other is $\sqrt{\frac{R}{g}}$ where R is some characteristic dimension, chosen to be the radius in the test case of the floating semi-circular cylinder. The justification for the latter is in terms of irregular frequencies, mentioned by Doctors [21], and it turns out that, regardless of the period of oscillation, it is quite important that the time step is small compared with the period of the first irregular frequency to obtain good results. In general, results show a superposition of the correct results and an oscillation at the irregular frequency that grows with time. The rate of growth increases as the time step size increases, but is negligible if the time step size is significantly smaller than the period of the irregular frequency, indicating that this component is erroneous. One might also consider the periods of the higher irregular frequencies, but as shown in figure 3-13 these irregular frequencies appear to have progressively less influence.

Again it is conceivable that these problems would be remedied with a lid, as they were

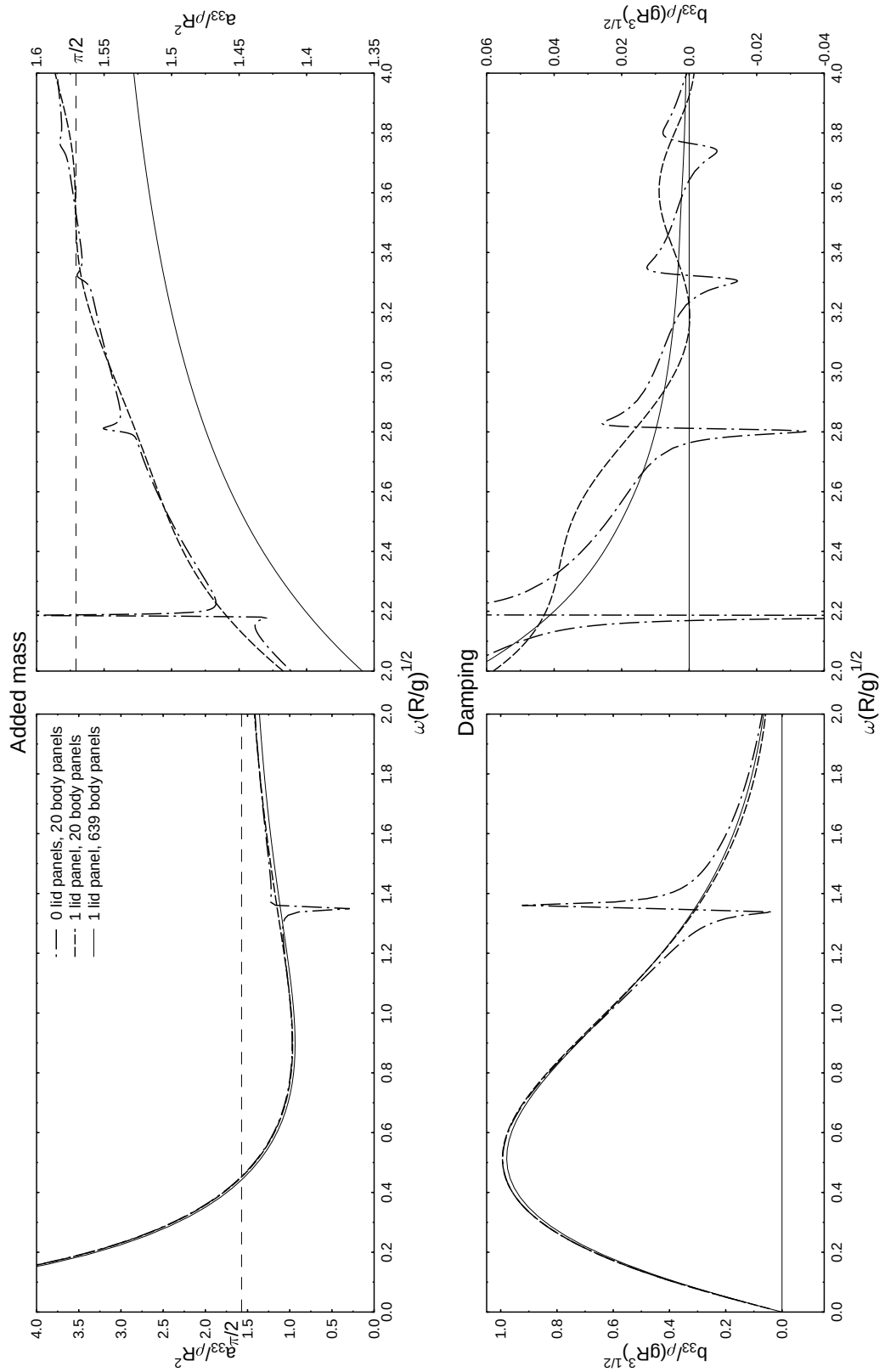

Figure 3-13: Irregular behaviour in Green function panel method solution for forces on heaving floating semi-circular cylinder

for the steady state periodic solutions. However, considering that large time simulations were not required in the intended final application and that the irregular frequency problem took considerable time to establish, the use of a lid was not investigated.

Figures 3-14 and 3-15 show a comparison between the time domain and periodic Green function solutions for a heaving floating semi-circular cylinder for various frequencies, each with identical body panelling. The two differ initially, as expected, but steady state appears to become established very quickly. The various curves on each graph show the effect of refining the time step size, and as with the translation motion it appears that quite small time steps are required for accurate results. At the lower frequencies (most obvious in figure 3-14 (a) and (b)), where larger time steps were used, the influence of the irregular frequencies on the result can be seen. The period of the observable irregular oscillation coincides with that of the first irregular frequency observed in the periodic solution (shown in figure 3-13).

Transient: simple source method and non-linear results

The focus in this section of work was on wave profiles, since most of the calculations involved in the generation of free surface heights are performed automatically as part of the solution process. An example of mildly non-linear wave motion is presented here merely for completeness, without any discussion of the validation process.

Figure 3-16 shows the free surface above a submerged cylinder in periodic sway motion, with a selection of wave profiles from the start of motion up to the elapse of approximately four cycles of oscillation. The cylinder was submerged to a centre depth of two radii, and its motion prescribed by $x = \frac{R}{4}(\cos(\omega t) - 1)$ where R is the cylinder radius and $\omega\sqrt{\frac{R}{g}} \simeq 0.7958$ ($\omega = 2.5$ rad/s for $R = 1$m). This frequency was chosen by running the linear frequency domain solution to find the range of frequencies for which significant wave motions occurred, and a frequency near the centre of the range was arbitrarily selected.

Both linear and non-linear solutions in figure 3-16 use 12 body panels and 281 free surface panels, the latter extending from -35 to $+35$, giving a panel length on the free surface of $\frac{R}{4}$, or approximately $\frac{1}{40}$th of the wavelength of the regular wave with frequency ω. A finer free surface panelling was tried for the linear solution with negligible difference. Also the extent of free surface was investigated and the length chosen represented a reasonable compromise, giving negligible error until about $\omega t = 20$ when small but noticeable errors started to grow inwards gradually from the extremities of the free surface.

The most interesting part of the comparison was the choice of time step. Time steps of $\omega\,\Delta t = 0.025$ and 0.05 were tried for the non-linear solution, with negligible difference being observed. However the same time steps used for the linear solution were too large to give acceptable results. Even a time step of $\omega\,\Delta t = 0.00625$, the value used in figure 3-16, gave a estimated error of about $1 - 2\%$ after the elapse of $\omega t = 25$. The different time step requirement for the two methods was unexpected since the finite difference approximation used for the free

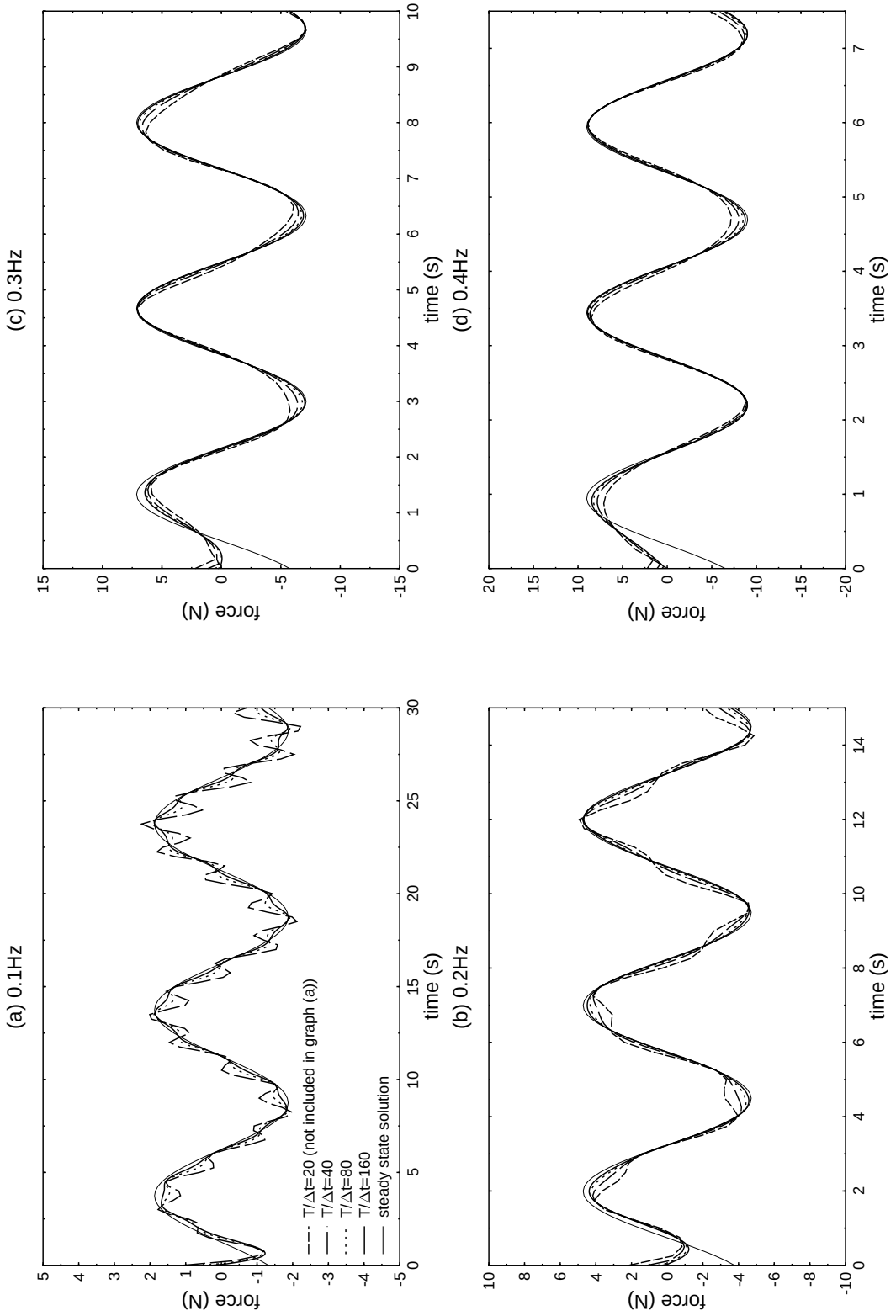

Figure 3-14: Effect of time step size on time domain Green function solution for periodic oscillation (frequency 0.1-0.4Hz)

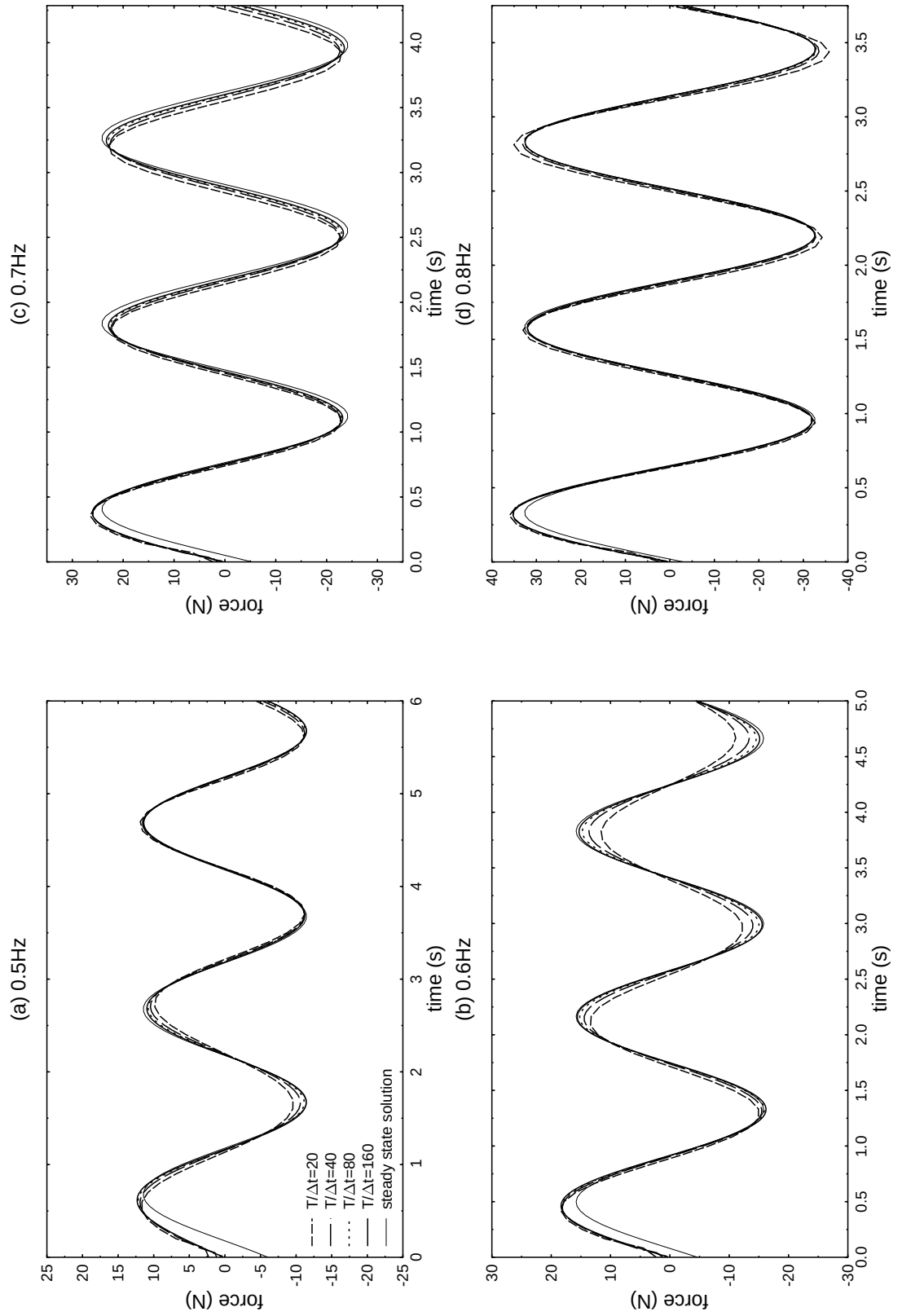

Figure 3-15: Effect of time step size on time domain Green function solution for periodic oscillation (freq. = 0.5-0.8Hz)

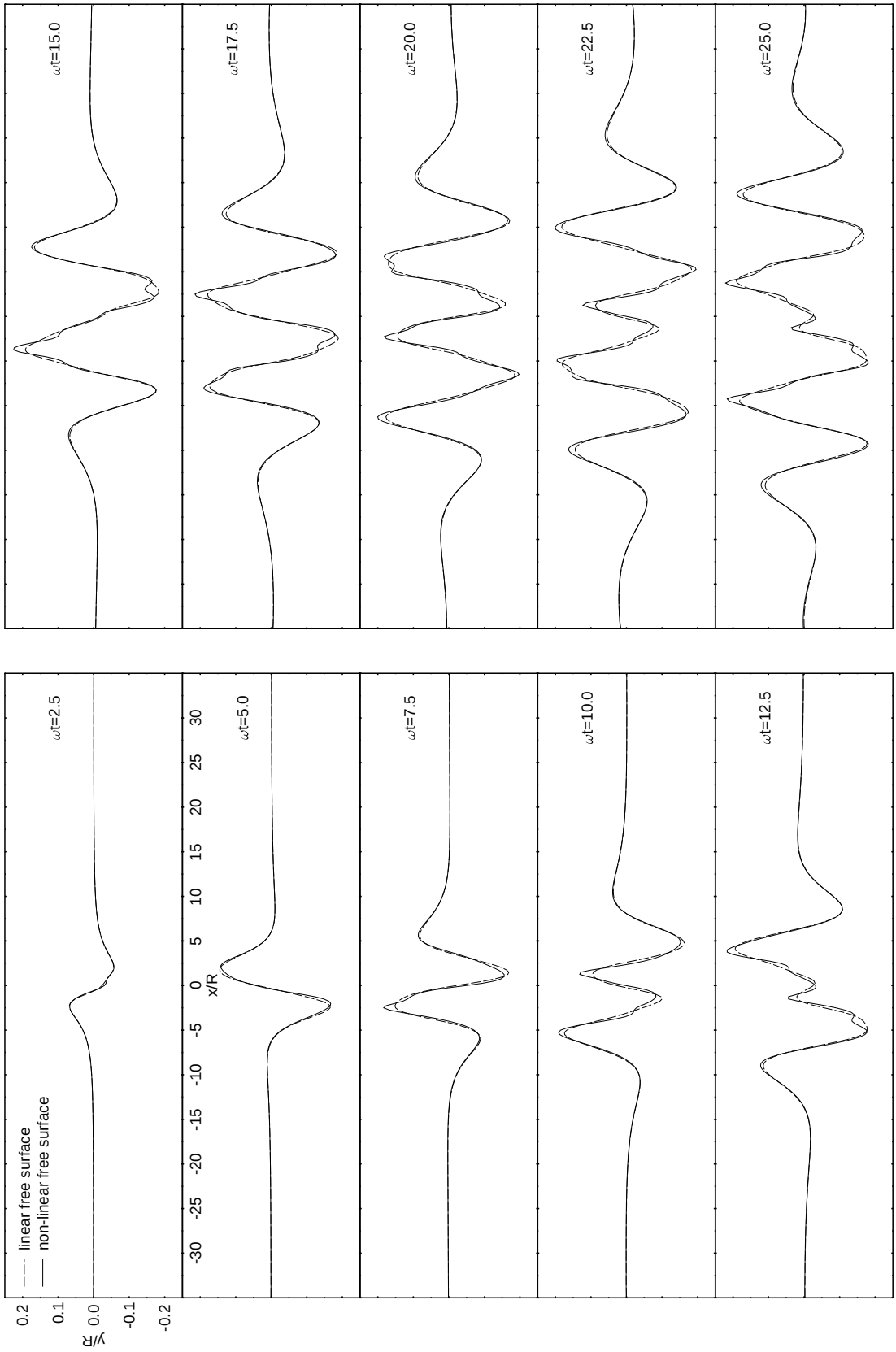

Figure 3-16: Comparison of non-linear and linear time domain free surface profiles above a submerged cylinder in periodic sway motion.

surface time derivatives was of the same order for both linear and non-linear solutions. Several factors listed below may have contributed to this anomaly, although these remain conjecture as the problem was not investigated.

- The free surface elevations are an essential part of the non-linear solution, while they are not required in the linear solution, and their more direct presence in the former may have led to better accuracy.
- The non-linear solution involved iterative improvement of the solution at each time step.
- The effect of additional terms in the non-linear boundary condition may have reduced the relative importance of and sensitivity to time derivative terms.

As a consequence of the requirement for a smaller time step to achieve the same accuracy the linear solution was actually slower than the non-linear solution, although the solution time per time step was faster. Furthermore the solution time per time step for the non-linear solution was slower by a smaller margin than expected. Given that there are approximately twice the number of unknowns in the non-linear solution (if the number of panels on the body is only a small proportion of the total number) one would expect a speed reduction factor of almost four in the matrix inversion alone, ignoring the need for iteration. However due to a considerable effort in optimising a specially dedicated matrix solver that took into account the structure of the Jacobian matrix, as well as introducing efficiencies in the iteration process, the total solution time per time step for the non-linear solution was only about 3.2 times that for the linear solution.

It is envisaged that the linear solution would always be faster that the non-linear solution if the same effort were put into optimising both, however the above observations indicate that the margin would not necessarily be very great.

Finally, the features that distinguish the non-linear and linear solutions are as expected. The non-linear solution has an obvious presence of higher harmonics, as well as exhibiting in most cases the classical sharpening of crests and flattening of troughs in the predominant waves. Other cases tested have also demonstrated that as the submergence is increased the two methods give the same results.

3.6.4 Transient motion of surface piercing bodies

Given that the intended end use for the time domain panel method program is for incorporation into a time domain strip theory program for the calculation of motions of surface piercing hull forms it is pertinent that validation includes test cases involving transient response to motions of surface piercing bodies. Two such examples for which analytical solutions exist are the wave form generated by a wavemaker, solved by [83], and the transient motion of a floating cylinder, solved by [67] and [93] for the semi-circular cylinder case. The latter has also been solved numerically by [99] for arbitrary shapes.

The wavemaker problem

[83] studied the problem of waves generated in an infinitely deep fluid bounded only on the left by a vertical wall, of which a section of depth d moves horizontally according to various prescribed motions. Other examples of analytical solution to the transient wavemaker problem include [51] and [58]. The former of these is similar to Roberts', except that the fluid is also bounded on the bottom at the depth of the moving plate, and surface tension effects are considered. The latter studies waves generated in a finite basin (bounded at both ends and the bottom) by a flap type wavemaker hinged at the channel bottom.

All three solutions linearise the free surface boundary condition in the same manner as the present time domain Green function panel method solution (if one ignores the contribution of surface tension in the case of [51]). They do not rely on assumptions of small time or local behaviour, and could all serve as test cases for validation of the present time domain panel method. Roberts' solution was chosen for comparison because the infinite fluid extent is most relevant to the intended application of the panel method, and because Roberts includes a comprehensive collection of cases for which simulations can be carried out. The stationary vertical wall below the wavemaker flap can be accounted for by the use of symmetry (in fact this is extremely similar to the case of a ship bow section piercing a two-dimensional strip of water, as will be evident in the discussion of a fixed reference frame time domain strip theory in chapter 4), and the absence of a channel bottom eliminates the need for extra panelling.

Before proceeding it should be pointed out that there is a problem with the vertical axis labels in Roberts' figures. His figures 3, 4 and 5 are labelled $\frac{\eta_0}{\alpha d}$, which should be but is not dimensionless[14]. Furthermore for linear problems (i.e. in the limit $\alpha \to 0$) $\frac{\eta_0}{\alpha d}$ is infinite. It is assumed that the vertical axis label should be $\eta_0\sqrt{\frac{g}{d}}$, which appears to be consistent with Roberts' equations and with limiting numerical values implied in the text, as well as with results given by the present time domain panel method. His figures 6, 7 and 8 are also incorrectly labelled. A label of $\frac{\eta_p}{\alpha}\left(\sqrt{\frac{g}{d}}\right)^{p+1}$ is consistent with the given results for figure 8, in which $p = 1$ (as well as for figures 3, 4 and 5, in which $p = 0$) but no simple combination of quantities was found that gave even approximately correct values for figures 6 and 7 (in which $p = -\frac{1}{2}$ and $\frac{1}{2}$ respectively)[15].

In modelling the problem numerically with the time domain panel method the choices of time step size and number of panels were the main issues. It was noted that Roberts gives results for the free surface elevation at $\frac{x}{d} \simeq 10^{-5}$ (see for example his figure 3(d)), suggesting that that was the order of the panel length required on the wavemaker near the free surface. Even with unequal panel lengths this would require a considerable number of panels since, as

[14] Respectively η_0, α, and d have dimensions of time, velocity, and length for the figures in question, thus $\frac{\eta_0}{\alpha d}$ has dimension (velocity)^2.

[15] Here p indicated the power of the plate velocity-time relationship (i.e. $U = \frac{\alpha t^p}{\Gamma(p+1)}$), and η_p the linearised free surface solution corresponding to that plate velocity relationship. Note also that Roberts uses η to indicate $\eta_p|_{p=0}$, and η_0 to indicate the first term in the power series for η. Thus $\eta_0 = \frac{\eta_p}{\alpha}$ for $p = 0$.

is well known in the use of panel methods, the ratio of lengths of adjacent panels should not be too great ([47] recommend a maximum of 1.5). However in practice it was found that the problem was independent of panelling, presumably due to some fortuitous geometrical property of a vertical wavemaker. The free surface elevation was calculated from $\frac{x}{d} = 10^{-5}$ to $\frac{x}{d} = 0.1$ with various numbers of panels ranging from a single panel to 60 panels, both with equal spacing and with geometric progression spacing. The results from all calculations differed only in the 7th significant digit, obviously due to machine roundoff. On the other hand it is expected that the pressure distribution on the wavemaker plate would not necessarily be calculated accurately since the source strengths were not constant for all panels.

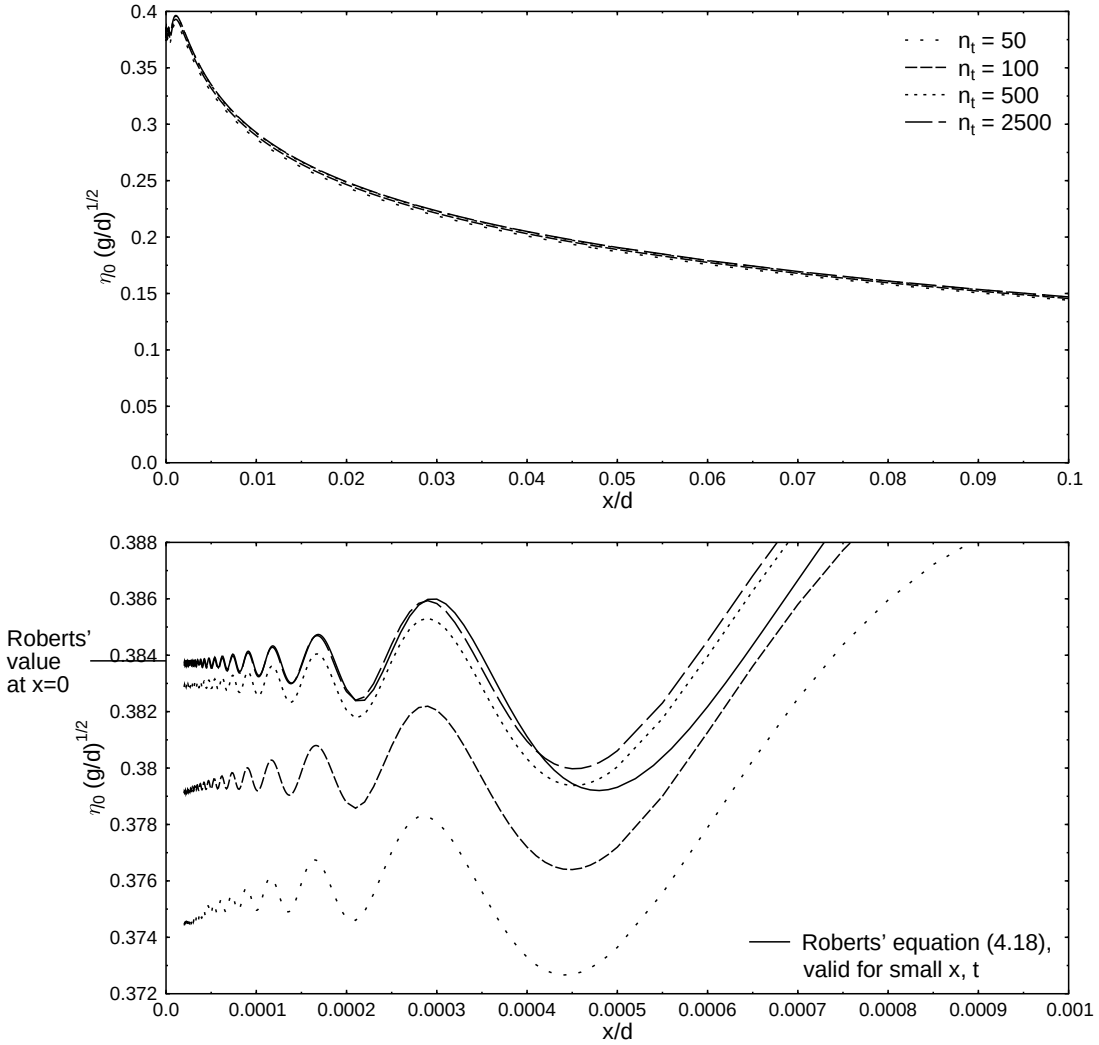

Figure 3-17: Effect or number of time steps on time domain panel method Solution for free surface elevation in front of wavemaker moving with constant velocity ($t\sqrt{\frac{g}{d}} = 0.1$).

The time step size proved to be far more critical in evaluating the free surface elevation at very small values of $\frac{x}{d}$. To explain this observation one can view the problem in Fourier space. It is evident that at any given maximum desired simulation time ($t_{\max}$) and minimum distance

from the wavemaker at which the free surface elevation is required ($x_{\min}$) only the frequency components having a group velocity exceeding a critical value $c_G = \frac{x_{\min}}{t_{\max}}$ sufficiently high to reach that point in the specified time will significantly influence the free surface elevation. The time step size Δt therefore needs to be significantly smaller than the period of this wave of critical group velocity. If Δt is chosen such that there are m time steps in this critical wave period (i.e. $\frac{2\pi}{\omega} = m\Delta t$) then the group velocity of this critical wave (in deep water) will be $c_G = \frac{gm\Delta t}{4\pi}$. The total number of time steps required ($n_t = \frac{t_{\max}}{\Delta t}$) in terms of dimensionless time ($t\sqrt{\frac{g}{d}}$) and dimensionless distance from the wavemaker ($\frac{x}{d}$) will then be

$$n_t = \frac{m\left(t\sqrt{\frac{g}{d}}\right)^2_{\max}}{4\pi\left(\frac{x}{d}\right)_{\min}}. \tag{3.38}$$

Thus, although the 2500 time steps used in figure 3-18 seems a large number, at $t\sqrt{\frac{g}{d}} = 0.1$ and $\left(\frac{x}{d}\right)_{\min} = 10^{-5}$ this corresponds to only $m = 30$. Smaller numbers of time steps gave noticeably poorer results at small values of $\frac{x}{d}$, as shown in figure 3-17, particularly when the error is viewed relative to the scale of the local oscillatory component of the free surface waves.

Figure 3-18 shows an example of the water surface profile calculated by the present time domain panel method for conditions equivalent to those in Roberts' figure 3, while figure 3-19 is reproduced from Roberts' original figure 3. The two show excellent agreement, and similar agreement was obtained for other figures of Roberts'.

Transient heave of an unrestrained floating body

The transient motion of a freely oscillating body in the free surface, in addition to calculation of the hydrodynamic force, poses the problem of integration of the equations of motion. These two aspects are interdependent since the forces depend on the motions, but in turn account for the accelerations. Direct integration of the accelerations is numerically unstable because implicit added mass effects in the hydrodynamic force causes the right hand side of the equation of motion to depend on acceleration, giving rise to feedback in the acceleration term being calculated on the left hand side, and amplifying any error that may be present. This will be discussed in detail in section 4.6 in connection with the time domain strip theory, where a successful and robust solution to the problem will be proposed. The method of integration proposed in that section has also been used successfully in solving the present problem of the transient motion of the freely oscillating body in the free surface, attesting to its accuracy and reliability.

Both [99] and [67] solve the two related problems of transient heaving motion due to an initial displacement and due to an initial velocity. Because they have solved a linear formulation of the problem one can in principle obtain motions resulting from any arbitrary initial condition as a linear combination of their initial displacement and initial velocity solutions. They both also note the property that the velocity history of the initial displacement problem is a multiple of the displacement history of the initial velocity problem (the multiple being $-\frac{2gH_0}{\pi a U_0}$ for a semi-circular body, where a is the body radius and H_0 and U_0 are respectively the initial heave displacement

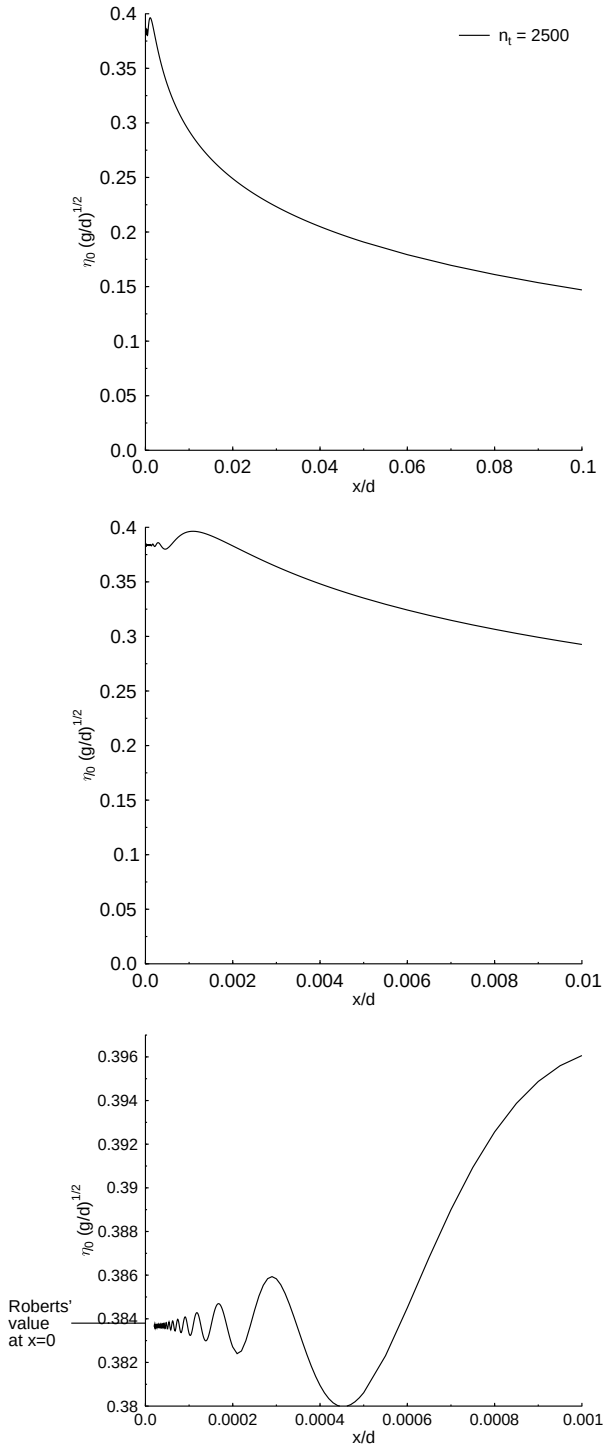

Figure 3-18: Free surface at time $t\sqrt{\frac{g}{d}} = 0.1$ in front of a wavemaker moving with constant unit velocity since $t = 0$.

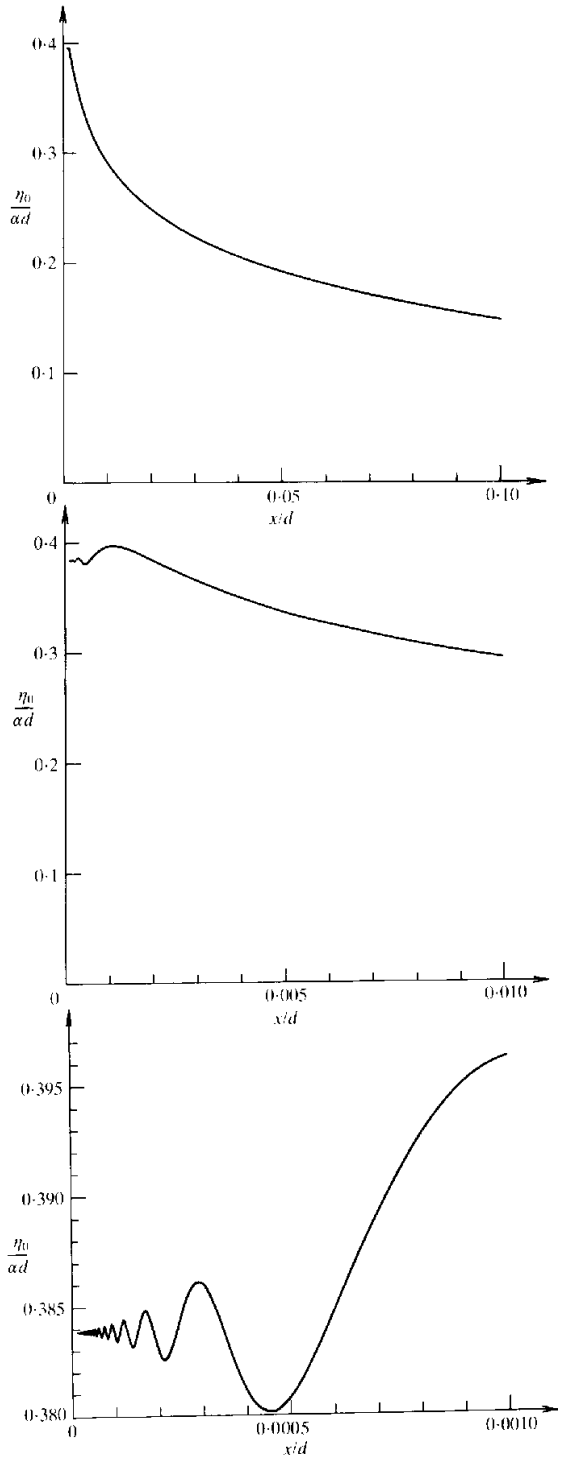

Figure 3-19: Reproduced from Roberts' figure 3(b)–(d) [83].

and velocity for the two problems).

[99], who uses a numerical method, considers semi-circular, rectangular and triangular bodies, while [67], who use an analytical method, consider only the case of a semi-circular body. Their results for the semi-circular problem are not as close as one might expect for such calculations. In particular the first trough for the initial displacement problem (estimated from enlarged copies of their figures to be -0.637 in the case of Yeung, and -0.663 in the case of Maskell and Ursell) differs by about 4%, and the first peak in the initial velocity problem (1.100 for Yeung and 0.718 for Maskell and Ursell) differs by about 2.5% (taking into account a $\frac{\pi}{2}$ factor difference in their normalisation). It is not known which of the two is more correct, although results from the present time domain panel method in all cases fell between the two and generally closer to Yeung's (the corresponding trough and peak being -0.642 and 1.109 using 24 body panels and a time step size $\Delta t\sqrt{\frac{g}{a}} \simeq 0.00783$, which are within about 0.8% of Yeung's values). On the other hand the time between zero crossings and the general form of the solutions corresponded very well between the three solutions.

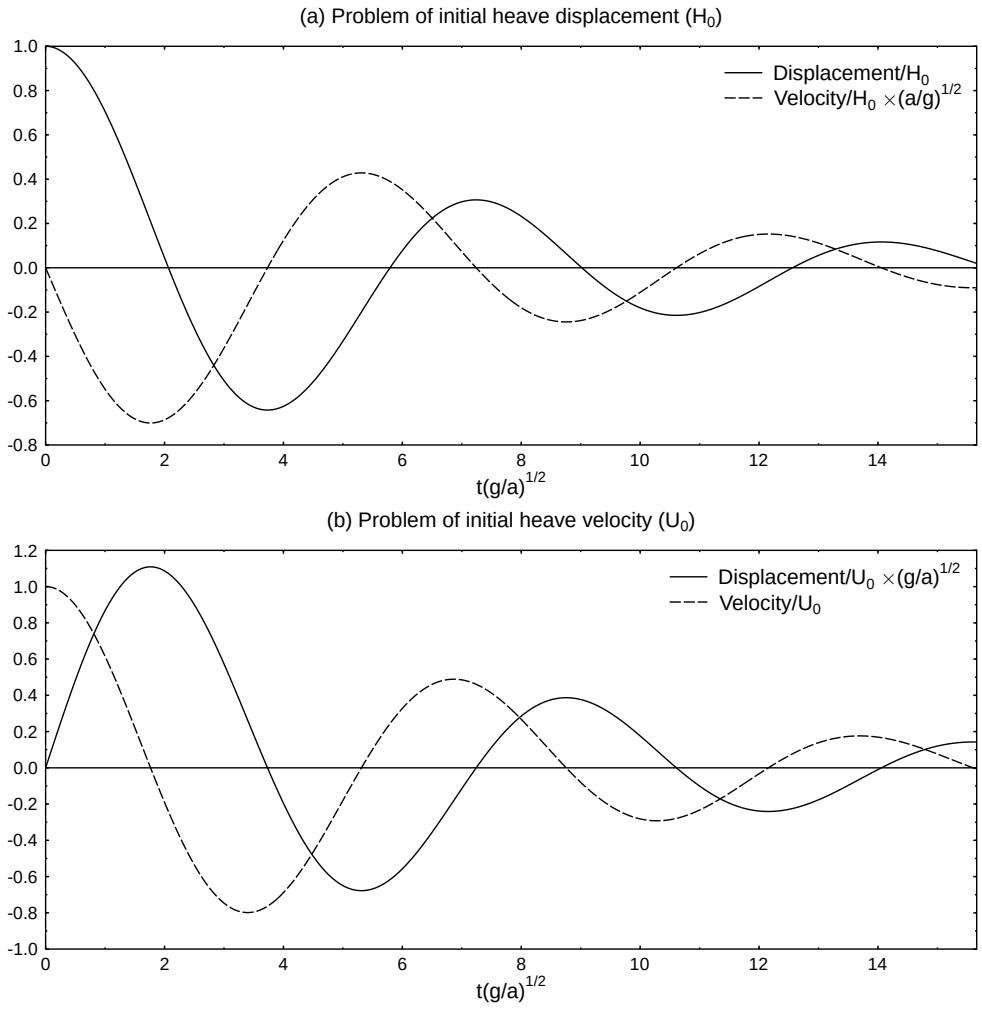

Figure 3-20: Transient heave response of a freely floating semi-circular cylinder.

Figure 3-20 shows responses to initial heave displacement and velocity for a semi-circular body calculated using the present time domain panel method, with 24 body panels on half the body (making use of symmetry) and a time step size of $\Delta t\sqrt{\frac{g}{a}} \simeq 0.00783$. These figures correspond to Yeung's figures 4 and 5, and to Maskell and Ursell's figures 2 and 3.

Another check on the solutions is a comparison of the velocity history of the initial displacement problem with the displacement history of the initial velocity problem. Yeung plots velocity in addition to displacement, and so a comparison can be made directly from his figures, showing a difference of about 0.6% for the first peak/trough (probably due mainly to estimation of numerical values from his figures). Maskell and Ursell do not plot velocities, but give analytical expressions for the asymptotic solutions for small and large time which can easily be differentiated. Their small time solutions correspond exactly, but their large time solutions (in the form of exponentially decaying sinusoids, and which have numerically determined coefficients) show a difference of about 1.0% in the amplitude and about $0.4\% \times 2\pi$ rad in the phase angle. In light of this, the corresponding difference of 0.7% (using 24 body panels on half the semi-circle, and a time step size $\Delta t\sqrt{\frac{g}{a}} \simeq 0.00783$) in the present time domain panel method seems entirely reasonable.

3.6.5 Conclusions

In summary, it is the time domain Green function method that is to form the basis of work in subsequent chapters, and a few precautions concerning the use of this technique deserve repetition here.

In general, for moving bodies, great care must be taken to ensure that the choice of time step size is sufficiently small. The problem appears to be primarily one of large changes in the body position between time steps. For motions typical of oscillating ship sections this is not a major concern since these motions involve oscillation about a mean position, and the problem in this case is the presence of extraneous forces due to irregular frequencies. Again, looking forward to later chapters, the proposed strip theory involves strips fixed in space, not moving with the ship, and therefore the hull section is not only oscillating but constantly changing shape as the ship passes through. Presumably too the irregular frequency is also changing, and the spurious oscillations (which appear to require some time to build up) would not have a chance to contaminate the solution. Furthermore, the solution for each strip is only carried for the time it takes for a ship to pass through that strip, giving very little time for any build up of errors. Presumably then a time step small compared with the period of oscillation would seems to be sufficient to represent this motion.

Little doubt remains as to the validity of the method in general, but it needs to be demonstrated for any particular case that the time step is sufficiently small for convergence to the continuous solution to be assumed. This requires no benchmark, but simply refinement of the time step in order to demonstrate negligible (or tolerable) change in the solution.

Chapter 4

Derivation and Implementation of a Time Domain Strip Theory for Pitch and Heave

4.1 Introduction

A time domain strip theory is proposed that differs fundamentally from all frequency domain strip theories in its treatment of the free surface boundary condition. This is achieved by rejecting the moving reference frame formulation, essential for the periodicity requirement of a frequency domain solution, and replacing it with a stationary reference frame. This eliminates the need for the $\frac{\partial}{\partial x}$ terms in the free surface boundary condition, necessarily absent but often required in the frequency domain theory.

We will first look at the difference in a rather intuitive physical description. Then a more rigorous mathematical comparison will be made in terms of the underlying assumptions that are required. Section 4.2 will then describe in more detail conventional strip theory, followed by the remainder of the chapter devoted to the present time domain fixed reference frame strip theory and its numerical implementation.

4.1.1 Physical interpretation of the new theory

Consider the following two scenarios for the strip theory calculation of hydrodynamic wave radiation forces on a hull moving at constant forward speed U in the $+x$ direction, initially ($t < 0$) with no other motion, then for $t > 0$ with periodic heave and/or pitch motion about its mean position superimposed. Through the application of conventional strip theory assumptions we will approximate the three-dimensional problem with a set of two-dimensional ones, combined in a way that exactly satisfies the slender hull boundary condition (as for example described by

Salvesen, Tuck and Faltinsen [84]).

Scenario 1: The computational domain for each two-dimensional solution is a strip that is stationary relative to the equilibrium position of the moving hull, (moving with speed U in the $+x$ direction relative to an absolute reference frame).

Strips that are ahead of or behind the moving boat will never experience any disturbance, while those in between will see a disturbance that grows in extent as time passes. In the limit as $t \to \infty$ this disturbance is asymptotic to the steady state periodic solution for the relevant section at the same frequency, in which waves extend infinitely in both directions. No strip has its solution influenced in any way by the waves or water motion created in adjacent strips.

The appropriate linearised free surface boundary condition is $\left(\frac{\partial}{\partial t} - U\frac{\partial}{\partial x}\right)^2 \phi + g\frac{\partial \phi}{\partial y} = 0$, which reduces to $-\omega^2\phi - 2i\omega U\frac{\partial \phi}{\partial x} + U^2\frac{\partial^2 \phi}{\partial x^2} + g\frac{\partial \phi}{\partial y} = 0$ at steady state when $t \to \infty$. This can not be satisfied exactly in a strictly two-dimensional solution since the $\frac{\partial}{\partial x}$ derivatives require consideration of the relationship between adjacent strips, and therefore, in addition to several other assumptions, the assumption that $\frac{U}{\omega}$ is in some sense small is implied. (As will be shown in more detail in section 4.1.2, $\frac{Uk}{\omega} = \tau < \frac{1}{4}$ is the principal requirement.)

This is conventional frequency domain strip theory.

Scenario 2: The computational domain for each two-dimensional solution is a strip that is fixed in an absolute reference frame (stationary relative to the equilibrium position of the water).

This strip remains undisturbed until the bow of the hull reaches it. It observes the oscillating hull passing through it, and waves are generated. (It is only in this second stage that any contribution is made to the hydrodynamic forces on the hull.) Finally, once the hull has completely passed through, the irregular wave pattern that has been generated gradually disperses, and no new waves are generated as this occurs. After some time an observer of this strip sees a central region with no waves, bounded by two regions containing waves, bounded again by two regions with no waves that extend infinitely. Under no circumstances (except at zero forward speed or an infinitely long hull) does a strip ever have waves extending infinitely, and the boat always leaves behind it a set of waves. The forces on each section are directly influenced by the waves created by forward sections earlier passing through the same strip.

Because the strip is stationary the appropriate linearised free surface boundary condition is $\frac{\partial^2 \phi}{\partial t^2} + g\frac{\partial \phi}{\partial y} = 0$, and no approximation of it is required for a two-dimensional solution.

This is essentially the time domain strip theory proposed here.

Of course *both* of the two scenarios suggested above will produce steady state periodic forces on the hull as $t \to \infty$, and both can be made to satisfy exactly the same hull boundary conditions, but only in the first can steady state ever be observed for an individual strip, and only in the second can the correct (linearised) free surface boundary condition for a strip ever be satisfied in a strictly two-dimensional solution with non-zero forward speed.

In spite of the fact that both solutions can reach steady state periodic motion when viewed

from the moving vessel, the two methods will only give identical results at zero forward speed and as $t \to \infty$. Note that the requirement is that $U = 0$, not $\omega \to \infty$, since the motion can only be periodic in a reference frame moving with the boat.

4.1.2 Strip theory assumptions

Strip theory, by definition, involves approximating the three-dimensional fluid around a vessel with a set of two-dimensional *strips* of fluid, generally with the object of predicting the vessel motions in the presence of waves. The three-dimensional wave field is a very complex one, containing up to six distinct sets of waves. The simplest equivalent wave system, that of a translating pulsating source, is described both mathematically and diagrammatically by Wehausen and Laitone [98] (equation (13.52) and figure 3), Havelock [37] (equation (6)), Becker [7] (figures 10, 11), and Yeung and Kim [102] (figure 3), and gives some indication of the wave system in the far field of an oscillating translating hull. In the near field the waves around the hull would presumably behave more like those due to a line distribution of such sources. We seek to determine under what conditions (particularly in the context of vessel motion prediction) it is valid to make a two-dimensional approximation to these near field waves. We further seek to demonstrate that a fixed reference frame approximation has a greater range of applicability than a moving reference frame one.

A mathematical description of the assumptions made in strip theory can be found in most of the standard references (for example [84], [72]). The following discussion will focus on their physical significance.

Before proceeding we must formally define the axis system. Let the origin be in the undisturbed free surface and coincident with the centre of mass of the boat in both horizontal directions, with x towards the bow, y to port, and z upwards, and assume the boat is travelling at constant forward speed U in the $+x$ direction. Let us further restrict ourselves to the case of regular head seas (waves travelling in the $-x$ direction). The applicability to irregular waves may be inferred through their Fourier spectrum. The following analysis may be extended to other sea directions, but we will only concern ourselves with head seas in the present work.

Dimensionless variables

At this point it is convenient to introduce some dimensionless variables that characterise the problem. First, in addition to variables already defined above, let ω_0 be the incident wave frequency with corresponding wave number k_0, and ω the wave encounter frequency with k being the wave number associated with a wave of this frequency in a stationary reference frame. The two are related for head seas through $\omega = \omega_0 + k_0 U$, and we also have the relationships in deep water $k = \frac{\omega^2}{g}$ and $k_0 = \frac{\omega_0^2}{g}$. One can therefore express ω_0 in terms of ω as the solution to a quadratic.

The dimensionless variables that will be used are

$$Fr = \frac{U}{\sqrt{gL}} \tag{4.1}$$

$$\left\{ \begin{array}{c} \tau \\ \tau_0 \end{array} \right\} = \frac{\left\{ \begin{array}{c} \omega \\ \omega_0 \end{array} \right\} U}{g} \tag{4.2}$$

$$\left\{ \begin{array}{c} \omega^* \\ \omega_0^* \end{array} \right\} = \left\{ \begin{array}{c} \omega \\ \omega_0 \end{array} \right\} \sqrt{\frac{L}{g}} \tag{4.3}$$

and these are related to each other through $\tau = \omega^* Fr$. Physically τ is the ratio of boat speed to two-dimensional wave speed (a large value of τ means the waves left behind the boat due to its oscillations will be confined to a narrow wedge), while $\frac{(\omega^*)^2}{2\pi}$ is the ratio of boat length to two-dimensional wave length.

Using these dimensionless variables the encounter frequency relation can be written as

$$\omega^* = \omega_0^* + Fr\,(\omega_0^*)^2 \tag{4.4}$$

or

$$\tau = \tau_0 + \tau_0^2, \tag{4.5}$$

from which

$$\tau_0 = \frac{1}{2}\left(\sqrt{1+4\tau} - 1\right). \tag{4.6}$$

Details of assumptions

Most assumptions relate directly to the propagated waves themselves. These waves are traditionally separated into *radiated* waves (the waves produced in otherwise calm water by the oscillating hull) and *diffracted* waves (the waves produced by the diffraction of the incident waves on a restrained hull), and it is convenient for this analysis to retain the distinction. The radiated waves should be viewed in a moving reference frame, and therefore have the same frequency as the boat oscillations, which is the wave encounter frequency, while the diffracted waves should be viewed in a stationary reference frame (as Newman [72] states, "the axial motion of a slender cylindrical body in an inviscid fluid has no effect on the inner flow except near the ends.") and therefore have the same frequency as the incident waves[1].

[1] Newman [72] (p.370) states "The only difference between the boundary-value problems for the functions Ψ_j [his sectional diffraction potential] and the corresponding forced-motion potentials Φ_j is that the frequency of encounter ω appears in (97) [the free surface boundary condition for Φ], whereas the incident wave frequency ω_0 appears in (115) [the free surface boundary condition for Ψ]. [Note that Newman, at this point, has ignored the exponential decay term in the hull boundary condition as a difference because he has excluded this term on the grounds that it is not of leading order.] *Thus the potentials Ψ_j can be regarded as forced-motion potentials, with oscillation occurring at the incident wave frequency ω_0, as measured in a fixed reference frame.* [Newman's emphasis.]" Newman subsequently points out (pp.371–373) that this is one of several ambiguities in the exciting

The fluid problem associated with ship motion calculations is for practical purposes specified by Laplace's equation, the free surface boundary condition, and the body boundary condition. (The equation of motion of the boat only enters when radiation and diffraction fields are combined, and a valid far field fluid boundary condition exists in the usual formulations).

The body boundary is known, therefore its boundary condition can always be completely and explicitly specified in a strip theory sense. On the other hand in any strip theory solution the x derivative in Laplace's equation will by definition always be missing.

Assuming linearisation of the free surface boundary on the basis of small amplitude waves to be valid, the free surface boundary condition is $\frac{\partial^2\phi}{\partial t^2} + g\frac{\partial\phi}{\partial z} = 0$, or $-\omega^2\phi + g\frac{\partial\phi}{\partial z} = 0$ in a fixed reference frame, and $\left(\frac{\partial}{\partial t} - U\frac{\partial}{\partial x}\right)^2\phi + g\frac{\partial\phi}{\partial z} = 0$ or $\left(i\omega + U\frac{\partial}{\partial x}\right)^2\phi + g\frac{\partial\phi}{\partial z} = 0$ in a moving reference frame, thus longitudinal changes only appears in the free surface boundary condition in a moving reference frame. In treating cross sections in isolation (as is usual in a strip theory[2]) it is not possible to include longitudinal terms in the free surface boundary condition, and the moving reference frame form, which should be used in traditional strip theories, is approximated as the fixed reference frame one.

It is worth noting that, as shown by the absence of terms dependent on x in the fixed reference frame linearised free surface boundary condition, it is Laplace's equation that makes the wave pattern intrinsically three-dimensional. The free surface boundary condition only creates three-dimensional waves through its interaction with Laplace's equation. An obvious illustration of this point is the lack of transverse waves in strip theories. Therefore in deciding whether a strip theory is appropriate in general, and a conventional frequency domain strip theory in particular, one must address two questions:

- When is it valid to ignore $\frac{\partial^2\phi}{\partial x^2}$ in Laplace's equation?
- When is it further valid to ignore $U\frac{\partial}{\partial x}$ terms in the moving reference frame free surface boundary condition?

Only the first of these needs to be addressed in a fixed reference frame formulation (as used in traditional strip theory).

Validity of a two-dimensional Laplace's equation

A physical interpretation of the first question may be gained from the orientation of the wave crests. In general if the waves are long crested and parallel with the hull then neglect of the $\frac{\partial^2}{\partial x^2}$ terms is probably reasonable.

force problem, and that Salvesen, Tuck and Faltinsen [84], as a consequence of the assumption $k = O\left(\varepsilon^{-1}\right)$ as opposed to $O\left(\varepsilon^{-1/2}\right)$, and using the Haskind relations (Newman, equation (6.172)), express the exciting force in terms of the forced-motion potentials, hence it becomes a function of ω rather than ω_0. However if $k = O\left(\varepsilon^{-1}\right)$ then the exciting force is negligible due to cancellation of phase along the hull length. I therefore subscribe to Newman's view of the problem.

[2]But not essential. See the discussion in section 4.3.

Some three-dimensional effects are obviously due to the variation of the hull cross section along the vessel length, and therefore the first important assumption is that this variation is small. This may be expressed mathematically by saying that hull slope in the x direction is much smaller than in the y or z directions. It is usual however to infer that this will be the case (at least for any realistic hull form) if the vessel is *slender*, i.e. that

$$\frac{\max(B,T)}{L} \ll 1 \tag{4.7}$$

where B = beam, T = draught, L = length (since we are considering only orders of magnitude it is immaterial whether these are nominal or actual values). This assumption breaks down near the bow and stern, but provided the hull is long compared with its cross section dimensions errors will be confined to the ends and will not significantly affect global forces and motions.

Consideration of end effects on the desired two-dimensionality of the generated waves requires in addition to slenderness that $\lambda \ll L$, or

$$\omega^* \gg \sqrt{2\pi} \simeq 2.5. \tag{4.8}$$

On the other hand in defence of strip theory the following observations can be made:

- For high speed vessels a clean separation of the flow off the transom effectively extends the length of the hull, displacing any three-dimensionality some distance away from the stern.
- Near the bow the hull section is usually very fine and fullness is gradually introduced. This will to some extent minimise the influence of errors due to poor prediction of the flow field near the bow when $\tau > \frac{1}{4}$. This will be discussed in more detail below.
- At long wavelengths the hydrodynamic forces are not dominant, and if the vessel is not near one of its resonant frequencies (where the wave or damping force, in spite of being small, is significant) then one usually gets good predictions anyway.

A further violation of the two-dimensional Laplace equation is at the transition from a subcritical to a supercritical wave pattern in the vicinity of $\tau = \frac{1}{4}$, where the linear three-dimensional wave radiation problem may become singular[3], as shown clearly in the numerical results of Sclavounos [86] and analytical results of Havelock [37]. The wave profile for this value of τ is highly three-dimensional, in particular with a leading front perpendicular to the direction of motion (obviously impossible to represent two-dimensionally in a transverse strip). Although the infinities would be smoothed over for real flows, mainly due to non-linearities, a strip theory is nevertheless inadequate in representing the situation accurately. We must therefore require

[3]The singularity always exists for a point source, but it has been shown [60] that the solution remains finite for some shiplike forms.

τ	$\mathbf{Fr}_{\min}$
0	.40
.25	.33
.5	.29
1	.25
2	.20

Table 4.1: Limiting Froude number for transverse wavelength to be longer than hull length

either

$$\tau \ll \frac{1}{4} \tag{4.9}$$

$$\text{or} \quad \tau \gg \frac{1}{4}. \tag{4.10}$$

The latter of these is not applicable however to traditional frequency domain strip theories, where it is assumed waves propagate infinitely in both lateral directions from each cross section. This contradicts the reality that for $\tau > \frac{1}{4}$ generated waves are confined to a narrow wedge, therefore near the bow in particular waves exist only a very small distance away from the hull. This point also follows from the discussion of the moving reference frame free surface boundary condition below.

Finally, the transverse wave system associated with a translating oscillating body is another example of waves not parallel with the hull. This will always be present, but it could be argued that the transverse waves will not significantly affect the hull forces and moments where its wavelength is long compared with the hull length[4]. This wavelength can not be predicted using two-dimensional analysis, however Becker [7] (in his Figure 11) plots its length (designated λ_1) as a function of τ, showing $\frac{\lambda_1}{U^2/g} = 2\pi\left(\frac{\tau+1/2-\sqrt{\tau+1/4}}{\tau^2}\right) \leq 2\pi$ always, from which it can be inferred that the requirement $\lambda_1 \geq L$ may be interpreted as

$$Fr \gg \frac{1}{\sqrt{2\pi}} \simeq 0.4. \tag{4.11}$$

(Note that this is necessary but not sufficient, table 4.1 shows Froude number limits for various τ.) Alternatively for a given Froude number there is a minimum τ, hence minimum ω^*.

Validity of the two-dimensional or fixed reference frame free surface boundary condition in a moving reference frame

Traditional periodic strip theory generally assumes a solution to the radiation problem of the form $\phi = A(x)\,\phi_0(y,z)$, where A is a function of both the cross section shape and the local heave motion, and ϕ_0, except for a local disturbance near the hull, is periodic in y with wavenumber

[4]One could argue on the other hand that any neglected wave system is a potential additional source of damping.

k. The requirement that $\left|U\frac{\partial\phi}{\partial x}\right| \ll |i\omega\phi|$ leads to the conclusion

$$\frac{U}{\omega}\frac{\frac{\partial A}{\partial x}}{A} \ll 1.$$

Ignoring cross section variation (which has been dealt with above in terms of slenderness), $\frac{\frac{\partial A}{\partial x}}{A} = \frac{\text{pitch}}{\text{local heave}}$. If dimensionless heave and dimensionless pitch are of the same order (where heave is normalised by the wave height H_w, and pitch by kH_w) this is approximately k. Putting $k = \frac{\omega^2}{g}$ gives $\frac{Uk}{\omega} = \tau \ll 1$, which basically restricts us to

$$\tau < \frac{1}{4}. \tag{4.12}$$

Since we cannot arbitrarily prescribe ω if we wish to investigate vessel response around its natural frequencies this confines the theory to low Froude numbers. Unfortunatelly this contradicts the restriction above relating to the transverse wave system.

Note also that we have assumed dimensionless heave and pitch to be of the same order, in other words if the motion is predominantly pitch this restriction needs to be more severe, but it may be less severe if motion is predominantly heave. The lesser applicability to pitch motion is a point noted above in reference to the two-dimensional Laplace's equation.

The diffraction problem, if it is viewed in a fixed reference frame (as advocated above), does not need to be considered, as there is no approximation to the (linear) free surface boundary condition. If it is viewed in a moving reference frame (as for example in the Salvesen, Tuck and Faltinsen theory [84]) then it has an assumed strip theories form of $\phi = e^{ik_0x}\phi_0(y,z)$, ($\phi_0$ also periodic in y with wavenumber k). Thus $Uk_0 \ll \omega = \omega_0 + Uk_0$, or (dividing by ω_0) $\tau_0 \ll 1 + \tau_0$, hence $\tau_0 \ll 1$, or again

$$\tau_0 < \frac{1}{4}. \tag{4.13}$$

The diffraction problem is less of a concern however, due to the ambiguity noted concerning its representation and to the fact that (for head seas) $\tau_0 < \tau$ (and for small τ_0 the two are similar). Most significantly however Magee and Beck [64] have shown that for at least several typical hull forms at low to moderate speeds (maximum Froude number of 0.3) the diffraction force is only a small component of the total incident wave force, which is dominated by the Froude-Krylov component.

Summary

In summary, for traditional strip theory some of these requirements contradict, and general opinion seems to be that the most important restriction is low froude number, followed by high frequency. Faltinsen [27] cautions against the use of (conventional) strip theory for $Fr \geq 0.4$. The fact that it can produce good results for Froude numbers even as high as that is more good fortune that anything else, but conversely it is generally regarded as poor at predicting local hull hydrodynamic forces. (This is discussed in more detail in section 4.3.) A fixed reference

frame theory can operate at moderate or even high speeds subject only to the restriction that $\omega^* \gg \sqrt{2\pi}$.

Finally one must also be aware that strip theories in general do not properly take into account the interaction of the steady wave system with the oscillatory one. (Exceptions are discussed in section 4.3.)

4.2 Conventional strip theory (frequency domain)

The original object of strip theory was to provide a method for predicting in a simple way the motions of a vessel in waves. This motion is a result of the hydrodynamic forces arising from the interaction of the hull and the waves. The simplification was achieved by slicing the boat into two-dimensional cross sections, or *strips*, justified on the assumptions listed in section 4.1.2, and representing the forces in terms of coefficients that could be derived or obtained experimentally for these two-dimensional sections. Thus a three-dimensional problem was approximated by a set of two-dimensional problems, a substantially easier task than undertaking the solution of the fully three-dimensional problem.

The original theory was proposed by Korvin-Kroukovsky and Jacobs [54]. Some of the terms in the equations were not correctly derived in this original theory, but were corrected in the now standard theory of Salvesen, Tuck and Faltinsen [84].

The following outline of the calculation of hydrodynamic forces is based on Newman [72] (section 7.7), which in turn is based on the theory of Salvesen, Tuck and Faltinsen [84]. To begin with we will make no assumptions about slenderness or small motions, but introduce these assumptions where they are required. Recalling from above, the coordinate system used has x towards the bow, y to port, and z upwards, hence heave is upwards and pitch is bow down. This differs from Newman [72], causing a difference of sign in some terms, but is the one adopted by the majority of researchers in the field (including Newman in some later works).

The forces and moments acting on a slender hull are a result of integrating pressures over the wetted hull surface. In particular *heaving* forces and *pitching* moments can be obtained by integrating the *vertical* components of pressure over the hull. (More generally $n_z x$ should be replaced with $(n_z x - n_x z)$, in equation (4.15) below, but for slender hulls $n_x z \ll n_z x$.) Here we are interested mainly in the hydrodynamic component of pressure since the hydrostatic component integrates to give the instantaneous buoyancy force and is a comparatively trivial exercise. If the flow field is represented by the potential function $\phi(x, y, z, t)$ then, ignoring the hydrostatic term, the pressure is given by the Bernoulli equation as $p = -\rho\left(\frac{\partial \phi}{\partial t} + \frac{1}{2}\nabla\phi \cdot \nabla\phi\right)$, hence

$$F_z = -\rho \iint_{hull} \left(\frac{\partial \phi}{\partial t} + \frac{1}{2}\nabla\phi \cdot \nabla\phi\right) n_z \, dl \, dx \tag{4.14}$$

$$M_y = \rho \iint_{hull} \left(\frac{\partial \phi}{\partial t} + \frac{1}{2}\nabla\phi \cdot \nabla\phi\right) n_z x \, dl \, dx. \tag{4.15}$$

Here n_z is the vertical component of the local hull unit normal vector pointing out of the fluid, which for slender hulls may be approximated to the unit normal in the cross section plane. Also l is a parameter representing distance in the girthwise direction on the hull around a given cross section of constant x, and the surface of integration *hull* is understood to mean the instantaneous wetted hull. At this stage, assuming that the three-dimensional potential (including the wave resistance effects of the forward motion of the boat) and the wetted hull boundary can be determined, there is no approximation beyond the assumption of inviscid flow.

Let us now assume that motions are small, allowing two significant simplifications. First, by assuming infinitesimal motions and waves we can reinterpret the surface of integration *hull* to be the portion of hull below the calm water line, making it a fixed surface. Second, the quantity $\frac{1}{2}\nabla\phi \cdot \nabla\phi$ will be of second order compared with $\frac{\partial\phi}{\partial t}$ and can be ignored.

To obtain a frequency domain solution it is necessary to change the reference frame to one moving with the boat. Only then can the motion be considered periodic. Redefining the potential function, if the boat is moving with constant forward speed U then $\phi_m(x_m, y, z, t) = \phi_f(x_f, y, z, t)$, where subscripts m and f refer respectively to the moving and fixed reference frames and $x_m = x_f - Ut$. We must also replace $\frac{\partial}{\partial t}$ wherever it occurs with $\left(\frac{\partial}{\partial t} - U\frac{\partial}{\partial x}\right)$ whenever taking the time derivative at a fixed position of a function expressed in its moving reference frame form.

With both the small motion and the moving reference frame modifications the hydrodynamic forces are now

$$F_z = -\rho \iint_{hull} \left(\frac{\partial\phi}{\partial t} - U\frac{\partial\phi}{\partial x}\right) n_z \, dl \, dx \tag{4.16}$$

$$M_y = \rho \iint_{hull} \left(\frac{\partial\phi}{\partial t} - U\frac{\partial\phi}{\partial x}\right) n_z x \, dl \, dx. \tag{4.17}$$

The x derivatives can be eliminated by integration (the moment expression must be integrated by parts), i.e. $\int \frac{\partial\phi}{\partial x} dx = \phi$ and $\int x\frac{\partial\phi}{\partial x} dx = x\phi - \int \phi \, dx$, giving expressions for hydrodynamic forces on the hull as

$$\begin{aligned} \frac{-F_z}{\rho} &= \iint_{hull} \frac{\partial\phi}{\partial t} n_z \, dl \, dx - U\left[\int_{section} \phi n_z \, dl\right]_{stern}^{bow} \\ \frac{M_y}{\rho} &= \iint_{hull} x\frac{\partial\phi}{\partial t} n_z \, dl \, dx - U\left(\left[x\int_{section} \phi n_z \, dl\right]_{stern}^{bow} - \iint_{hull} \phi n_z \, dl \, dx\right) \end{aligned}$$

Simplifying the notation and assuming that the cross section vanishes at the bow but not necessarily at the stern we may rewrite these as

$$F_z = -\rho\left\{\int_{stern}^{bow} p \, dx + UP^A\right\} \tag{4.18}$$

$$M_y = \rho\left\{\int_{stern}^{bow} (xp + UP) \, dx + Ux^A P^A\right\} \tag{4.19}$$

where

$$p = \int_{section} \frac{\partial\phi}{\partial t} n_z dl, \quad P = \int_{section} \phi n_z dl \tag{4.20}$$

and the superscript ^{A} refers to the aft or stern section.

Up to this point the periodicity of the motion has deliberately been ignored in order to represent the equations in a form suitable for adaptation to the time domain in the next section.

The next step is to decompose ϕ into two sets of components, one independent of the boat motion and the other dependent on it, allowing, in the case of sinusoidal motion, isolation of the boat motions in the equations of motion so that an explicit solution may be obtained. That is we can consider the potential to be the sum of effects due to the forced oscillation of the boat with steady forward speed in calm water and due to the incident wave acting on a forward moving boat restrained from oscillation. Recall that the small amplitude assumption means that the problem is linear, and we can add and subtract the various solutions for the components of ϕ.

Let the generalised vessel displacement amplitudes be ξ_i, where $i = 1, 2, 3$ correspond to displacements in the x, y, z directions and $i = 4, 5, 6$ correspond to rotations about the x, y, z axes, then the vessel heave displacement amplitude is ξ_3 and vessel pitch amplitude is ξ_5. We can also define a generalised force in the same manner, giving for the heave force and pitching moment amplitudes respectively F_3 and F_5, indicating the components due to the boat motion as $F_3(\xi_3, \xi_5)$ and $F_5(\xi_3, \xi_5)$, and the components due to the wave action on the fixed hull (independent of the ξ_i's) as $F_{3,W}$ and $F_{5,W}$. Note that in addition to the hydrodynamic components defined in equations (4.18) and (4.19) these forces also contain hydrostatic components due to the changing hull immersion. By considering sinusoidal waves and motions at an encounter frequency ω the equations of motion after decomposing ϕ can be written as

$$\begin{aligned} e^{i\omega t}\left[F_{3,W} + F_3(\xi_3, \xi_5)\right] &= -\omega^2 e^{i\omega t} M \xi_3 \\ e^{i\omega t}\left[F_{3,W} + F_5(\xi_3, \xi_5)\right] &= -\omega^2 e^{i\omega t} I_5 \xi_5 \end{aligned}$$

where M and I_5 are the mass and the pitch moment of inertia of the boat, it is assumed that the coordinate system has its origin in the waterplane horizontally aligned with the centre of mass (the vertical shift is for convenience only and for slender vessels has negligible effect on the equations of motion and calculation of forces) eliminating the products of inertia $I_{5,3}$ and $I_{3,5}$, all quantities except M and I_5 are time complex (allowing for arbitrary phase), and the real parts of the equations are to be assumed. Note that ω is the frequency at which the boat oscillates, which must equal the frequency at which waves are encountered in the moving reference frame (the *encounter frequency*), and for head seas we recall from section 4.1.2 that it is related to the wave frequency in a stationary reference frame, ω_0, by $\omega = \omega_0 + Uk_0$ where $k_0 = \frac{\omega_0^2}{g}$ in deep water. The forces $F_3(\xi_3, \xi_5)$ and $F_3(\xi_3, \xi_5)$ are linear functions of the ξ_i's and can therefore be expressed as the product of the forces resulting from motions of unit amplitude and the motion amplitudes (i.e. $F_i(\xi_3, \xi_5) = \frac{\partial F_i}{\partial \xi_3}\xi_3 + \frac{\partial F_i}{\partial \xi_5}\xi_5$). Dividing by $e^{i\omega t}$ and rearranging gives

$$\begin{bmatrix} -\omega^2 M - \frac{\partial F_3(\xi_3,\xi_5)}{\partial \xi_3} & -\frac{\partial F_3(\xi_3,\xi_5)}{\partial \xi_5} \\ -\frac{\partial F_5(\xi_3,\xi_5)}{\partial \xi_3} & -\omega^2 I_5 - \frac{\partial F_5(\xi_3,\xi_5)}{\partial \xi_5} \end{bmatrix} \begin{Bmatrix} \xi_3 \\ \xi_5 \end{Bmatrix} = \begin{Bmatrix} F_{3,W} \\ F_{5,W} \end{Bmatrix}. \tag{4.21}$$

Once the forces are evaluated (the main task in solving the problem) it then requires only a simple matrix inversion to complete the solution.

We can consider sinusoidal waves without any loss of generality since any time response can be represented as a Fourier spectrum and the assumed linearity of the problem allows us to add the various frequency components.

As an illustrative exercise let us focus our attention on the components of ϕ due to the boat motions. These can be represented in terms of added mass, $A_{i,j}$, and damping, $B_{i,j}$. The subscripts i, j mean the force in the ith direction due to motion in the jth direction. Conceptually the added mass is so named because it is the component of the force with a phase difference from the motions of π (in phase with the acceleration), and it can be thought of as the inertia of the water surrounding the hull but moving with it. The damping force is the force component with a $\frac{\pi}{2}$ phase difference from the boat motion (in phase with the velocity) and this represents the radiating energy in the outgoing wave system generated by the oscillating boat. The added mass and damping are derived from the forces for a unit amplitude boat motion. There is also an in-phase component which is the hydrostatic force due to a unit change in hull immersion, but its calculation is trivial by comparison and requires no detailed explanation.

The equations of motion (4.21) can now be expressed as

$$\left(-\omega^2 \left(A_{3,3} + M\right) + i\omega B_{3,3} + C_{3,3}\right) \xi_3 + \left(-\omega^2 A_{3,5} + i\omega B_{3,5} + C_{3,5}\right) \xi_5 = F_{3,W} \quad (4.22)$$

$$\left(-\omega^2 A_{5,3} + i\omega B_{5,3} + C_{5,3}\right) \xi_3 + \left(-\omega^2 \left(A_{5,5} + I_5\right) + i\omega B_{5,5} + C_{5,5}\right) \xi_5 = F_{5,W} \quad (4.23)$$

where $C_{i,j}$ are the hydrostatic stiffness terms mentioned above. Recall that the quantities ξ_i and $F_{j,W}$ will be time complex.

At this stage we shall invoke the slenderness assumption. This means that we assume the maximum hull cross section dimension to be small compared with the hull length, and that cross section properties and ϕ vary slowly in the x direction. This assumption is quite consistent with typical hull geometries with perhaps the exception of the sudden area reduction at the stern. Salvesen, Tuck and Faltinsen [84] point out in defence of this criticism that at higher speeds the flow separates from the stern and does not have any sudden jumps, and more importantly that the computed results agree best with the transom terms included. As a consequence we can now treat ϕ as a set of potentials defining the two-dimensional flow fields in planes of constant x around cross sectional slices of the hull.

Looking now at individual strips we can derive heave sectional added mass and damping coefficients, a and b, from the sectional forces (equation (4.20)) and using equations (4.18) and (4.19) combine these to give the added mass and damping coefficients, $A_{i,j}$ and $B_{i,j}$, for the whole hull.

As well as the free surface boundary condition the potential in each strip must satisfy a condition of compatibility of normal velocities between the fluid and hull in a fixed reference

frame, i.e. if η is the vertical displacement of the cross section of interest then

$$\frac{\partial \phi}{\partial n} = \left(\frac{\partial \eta}{\partial t} - U \frac{\partial \eta}{\partial x} \right) n_z. \tag{4.24}$$

For a section located at x the local heave displacement is related to the boat heave and pitch by

$$\eta = e^{i\omega t} \left(\xi_3 - x\xi_5 \right)$$

recalling that the ξ_i's may be complex and the real part of η is assumed. Thus if we assume $n_x \ll 1$ (hence $\frac{\partial \eta}{\partial n} = \xi_5 e^{i\omega t} n_x$ can be ignored) it can easily be shown that equation (4.24) is satisfied by

$$\begin{aligned} \phi &= \left(\frac{\partial}{\partial t} - U \frac{\partial}{\partial x} \right) \left[e^{i\omega t} \left(\xi_3 - x\xi_5 \right) \right] \phi_0 \\ &= i\omega \left(\xi_3 - \xi_5 \left(x - \frac{U}{i\omega} \right) \right) e^{i\omega t} \phi_0 \end{aligned} \tag{4.25}$$

where the derivative of ϕ_0 in the direction normal to the hull satisfies

$$\frac{\partial \phi_0}{\partial n} = n_z \tag{4.26}$$

on the hull surface. The second form of (4.25) is preferred since we need eventually to separate the contributions from ξ_3 and ξ_5 before using equations (4.22) and (4.23). Defining now the sectional added mass and damping coefficients for heave, a and b respectively, as

$$a + \frac{b}{i\omega} = Z\left(x, \omega\right) = \rho \int_{section} \phi_0 n_z \, dl \tag{4.27}$$

we obtain from (4.20), (4.25) and (4.27) that

$$P = \frac{e^{i\omega t}}{\rho} \left(\xi_3 - \xi_5 \left(x - \frac{U}{i\omega} \right) \right) i\omega Z \tag{4.28}$$

and

$$p = i\omega P = -\frac{e^{i\omega t}}{\rho} \left(\xi_3 - \xi_5 \left(x - \frac{U}{i\omega} \right) \right) \omega^2 Z. \tag{4.29}$$

Substituting these expressions for p and P into equations (4.18) and (4.19) gives the hull added mass and damping coefficients in the form analogous to Newman's equations (7.106 and 7.107) [72], (note that Newman assumes the terms UP^A and $Ux^A P^A$ to be zero, and also has an error in the sign of $\frac{U^2}{\omega^2}$ in the moment expression, noted also in [73])

$$\frac{F_3}{e^{i\omega t}} = \omega^2 \int_{stern}^{bow} \left(\xi_3 - \xi_5 \left(x - \frac{U}{i\omega} \right) \right) Z \, dx - i\omega U Z^A \left(\xi_3 - \xi_5 \left(x^A - \frac{U}{i\omega} \right) \right) \tag{4.30}$$

$$\begin{aligned} \frac{F_5}{e^{i\omega t}} &= -\omega^2 \int_{stern}^{bow} \left[\xi_3 \left(x + \frac{U}{i\omega} \right) - \xi_5 \left(x^2 + \frac{U^2}{\omega^2} \right) \right] Z \, dx \\ &\quad + i\omega U x^A Z^A \left(\xi_3 - \xi_5 \left(x^A - \frac{U}{i\omega} \right) \right). \end{aligned} \tag{4.31}$$

We can write the hull added mass and damping coefficients for pitch and heave as

$$A_{i,j} = -\operatorname{Re}\left\{ \frac{\frac{\partial F_i}{\partial \xi_j}}{-\omega^2 e^{i\omega t}} \right\}, \quad B_{i,j} = -\operatorname{Re}\left\{ \frac{\frac{\partial F_i}{\partial \xi_j}}{i\omega e^{i\omega t}} \right\}. \tag{4.32}$$

This follows directly from comparing equations (4.22) and (4.23) with (4.21).

Taking the components defined by (4.32) of the forces given by the equations (4.30) and (4.31) and recalling that $Z = a + \frac{b}{i\omega}$ we obtain the added mass and damping coefficients in the form in which they are normally expressed:

$$A_{3,3} = \int a\, dx - \frac{U}{\omega^2} b^A \tag{4.33}$$

$$A_{3,5} = -\int \left(ax + \frac{bU}{\omega^2} \right) dx - \frac{U}{\omega^2} \left(a^A U - b^A x^A \right) \tag{4.34}$$

$$A_{5,3} = -\int \left(ax - \frac{bU}{\omega^2} \right) dx + \frac{U}{\omega^2} b^A x^A \tag{4.35}$$

$$A_{5,5} = \int a \left(x^2 + \frac{U^2}{\omega^2} \right) dx + \frac{U x^A}{\omega^2} \left(a^A U - b^A x^A \right) \tag{4.36}$$

$$B_{3,3} = \int b\, dx + U a^A \tag{4.37}$$

$$B_{3,5} = -\int (bx - aU)\, dx - U \left(a^A x^A + \frac{b^A U}{\omega^2} \right) \tag{4.38}$$

$$B_{5,3} = -\int (bx + aU)\, dx - U a^A x^A \tag{4.39}$$

$$B_{5,5} = \int b \left(x^2 + \frac{U^2}{\omega^2} \right) dx + U x^A \left(a^A x^A + \frac{b^A U}{\omega^2} \right) \tag{4.40}$$

where all integrals are from the stern to the bow (in practice these would be integrated numerically by summing the section coefficients).

It should be pointed out that we have so far neglected how to obtain the coefficients a and b (or the equivalent problem of obtaining ϕ_0). Although this is very much a related problem it is not part of the theory since several legitimate methods of evaluating these coefficients exist, including experimentation. If one wishes to obtain a purely mathematical solution one must use methods such as finite elements, finite differences, or boundary elements (panel methods and Frank close fit) for arbitrary shapes; or, for particular families of shapes, analytic solutions (such as Lewis forms, whose hydrodynamic properties can be obtained from conformal mapping of the floating semi-circle solution, for example Ursell's solution for heave [92]). The present work makes use of panel methods, and these were discussed in the previous two chapters.

In order to obtain numerical solutions for a and b by any method we need as well as the body boundary condition (4.26) a free surface boundary condition, a point that has been neglected until now. This boundary condition, ignoring non-linear terms, is derived by combining the dynamic condition that the pressure (for small amplitude waves) is hydrostatic, i.e. $\frac{\partial \phi}{\partial t} = \rho g \eta$ on $z = 0$ (where η is the wave height), and the kinematic condition that the vertical water velocity at the water surface is equal to the rate of change of wave height, i.e. $\frac{\partial \eta}{\partial t} = \frac{\partial \phi}{\partial z}$ on $z = 0$. Eliminating η one obtains

$$\frac{\partial^2 \phi}{\partial t^2} + g \frac{\partial \phi}{\partial z} = 0 \quad \text{on} \quad z = 0 \tag{4.41}$$

in a fixed reference frame, or

$$\left(\frac{\partial}{\partial t} - U \frac{\partial}{\partial x} \right)^2 \phi + g \frac{\partial \phi}{\partial z} = \frac{\partial^2 \phi}{\partial t^2} - 2U \frac{\partial^2 \phi}{\partial t \partial x} + U^2 \frac{\partial^2 \phi}{\partial x^2} + g \frac{\partial \phi}{\partial z} = 0 \quad \text{on} \quad z = 0. \tag{4.42}$$

in a moving reference frame. The second of these can not ever be satisfied in a two-dimensional formulation if strips are considered in isolation to each other, and generally (4.41) is taken to adequately represent the required boundary condition[5]. The validity of this approach has been discussed in section 4.1.2. In fact, as pointed out by Newman [72], consistency should require that all terms involving $\frac{U}{\omega}$ in the coefficients given in equations (4.33)–(4.40) should be discarded. Consistent higher order theories in a moving reference frame have been derived (for example [77]), but, with the exception of cross coupling coefficients, the neglected higher order effects tend to cancel. These theories, because of the additional complexity, are not extensively used.

To complete the analysis we need to evaluate the wave forces. The wave forces are made up of Froude-Krylov (or Kriloff) forces and diffraction forces, the latter of which is calculated in a manner very similar to that of the calculation of the forces due to the boat motion, except that the body boundary condition required for the calculation of the potential field differs slightly. The result is a set of coefficients similar to the added mass and damping coefficients, but referred to as the *Smith-weighted added mass and damping coefficients*. This will be described in more detail after an explanation of the Froude-Krylov force.

The Froude-Krylov forces are the dynamic pressure forces that would exist on a hypothetical surface identical to the hull surface in the wave field but in the absence of the hull. These can be computed using the pressure field under a regular wave, which in a moving coordinate system for a unit wave amplitude in head seas (ignoring hydrostatic and non-linear terms) is

$$p = -\rho\left(\frac{\partial\phi}{\partial t} - U\frac{\partial\phi}{\partial x}\right) = -\rho\left(\frac{\partial}{\partial t} - U\frac{\partial}{\partial x}\right)\left[\frac{ig}{\omega_0}e^{k_0 z + i(k_0 x + \omega t)}\right] = \rho g e^{k_0 z + i(k_0 x + \omega t)}. \qquad (4.43)$$

(This can be generalised to include waves other than head seas by replacing x with $-(x\cos\theta + y\sin\theta)$ where θ ($= \pi$ for head seas) is the direction of propagation of the incident waves measured from the x axis in the direction of the y axis. The relationship between the wave and encounter frequencies will also change to $\omega = \omega_0 - k_0 U\cos\theta$) Note that z is negative so this pressure decays exponentially with depth.

The Froude-Krylov force is not on its own equal to the dynamic wave force since the fluid velocities under a regular wave in the absence of the boat hull violate the body boundary condition

$$\frac{\partial\phi}{\partial n} = 0 \quad \text{on the hull surface, in the moving reference frame.} \qquad (4.44)$$

(Recall that in calculating the wave forces we assume the boat not to be oscillating.) This can be remedied by adding to the Froude-Krylov force the force from the pressure field resulting from the diffracted wave potential. The diffraction potential then is the potential field which

[5]This approximation is somewhat analogous to interpreting the strips as being made up of a half plane on each side of the boat, each of which is not perpendicular to the x axis but angled backwards at an angle whose tangent is the ratio of boat velocity to wave velocity. The time domain strip theory, as we will see later, is able to address this problem.

when superimposed on the incident wave potential must satisfy (4.44), or

$$\frac{\partial \phi_{\text{Diffraction}}}{\partial n} = -\frac{\partial \phi_{\text{Incident wave}}}{\partial n}$$

in a reference frame moving with the boat. Putting $\frac{\partial \phi}{\partial n} = \frac{\partial \phi}{\partial z} n_z + \frac{\partial \phi}{\partial x} n_x \simeq \frac{\partial \phi}{\partial z} n_z$ (since due to the slenderness assumption $n_x \simeq 0$)

$$\frac{\partial \phi_{\text{Diffraction}}}{\partial n} = \frac{\partial}{\partial z}\left[\frac{ig}{\omega_0} e^{k_0 z + i(k_0 x + \omega t)}\right] n_z = -i\omega_0 e^{k_0 z + i(k_0 x + \omega t)} n_z. \tag{4.45}$$

This is analogous to the potential problem defined by equation (4.26) except that the exponential decay of the velocities must be taken into account (rather like stretching and contracting the hull section at the wave frequency in the vertical direction by an amount that decays exponentially with depth, and then solving as before). For wavelengths that are large compared with the maximum draught the term $e^{k_0 z} \simeq 1$, and the Smith-weighted sectional added mass and damping coefficients become identical to the ordinary added mass and damping coefficients except that the encounter frequency must be replaced with the wave frequency. Details are given in Newman p368ff [72].

The hull coefficients for the diffraction force are derived from the section coefficients in a manner analogous to the $A_{i,j}$'s and $B_{i,j}$'s (equations (4.33)–(4.40)), noting that phase for the wave force is a function of x.

4.3 Other strip theories

4.3.1 Overview

Although considerable progress has been made on numerical solutions to the three-dimensional unsteady flow problem (see for example Nakos and Sclavounos [70]; Beck and others [4], [5], [3], [6]; Zhu and Katory [107]) there is still a place for strip theories. They are simpler to program and quicker to run, and in many situations give satisfactory or even good results. Also, there still remain many unsolved problems and features that are impractical to implement with currently available computing resources in the three-dimensional theories. Nevertheless, because the approximations involved in strip theories rely on certain assumptions that may not be valid for a particular boat, they are not universally applicable.

The limited applicability of conventional strip theory, particularly in representing unconventional ships, leaves much scope for theories intermediate between it and fully three-dimensional theories. These limitations relate to the assumptions described in section 4.1.2, and can be summarised as short wavelength (or high frequency), slow speed, and slender hull form. Various strip or strip-like[6] theories have been proposed to overcome one or more of the first two of

[6] By 'strip-like' it is meant a theory that is only partly two-dimensional, usually in the description of flow near the hull, and this is matched to a three dimensional description of the far-field flow. Such theories are sometimes also referred to as $2\frac{1}{2}$-dimensional theories. These are the "slender hull, any λ" theories in table 4.2.

these limitations, but essentially a three-dimensional theory is required to represent validly a non-slender hull. Table 4.2 shows some examples of important contributions in this area, their relation to each other, and the particular restrictions of conventional strip theory that they seek to overcome. Each of these theories (except that of Salvesen, Tuck and Faltinsen, which was described in section 4.2) will be briefly discussed below. A separate row in table 4.2 for *high Froude number with steady interaction* has been included because of the importance many authors place on it. It is an extension of the basic high Froude number problem, but obviously becomes more important as the hull becomes less slender.

In addition to the broad categories suggested in table 4.2 one may wish to address more specific issues, such as non-linearities, or the question of frequency or time domain. Choices regarding many of these issues are already implicit in the method used. For example the *low Froude number* theories are frequency domain theories[7], and do not include any non-linear effects. However the *high Froude number with steady interaction* theories preclude the use of Green functions to represent the free surface because the free surface boundary condition for the unsteady part of the solution is linearised (if at all) about the steady free surface, not the undisturbed free surface. Generally the more complete theories (i.e. as one moves to the bottom right corner of table 4.2) offer more scope for inclusion of these types of effects, but at a cost of increased complexity.

	slender hull		non-slender hull
	short λ	any λ	(any λ)
low Fr	Salvesen, Tuck and Faltinsen [84]	Newman (unified)[73]	Newman (3D) [74]
any Fr	Yeung and Kim [100]	Yeung and Kim (comprehensive) [102]	linear 3D
high (i.e. any) Fr with steady interaction	Faltinsen and Zhao [26]		Nakos and Sclavounos [70]

Table 4.2: Relationship between various strip or strip-like theories and some 3D theories

4.3.2 Limitations of standard strip theory

High speed, low frequency

Conventional strip theory (such as that of Salvesen, Tuck and Faltinsen [84]) developed initially from a need for analysing the seakeeping of conventional boats, and as such all authors agree that it is not valid for low frequencies or high speeds (although curiously many of the same authors list $Fr = O(1)$ as one of the starting assumptions). Typical comments include: "strip theory is invalid at low frequencies of encounter" [73], "This is the short wavelength theory"

[7] While they could be adapted to the time domain, there would generally be little advantage in doing so.

[102], "The conventional strip theory is deficient not only for low frequencies, but also for high speeds" [73], "Strip theories have no justification for high speed" [26], "The strip theory as described does not have any three-dimensional effects representing interactions between sections nor any forward-speed effects on the free-surface condition. It is known to be incorrect in the low frequency limit" [102].

Often cited is the inconsistency in conventional strip theory of applying forward speed corrections on the hull boundary condition but not on the free surface boundary condition, although some versions (for example Ogilvie and Tuck [77]) do contain higher order terms on the free surface. Faltinsen [28] states "for high Froude numbers unsteady 'divergent' wave systems become important. This effect is neglected in [conventional] strip theory...". By this he was probably referring in particular to the wedge shaped three-dimensional wave pattern characteristic of the case $\tau = \frac{U\omega}{g} > \frac{1}{4}$, as opposed to the infinite lateral propagation of waves of the steady state periodic solution for a two-dimensional strip. All the high speed theories presented below (sections 4.3.4, 4.3.5 and 4.3.6, as well as 4.4), by inclusion of forward speed terms in the free surface boundary condition, contain the divergent wave system that Faltinsen was referring to.

Newman [74] questions the use of forward speed corrections altogether in conventional strip theory. He gives an example where (at a Froude number of only 0.2) some of the hydrodynamic coefficients are predicted worse if the forward speed terms are omitted while an equal number are predicted better. The findings of the current research are that this is by no means an isolated occurrence. Results from the conventional strip theory program *HYDROS* presented in chapter 6 of this thesis suggest in some cases that motions at high speeds are only predicted accurately presumably because they resemble the zero speed result, but that incremental changes in the magnitude of resonant peaks as speed is increased are not necessarily in the right direction.

It is typically the coupling between heave and pitch motions that is predicted most poorly by strip theory (see for example [86], [102], [74], [11]), and given that coupling effects are introduced as a result of the hydrodynamic asymmetry caused by forward speed [32] the use of forward speed corrections must further come into question.

In spite of this Faltinsen [28] states that conventional strip theories, although theoretically questionable, are "still the most successful theories for wave-induced motions of conventional ships at forward speed." This is perhaps as much a comment on conventional ships as it is on conventional strip theories.

In relation to the low frequency limitation, Newman [73] states that conventional strip theory makes "reasonable predictions" for long wavelength and zero speed, although "An explanation of this fortunate situation is the disparity between the natural frequencies and the wave frequencies where the exciting force and moment are significant." In other words, if the encounter frequency is near or above resonance the accurate prediction of dynamic response characteristics is unimportant if the forcing is negligible, while significantly below resonance hydrostatic forces dominate and one can get away with poor estimates of added mass and damping as long as

the exciting force can be calculated with reasonable accuracy (which turns out to be possible since this is usually dominated by hydrostatic and Froude Krylov components: Gerritsma [32] states that, except for short incident waves, the diffraction force is small compared with the Froude-Krylov force, and "Even gross errors in the computed diffraction forces may be masked in the predicted total wave force."). Newman [73] also shows, by considering typical relationships between displacement, waterplane area and length, that for conventional boats "resonance will occur in combination with significant wave excitation only if the frequency of encounter is substantially greater than the wave frequency", which of course is the case only at high speeds.

In the short wavelength regime the three-dimensional wave pattern in the near field of the hull is equivalent to the strip theory solution (except perhaps near the bow and stern), as can be shown by consideration of the high frequency limit in Newman's *unified theory* (described in section 4.3.3), and strip theory in this case is entirely appropriate.

Actual estimates of limits of Froude number or dimensionless frequency for which strip theory is valid vary considerably from one author to another, and depend on the type of vessel, the information sought, and the criteria for judgement. For example Gerritsma [32] suggests $Fr < 0.4$ for reasonable predictions of damping for conventional ships, while in the same paper he cites a case where some motions were well predicted at $Fr = 1.14$. Gerritsma also investigates wavelength effects by comparing the strip theory predictions of added mass and damping distributions at zero forward speed with predictions from a three-dimensional panel method and with experimental results. He shows some significant discrepancy at a frequency of $\omega\sqrt{\frac{L}{g}} = 1.9$, but claims very little difference at higher frequencies. Generally speaking, because of cancellation of opposing errors, overall motions tend to be better predicted than individual coefficients or local forces.

Effect of steady wave pattern

Inclusion of steady wave pattern effects is considered important both at high speed ("The interaction between the unsteady and the local steady flow is important at high forward speed." [28]) and for full bodied hulls ("There is growing evidence that the influence of the steady-state velocity field is important, and the degree of completeness required to account for the steady field depends on the fullness of the ship." [74]). It is in these two situations that significant waves are generated by the steady forward motion of the ship.

Opinion differs regarding the importance of the steady wave system. Newman's [74] view is that "In the perturbation hierarchy any attempt to analyse these unsteady motions must be preceded by a solution of the basic steady-state flow", while Yeung and Kim [102] say "In as much as the steady-state potential ϕ_s is not immediately amenable to reliable numerical description even with present state-of-the art computational techniques, and that there is already considerable amount of complexity in tackling just the homogeneous equation of (2.7) alone, it is a little premature to consider the inclusion of these interactive terms at this time".

Interaction between steady and unsteady wave patterns should in particular be considered however in the calculation of added resistance in waves [28].

Steady wave effects fall into three main categories.

First is the question of linearisation of the free surface. This is only a problem in frequency domain theories, in which the steady and unsteady potentials must be solved separately. The free surface boundary condition with interaction includes cross products of the two potentials. Since the two potentials are not necessarily of the same order it is difficult to justify which, if any, of the terms should be discarded in a linerised form of the boundary condition. In a time domain theory the steady and unsteady problems can be solved simultaneously, and use of a linearised free surface boundary condition will automatically distinguish which is of higher order.

Second is the calculation of the so called 'm_j-terms' in the body boundary condition. The boundary condition on the hull for the potential corresponding to the jth mode of motion ($j = 3$ for heave and $j = 5$ for pitch) can be written in the form $\frac{\partial \phi_j}{\partial n} = i\omega n_j + U m_j$, where n_j is the jth component of the unit normal, $m_3 = -\frac{\partial^2 \phi_s}{\partial z \partial n}$, $m_5 = -Un_3 - xm_3$, (and the other m_js similarly defined) and ϕ_s is the steady potential. In the simplest case, corresponding to the slender ship assumption of strip theory, ϕ_s is approximated as $-Ux$ (the free stream flow), and all interaction with the steady potential disappears. The next level of sophistication is to use the double body flow as an approximation to ϕ_s (as was done in the three-dimensional theory of Nakos and Sclavounos [70]), and finally the full calculation of ϕ_s must take into account the steady wave system generated by the forward motion of the boat. A particular difficulty associated with calculating the steady interaction term $\frac{\partial^2 \phi_s}{\partial z \partial n}$ is the fact that it is singular at sharp corners because the normal direction changes abruptly (for example at chines), and may also be very large at the intersection between the free surface and the hull where the latter is not vertical (see [26], [28]). Again the problem can be avoided in the time domain using a 'body-nonlinear' approach in which the body boundary condition is satisfied at the exact body position at each time step: "This approach obviates the need to consider the troublesome m-factors, and the ships motion may be prescribed arbitrarily, in principle" [74].

Third is the effect of sinkage and trim. Although this is indirect it may nevertheless be important. An example of significant interactions with motions, particularly as a result of trim, is the lifting effects associated with high speed vessels with ventillated transoms (to be discussed in section 6.5.1).

Other limitation

A limitation not only of strip theory, but of most unsteady motion theories, is the inability to adequately represent the tangential separation of flow at a transom stern in the downstream direction and the resulting atmospheric pressure. (At slower speeds there may be a head of water built up above the streamline separating tangentially from the transom, but if this is of

constant depth the unsteady component of the transom force is still zero.)

Although the theory of Salvesen, Tuck and Faltinsen [84] contains transom terms these are not to be confused with the issue in question here. The transom terms in strip theory give rise to the forces that would in theory be present if the hull were extrapolated rearward. The actual force that would be present with atmospheric pressure at the transom is of course zero, meaning that the added mass force per unit length should exactly cancel with the restoring force per unit length, and the damping should be zero. Faltinsen and Zhao [26] demonstrate that this is not the same as the values predicted by strip theory. However Faltinsen [28] concludes from actual force measurements "...that there must be a rapid change of pressure back to atmospheric pressure in a small neighbourhood of the transom stern." This means that in terms of motion predictions the error is not critical, but it would make a difference in predicting loads very near the stern.

Conventional strip theory also represents the radiated and diffracted waves simplistically. They are assumed to propagate perpendicularly to the hull, extending an infinite distance laterally, and none of the three-dimensional characteristics of the wave pattern due to a translating and pulsating source are present. In particular the two-dimensionality of the representation precludes the presence of any waves with characteristics at all similar to the transverse waves in the three-dimensional solution. While these approximations may seem very severe they are actually nothing more than the physical manifestations of the high-frequency low-speed assumptions.

Finally, conventional strip theory assumes small motions and wave heights, and therefore a linear relationship between the two.

4.3.3 Newman's unified theory [73]

In conventional strip theory the two-dimensional hydrodynamic solutions for each strip are obtained in complete independence of each other. There is therefore no interaction between them, and three-dimensional effects are glaringly absent. This is adequate if longitudinal changes of hull geometry are gradual and the radiated wave are short, but for low encounter frequencies this will not be the case. There is some attempt to link the solutions, but this occurs only *after* the strip forces have been calculated, and is only intended to take into account some forward speed effects in the hull boundary condition, and not three-dimensional effects.

Newman [73] proposed a 'unified' theory, so called because the individual two-dimensional strip solutions are modified to match a common three-dimensional solution, thus unifying the strip solutions by imposing some genuine interaction between them.

The two-dimensional solutions for each strip are unique only if a radiation condition is imposed. In conventional strip theory the radiation condition requires the presence of only outgoing waves, as would be the case in the time-asymptotic solution of the equivalent transient problem in which the initial state contains no waves. Without this condition the solution is not unique, but could in general be expressed in the form of a particular solution (such as the

one with only outgoing waves) combined with an arbitrary multiple of a non-trivial solution to the equivalent homogeneous problem (in which a zero normal velocity boundary condition is imposed on the hull). For example, with lateral symmetry the homogeneous solution could be thought of as the sum of the wave pattern resulting from the diffraction of a regular wave train incident from one side and its symmetrical reflection, producing a standing wave pattern oscillating at the same frequency as the particular solution in the far field. Uniqueness may be restored by specifying a radiation condition, and the essence of Newman's theory [73] is to use a suitable three-dimensional wave pattern for choosing the appropriate radiation condition that will properly 'unify' the strip solutions.

The set of two-dimensional strip solutions described in the previous paragraph is referred to by Newman as the 'inner' solution, and in the absence of the homogeneous component corresponds exactly to the conventional strip theory solution. The inclusion of the homogeneous component introduces a number of free parameters to be determined, defining its magnitude and phase at each strip.

An 'outer' solution is generated by distributing three-dimensional sources (for symmetric modes of motion, or dipoles for the antisymmetric modes) on the hull centreline. Green function sources are used to automatically satisfy three-dimensional free surface and radiation conditions, but the behaviour of the outer solution on (or near) the actual ship hull is unimportant. In the absence of the hull boundary condition, or its equivalent, the outer solution therefore also has a number of unknowns corresponding to the strengths and phase of the sources.

If the source strengths are appropriately chosen the outer solution becomes identical in the far field to the fully three-dimensional wave pattern generated by the oscillating ship. Similarly the inner solution will be an accurate representation of the true flow near the hull if the coefficients of the homogeneous components are correctly chosen. On the other hand, behaviour of the outer solution near the hull or the inner solution in the far field are both incorrect physically, but there will be an intermediate overlapping region where both solutions are satisfactory. This overlap region is chosen sufficiently distant from the hull for the outer solution to be insensitive to fine details of the ship hull geometry while close enough that three-dimensionality may be neglected in the inner solution. Essentially the distance is determined by minimising errors in both approximations.

The problem then reduces to one of determination of the unknowns in the two solutions by matching in the overlap region.

After taking Fourier transforms with respect to the longitudinal coordinate (i.e. in wave number space), the asymptotic behaviour of the outer solution near the hull and of the inner solution far from the hull can both be expressed in terms of a general two-dimensional Green function and a general three-dimensional Green function. The set of coefficients of these Green functions can be expressed in wave number space in terms of the Fourier transform of the source strengths, or the Fourier transform of the coefficients of the homogeneous component, in the case

respectively of the outer, or inner, solution. By equating inner and outer solution coefficients for both the two and three-dimensional Green functions in the overlap region a sufficient number of equations are obtained to solve for all the unknowns.

The total solution is completed by calculation of the hydrodynamic forces in terms of the now fully specified inner solution.

Yeung and Kim [102] note that the true three-dimensional solution in the presence of forward speed contains several wavelengths, and it should dictate the nature of the waves produced in the inner solution rather than vice versa. Contrary to this the strictly frequency dependent nature of the *inner* solution in Newman's unified theory and the lack of speed dependent terms in its free surface boundary condition mean it

> ...is still basically one corresponding to a single wave length, [therefore] it is not compatible with waves generated in a three-dimensional flow with forward speed. This difficulty showed up in Newman's (1978) matching procedure when some of the wave components from the outer approximation were forced to be the same wave length as those from the inner problem. It would seem that the three-dimensional flow should dictate the inner behaviour rather than be dictated by the inner flow. This difficulty cannot be easily rectified in Newman's formulation since the inner region is assumed to be non speed-dependent to start with. [102]

In other words, the unified theory addresses the long wavelength limitations of conventional strip theory but not the speed problem.

The theory has been quite popular, and has been used by others such as Sclavounos [86], Børresen and Faltinsen [11], and Kashiwagi and Ohkusu [52].

Sclavounos [86] presents comparisons with strip theory and with model tests for hydrodynamic coefficients, forces and motions. Apart from being able to predict a singularity at $\tau = \frac{1}{4}$ (which is not actually evident in the experimental results because of the range of frequencies chosen) there is no real evidence in the results presented of an improvement over strip theory. However one can not exclude the likelihood of an advantage at lower frequencies since the unified theory and strip theory differ most (as expected) at low frequencies, but experimental results are only given for moderate to high frequencies[8], preventing a proper judgement of the low frequency results.

Børresen and Faltinsen [11] used the theory to investigate motions in shallow water. They state "It is difficult to conclude that the 'Unified Theory' gives better results than 'Strip Theory' in finite water depth." Again though their comparisons do not extend far into the low frequency region.

Kashiwagi and Ohkusu [52] use the theory to investigate towing tank side wall effects, and

[8]This appears to be because they were taken from a report by Gerritsma and Beukelman that did not investigate the lower frequencies.

their calculations of the hydrodynamic coefficients of a prolate spheroid show very favourable agreement with a three-dimensional panel method.

4.3.4 The forward-speed theory of Yeung and Kim [100] [102]

Yeung and Kim [100] (also described in [102]) proposed a *forward speed* strip theory in which a "pseudo-time" variable, $t^* = \frac{-\left(x-\frac{L}{2}\right)}{U}$, was introduced so that the $U\frac{\partial}{\partial x}$ terms in the free surface boundary condition could be reinterpreted as time derivatives, allowing forward speed terms to be effectively retained within the limitation of a two-dimensional solution at each strip. In addressing these forward speed terms the theory was therefore intended as a solution to the high speed restrictions of conventional strip theory.

In Yeung and Kim's theory each strip solution is transient in pseudo-time (i.e. with the real-time variable kept constant), but periodic in real-time (with the pseudo-time, or equivalently, longitudinal position, constant). The real-time dependence could therefore be implied by the use of complex variables, provided the unsteady part of the body boundary condition was linearised about its mean position[9], and the pseudo-time response of a strip is then described by the initial value problem representing the convection of a strip from the bow to the stern. The theory is mathematically similar, although conceptually quite different, to the theory to be proposed in section 4.4, with the main exception being that the latter is a full time domain theory and can therefore represent the exact body boundary condition.

The *forward-speed theory* "has only quasi-three-dimensional effects" since "downstream sections experience a wave field generated by all upstream ones, but not vice-versa" [102]. This means that the divergent waves in the unsteady wave field are represented, but not the transverse ones. Also, the zero initial disturbance condition imposed at the bow is somewhat arbitrary, and is obviously not strictly valid if $\tau = \frac{\omega U}{g} < \frac{1}{4}$, when waves from the unsteady motion exist ahead of the boat. In spite of this, "The improvements over strip-theory results in the hydrodynamic coupling coefficients of heave and pitch were particularly striking for a number of realistic hull forms." [102].

The theory forms the basis of a more sophisticated theory by the same authors, described in the next section.

4.3.5 Yeung and Kim's comprehensive first order theory [102]

Yeung and Kim [102] present "a comprehensive theory of the first-order problem, in which no restrictions need to be placed on the frequency of oscillation ω and the forward speed U of the ship", although slenderness is still assumed.

[9] Yeung [99] showed in the related problem of the transient heaving response of a floating cylinder (with the free surface and body boundary conditions both linearised) that the response with initial velocity is directly related to the time derivative of the response with initial displacement. Thus the one solution with a time complex amplitude can be used to represent both problems, or a combination with arbitrary phase.

Yeung and Kim's *comprehensive theory* proposed accounting for forward speed in a manner analogous to their *forward-speed theory* (described in section 4.3.4) and for low frequencies in a manner analogous to Newman's *unified theory* (section 4.3.3). Newman's technique of unification [73] is used to account for three-dimensional effects associated with long wavelengths.

The *outer* solution of Newman's theory [73] takes into account both forward speed and three-dimensionality, and is therefore directly applicable to Yeung and Kim's *comprehensive theory* [102]. Yeung and Kim did show however that where forward speed was present an accurate matching with the inner solution required that the sources associated with the outer solution not be restricted to being distributed only over the hull length, as they are in the *unified theory*.

The inner solution of Newman's *unified theory* does not take into account speed dependent terms in the free surface boundary condition, so in the present *comprehensive theory* it is replaced with one analogous to the *forward-speed theory* of Yeung and Kim [100], which does contain the required speed dependent terms. As in Newman's theory, the matching process requires the addition of an arbitrary periodic function to the inner Green function of the basic forward speed theory, which must satisfy the homogeneous hull body boundary condition.

The *inner* solution of the forward speed theory is referred to as the *pseudo-time forward-flow* function, because it assumes homogeneous initial conditions on the free surface (no disturbance ahead of the bow), and therefore is associated physically with the forward movement of the boat through the water. The nature of the time dependent form of the free surface boundary condition is such that a valid solution could be reversed in time. Therefore a problem with known end conditions but unknown initial conditions could be solved as if it were a reverse time problem (and therefore in this case reverse flow direction since it is pseudo-time) with known initial conditions. This gives rise to an equivalent *pseudo-time reverse-flow* function, introduced to allow for arbitrary initial conditions in the *forward-flow* function. Since the forward and reverse flow functions both satisfy the same body boundary condition, and the two correspond to different initial conditions in the forward time direction and are therefore not identical, their difference must be a non-trivial solution to the equivalent homogeneous body boundary condition problem[10]. This is almost the required additional component in the inner solution. Finally, a convolution of this homogeneous solution with an appropriate 'modulation' function (determined by matching with the outer solution — its definition is one of the main results of the theory) gives the appropriate weighting of the homogeneous solution for each strip. As in the unified theory, matching is done in wave number space by taking Fourier transforms of both the inner and outer solutions.

A significant result is that an explicit expression for the 'modulation' function is predetermined as part of the theory, and therefore no three-dimensional Green functions associated with the outer solution need be evaluated during computations.

[10] This is of course a rather intuitive argument, and not the one presented by Yeung and Kim [102], who arrive at the same result through mathematical analysis.

Yeung and Kim do not show numerical results in their 1985 paper [102], but show that in various limits the theory reduces to some of the simpler theories discussed above.

In the zero speed limit, for example, their *comprehensive theory* reduces to Newman's *unified theory* [73]. In the presence of forward speed however the two differ. The inner solution of the *unified theory* with forward speed "does not contain wave characteristics that are entirely compatible with those of the three-dimensional field" [102]. In contrast to this the wave numbers associated with the homogeneous part of the inner Green function of the *comprehensive theory* are identical to those associated with the transverse waves of the three-dimensional pattern due to a translating and pulsating source, while those associated with the non-homogeneous (*pseudo-time forward-flow*) part give rise to the divergent wave system.

In the high frequency limit the homogeneous part of the inner solution of the *comprehensive theory* vanishes and the theory reduces to Yeung and Kim's *forward-speed* theory [100]. This contains all of the divergent wave system but none of the transverse wave system.

Finally, in the zero frequency limit Yeung and Kim suggest that a new slender-ship wave-resistance theory is obtained that does not necessitate the use of three-dimensional Green functions.

4.3.6 High speed theory of Faltinsen and Zhao [26] [29]

Faltinsen and Zhao's theory [26] [29] for heave and pitch is based on a similar method proposed by Chapman [15] for yaw & sway motions. Its main objective was to include interaction between the local steady flow (calm water wave resistance problem) and the unsteady (seakeeping) problem. However an important consideration was to maintain a practical theory, which "rules out a complete three-dimensional theory" [26]. It differs both in its objectives and in its formulation from either of the theories of Yeung and Kim described in sections 4.3.4 and 4.3.5.

The approach essentially consists of first solving the steady flow problem. Then the unsteady part of the flow is solved, but with the free surface boundary condition linearised about the steady flow solution rather than the usual linearisation about the undisturbed free surface (this necessitates the use of a Rankine method — see section 2.3.6). Also the steady free surface could be solved as a non-linear problem if desired. Faltinsen and Zhao present results using both linear and non-linear solutions to the steady part of the problem (at $Fr = 1.14$), and the latter shows significantly better agreement with experimental results.

A three-dimensional theory was avoided by solving both problems in a strip sense. This involved the assumption of slenderness, so that some terms involving longitudinal derivatives, including the one in Laplace's equation, could be neglected. The partial differential equations representing the free surface could also be written as linear functions of the longitudinal derivatives of free surface quantities (that is, $\frac{\partial}{\partial x}$ could be separated, x being in this case the longitudinal coordinate). The problem could then be solved by stepping the free surface from the bow to the stern, solving a two-dimensional potential problem at each step.

In the stepping scheme it was necessary to specify starting conditions at the bow in order to solve the problem[11]. The assumption made was that there was no disturbance ahead of the vessel. This is a reasonable assumption at high speed, and without resorting to a theory with three-dimensional far field effects (such as the *comprehensive theory* of Yeung and Kim [102]), or three-dimensional local effects (such as has been introduced more recently by Fontaine and Faltinsen [30], in which the bow wave is predicted by asymptotically matching a three-dimensional near-bow solution and the two-dimensional far field solution), one could not justify an alternative.

The high speed theory of Faltinsen and Zhao represents well the diverging waves of both the steady and unsteady wave systems, but transverse waves are necessarily completely neglected. Faltinsen and Zhao state "The [steady] solution is appropriate for the bow flow of any fine ship at any Froude number. The higher the Froude number is, the longer is the distance along the ship where the solution is appropriate.", and similarly for the unsteady solution. Furthermore, because of the choice of starting conditions for the free surface at the bow in the longitudinal integration, one must assume only downstream waves in the unsteady solution, hence $\tau = \frac{U\omega}{g} > \frac{1}{4}$.

The theory is inappropriate for long wavelength due to the lack of 'unification' — it still uses only two-dimensional solutions at each strip (the assumption of slenderness is used to justify the two-dimensional form of Laplace's equation), and initial conditions at the bow are somewhat arbitrary. In this sense it is similar in objective to the *forward speed* theory of Yeung and Kim [100], but its main advantage is that by separating the waves into their steady and unsteady (periodic) components Faltinsen and Zhao have been able to consider non-linearities in the former. Furthermore, although by the inclusion of appropriate terms in the body boundary condition the two theories of Yeung and Kim [102] can include some steady wave *effects*, they do not contain any *interaction* between these and the unsteady waves. It is only by linearising the free surface boundary condition about the steady free surface position, as Faltinsen and Zhao have done (whether it be the linear or non-linear one), or by solving the problem entirely in the time domain, as proposed in section 4.4, that genuine interaction can be accounted for. The theory is therefore applicable to high Froude numbers and high frequencies; it can tolerate some fullness to the hull form, but is largely aimed at incorporating the steady wave interaction effects that are specifically due to high forward speed.

Numerically computed added mass and damping distributions along a hull at high Froude number are presented graphically by Faltinsen and Zhao [26], showing, as expected, improved agreement with experiment as frequency is increased. The wave profile along the hull and force distribution for steady flow are also shown, showing some improvement due to consideration of non-linear terms in the free surface boundary condition.

[11] Alternatively one could perhaps have specified conditions at the stern, or some other position, and integrated in the forward direction, except that no rational or intuitive method of establishing appropriate starting conditions is available in a theory such as this that lacks a three dimensional radiation conditions. (See section 4.3.5.)

4.3.7 Newman's simplified 3D theory [74]

This theory is not a strip theory at all, but is of interest to the present discussion because it is able to answer some questions relating to three-dimensional and forward speed effects.

It is a three-dimensional analysis in which the principal approximations are (1) to simplify calculation of the interaction between the steady and unsteady flows by considering only the free stream component of the former in the body boundary condition for the latter, and (2) to base the unsteady (periodic) flow component on the three-dimensional zero speed wave radiation and diffraction solutions, but manipulating them (after calculation) in a manner equivalent to that in the strip theory of Salvesen, Tuck and Faltinsen [84] to satisfy forward speed effects in the hull boundary condition. Thus essentially the theory is restricted to slow speeds but can handle both low and high frequencies. The theory can also tolerate some degree of fullness in the hull body shape because it is three-dimensional right up to the hull boundary, although this conflicts with the first of the two main approximations cited above.

Newman's simplified three-dimensional theory is appropriate for slow speed non-slender hulls. It seems to offer little advantage over the unified theory: while the unified theory was limited by its inner solution it did include free surface forward speed effects in its three-dimensional outer solution, but these are absent in this simplified three-dimensional theory.

It is mainly of interest in what it reveals about which effects are due to forward speed and which to three-dimensionality, confirming that conventional strip theory is inappropriate in the presence of forward speed.

Newman [74] compares results from his simplified three-dimensional theory with those from strip theory, experiments, and calculations by Nakos and Sclavounos [70] using a more complete three-dimensional theory with proper treatment of forward speed effects in the free surface boundary condition. Interestingly, there is a strong correlation between the simplified three-dimensional theory and strip theory, both of which include forward speed terms in the body boundary condition but not for the free surface, and also between the complete three-dimensional theory and experiments, both of which contain forward speed effects on the body and free surface. The difference between the two pairs of results is particularly evident for the cross coupling terms, and to a lesser degree also the damping terms. This agrees with the findings of Yeung and Kim quoted in section 4.3.4, which also relate to a theory with free surface forward speed effects. On the other hand, the strong correlation between the simplified three-dimensional theory and strip theory suggests a lack of importance of three-dimensional effects at the frequencies considered. Newman's comparison therefore suggests that the differences in this case are due to forward speed rather than three-dimensionality.

4.4 A new high speed time domain strip theory

4.4.1 Introduction

There are at least three motivations for developing a time domain strip theory. First, it facilitates the introduction of non-linear behaviours, second, it allows rational consideration of speed effects in the hull boundary condition while obviating the need to ignore them in the free surface boundary condition, and third, it opens up possibilities for the operation of active ride control systems on boats. The second has been discussed at some length in sections 4.1.2 and 4.3, and is of particular relevance to high speed vessels such as catamarans and SWATHs. The present theory differs from those described in section 4.3 in that it solves the potential problem for each strip in a stationary reference frame, and the free surface boundary condition therefore does not contain any speed dependent terms. In doing so some of the complications that arise when solving the problem in the usual moving reference frame formulations are significantly simplified. Regarding the third, while the theory proposed in this chapter would not be suitable for calculations as part of an active control system in real time with present computing power it could be used to calibrate a more empirical formulation and thus have application in ride control. Some useful non-linear aspects on the other hand are certainly capable of being handled by the proposed theory.

Non-linearities fall into a number of categories, each of which will be discussed briefly.

- There is the slenderness assumption inherent in strip theory, which can not be avoided without attempting a fully three-dimensional theory and by definition that would not be a strip theory. Such a solution, particularly in the time domain, would be prohibitively slow, and the proposed theory is seen as a compromise between this and frequency domain strip theory.

- Non-linearities are present (to varying degree) in the free surface boundary conditions and in the calculation of pressures on the hull surface. In the case of the radiated and diffracted waves the fully non-linear wave field can be calculated (although at great computational cost). In the case of the incident wave potential this is much more difficult to do, particularly for irregular waves. As an illustration, for regular Stokes waves the first order potential is identical to the third order potential, but the wave height of the third order wave is made up of three different frequencies. If the wave is defined for example as a frequency spectrum based on wave heights it becomes very difficult to determine how much of a particular frequency component results from the potential of the same frequency and how much of it is a higher harmonic of a lower frequency potential component. In fact Hutchison [49] (p.297) states that "Since there is really no hydrodynamic model for the non-linear irregular wave field, there has yet been no attempt to develop a higher order operator theory for non-linear responses in a non-linear irregular sea". Since the incident

waves are of similar size to the radiated waves it makes no sense to represent one as a linear potential field and then to apply non-linear free surface boundary conditions for the other, and the latter would not be legitimate in any case unless the two potential fields were considered together. A possible further justification for using a linear free surface boundary condition could be argued on the following grounds. Linearisation relies either on the assumption of deeply submerged disturbances or small amplitude motions. Suppose we wish to study finite amplitude motions. Near the keel this could be justified on the grounds of deep submergence. If we are interested in heave motion for the hull sections (i.e. heave and pitch for the whole hull) and our hull is steep near the waterline a finite vertical motion of the section could be considered to produce small motions near the water surface. In both cases there is some justification for using a linear theory.

- A further argument for ignoring non-linearities in the free surface boundary condition in a strip theory is that the incoming wave field is not in the same plane as the radiated waves. For example in head seas a regular incoming wave will be two-dimensional in the xz-plane, while the outgoing waves as calculated by a strip theory will be in the yz-plane. Superposition is therefore impossible without resorting to three dimensions, which rules out strip theory and, as noted in the first point, is not the desired objective.

- The assumption of inviscid flow is inherent in any potential flow method used to evaluate force or coefficients. A viscous flow solution would not normally be justified in terms of the improved accuracy achievable and the additional computational cost involved, but viscous effects may be considered empirically. With some exceptions, such as roll damping for monohulls, viscous effects are usually small, and particularly so for hulls without chines.

- A non-linearity that can quite easily be accounted for in the proposed theory, and probably the one having the most dominant effect, is the changing hull submergence. In particular for hulls such as SWATHs, wave piercing catamarans and bulbous bows a bow section may at one instant be completely submerged and at another completely out of the water. The proposed theory uses a free surface Green function panel method to eliminate the need for source distributions on the free surface, and hence can represent changing waterlines without any need for special treatment where the hull intersects the water surface. The only approximation is the linearised free surface boundary condition, which will of course be violated in cases where sections impact the free surface, or where there is a rapid change of beam. However the discussion of figure 6-3 will show that the method may be surprisingly insensitive to this source of error. This is sometimes referred to as the *body-exact* problem.

It is this last non-linearity that this time domain theory seeks to address.

4.4.2 Calculation of forces

In the time domain it is not possible to assume that the boat motions will always be periodic, so there is not necessarily any advantage in working in a moving coordinate system. We therefore have a choice of whether to express the hydrodynamic forces in a moving reference frame as in equations (4.18) and (4.19) or to use the equivalent fixed reference frame forms

$$F_3 = F_z = -\rho \left\{ \int_{stern}^{bow} p \, dx \right\} \tag{4.46}$$

and

$$F_5 = M_y = \rho \left\{ \int_{stern}^{bow} xp \, dx \right\} \tag{4.47}$$

recalling that $p = \int_{section} \frac{\partial \phi}{\partial t} n_z dl$ (equation (4.20)). It has been shown in section 4.1.2 that the fixed reference frame form is preferable from a mathematical standpoint, and we will see below that significant computational advantages may also be gained by using a fixed reference frame for a time domain strip theory solution.

When working in the time domain the form of the solution is unknown and equations analogous to (4.21) can not be derived. Instead one must work with the differential equations of motion

$$\begin{aligned} [F_{3,\text{hydrostatic}} + F_3(\xi_3, \xi_5)] &= M\ddot{\xi}_3 \\ [F_{5,\text{hydrostatic}} + F_5(\xi_3, \xi_5)] &= I_5\ddot{\xi}_5 \end{aligned} \tag{4.48}$$

where all components of the force are now on the left hand side of the equations. There is no longer any advantage in decomposing ϕ into a set of components independent of the boat motion and one dependent on it, in fact there is a considerable disadvantage in doing so. This is because all components of ϕ can be solved for simultaneously by combining the boundary conditions, and calculation of the boundary conditions represents an almost insignificant fraction of the total computation time. In fact the analysis presented after equation (4.20) in the previous section becomes mostly irrelevant, including the concepts of added mass and damping. It is more efficient just to calculate forces and substitute them directly into equation (4.48) without trying to interpret them as added mass and damping first.

The final formulation may look quite different from conventional strip theory, but it is nevertheless a strip theory in the sense that slenderness and related assumptions are used to justify representing a complicated three-dimensional problem as a set of simpler two-dimensional problems.

In order to use a fixed reference frame consider now the strips not to be slices of the boat but to be slices of the water (still in planes parallel to the yz plane) through which the boat is passing. Assuming slenderness still to be valid there is no need to represent strips ahead of the boat until the boat reaches them or to retain strips astern of the boat after the boat has passed through them. If the time step Δt is chosen to be related to the strip width Δx by

$U = \frac{\Delta x}{\Delta t}$ and at each time step a new strip is added at the bow and the stern strip discarded, then in effect we have exactly the same strips as in the moving reference frame, although their treatment computationally is totally different.

Not only are the fixed reference frame equations considerably simpler but very importantly it is no longer necessary to approximate the free surface boundary condition (equation (4.42) in a moving reference frame, but taken to be equation (4.41)) when solving for the potential field of each strip. As an illustration consider for example a very long slender vessel, prismatic except perhaps for a fine bow, in calm water in forced periodic heave. The two-dimensional steady state periodic solution represents well the flow pattern for sections near the stern, where the waves have radiated a considerable distance, but is quite inadequate near the bow where there are no waves beyond a short distance laterally of the hull. This raises the question of how adequate the conventional added mass and damping concept is, particularly for bow sections.

A further advantage of the fixed reference frame is that calculation of P (equation (4.20)) is not required (compare equations (4.18) and (4.19) with equations (4.46) and (4.47)). This is a considerable saving, particularly when using Green function panel methods, in which the calculation of P would double the total number of Green function evaluations required.

Also when using Green function methods the flow field is represented as a convolution integral and the number of calculations required is approximately proportional to the square of the number of time steps in the convolution integral. In a moving reference frame this number is equal to the total number of time steps completed to that point, which increases indefinitely, whereas in a fixed reference frame it is limited to the number of time steps required for the boat to travel one boat length (i.e. the number of strips if Δt is chosen as above). The savings here are considerable.

The entire method is summed up in equations (4.46), (4.47) and (4.48), and two tasks remain: to calculate the sectional forces, and to integrate the equations of motion. Both these tasks offer some scope for different methods of treatment, and the remaining sections of this chapter will describe the approach taken in the present work.

4.5 Incorporation of panel methods into the time domain strip theory

The function of panel methods in a strip theory is to calculate the hydrodynamic forces on each hull section. One can use other methods, as described in section 4.2, but panel methods offer by far the best combination of versatility (in particular the ease with which arbitrarily shaped hull sections can be entered) and computational efficiency. For reasons outlined in the introduction to the previous chapter a linear time domain Green function panel method was chosen.

The numerical details of solving the time-domain panel method have been described in the previous chapter, but it still remains to specify the boundary conditions that must be fed into

the method in order to incorporate it into the proposed strip theory. In addition the present section will describe the method used for interpolating the coordinates that define new sections. In taking into account some non-linearities a dynamic waterline has been adopted, and some particular considerations that arise from this are also discussed below.

A complete calculation of forces also includes the evaluation of hydrostatic and Froude-Krylov forces, which is not strictly part of the panel method solution, but it is most appropriate to include these at the end of the current section.

4.5.1 Interpolation of new panel coordinates for each section

The dynamic waterline, which accounts for the relative displacement between the water surface and the hull in solving the non-linear hull boundary condition problem, was incorporated into the two-dimensional solutions by placing the horizontal axis for each strip at each time step on the line of intersection of the undisturbed incoming wave with the hull section in question at its instantaneous position. The shape and length of the curve defining this section changes with time not only through the influence of the boat and wave motions, but simply because the boat is passing through the strip and is not prismatic.

All three of these effects influence the hull boundary condition, which will be described in section 4.5.3. However the first two in particular also necessitate redefining the section curves at each time step[12]. The interpolation of new panel coordinates at each time step is therefore an essential component of the boundary element solution with dynamic waterline, and some consideration must be given to the process of interpolation to avoid unwanted errors.

One feature that requires consideration is chines. An approach sometimes taken is to tag the location of the chine so that panels can be interpolated separately on either side, meeting at the chine in a corner. This is impossible in the present type of problem since the chine may vary in its relative position between the keel and the waterline, or even rise above the waterline, causing dramatic and undesired differences in panel length on either side of the chine. One would have to allow the chine to float from one panel to another to avoid this, involving some extremely messy algebra (particularly in the time derivatives). It is far simpler to ignore the chine altogether, and to refine the panel length until the effect of approximating the chine in this way becomes negligible. This can be justified on two grounds. First, as was shown in section 2.1.2, there is no requirement that the source panels lie on the fluid boundary, only that they do not lie within it (outside the hull) and that the collocation points lie on it. There is no reason why an interpolation procedure in which the source panels are always exactly on the boundary should necessarily produce better results. Second, because of flow separation effects the streamlines

[12]If the hull boundary condition were linearised then the only contribution to the change of section would be from the forward motion of the boat, and each new hull cross section at a given time step would be identical to that of the next rearward section at the previous time step. It would therefore not be necessary to recalculate section shapes at each time step.

are unlikely to follow the hull boundary exactly at the chines. An interpolation procedure in which the chines are ignored will smear the sharp edges numerically, mirroring what viscosity does physically. In summary, the special treatment of chines would add considerable complexity to the program, and it is unwarranted in terms of improved results.

Another difficulty that the panel interpolation procedure must overcome is submerged sections. Consider for example the hydrodynamic solution for a strip of water through which a hull with a submerged bow section (such as a SWATH hull) passes. The strip is initially penetrated by a submerged point, and this grows laterally as the submerged bow section becomes fuller. A small time later, when the forward perpendicular reaches the strip, the strip suddenly observes a section that extends all the way to the free surface. This may be viewed either as a very sudden vertical growth of the submerged section, or as a lateral expansion of an infinitely thin newly created vertical extension to the section. Numerically the former view is unacceptable since it means that a panel, at one instant on the submerged section, may suddenly jump at the next time step to near the free surface. This causes singular behaviour in the derivatives. The latter view is acceptable numerically, but can be modelled in two ways. The least desirable of the two is to adjust the number of panels as the solution progresses to account for the sudden creation (or extinction) of part of a section. This approach gives rise to considerable housekeeping problems in the computer program, and an alternative was sought. In fact it is immaterial whether the infinitely thin vertical extension was newly created at the instant of the forward perpendicular intersecting the strip of water or whether it was pre-existing. The alternative therefore to the creation of part of a section is to view the section always as a surface piercing section but with an infinitely thin local beam above the true submerged section. This *vertical cut* (as it will subsequently be referred to) may then open laterally at the moment that the additional part of the section needs to be created. This alternative approach allows numerically valid modelling of the phenomenon in question while retaining a fixed number of panels, the latter avoiding the programming difficulties of varying panel numbers. It is the method that was chosen for the modelling of submerged sections.

The vertical cut method of modelling submerged sections, although superior to the alternatives considered, does present its own numerical and programming problems. If symmetry is not exploited then the coincidence of a panel on one side of the vertical cut with the corresponding panel on the other side of the cut results in a singular matrix representing the influence of the unknown source strengths on the boundary conditions. Symmetry could easily be exploited for the case of pure head seas, in which a source and its reflection can be shown to have identical values, or pure beam seas, in which a source and its reflection can be shown to have identical magnitude but opposite sign. There is an additional benefit of a twofold increase in computational speed[13].

[13]In terms of matrix inversion, which is an order n^2 process, one might at first expect a fourfold increase in speed. However the evaluation of the convolution integral contribution to the right hand side vector (also an order n^2 process) is very computationally intensive because of the Green functions involved, and by far accounts for the majority of the total computational time. Unfortunately only a twofold increase in speed is able to be

The problem is a little more difficult in cases with asymmetric boundary conditions, such as quartering seas. These can be solved (although not trivially) by decomposing the boundary conditions into symmetric and antisymmetric components, solving the two problems separately, and superimposing the solutions to give the complete velocity field. The requirement to solve two problems exactly negates the twofold increase in speed, and this works out to be identical in speed to solving the problem without the use of symmetry.

Only head seas were modelled in the current work. A difficulty is *possibly* envisaged for catamarans in cases where both hulls must be represented, and it may be necessary to abandon use of symmetry and restrict applicability to conventional hull forms (i.e. not with submerged bow) to avoid the singularity that exists when the vertical cut is used without exploiting symmetry.

A final difficulty that exists only for conventional hulls (i.e. hulls that do not have submerged bow sections) or hulls with submerged bow sections in extreme motions is the changing waterline length as bow moves in and out of water. This results in a changing number of strips. If one excludes the unlikely event of a combination of waves and motions in which a strip of water experiences a window of time when it *is not* pierced by a hull section, between two points in time when it *is*, then the difficulty of emerging bow (or stern) sections can be solved by starting the hydrodynamic solution for a strip later (or finishing it earlier), and it reduces to a problem of programming housekeeping. It would also require one or two "spare" strips ahead of the nominal forward most strip of the hull in its equilibrium position. Although no attempt was made to handle this feature in the current program it is not expected that it would be very difficult to implement.

The method finally settled upon for the interpolation of panels in the current version of the program was as follows:

- Define input data for the section curves as a set of arbitrarily spaced points defining straight line segments. (Higher order discretisation may be used if desired.) Preferably the spacing of points should be significantly smaller than that required in the final interpolation of panels (unless a part of the curve is straight) so that the accuracy of the interpolated curve is not limited by that of the input data. The curve should also extend above the free surface to at least the highest waterline that is expected to be encountered for that section during the solution.

- Calculate the instantaneous line of intersection of the hull section in question with the free surface, based on the incoming wave height and the vessel motion.

- If the section does not intersect the free surface (for example submerged sections, or surface piercing sections that have been defined with insufficient freeboard on input) then extend it by the addition of a vertical line from the top of the section as it is currently defined to

realised in the convolution integral evaluations when using symmetry to halve the number of points because the use of symmetry also necessitates twice as many evaluations per Green function.

the free surface.

- Calculate the instantaneous total length of the section curve from the free surface to the keel (including any *vertical cut* created at the previous step). Divide by the number of panels being used to give the nominal panel length for that section at that time step.
- Divide the section curve into equal length panels, and store either the panel midpoint coordinates, slope and length, or panel endpoint coordinates. (The two are equivalent and require identical storage space. The choice is mainly a matter of preference, and the former was used in the current program.)

4.5.2 Wave information

The hull boundary condition for the time domain panel method is a kinematic one, so it is essential to know the velocity field beneath the incoming wave for a complete solution of the hydrodynamic forces. This contributes to the diffraction potential in traditional (frequency domain) strip theory, but in the present method the diffraction and radiation potentials are solved simultaneously. In addition information about the incoming wave is required for the evaluation of hydrostatic and Froude-Krylov forces.

Representation of the wave

It is assumed that the wave is travelling in the $-x$ direction. This corresponds to head seas, although it is not difficult to generalise to other directions by replacing x with $(x\cos\theta + y\sin\theta)$ as suggested in reference to equation (4.43). Initially we will deal with regular waves. The incoming wave is fully defined in a fixed reference frame by the potential function

$$\phi = \frac{H_w g}{2\omega_0} e^{k_0 z} \cos\left(k_0 x + \omega_0 t\right) = \frac{H_w \omega_0}{2k_0} e^{k_0 z} \cos\left(k_0 x + \omega_0 t\right), \tag{4.49}$$

from which the quantities required for the complete strip theory solution are the wave height

$$\eta = \frac{H_w}{2} \sin\left(k_0 x + \omega_0 t\right) \tag{4.50}$$

the hydrodynamic component of pressure head

$$\frac{p}{\rho g} + z = -\frac{1}{g}\frac{\partial \phi}{\partial t} = \frac{H_w}{2} e^{k_0 z} \sin\left(k_0 x + \omega_0 t\right) = \eta e^{k_0 z} \tag{4.51}$$

and the vertical velocity

$$w = \frac{\partial \phi}{\partial z} = \omega_0 \frac{H_w}{2} e^{k_0 z} \cos\left(k_0 x + \omega_0 t\right). \tag{4.52}$$

Other quantities not needed at this stage are the two horizontal velocity components

$$u = \frac{\partial \phi}{\partial x} = -\omega_0 \frac{H_w}{2} e^{k_0 z} \sin\left(k_0 x + \omega_0 t\right)$$

$$v = \frac{\partial \phi}{\partial y} = 0,$$

but these would be required for conditions other than head seas.

Repeating in a coordinate system stationary in the x direction but moving vertically so that the origin always coincides with the water surface,

$$\eta_{rel} = 0$$

$$\frac{p}{\rho g} + z_{rel} = -\frac{1}{g}\frac{\partial \phi}{\partial t} - \eta = \frac{H_w}{2}\sin\left(k_0 x + \omega_0 t\right)\left\{e^{k_0 z} - 1\right\}.$$

This expression is still linearised about the plane $z = 0$, and if we wish it to be linearised about $z_{rel} = 0$ we must replace z with z_{rel} in the right hand side to fulfil the requirement that $p = 0$ on $z_{rel} = 0$. Thus

$$\frac{p}{\rho g} + z_{rel} = -\frac{1}{g}\frac{\partial \phi}{\partial t} - \eta = \frac{H_w}{2}\sin\left(k_0 x + \omega_0 t\right)\left\{e^{k_0 z_{rel}} - 1\right\} \tag{4.53}$$

and similarly

$$w_{rel} = \frac{\partial \phi}{\partial z} - \frac{\partial \eta}{\partial t} = \omega_0 \frac{H_w}{2}\cos\left(k_0 x + \omega_0 t\right)\left\{e^{k_0 z_{rel}} - 1\right\} \tag{4.54}$$

$$u_{rel}\left(z_{rel}\right) = u\left(z\right) \tag{4.55}$$

$$v_{rel}\left(z_{rel}\right) = v\left(z\right). \tag{4.56}$$

4.5.3 Panel method boundary conditions and hydrodynamic force

We will first assume a rigid body, such as might represent a fully submerged section. (*Rigid* here refers to a body described by a surface of fixed size and shape, and excludes the wetted hull of a surface piercing vessel, in which the line of intersection of the free surface and the hull changes with time.) The resulting equations will then be adapted to account for the changing submergence of a surface piercing section. Finally we also acknowledge that there is a contribution to the change of shape of a section from the longitudinal motion of the boat through a stationary strip. According to linear theory this should affect only the trim and not motions. However it was actually found to make a significant difference to the computed motions, and has therefore been included in the present work.

Rigid body in fixed coordinates

Let us introduce the following notation:

- $X_s = x$ coordinate of hull section relative to the vessel centre of mass
- $h =$ local heave $= \xi_3 - X_s \xi_5$ (noting that positive pitch is bow down).

The strip solution must satisfy a zero normal velocity condition relative to the moving hull boundary. The total velocity field is made up of the velocity field of the undisturbed wave and the combined radiated and diffracted fields. The latter two make up the computed velocity

field, while the former, along with the hull boundary velocities, forms the boundary condition. Although the computation treats the radiated and diffracted waves simultaneously the computed velocity field does need to be separated into two components to obtain a solution. These two components are effects dependent on the unknown source strengths of the current time step (*impulsive* component) and those dependent on the past history of known source strengths (*convolution* component). Thus one could write $\vec{v}_{fluid} \cdot \hat{n} = (\vec{v}_{wave} + \vec{v}_{imp} + \vec{v}_{conv}) \cdot \hat{n} = \vec{v}_{hull} \cdot \hat{n}$. Separating unknowns from knowns we end up with

$$\vec{v}_{imp} \cdot \hat{n} = (\vec{v}_{hull} - \vec{v}_{wave} - \vec{v}_{conv}) \cdot \hat{n} \tag{4.57}$$

in which we seek the solution to $\vec{v}_{imp}$, and the right hand side can be evaluated at any time step. For two-dimensional strip solutions we are only interested in y and z components of these velocities.

Evaluation of $\vec{v}_{conv}$ is discussed in the previous chapter, and $\vec{v}_{wave}$ is given above in section 4.5.2 in terms of its vertical and lateral components, w and v.

Clearly $\vec{v}_{hull} = \frac{dh}{dt}\hat{z}$ as observed in a fixed reference frame, but the local heave of a section is expressed in terms of the global heave and pitch of the vessel, which is defined in a reference frame moving forward at the same speed as the vessel. It is therefore necessary to adapt this to a stationary reference frame to be compatible with the rest of the two-dimensional strip solution. Putting $x = Ut + X_s$ we have for constant x that $\frac{dX_s}{dt} = -U$, thus

$$\begin{aligned} \vec{v}_{hull} &= \left\{ \left(\frac{dh}{dt} \right)_{\text{fixed reference frame}} \right\} \hat{z} \\ &= \left\{ \frac{d\xi_3}{dt} - X_s \frac{d\xi_5}{dt} - \xi_5 \frac{dX_s}{dt} \right\} \hat{z} \\ &= \left\{ \left(\frac{dh}{dt} \right)_{\text{moving reference frame}} + U\xi_5 \right\} \hat{z}, \end{aligned} \tag{4.58}$$

with the vertical direction being implicit for each of these velocity terms.

Rigid body in coordinates moving vertically with wave

As far as the body boundary condition is concerned it is only necessary to subtract $\frac{\partial \eta}{\partial t}\hat{z}$ from both $\vec{v}_{hull}$ and $\vec{v}_{wave}$ in equation (4.57) in order to represent the problem in coordinates relative to the wave. The latter is then given by equation (4.54), while the former becomes

$$\vec{v}_{hull} = \left\{ \left(\frac{dh}{dt} \right)_{\text{moving reference frame}} + U\xi_5 - \frac{\partial \eta}{\partial t} \right\} \hat{z} \tag{4.59}$$

Other changes include modifying the calculation of the Froude-Krylov and hydrostatic forces, described in section 4.5.4. These changes have no net effect for a rigid body, while for surface piercing bodies the only difference is the extent of the wetted hull surface over which the potential problem is solved. However other effects relating to the discretisation of the hull must be considered for surface piercing bodies, and these will be discussed below.

One question that arises is the validity of the panel solution itself in a vertically moving reference frame. In particular if the reference frame is accelerating vertically (which it must eventually be if it is attached to the wave) the dynamic boundary condition on the free surface differs from the fixed reference frame version, and the Green function that the method is based on, unless it is changed accordingly, is no longer valid.

The effect of a moving reference frame may be apparent either in solving for the source strengths or in the subsequent calculation of body pressures. It is argued below that, if treated properly, it does not invalidate the solution.

In solving for source strengths we note that the matrix of influence coefficients is only a function of the relative positions of panels. The dependence of the panel geometry on the free surface location means that the influence coefficient matrix can be affected by the position of the free surface, but it can in no way be affected by whether the reference frame is moving or stationary. Also the $(\vec{v}_{hull} - \vec{v}_{wave})$ terms in the right hand side vector are independent of the reference frame velocity since the effect of any change in reference frame will be cancelled. Only the $\vec{v}_{conv}$ term in the right hand side vector can contain any information that the instantaneous position of the reference frame origin differs from its past positions. No velocity or acceleration terms appear in the calculation of $\vec{v}_{conv}$ however, so the method remains valid. This is consistent with the fact that solving for source strength values is a problem of kinematics.

In calculating the body pressures one needs to evaluate $\frac{\partial \phi}{\partial t}$. This problem is one of dynamics, and some care must be taken to ensure that the Green function satisfies the correct free surface boundary condition. Again the convolution term only perceives any change of reference frame through the change in position of past panels relative to current positions, but the full expression for $\frac{\partial \phi}{\partial t}$ does now contain velocity terms in the body and image contributions. The solution is to view the reference frame for the purposes of the potential flow solution not as moving, but as temporarily stationary and coincident with the instantaneous free surface. This is achieved by expressing any velocities that appear in the body and image terms as absolute velocities, and not as velocities relative to the moving free surface. The approach of fixing the reference frame instantaneously at the height of the free surface is equivalent to linearising the free surface boundary condition about that height, which gives a boundary condition identical to the one linearised about the line $z = 0$. The Green function used in the panel method solution therefore remains valid.

Surface piercing body modifications

The essential difference between a surface piercing body and a rigid body is that in the former the curve that defines the section is extended or shortened as the waterline moves up or down relative to the hull. In the present method the panels are interpolated so that their length is a constant throughout a given section for a particular time step. As the section curve changes with time the panel length must change proportionally, and all panels must be reinterpolated.

Panels therefore move relative to the hull, and the following section details how to incorporate the resulting panel velocity into the hull boundary condition. It could equally well apply to the panel velocity that results from the forward motion of the boat through a computational strip of water coupled with the variation of hull shape along its longitudinal axis.

In this section (up to and including equation (4.62)) it is convenient to use complex variables, so the notation will revert to that used for two-dimensional problems, as in the previous chapter, in which x and y refer to the lateral and vertical directions respectively, and $z = x + iy$. The longitudinal coordinate of the hull cross section will be denoted X_s.

Assume that each two-dimensional section is symmetric and its starboard half defined by a curve S represented numerically by equally spaced points p, numbered $0, 1, 2 \ldots n_p$ ordered from the waterline to the keel. Each point has complex coordinates $z_p = x_p + iy_p$. These points, although constrained to move along curve S, are not fixed to the section but move such that the criterion of equal spacing (arbitrarily imposed in section 4.5.1) is maintained as the section goes in and out of the water. Only point $p = n_p$, attached to the keel, has the same motion as the section as a whole, equal to $\vec{v}_{hull}$ for the rigid hull given in equation (4.58) or (4.59) as appropriate. Hence

$$\frac{dz_{n_p}}{dt} = i\left(\frac{dh}{dt}\right)_{\text{fixed reference frame}}.$$

(Until otherwise stated, $\frac{dh}{dt}$ will be assumed to be evaluated in a fixed reference frame.)

If s_p is the distance measured along S from point n_p to point p then z_p in general will be a function of s_p and h for a given curve S, thus, noting that $\frac{\partial z_p}{\partial h} = i$,

$$\frac{dz_p}{dt} = \frac{\partial z_p}{\partial s_p}\frac{ds_p}{dt} + i\frac{dh}{dt}.$$

The equal spacing criterion requires $\frac{ds_p}{dt} = \frac{ds_0}{dt}\left(\frac{n_p - p}{n_p}\right)$ where s_0 is the total length of the section from the keel to the waterline. Also, since z_p is constrained to move along S, $\frac{\partial z_p}{\partial s_p} = -e^{i\theta_p}$ where θ_p is the tangential direction to S at point p with the normal pointing into the fluid. Furthermore point $p = 0$ remains fixed to the free surface, and moves only horizontally, thus $\text{Im}\left\{\frac{dz_0}{dt}\right\} = 0$. By substitution into the above equations this can be written as $\text{Im}\left\{-e^{i\theta_p}\frac{ds_0}{dt} + i\frac{dh}{dt}\right\} = 0$, hence

$$\frac{ds_0}{dt}\sin\theta_0 = \frac{dh}{dt}.$$

Combining these gives the final expression for $\vec{v}_{hull}$, now taken to mean the local hull panel velocity, as

$$\vec{v}_{hull} \cdot (\hat{x} + i\hat{y}) = \frac{dz_p}{dt} = \left(i + \frac{e^{i\theta_p}}{\sin\theta_0}\left(\frac{p}{n_p} - 1\right)\right)\frac{dh}{dt}. \tag{4.60}$$

(Note that this expression is interpreted as the time derivative of position rather than complex velocity, so, contrary to convention, the vertical component of velocity here is taken as positive imaginary.)

Taking the normal component as is required for the boundary condition we find the expression simplifies to

$$\frac{dz_p}{dt} \cdot \hat{n} = \mathrm{Im}\left\{ \frac{dz_p}{dt} e^{-i\theta_p} \right\} = \frac{dh}{dt} \cdot \hat{n}. \tag{4.61}$$

The full form of $\vec{v}_{hull}$ (equation (4.60)) might appear therefore to be unnecessary, but it must still be evaluated for two reasons: first and most important is that it is required in other parts of the solution in its full form, in particular the $\frac{dc}{dt}$ terms in the expression for $\frac{\partial \phi}{\partial t}$ (equation (3.12)), and second, by having an expanded form of $\vec{v}_{hull}$ the longitudinal derivative terms (to be described below under the heading *Non-rigid body modification*) may be more easily included in the hull boundary condition.

The wave velocity component of the hull boundary condition is not affected by the need to reinterpolate the hull panels for surface piercing sections, and remains unchanged from its submerged section form.

Non-rigid body modification

To an observer in a stationary two-dimensional strip of water the hull cross section of a non-prismatic ship (i.e. an arbitrary real ship) appears to change shape. Hence the hull cannot be represented as a rigid body for the purposes of the two dimensional strip solution in the present fixed reference frame time domain strip theory.

An additional term, $-U\frac{\partial z_p}{\partial X_s}$, must be introduced to account for the component of velocity of the pth panel of a given section resulting form this longitudinal variation of hull cross section shape of a non-prismatic hull, but in the absence of heave and pitch velocities. In doing this it must be noted that the angle of attack term $U\xi_5$ is no longer required *if* the body boundary condition is satisfied on the instantaneous rather than mean body location (hull coordinates re-interpolated at each time step based on current heave and pitch displacements) because it is then implicit in the $-U\frac{\partial z_p}{\partial X_s}$ term (i.e. there is a component of the longitudinal variation of hull cross section shape due to an instantaneous pitch)[14]. A similar compensation must be made for the fact that in the computer program the vertical coordinates of points on each hull section are expressed relative to the actual free surface elevation of the incident wave. Thus $\left(\frac{\partial \eta}{\partial t}\right)_{\mathrm{MRF}}$ must be subtracted from $\frac{dh}{dt}$ in equation (4.60) and $\left(\frac{\partial \eta}{\partial t}\right)_{\mathrm{FRF}}$ added to the total velocity (where $_{\mathrm{MRF}}$ and $_{\mathrm{FRF}}$ refer to moving and fixed reference frames). The complete form of the panel velocity component of the hull boundary condition (equation (4.60)), with the addition of the $-U\frac{\partial z_p}{\partial X_s}$ term, is then

$$\vec{v}_{hull} \cdot (\hat{x} + i\hat{y}) = \frac{dz_p}{dt} = -U\frac{\partial z_p}{\partial X_s} + \left(i + \frac{e^{i\theta_p}}{\sin\theta_0}\left(\frac{p}{n_p} - 1\right)\right)\left(\frac{\partial\left(h-\eta\right)}{\partial t}\right)_{\mathrm{MRF}} + i\left(\frac{\partial \eta}{\partial t}\right)_{\mathrm{FRF}}, \tag{4.62}$$

[14] The component of $\frac{\partial z_p}{\partial X_s}$ due to the difference between the instantaneous and mean hull geometries corresponds to the m_j terms in conventional strip theory.

where

$$\left(\frac{\partial\left(h-\eta\right)}{\partial t}\right)_{\text{MRF}} = \frac{d\xi_3}{dt} - X_s\frac{d\xi_5}{dt} - \left(\frac{\partial\eta}{\partial t} + U\frac{\partial\eta}{\partial X_s}\right)_{\text{FRF}}.$$

Final boundary condition, solution for source strengths, and evaluation of hydrodynamic forces

Radiated and diffracted waves may be solved simultaneously by combining equation (4.62)[15] and equations (4.56) and (4.54) into a single boundary condition, as in equation (4.57). The right hand side of equation (4.57) at any panel collocation point is equivalent to equation (3.37) of the time domain panel method, where $(\vec{v}_{hull} - \vec{v}_{wave}) \cdot \hat{n}$ and $-v_{conv} \cdot \hat{n}$ respectively in the former are the same as $\vec{V} \cdot \hat{n}$ and the remaining term in the latter. The left hand side of (4.57) at any panel is represented by elements of the vector $[A]\{Q\}$, where A_{ij} is given by equation (3.36) and Q_j are the unknown source strengths at the current time step. Solution of the resulting system of equations yields the vector of unknown source strengths $\{Q\}$.

Once source strengths are known the hydrodynamic heave force and pitch moment on the hull can be evaluated using equations (4.46), (4.47), (4.20) and (3.12). The $\frac{dc}{dt}$ term (A_k) in equation (3.12) is the panel end point velocity, which is given by equation (4.62).

4.5.4 Hydrostatic and Froude-Krylov forces

The hydrostatic force is simply the weight of the water displaced by the hull. The wave elevation can be taken into account by the use of the dynamic waterline in calculating the displaced volume. However we recall that the pressure distribution beneath a wave is not hydrostatic except at points of zero wave height (equation (4.51)), and the correction necessary to the force to account for the deviation of pressures from hydrostatic is called the Froude-Krylov force. It can be calculated by adding the vertical component of the integral of $p + \rho g z_{rel} = \rho g \eta \left\{e^{k_0 z_{rel}} - 1\right\}$ (where notation has reverted to the three-dimensional coordinate system — x, y, z being forward, port and upwards) over the hull boundary.

Alternatively one can calculate a combined hydrostatic and Froude-Krylov force using a modified hull volume. The submerged volume of a unit length of hull is its cross section area, $\int_S -z_{rel}\, dy$, and with the Froude-Krylov correction becomes

$$\int_S \left\{-z_{rel} + \eta\left(e^{k_0 z_{rel}} - 1\right)\right\} dy \tag{4.63}$$

where S is the curve that defines the section (starting on the $-y$ side and ending on the $+y$ side) and z_s is the local wave height. Note that submerged or small waterplane sections are correctly accounted for in equation (4.63) since dy is negative above the points of maximum beam.

[15] Strictly speaking this equation represents velocities at panel end points. For the panel method boundary condition the velocity at the mid point is required, which may be obtained by averaging the values for its two end points.

4.6 Integration of the equations of motion

4.6.1 Development of an algorithm

The time domain equations of motion are of the form $F = m\ddot{x}$, where F denotes all forces acting on the hull (traditionally separated into radiation, diffraction, hydrostatic and Froude-Krylov forces), and in general is a complicated function of the current boat position, its velocity, and the history of these motions. (We take x and F here as being generic motion and force variables. The discussion applies equally well for example to heave, pitch and two degrees of freedom.) The dynamic part of F is obtained by solving for the flow potential about the hull and differentiating with respect to time. It involves terms dependent on the vessel velocity and acceleration, and is closely analogous to the conventional frequency domain approach involving added mass and damping terms.

Although it would appear to be a simple matter to integrate these equations they are inherently unstable due to feedback from the acceleration terms in F appearing directly as well as implicitly through the history terms. Some authors have avoided the problem (perhaps intentionally?) by calculating radiation and diffraction forces separately. On the other hand Beck et al. [5] offer a solution to the problem. They argue that $\frac{\partial \phi}{\partial t}$ is critical to the calculation of hydrodynamic forces, and the fact that ϕ is only known up to the current time step means that a backward difference must be used to obtain $\frac{\partial \phi}{\partial t}$. The backward difference gives a poor estimate of the derivative, which leads to the observed instability. However, noting that $\frac{\partial \phi}{\partial t}$ satisfies the same partial differential equation as ϕ one can compute it directly, avoiding the need for the backward difference. In fact the same form of singularity may be used for both ϕ and $\frac{\partial \phi}{\partial t}$, avoiding the need to create and invert another influence matrix. Unlike ϕ, which only requires body velocities in its boundary condition, $\frac{\partial \phi}{\partial t}$ requires body accelerations. He assumes an acceleration, calculates $\frac{\partial \phi}{\partial t}$ and hence F, and from F calculates the new acceleration. Stability is achieved by iterating the process until the assumed and calculated accelerations agree to within a given tolerance.

The method of Beck et al. [5] is ideal for non-linear problems, in which most of the computational effort is in assembling and inverting the influence matrix. However, using the present Green function method, even with no iteration, it would involve twice as many convolution integral evaluations, which in this method account for almost all of the computational time. Furthermore, since the exact body boundary condition is being used, every iteration would require a further complete set of convolution integral calculations. A more appropriate method of stabilisation was sought.

A successful and completely explicit method of integrating the equations of motion has been developed that overcomes the instability problem, involving the combination of two estimates of the solution, each unstable on its own, but whose errors cancel sufficiently to stabilise the solution. It will be demonstrated that stability is achieved without loss of accuracy. No iteration

is required, and the additional computational cost is negligible.

To identify the source of instability one can rewrite the equations in their frequency domain form, using added mass and damping notation for the hydrodynamic radiation forces. The heave equation is

$$(m + A)\,\ddot{x} + B\dot{x} + Cx = F_w, \tag{4.64}$$

where F_w is the wave force (Froude-Krylov and diffraction), and is independent of x. Applying this to the time domain we must recognise that A, B and C are (generally weakly) time (or more strictly frequency) dependent, but if we integrate with a small time step we can treat them as constants. In the present time domain formulation all hydrodynamic forces acting on each strip are evaluated simultaneously and there is no way of distinguishing components depending on water inertia (added mass), wave radiation (damping) etc.. This is equivalent to rewriting equation (4.64) as

$$\ddot{x} = \frac{-1}{m}\left(A\ddot{x} + B\dot{x} + Cx - F_w\right) \tag{4.65}$$

where the right hand side as a whole is known but the individual terms that it contains are not. If there is a small error ϵ in the inertia term, which might for example originate in the evaluation of $\frac{\partial\phi}{\partial t}$ due to inconsistent initial conditions, roundoff or truncation errors, this will be represented in the $\ddot{x}$ term on the right hand side of equation (4.65), and will cause an error of $-\alpha\frac{A}{m}\epsilon$ in the calculated value of $\ddot{x}$ (the factor α is included to account for additional effects such as differences between the analogous and the actual problems, factors dependent on the particular numerical integration method, the dependence of A on $\ddot{x}$, and feedback through the $\dot{x}$ and x terms). Recall that we can not write an explicit expression for $\ddot{x}$ since A can not be isolated. It is clear that at each time step the error will be amplified by a factor of order $-\frac{A}{m}$ (assuming α to be of order 1) and that this amplification factor must have an absolute value less than 1 for the method to be stable.

The solution of the flow potential and calculation of the forces were ruled out as sources of instability since the program was successfully able to calculate realistic forces when the boat motion was prescribed, leaving only the numerical integration of the equations of motion as the offender. Again this is consistent with the findings of Beck et al. [5]. Estimates from initial runs of the program give $\frac{A}{m} \approx 0.82$ and the corresponding error amplification factor ≈ -3.5 with the current integration method (of course these values depend on model geometry and motions, and integration method). Furthermore extensive comparisons between the actual strip theory program, which calculates forces from the time domain potential flow field, and a simplified analogous program based on constant added mass, damping and stiffness coefficients as in equation (4.65) (coefficients being empirically determined from the actual program) give virtually identical behaviour, confirming the implied inertia term in the hydrodynamic force as the origin of instability.

Owing to its success in simulating the instability the *constant coefficient program* was used extensively to investigate causes and remedies before testing the latter in the actual strip theory

program. This allowed several hours of running time to be simulated in a fraction of a second. It revealed for example that the true error multiplication factor behaves like $-\left(1+\frac{A}{m}\right)$ rather than $-\frac{A}{m}$ when using an Euler integration (or worse with higher order methods), making the problem a very serious one since any finite positive value of $\frac{A}{m}$ is sufficient to cause instability.

The differential equation literature refers to this type of problem as *stiff*, and favoured methods of solving such equations are generally implicit methods (such as Adams-Bashforth-Moulton predictor-corrector solvers). See for example references [79], [31] or [34].

The usual cause of stiffness is greatly differing time constants. An example is the set of equations whose solution includes

$$x\left(t\right)=Ae^{-\alpha t}+Be^{-\beta t};\quad \alpha\gg\beta>0, \tag{4.66}$$

and the focus of implicit methods in this context is to overcome this and related difficulties.

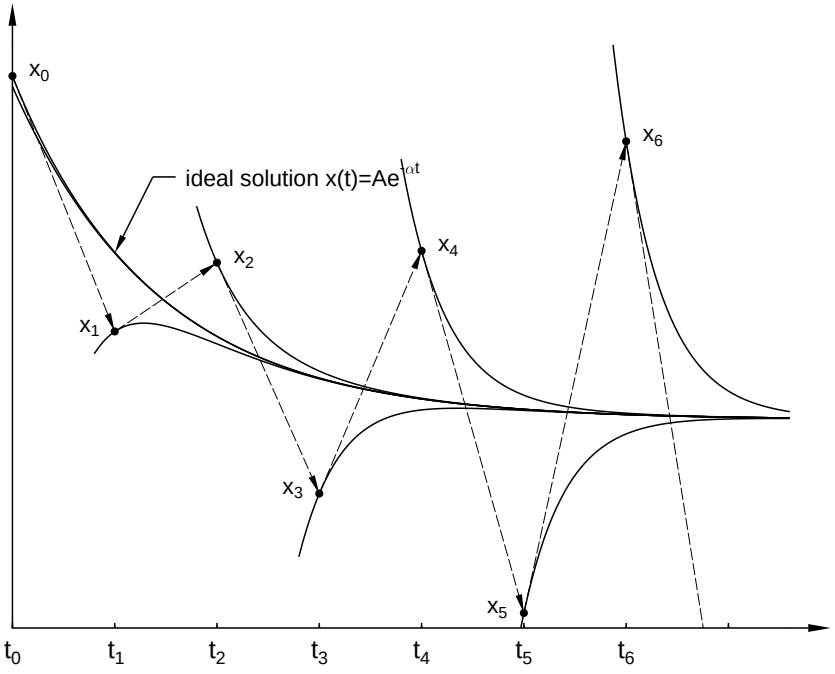

Figure 4-1: Error propagation in Euler integration of stiff differential equation.

Figure 4-1 shows graphically the solution to equation (4.66) using forward Euler estimates. Each curve in the diagram is a valid solution but with different initial conditions (the same values for A, α and β in equation (4.66), but different values for B). If the ideal solution has $B=0$ then errors are represented by the curves corresponding to non-zero values for B. Since these curves are steep (decay rapidly to the ideal solution) the solution always overshoots if the time step is not small compared with the shorter of the two time constants. The diagram shows how this can lead to instability.

One approach is to refine the step size so that the solution does not overshoot (or at least overshoots by an amount less than the error at the current time step). An alternative approach is

to use backward Euler steps, illustrated in figure 4-2. By working backwards from the unknown value at the next time step (hence the method is implicit) the solution can be stabilised. The slowly decaying exponential can be well represented by the coarser time steps, but at the cost of losing detail in the rapidly decaying exponential.

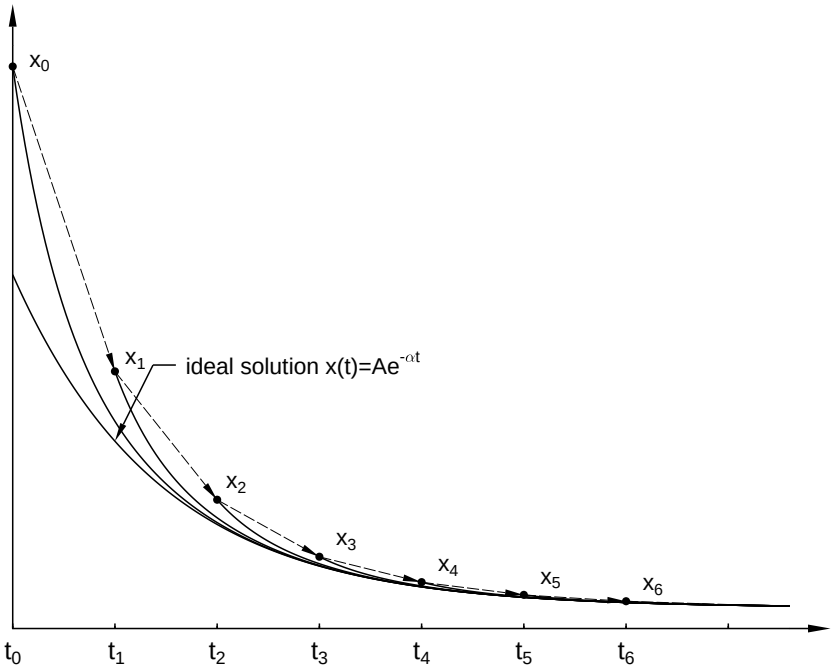

Figure 4-2: Stabilisation of errors using backward Euler integration.

The present problem does not fall into the aforementioned stiff behaviour category, and although only a few such methods were tried the results were disappointing. An important distinction is that in the present problem the propagation of error at each time step is independent of the step size (in fact refining the step size only means that the errors are multiplied by the same factor a larger number of times) whereas in stiff problems of the above type a stable solution can always be obtained by refining the time step. (In [79] an example is cited in which a stiff problem is solved to a given accuracy using a Rosenbrock method for stiff equations in 29 time steps, while the same problem takes 51012 steps using a standard Runge-Kutta method.) Furthermore implicit methods require multiple evaluations of the right hand side, which in the present problem are extremely computationally intensive and turned out to be unnecessary since a better solution was found.

A method was sought that

1. was stable and insensitive to errors in initial conditions
2. required a minimum of right hand side evaluations
3. gave accurate results.

4. preferably evaluated solutions at equal time intervals without the need to evaluate intermediate values. (This is because of the way the vessel is divided into "strips" whose width is the distance the vessel travels in a time step. Violation of this requirement would necessitate interpolation between discrete solutions, causing a loss in accuracy. This puts Runge-Kutta and Richardson methods low on the list of options.)

A suitable explicit technique was developed that requires only one evaluation of the right hand side per time step. It involves setting the acceleration at each time step at a weighted average of the value calculated from the force and a value estimated from recent velocities. Neither gives a stable correct solution on its own, but they have error terms in opposing directions, and a combination of the two gives remarkably accurate results. The modified acceleration can then be combined with almost any integration method. The analysis that follows will be based on an Euler integration for clarity and simplicity, but the actual method used was a higher order Taylor method. The analysis was further simplified by considering only the homogeneous single degree of freedom problem, which exhibits identical instabilities to the general problem.

Consider the force acting on the hull, F, to consist of components proportional to the instantaneous position, velocity and acceleration, which are respectively Cx, $B\dot{x}$, and $A\ddot{x}$. Recall that precise values of these individual components are unknown, but assume that they may be estimated. Thus our calculated (denoted by subscript $_c$) acceleration, $\ddot{x}_c$, is given by $\ddot{x}_c = \frac{F}{m} = -\frac{1}{m}\left(A\ddot{x} + B\dot{x} + Cx\right)$. Suppose we estimate (subscript $_e$) the added mass and acceleration as A_e and $\ddot{x}_e$ respectively then we can write

$$\ddot{x}\left(m + A_e\right) = -\left(\left(A - A_e\right)\ddot{x} + B\dot{x} + Cx\right) = F + A_e\ddot{x} \approx F + A_e\ddot{x}_e.$$

Note that if A_e and x_e are good estimates we have removed the $\ddot{x}$ term from the right hand side, stabilising the problem. From this, putting $\frac{F}{m} = \ddot{x}_c$, we get

$$\ddot{x} \approx \frac{F + A_e\ddot{x}_e}{m + A_e} = \left(\frac{m}{m + A_e}\right)\ddot{x}_c + \left(\frac{A_e}{m + A_e}\right)\ddot{x}_e. \tag{4.67}$$

Errors in $\ddot{x}_c$ are now multiplied by a factor that behaves like $-\left(\frac{A+m}{m}\right)\left(\frac{m}{m+A_e}\right) \approx 1$, so we are already much better off. However the choice of A_e is still guesswork, and we do not wish the solution to be sensitive to its value. Furthermore we have said nothing about how we obtain $\ddot{x}_e$ or about the behaviour of errors present in it. Obviously if the estimate $\ddot{x}_e$ were sufficiently good and errors did not propagate we could ignore $\ddot{x}_c$ altogether. We shall see in a moment that our only requirement for $\ddot{x}_e$ is that its errors diverge rather than oscillate (i.e. that its error is always of the same sign if not corrected) and that the error is approximately sequential, although it is unnecessary to be able to predict its pattern to any significant accuracy.

Based on equation (4.67) one could write

$$\ddot{x} = \mu\ddot{x}_c + \left(1 - \mu\right)\ddot{x}_e, \tag{4.68}$$

where μ is a coefficient to be determined, equivalent to $\frac{m}{m+A_e}$ in the equation (4.67). Suppose that the solutions based only on $\ddot{x}_c$ ($\mu = 1$) and only on $\ddot{x}_e$ ($\mu = 0$) have errors that are respec-

tively multiplied at each time step by $-\rho_c$ and $+\rho_e$, where ρ_c and ρ_e are both > 1, i.e. that neither solution on its own will converge to the correct solution (if one did the problem would be trivial), but that they each propagate errors in opposite directions. The error in $\ddot{x}$ will be multiplied at each time step therefore by $\mu\rho_c + (1-\mu)\,\rho_e$ and we require the absolute value of this to be less than 1. This gives us

$$\frac{\rho_e - 1}{\rho_e + \rho_c} < \mu < \frac{\rho_e + 1}{\rho_e + \rho_c}. \tag{4.69}$$

A successful solution can thus be obtained for a range of μ values.

The method chosen to calculate the estimate $\ddot{x}_e$ was a second order backward difference approximation to the derivative of the velocity, i.e.

$$\ddot{x}_e\,(t) = \frac{3\dot{x}\,(t) - 4\dot{x}\,(t-\Delta t) + \dot{x}\,(t-2\Delta t)}{2\Delta t}. \tag{4.70}$$

This is a very good estimate of the current acceleration if Δt is small and the solution (including velocities) up to the present time step is reasonably good, but it does not on its own lead to a convergent solution. A solution based on this would have constant curvature, resulting in a parabolic solution rather than the correct decaying oscillatory solution. It does however fulfil our requirements of having $\rho_e > 1$. To illustrate this, if we choose μ to completely eliminate any error then we can ignore the effects of feedback from errors beyond the immediately previous time step and interactions between the two methods of solution in equation (4.68), in which case using an Euler integration it follows from equation (4.70) that $\rho_e = \frac{3}{2}$. In general the value will differ slightly from this and numerical experiments suggest that $\rho_e \approx 1.3$ is a sufficiently conservative estimate for general use, while with $\frac{A}{m} \approx 0.8$ stable solutions were obtained for $(0.15 <)\,\mu < 0.82$ (the lower limit varied quite considerably depending on the time step size), giving an estimated $\rho_c \approx 1.5$. Significant variation of ρ_e and ρ_c may be observed due to interactions between the two methods (i.e. they may be a function of μ). The values also depend on the particular problem and method of integration, but the important feature is that an accurate[16], stable and consistent solution is obtained for a reasonably wide range of μ values. Therefore one may be confident of solving a range of problems with a single μ value. Furthermore the deterioration of the solution as μ passes out of the acceptable range is rapid, so there is little danger of accepting an erroneous solution.

The fact that explicit integration methods using this corrected acceleration are stable implies that the difficulty lies in the evaluation of the derivatives and not in the method of integrating, and that recourse to methods specifically designed for stiff equations is unnecessary. The method of integration chosen was a third order Taylor series, with the third derivative approximated from previous second derivative values. This was an extremely simple method to implement, while giving significantly better results than the second order Taylor series. The details of the final algorithm are given below. Note that x, F and m may refer to heave, heave force and mass,

[16] Only stability, not accuracy, has been dealt with specifically so far. The issue of accuracy will be discussed in detail in section 4.6.2.

or to pitch, pitch moment and moment of inertia. Heave and pitch equations may be integrated independently because all coupling effects are implicit in F.

$$\ddot{x}_c(t) = \frac{F}{m} \tag{4.71}$$

$$\ddot{x}_e(t) = \frac{3\dot{x}(t) - 4\dot{x}(t-\Delta t) + \dot{x}(t-2\Delta t)}{2\Delta t} \tag{4.72}$$

$$\ddot{x}(t) = \mu\ddot{x}_c(t) + (1-\mu)\ddot{x}_e(t) \tag{4.73}$$

$$\dddot{x}(t) = \frac{3\ddot{x}(t) - 4\ddot{x}(t-\Delta t) + \ddot{x}(t-2\Delta t)}{2\Delta t} \tag{4.74}$$

$$\dot{x}(t+\Delta t) = \dot{x}(t) + \Delta t\,\ddot{x}(t) + \frac{\Delta t^2}{2}\dddot{x}(t) \tag{4.75}$$

$$x(t+\Delta t) = x(t) + \Delta t\,\dot{x}(t) + \frac{\Delta t^2}{2}\ddot{x}(t) + \frac{\Delta t^3}{3!}\dddot{x}(t) \tag{4.76}$$

4.6.2 Validation of the algorithm

Validation consists of three parts:

- Demonstration that the simplified analogy (constant coefficient program) accurately models the essential features of the full time domain strip theory program, including prediction of the onset of instability.
- Validation of the concept of combining the two solutions $\ddot{x}_e$ and $\ddot{x}_c$, which requires only that in the limit $\Delta t \to 0$ the solution is independent of μ for some range of values as implied in equation (4.69).
- Estimation of the error involved in the particular integration method used, and the size of Δt required to keep this acceptably small. This was done using only the constant coefficient program because the corresponding analytical solution is known, and also because it allowed large numbers of test cases to be run in a reasonable time.

The constant coefficient program

By far the most time consuming task in solving the set of equations (4.71)–(4.76) is the panel method solution required to obtain F at each time step in equation (4.71), and this task was substantial enough to hinder progress on the development of integration algorithms. However in developing and testing algorithms it was only necessary to represent F qualitatively and to approximate it sufficiently well to reproduce the instability. This was done by assuming the force to behave according to

$$F = -(A\ddot{x} + B\dot{x} + C) \tag{4.77}$$

where A, B and C are treated as constants and $\ddot{x}$ was taken as the estimated value, $\ddot{x}_e$, given in equation (4.72). Thus testing time was reduced by a factor of the order of 10^4.

Initially it was not even necessary that the values for A, B and C realistically modelled the actual problem, but once a stable algorithm had been developed the full strip theory was run to determine more appropriate values for these coefficients. (All the results presented below use the latter coefficients.) These initial runs on the true strip theory program also established that the assumption of representing the force with constant coefficients was an excellent approximation to the true behaviour, and therefore that, at least in principle, the constant coefficient program could be used for testing algorithms.

The only remaining question regarding the validity of the constant coefficient program was whether the use of the estimate $\ddot{x}_e$ instead of the unknown $\ddot{x}$ in equation (4.77) would reproduce the appropriate instability behaviour, and it will be evident from the discussion of figures 4-3 and 4-4 below that it was extremely successful in this regard.

The constant coefficient program was used to determine relative merits of integration methods, including the effect of μ. The method described by equations (4.71)–(4.76) was found to be very accurate without sacrificing stability. It was also favoured over methods such as Runge-Kutta because it required only one evaluation of F per time step. The third derivative terms in equations (4.75) and (4.76), although only extrapolated from past accelerations (equation (4.74)), gave a substantial improvement in accuracy over a second order Taylor series, allowing the use of larger time steps.

Initially the case of a single degree of freedom and no external forcing was investigated, and these results will be presented below since they illustrate clearly the important features without introducing unnecessary complexity. The constant coefficient program was then extended to include effects of wave forcing and of two degrees of freedom, and the integration algorithm performed equally well with these features included.

Demonstration of the independence of the solution from the choice of μ

Equation (4.69) shows that there is an upper and lower limit for μ for which a stable solution may be obtained, but this does not necessarily imply accuracy of the solution. It will be shown that accuracy limits roughly, but not exactly, correspond to the stability limits, with higher values of μ giving more accurate results.

Figure 4-3 shows the behaviour near the upper stability limit for the case of free oscillation in the heave mode (pitch is restrained) with an initial heave displacement[17]. The initial instability in the strip theory program is because the hydrodynamic force calculated at the first time step is not necessarily consistent with the implied prior acceleration resulting from arbitrarily

[17]The strip theory results are for a model of 22kg displacement, and the coefficients in the constant coefficient program were chosen to give as nearly similar behaviour as possible. Initial conditions differ slightly between the two, accounting for a slight phase difference. In particular the former was restrained in pitch for three time steps to allow sufficient initialisation of variables to calculate meaningful derivatives, and the latter has a unit initial displacement (which, because of the linearity resulting from the use of constant coefficients, does not affect the general shape). All subsequent results presented in this chapter consider this same case.

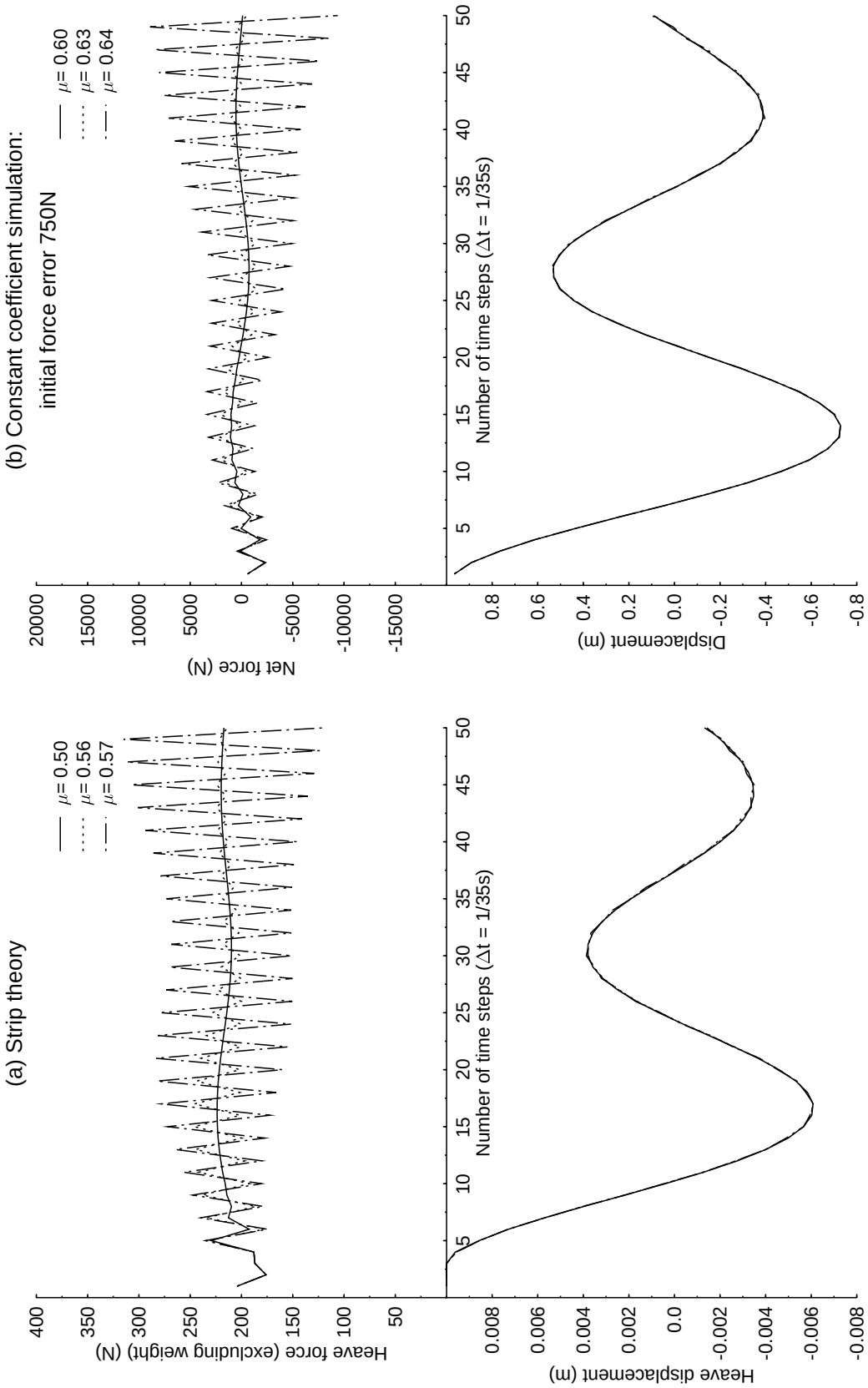

Figure 4-3: Behaviour of the numerical integration for values of μ near the upper stability limit.

defined initial conditions. This could also be viewed as a step function in the externally applied force, which is physically plausible but, because of the associated infinite derivatives, cannot be modelled well numerically over short time scales. In fact a requirement of the integration method used was that it was robust to this kind of interference. For the constant coefficient program it was necessary to artificially introduce a large error in the force to simulate the behaviour of the strip theory. Instability could still occur without this, but it would take much longer to be visible, and nothing of interest would be visible at all for the stable solutions.

For the constant coefficient program any oscillating errors decay for $\mu \leq 0.63$, and the solution is therefore stable, while the error grows for $\mu \geq 0.64$. The cutoff point is $\mu = 0.56$ for the strip theory, but otherwise the two methods exhibit virtually identical features. As expected the rate of decay (or growth) of error increases as μ is decreased (or increased) from the limiting value of 0.63 or 0.56. The higher limit for the constant coefficient program is attributed to a stronger correlation between $\ddot{x}_e$ and $\ddot{x}_c$ due to the use of $\ddot{x}_e$ in calculating F (equations (4.71) and (4.72)), which causes better cancellation of errors.

Because of the high frequency of the error oscillations they are hardly visible after integrating twice to obtain displacements, and when instability is present it will therefore take much longer to affect displacements. It can be seen that the final solution, ignoring the oscillations due to instability, is not affected by the choice of μ, and therefore accuracy can be assumed to be a function of Δt. This is apparent in both the force and displacement graphs, and surprisingly is even the case when instability is present. Presumably then the accuracy limit (if it exists) for μ is much higher than the stability limit, but further investigation was pointless because an accurate solution is useless if it is unstable.

In general the force graph shows most clearly the stability or otherwise of the solution while the displacement graph shows better the overall accuracy.

The effect of refinement of the time step size was investigated using the constant coefficient program. In general the growth or decay of instability errors tended to be more a function of the number of time steps than of the actual length of time simulated. Therefore the use of a smaller time step improved the stability of a stable solution while making an unstable one worse. The value of μ above which the solution became unstable was unchanged.

The behaviour near the lower stability limit for μ was not as clear cut as that near the upper limit, mainly because accuracy deteriorated before stability. Figure 4-4 shows the same cases presented in figure 4-3 solved with lower values of μ. It shows that in the range $0.20 \leq \mu \leq 0.50$ there is only minimal effect of μ on the solution. For $\mu = 0.10$ the solution appears to be significantly contaminated with oscillations at a frequency somewhat higher than the true natural frequency, but again on integrating twice the effect is not too obvious apart from a frequency shift. The undesired oscillation is decaying, thus the solution is stable, but its rate of decay is about the same as that of the boat motions and so the solution will never be accurate. The stability limit, at which the undesired oscillations start to grow in magnitude, appears to have

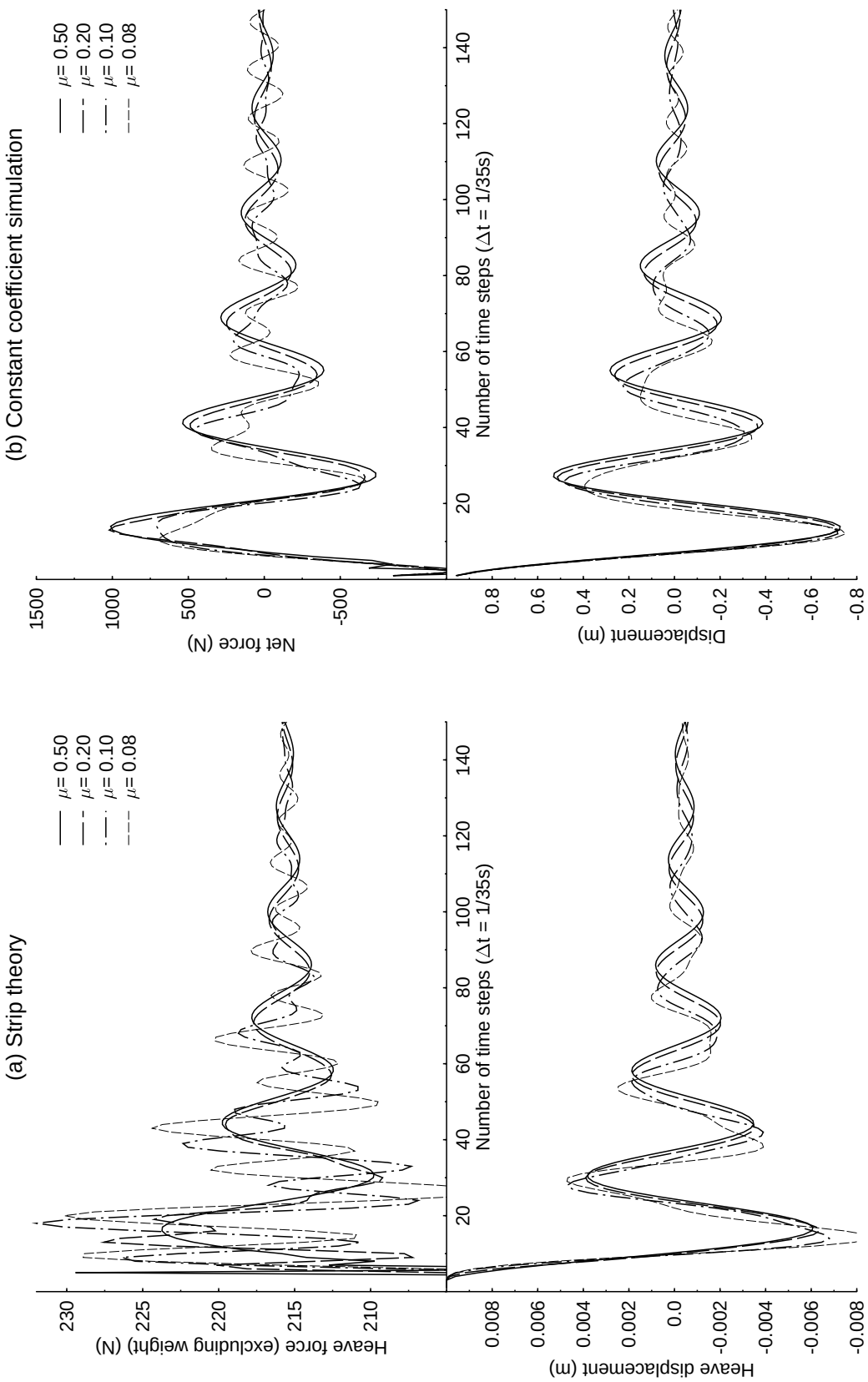

Figure 4-4: Behaviour of the numerical integration for values of μ near the lower stability limit.

been just reached at $\mu = 0.08$ in the constant coefficient program but is slightly lower for the strip theory program. After only a few periods of oscillation there is nothing meaningful left in either solution with $\mu = 0.08$.

Once again both the strip theory and constant coefficient programs show virtually identical behaviour once the noise present in the former due to the inconsistent initial conditions (discussed above) has died away. The similarity between the two for $\mu = 0.10$ is particularly remarkable.

Factors influencing accuracy

Having established the validity of the constant coefficient program in simulating the strip theory it can be used with confidence to investigate accuracy. Figure 4-5 shows the accuracy of the constant coefficient solution over the entire stability range, with two different time step sizes. Note that the result is shown after large time (starting after slightly over seven periods) and so the effect of any inaccuracy has had time to accumulate and errors are magnified. The corresponding analytical solution, also shown in the figures, is the product of a decaying exponential and a sinusoid. The error in the time constant of the exponential for $\mu = 0.30$, $\Delta t = \frac{1}{35}$s, is estimated to be 3.3%, while the error in the frequency is about 1.2%.

Accuracy is highest for μ near its upper stability limit. It can be shown, by comparison with the solution to the corresponding stable differential equation, $\ddot{x} = \frac{-B\dot{x}+Cx}{A+m}$, that the error for these values of μ is mainly due to the time discretisation and integration method rather than due to the effect of μ. However as μ is decreased the accuracy degrades, and does so more rapidly as μ approaches its lower limit.

The best strategy then is to choose a value of μ near its upper stability limit. This is generally a safe strategy since it is immediately apparent from inspection of the force output when the chosen value is too high. The fact that the deterioration of the solution at the upper stability limit is sudden and highly recognisable, combined with the fact that there is no degradation of general accuracy corresponding to the onset of instability, means that there is no danger of accepting an erroneous solution. This is in complete opposition to the behaviour near the lower stability limit.

The effect of reducing Δt is twofold. As one would expect, it causes the discrete (numerical) solution to better approximate the ideal continuous (analytical) one, but it has the added benefit of reducing the influence of μ on the accuracy of the solution.

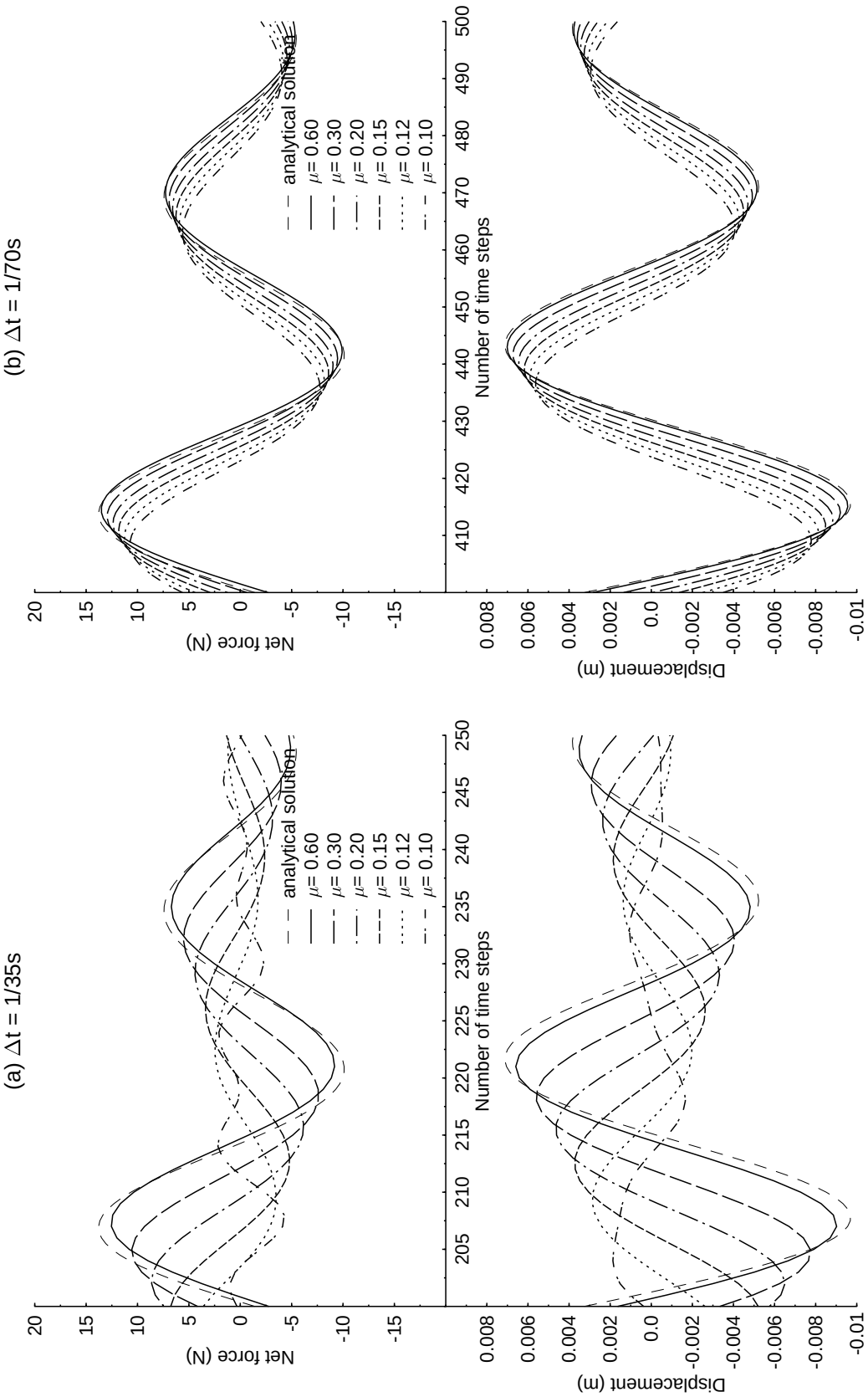

Figure 4-5: Accuracy of the numerical integration after large time as a function of μ and Δt.

Chapter 5

Towing tank testing

5.1 Design of models

5.1.1 Model design objectives

Large high speed passenger ferries present a range of technological problems that have either emerged for the first time or have been exaggerated by the increased demands of higher speeds. One of these issues is seakeeping. Poor seakeeping occurs when resonance of motions occurs in combination with significant excitations. The resonant frequency and associated damping ratio of a given boat, although a function of parameters such as speed and loading, does not change greatly under different conditions. On the other hand as the boat speed increases this frequency is encountered (for head seas) in longer waves. For conventional hulls at slow speeds the waves corresponding to the heave and pitch resonant frequencies are generally shorter than the hull length, and the associated heave force and pitching moment are small or even negligible. This is a consequence of cancellation effects when integrating pressures over the hull (at certain wavelengths, where equivalent volumes of the boat may be at wave troughs and wave crests, the net force may be close to zero) and of the decay with depth over a length scale proportional to the wavelength of the non-hydrostatic component of pressure. The wave force for a given wave height will be at a maximum, and equal to the equivalent hydrostatic force, for wavelengths significantly longer than the hull, and any vessel fast enough for this to coincide with its natural frequency has potential for seakeeping problems.

Early development of high speed ferries naturally focused on resistance and propulsion. In terms of meeting contract obligations these problems have been largely overcome, although they continue to be of interest as builders and operators demand bigger, faster, or more efficient vessels, and tighter design margins, in order to secure an advantage over their competitors. On the other hand these vessels have developed a reputation for poor seakeeping, and consequently there is now a greater emphasis on motion prediction in the research activities. There is also a rapidly growing interest in dynamic sea loads and their influence on structural fatigue.

The effect of motions on passengers may be quantified in terms of *motion sickness incidence* or *motion sickness index* (MSI), defined by Mandel [65] as "the percent of individuals who would vomit if subjected to motions of prescribed characteristics for a given time interval t_1", and discussed also in [66] and [78]. Figure 5-1 shows MSI as a function of frequency and acceleration for sinusoidal vertical motions. This shows the worst range of frequencies to be about 0.06–0.4Hz (0.4–2.5r/s). Unfortunately this coincides with the typical range of natural frequencies for most large high speed passenger ships.

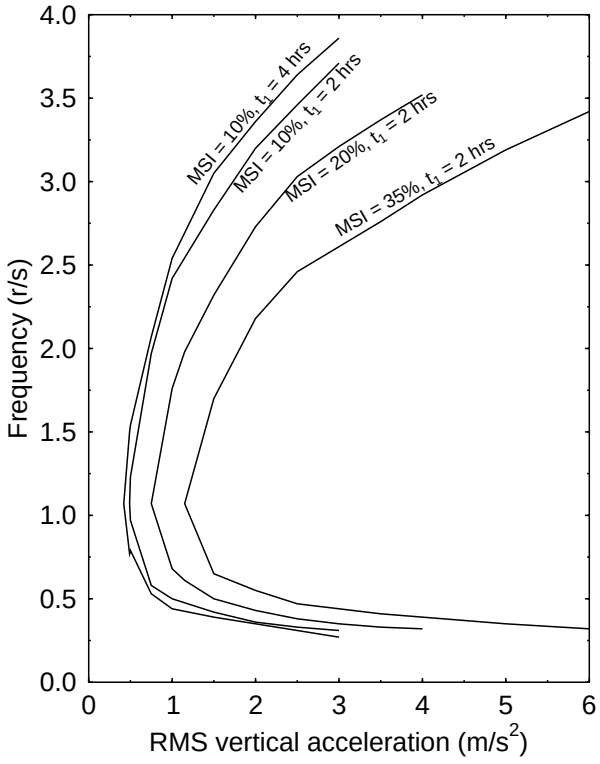

Figure 5-1: Contours of motion sickness incidence as a function of frequency and vertical acceleration (based on tabulated data in Mandel [65]).

In addition to passenger comfort is the problem of dynamic structural load and slamming. The high speed of these vessels means that dynamic structural loads and slamming events are likely to be both more severe and more frequent than for conventional vessels. Slamming, as well as introducing very high local stresses, initiates high frequency global vibrations with very low damping, which in turn is associated with high global stresses ([2] and [12], as well as preliminary results of research in progress by Roberts, Watson and Davis at the University of Tasmania). This has serious implications for fatigue, particularly as this type of vessel is generally made of aluminium in order to overcome the increased drag or decreased payload capacity associated with excess structural weight.

The dynamic load and slamming problem is a major concern in the classification of high speed ferries, and the lack of a sufficiently large body of related research has meant that many

of the design rules are extrapolated from research on more conventional types of boats. Naturally in such cases the classification societies have to be conservative in making the rules, while the builders are concerned about unnecessary structural weight and the impact it has in terms of speed reduction, lost payload, or additional propulsive power requirements. Unlike civil engineering construction for example, where the regulatory bodies have a monopoly, there is open competition in the market for boat classification, and therefore the builders and the classification societies both have an active interest in better load prediction and less conservative rules based on accurate and more comprehensive information. The prediction of dynamic sea loads follows as a logical consequence of the computational methods developed in this thesis. However, slamming, if defined as the high local loads that develop rapidly (inertia dominated) when hull surfaces of significantly non-vertical inclination impact with the free surface, accompanied by significant wave breaking, would demand a more customised local analysis that is not directly the subject of the present thesis. Nevertheless the methods developed here have potential application to the prediction of slamming loads, and also to the damping and decay of the higher frequency global modes of vibration which have recently been observed to be initiated by slamming events.

The usual solution to the seakeeping problem is to install a ride control system, either active or passive, which make use of lifting surfaces. Considerable research has already been done and is still being undertaken in the area. However appendages have disadvantages, including additional drag and proneness to damage. In the last few decades designers have been considering alternative hull forms to minimise motions. One such form is the *small waterplane area twin hull* (SWATH), and, more recently, shapes intermediate between this and conventional hulls (semi-SWATH) have also been tried.

Examples of semi-SWATHs include boats designed and built in Australia by Austal Ships (in Fremantle, Western Australia) and NQEA (in Cairns, Queensland, who have originated the *Seajet* design built in Denmark), as well as the 128m "HSS" built for STENA in Finland. The Australian built example has been at a scale where an element of speculation has been possible without too much financial risk, as the semi-SWATH treatment in the Austal design is little more than a modest submerged bulbous bow faired into the underwater hull. The HSS however is not only considerably larger than anything else of its type in the world, but it in particular represents a very substantial departure from a conventional hull form, with a significant reduction of waterplane area along the whole hull length and a large submerged bow. However in spite of being the subject of considerable research it has not met the expectations of all observers. In particular this vessel, as well as the *Seajet* and other vessels without substantial reserve buoyancy above the waterline forward, have shown themselves to be very prone to nose-in incidents in following seas or even during crash stops. This illustrates the overall complexity of the design process, as the consideration of such events involves significant surge inertia terms which are not the subject of the present work. However, there is potential for the computational methods developed here to provide a basis for analysis of these aspects.

The basic premise of the SWATH concept is that a lower natural frequency (due to reduced hydrostatic stiffness for the same or similar effective mass) has associated with it lower accelerations for a given amplitude of motion. This is partly offset by increased motion amplitudes due to an increased wave force associated with the longer wavelengths at resonance (this will be described in detail in the following chapter), and possibly also due to slightly poorer damping characteristics of SWATH type hull forms. Generally however for high speed vessels there is a significant net reduction in accelerations. Motion sickness incidence is basically a function of acceleration and frequency, but for frequencies near the natural frequency of typical ships in heave and pitch the motion sickness incidence is near its maximum and is only weakly frequency dependent. Therefore a reduction in accelerations will in general improve comfort for passengers. It does not necessarily imply however an improvement in the structural aspects of seakeeping, although global dynamic sea loads and impact velocities in slamming events will probably also be lower. Also a lower natural frequency allows more response time for ride control systems, as well as smaller force requirements.

Obviously, given that conventional boats are still far more common, the seakeeping advantages of SWATHs are gained at some sacrifice. The buoyant part of the hull form, being largely submerged, creates smaller waves than conventional hull forms due to its dynamic motions. As a consequence there is less damping near the natural frequencies, and motions may be large. Furthermore the lower natural frequency means that resonance occurs in longer waves, also contributing to larger motions. In terms of passenger comfort there is usually still a net benefit, but structural or safety problems may arise. Therefore SWATHs are rarely built without some form of ride control system (although the HSS has hull appendages designed to reduce vertical motions and does operate without an active ride control system). Other disadvantages of SWATHs include sensitivity to load (hence ballast and/or appendages are required, which contribute to drag), higher resistance (although wave resistance is usually less, the frictional resistance and other viscosity related components more than offset any gain), difficulty of manufacture (they tend to have more curved surfaces than conventional hulls), and machinery arrangement is more difficult (because the narrow waterplane restricts free access to the hulls).

The semi-SWATH concept is an obvious opportunity to exploit the positive aspects of both SWATH and conventional hulls, but without a better understanding of which major features of the hull (which is basically an infinitely variable surface) are important, and how they affect global behaviour, there is no guarantee that such a hybrid will be better than either of its antecedents. Fundamental questions include whether to have waterline beam reduction for the whole length of the boat or only for part of the length (for example only for the forward half), whether or not to have a submerged or bulbous bow (and if so the shape, size, and depth), the optimum use of flat surfaces, curved surfaces, and chines, design for slamming, and safety against nose-in incidents in following seas. Even in this list there is considerable scope for variations, and as there is yet no “normal” semi-SWATH design.

Seakeeping studies have been done on specific SWATH hulls, but unfortunately there is not a great amount of information publicly available about the general behaviour of this class of vessel (such as the type of extensive systematic series data frequently seen for conventional hull forms) and there is even less publicly available for semi-SWATHs. Some exceptions to this include Doctors [24] and Schack [85]. Rapid progress therefore requires intelligent interpretation of results and not just a mass data or trial and error approach. Once the relative importance and general effects of various features have been identified systematic studies may be beneficial in refining and optimising design.

The models tested as part of this project are intended to represent a significant departure from the conventional, with the object of gaining a better understanding of some semi-SWATH design issues.

Finally, one of the objectives of the strip theory of the previous chapter was the modelling of high speed vessels, as was highlighted in the section dealing with the strip theory assumptions, and there is an obvious application to the high speed ferries of the type discussed above. Therefore, in addition to addressing some issues associated with unconventional hull forms, and in particular semi-SWATHs, the models tested in the experimental programme were also designed to providing a challenging test case for the validation of the new strip theory.

5.1.2 Reference hull

As a point of reference in comparing the semi-SWATH hulls to be tested in the experimental programme an Incat 74m wave-piercing hull was selected as a benchmark. The semi-SWATH hulls were therefore designed to be in some sense a variation of the Incat 74m hull, and similarities and differences will be described below, although obviously the main feature was a reduction in waterplane area.

The Incat hull, apart from its slenderness, is a very conventional hull when viewed below its calm water line. The bow only takes on its wave-piercing properties when it has significant downward motion relative to the water. It was chosen because it was a real boat, it represented a typical example of a conventional high speed ferry hull, and because some information about its shape was available.

5.1.3 Models

Two semi-SWATH models were designed. Each had identical buoyancy distribution to the Incat hull at the nominal displacement. This guaranteed the same nominal wetted length and displacement. Obviously with differing waterplane areas it was not possible in general to maintain the same buoyancy distribution at any other draught without the hulls being mere copies of the original with different scaling factors in the vertical and lateral directions. This was not desired not only because it did not represent a significant enough change, but because it would have resulted in very large draughts as the waterline was reduced. The intention was to confine

the cross sections to similar beams and draughts to the Incat ones within the constraints of a plausible real hull form, both to maintain a similarity between the new hulls and the original Incat one, and because the author's view of the distinction between a SWATH (or semi-SWATH) and a conventional hull is that the waterplane area in the former should be smaller than the maximum submerged plan area, that is the waterline beam for at least some sections is smaller than maximum beam at the same sections.

With the focus being on the waterplane area it was decided also to keep the shape of this constant in dimensionless terms (i.e. if the lateral coordinates were expressed in units of the maximum beam, and the longitudinal coordinates in terms of the waterline length, the waterplane area would fit within a unit square, and this shape was fixed). The aft end of the waterplane was also kept at the stern, so that as the length was reduced the point where the bow cut the calm water surface was moved aft and, because the wetted length was fixed, a submerged bow was created rather like an exaggerated bulbous bow.

There were two controlled differences between the various hulls. These were the waterplane area and the longitudinal centre of floatation (LCF) (or centre of waterplane area, which is the point of action of the incremental hydrostatic restoring force for an infinitesimal heave displacement), and the specification of these two quantities uniquely determined the lateral and longitudinal scaling factors to be used for the waterplane area shape (or vice versa). The significance of the LCF is that for small amplitude motions and zero frequency it is the point of action of the net force acting on the hull. For conventional hulls the LCF is always forward of the LCB, and typically motions at the bow are greater than at the stern. The two can be made to coincide if a submerged or bulbous bow is present, and this tends to reduce pitching moments and hence to some extent overall motions.

The two models, subsequently to be referred to as *SWATH #1* and *SWATH #2* are shown in body view in figure 5-2, with equal section spacings of 250mm. Both have a total length of 2.5m, and were tested as demi-hulls with a design displacement of 22.00kg. (Note that not all of the freeboard is shown in this figure: the SWATH #1 model has a freeboard of 125mm, while the SWATH #2 model has a freeboard of 200mm.) SWATH #1 has 40% of the waterplane area and $\frac{5}{6}$ of the waterline length as the Incat 74m reference hull (giving 48.0% of the maximum waterline beam) while for SWATH #2 the corresponding values are half way in between at 70% waterplane area and $\frac{11}{12}$ waterline length (giving 76.4% beam). The position of the LCB for all hulls is 39.1% of the length, measured from the stern, and for the LCF it is 35.5%, 39.0%, and 42.5% respectively for SWATH #1, SWATH #2 and the reference hull. (Here the length is taken as the wetted length, and is therefore the total length for the SWATH models and the waterline length for the Incat hull.) Note that the LCB and LCF are almost coincident for SWATH #2, and for SWATH #1 the LCF is aft of the LCB. This will tend to decrease bow motions while increasing stern motions. It was suspected that the optimum position for the LCF was in fact slightly aft of the LCB because of the greater added mass coefficients of typical stern sections

contributing to a slight rearward shift of the *effective* centre of mass. In addition if the LCF is moved far enough aft that motions are greatest at the stern then there is the possibility of improved controllability through the use of stern tabs. It transpires that something like this approach may have been adopted in the HSS, but with aft end vertical motions constrained or damped by appendages and bilge keel like features. This vessel has accommodation for passengers right at the forward bow, a feature giving greater incentive to move the LCF well aft but also raising the issue of general safety and passenger exposure to bow damage.

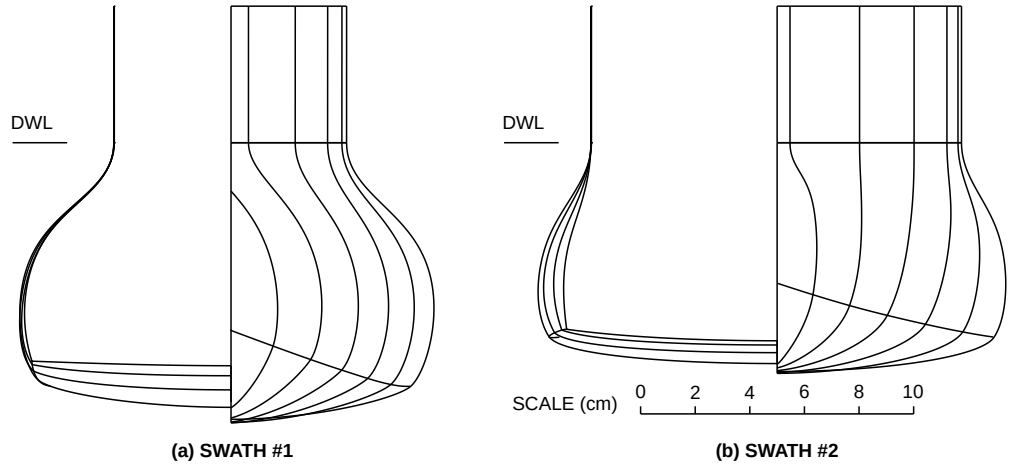

Figure 5-2: Semi-SWATH models.

The reference hull had chines at the stern extending for most of the length of the hull, as well as a V-shaped keel, the angle of which increases from the bow to the stern. The SWATH models were similar, except that the chines were made to vanish after about one third of the length, and the V of the keel also was made to disappear, creating an almost flat bottomed stern.

The shape of the semi-SWATH models above the waterline was not given as much consideration as the shape below. It was decided for simplicity to have vertical sides above the waterline, giving the added advantage that the hull did not become too narrow at any point (if the sides were sloping at the waterline then the waterline would no longer be the narrowest part of the boat). It is envisaged that in later testing the semi-SWATH models can be modified above the waterline to provide for testing of the effects of a more realistic outward expansion of the hull beam above the waterline.

Most other model design features were governed by practical considerations. These include in particular the shapes of the bow and stern. The bow shape in particular can have a dramatic effect on seakeeping. In particular a wide flat bow (even neglecting viscous effects) introduces substantial damping in the motions, which is highly desirable. However if a slamming incident were to occur with this type of bow the effect could be quite damaging. The most desirable shape from the point of view of slamming pressures is a narrow vertical shape, and, given that high speed vessels are susceptible to slamming, this is the general shape that was chosen for the

models to be tested. It is also more similar to the form of the HSS bow. A compromise between the two would be a round bow, as would be typical but on a smaller scale for bulbous bows (as in the Austal designs), and most of the semi-SWATH designs currently being built have opted for this.

The stern of most semi-SWATHs currently being built are generally very similar to conventional hulls, although the STENA HSS is a notable exception. Obviously, given the waterline constraints arbitrarily imposed above, the present models have as much waterline beam reduction at the stern as anywhere else, which is actually even more reduction than in the STENA HSS. This does however present possible difficulties when considering space requirements for the propulsion system. Therefore the transom shape was chosen to maximise the possible jet duct diameter for a specified waterline beam and submerged area while maintaining a plausible shape.

Finally fairness of the hull form was an important consideration. This, in combination with the other chosen restrictions, to a large extent dictated the shape of the keel line and bow profile. This was especially true of the bow shape, where the buoyancy distribution of the wave-piercing catamaran hull was not ideally suited to the very different submerged bow sections of the semi-SWATHs. This was particularly true at the point at which the stem of the latter cut the waterplane, where it was difficult to contain a tendency for the cross section area to increase rapidly in the aft direction while still retaining fairness.

It was decided to make the models 2.5m long, giving a scale of 1:24[1]. This was actually quite long relative to the tank dimensions, but because the hulls were very slender the cross sections were actually quite small. The displacement at the nominal draught was only 22kg and the maximum draughts at the nominal waterline were respectively about 84.5 and 102.6mm for the two models.

The size of the models gave rise to some problems in testing, including finite depth effects and difficulties in obtaining the required low frequency data. This is discussed in more detail in section 5.4, and in hindsight a slightly smaller scale would have been chosen.

A summary of the SWATH model particulars is given in table 5.1.

Model	**L/B**	**B/T**	$\mathbf{C}_b$	**LOA** (m)	**LCB** (m)	**RofG** (m)	**WSA** (m^2)	$\boldsymbol{\Delta}$ (kg)
#1	16.12	1.511	0.553	2.5	0.977	0.775	0.716	22.00
#2	14.28	2.072	0.593	2.5	0.977	0.775	0.642	22.00

Table 5.1: SWATH model parameters

[1] Although the reference hull was 74m in total the waterline length was only 60m. It has a large centre bow for reserve buoyancy that extends well forward of the two demi-hulls.

5.2 Towing tank set-up

Testing was carried out at the towing tank at the Australian Maritime College in Launceston, Tasmania. The tank itself is 60m long × 3.5m wide, with a maximum water depth of 1.6m (although testing in waves is generally restricted to a maximum of 1.5m depth). The carriage has a maximum speed of 4.5m/s, although the tank is too short to get much useful length of steady state data above 4.0m/s. The maximum speed is further restricted for heavy models to avoid damage to strain gauges during starting and stopping, although this was not a problem in the present tests.

The wave maker is a bottom hinged wet back flap type hinged at the tank floor, driven by a hydraulic ram powered by a 54kW hydraulic pump. It could nominally produce waves up to a frequency of 2.0Hz or a wave height of 250mm, but in practice the output was limited by non-linearities and eventual breaking of the wave, not by the paddle. For example a 1.4Hz wave becomes significantly distorted at a wave height of 80mm, and its theoretical breaking limit is 113mm. At the low frequency end of the spectrum the hinged type paddle distorted the wave, and this limited the frequency to a minimum of about 0.4Hz. Other problems arose at the low frequencies, including finite depth effects and high wave velocities, the latter of which could result in contamination by reflections at lower model speeds. These are not in themselves problems, but they limit the applicability of results, and will be discussed in more detail in section 5.4.

Input of the wave form to the wave maker is via a computer, and the software allows regular waves, irregular waves based on a comprehensive repertoire of predefined spectra, or arbitrary user defined forms. The use of irregular waves was however limited by the calibration of the system, and this too will be discussed in more detail in section 5.4.

The model was supported so that it was free to move in heave and pitch, but restrained for the other degrees of freedom. This was achieved by attaching the boat to the carriage at two points one metre apart, approximately equal distances from the centre of mass of the boat. The aft support was free to move vertically only, and attached to the hull via a ball and socket hinge, which in turn was connected to a slide that allowed longitudinal movement between the hull and its support (this allows compensation for the slight change in the horizontal distance between the two attachment points on the hull as it pitches). Relative motion between the support and hull was therefore constrained only vertically and laterally. The forward support was also free to move only vertically, but was attached to the hull via a fixed hinge, allowing rotation about the lateral axis. Thus relative motion was constrained in all translation modes, and in rotation about vertical and longitudinal axes.

Instrumentation used for the tests consisted of two linear variable displacement transducers (LVDTs) for measuring the vertical motion of the supports (and hence heave and pitch), a strain gauge for measuring resistance (only connected for some of the tests), and a capacitance type wave probe. Waves were recorded by a static wave probe mounted near the wave maker as was

the standard practice at the towing tank at which the tests were conducted. Because of the problems in maintaining an electrical connection with the wave probe, the wave measurements had to be taken before moving the carriage. This was not a problem as the recording of the signal was normally complete well before the waves had approached the carriage, but for the lower frequency (higher speed) waves timing of the process was quite critical in order that the carriage could be started before the waves were reflected.

5.3 Testing programme

5.3.1 Tests conducted

Calm water resistance

A set of calm water resistance measurements was made for both SWATH models, for speeds from 0.4m/s to 4.0m/s in steps of 0.2m/s, at the nominal displacement. These are compared in figure 5-3, in which the results have been scaled to a full size of 60m using the ITTC friction line with the form factors indicated. The corredponding model sinkage and trim are indicated by figure 5-4.

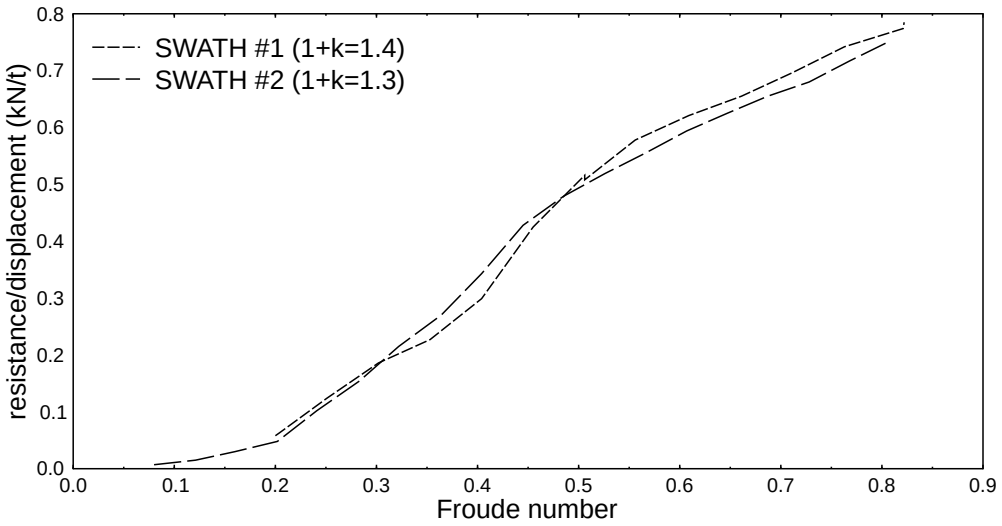

Figure 5-3: Comparison of full scale total resistance of SWATH #1 and SWATH #2

The form factors used in figure 5-3 were obtained from Prohaska plots, which are based on the premise that the wave resistance coefficient, C_W, is proportional to Fr^4 (at least at low Froude number), and that the total resistance coefficient is given by $C_T = C_W + (1+k)\,C_f$, hence $\frac{C_T}{C_f} = m\left(\frac{Fr^4}{C_f}\right) + (1+k)$, giving a straight line with vertical axis intercept $(1+k)$. (In fact it is not necessary that $C_W \propto Fr^4$, merely that $\lim_{Fr\to 0} \frac{C_W}{Cf} = 0$.) Application of the form factor thus obtained to the resistance results relies additionally on the assumption that k is a constant over the entire Froude number range, which is highly questionable for the SWATHs (both of

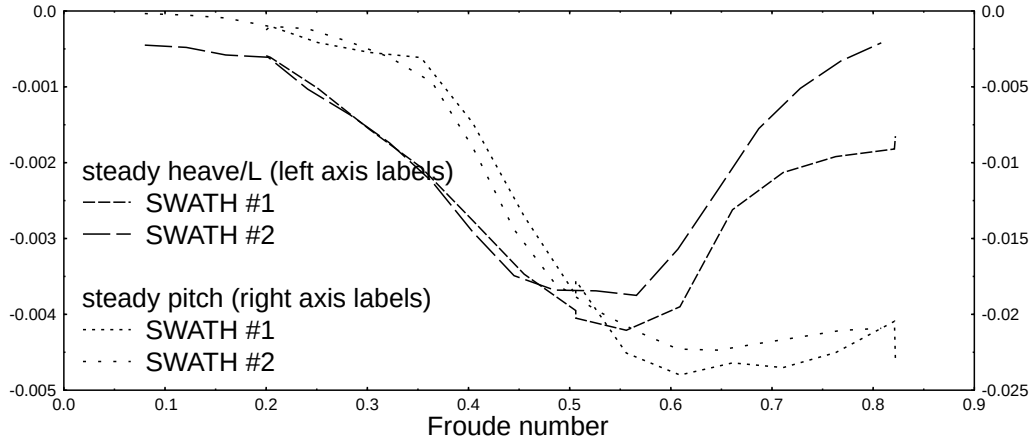

Figure 5-4: Steady state heave and pitch (positive bow down) in calm water for SWATH models as a function of Froude number

which have submerged transoms) considering the different transom flow regimes at low and high Froude number. The inapplicability to other than slow vessels without immersed transoms is also noted by Couser et al. [18], who also cite numerous other methods of estimating form factors showing both a significant variation with Froude number and considerable disagreement of results for a given hull.

Estimation of form factors by this method can only be done with any certainty in the case of SWATH #2 since SWATH#1 has limited resistance data at low Froude number, although the sequence formed with the reference hull form factor of $1 + k = 1.05$[2] is consistent with the ranking of the three hulls as members of a semi-SWATH family. Furthermore the sensitivity of the comparison to the choice of k does not appear to be very great. Given the dubious nature of calculating form factors and the huge variation with different methods of calculation [18], it is impossible to tell on the basis of information at hand how indicative the results presented here are of the true resistance.

As might be expected because of its greater surface area, SWATH #1 has in general a slightly higher resistance, particularly at higher speeds where the frictional component of resistance dominates. In the near vicinity of a Froude number of about 0.4 the trend is reversed, however the difference is not particularly significant, and may even be due to experimental factors. It could alternatively be explained in terms of the hump in the wave making component of resistance, which might be smaller for the SWATH #1 because of its finer waterlines and more deeply submerged hull. The reference hull resistance results broadly follow the trend established by the two SWATH models, although the comparison should be made with caution because of its different test conditions[3].

[2]The reference hull was tested by MARIN, who used this value. It is not known how the value was obtained, but it could not have been obtained using Prohaska's method from the resistance data presented by MARIN in their test report.

[3]The reference hull results have not been included in figure 5-3 in accordance with confidentiality requirements

In addition to their larger wetted surface area the SWATHs may show higher resistance because of their large deeply submerged transom areas (contributing significantly to both form drag and wave-making drag). However it should be pointed out that no effort was made to optimise the SWATHs for resistance, and considerable scope is left for improvement.

In summary, although the SWATH models most likely had a significantly higher resistance, this should not imply that SWATHs in general are significantly worse. A well designed SWATH (or semi-SWATH) should have only slightly greater resistance than an equivalent catamaran, and this may be a worthwhile sacrifice if seakeeping properties are improved.

Regular seas

Seakeeping tests in regular waves were conducted for both models at their nominal draught (22.00kg) and at a draught deeper by 25mm (corresponding to 25.72kg for SWATH #1, or 28.50kg for SWATH #2) for various speeds wave heights, and frequencies. The ranges of frequencies chosen differed depending on speed, but in most cases were sufficiently extensive to clearly define the resonant peaks in the transfer functions. The only exceptions to this was at the higher speeds, and particularly for SWATH #1, which had a lower resonant frequency. In these cases the wave frequency corresponding to the encounter frequency that caused resonance was too low to be produced in the tank without major problems (these problems and others will be discussed in section 5.4).

Speeds and wave heights at which tests were conducted are shown in table 5.2 for the two models and two draughts used. The speeds cover the range up to a maximum of 3.5m/s, corresponding to about 37kt full scale. The effect of wave height was only investigated for three combinations of model and speed, and found to be fairly linear, so further investigation was not considered warranted. At greater wave heights there was also a practical operational problem with the first SWATH model of swamping near the resonant frequency, and the shape of the hull made it very difficult to remove the water. The second model was built with more freeboard, but near its resonant frequency it almost hit the carriage at larger wave heights.

	speed (m/s)					
	1.0	**1.5**	**2.0**	**2.5**	**3.0**	**3.5**
SWATH #1, 22.00kg	40	40	40	40	40	20, 40
SWATH #1, 25.72kg	30		30		30	
SWATH #2, 22.00kg	40	40	20, 40	40	20, 40, 60	40
SWATH #2, 28.50kg	40		40		40	

Table 5.2: Showing wave heights (mm) for which tests in regular waves were conducted

Results of these tests will be presented in chapter 6.

of Incat.

Random seas

Some preliminary tests in irregular waves were conducted for SWATH #1, but, mainly because of the short tank length, and high speed and low natural frequency of the model, irregular wave testing was discontinued. More detail is given in section 5.4.

5.3.2 Conventional hull form results

It was originally envisaged that the semi-SWATH results be compared with comparable results for their reference hull, the Incat 74m wave piercing catamaran. However there were problems with access to the relevant data for commercial reasons. On the other hand, data relating to the seakeeping of a systematic series of conventional high speed hull forms was available through the Australian Maritime Engineering Cooperative Research Centre (AMECRC) ([63] and [10]).

Two contrasting examples from the AMECRC systematic series were taken as representative of conventional hull forms. These are shown in figure 5-5, and principal particulars are shown in table 5.3. These formed the basis for comparison with the semi-SWATH results, and will

Model	**L/B**	**B/T**	$\mathbf{C}_b$	**LWL** (m)	**LCB** (m)	**RofG** (m)	**WSA** $\left(\mathrm{m}^2\right)$	$\boldsymbol{\Delta}$ (kg)
#04	8.00	4.00	0.447	1.6	0.7136	0.400	0.3056	7.158
#05	4.00	4.00	0.395	1.6	0.7136	0.400	0.6297	25.344

Table 5.3: Relevant AMECRC systematic series model parameters

subsequently be referred to as *AMECRC #04* and *AMECRC #05*.

Of these AMECRC #05 was closest in displacement and draught to the two semi-SWATH models, while AMECRC #04 was closest in beam.

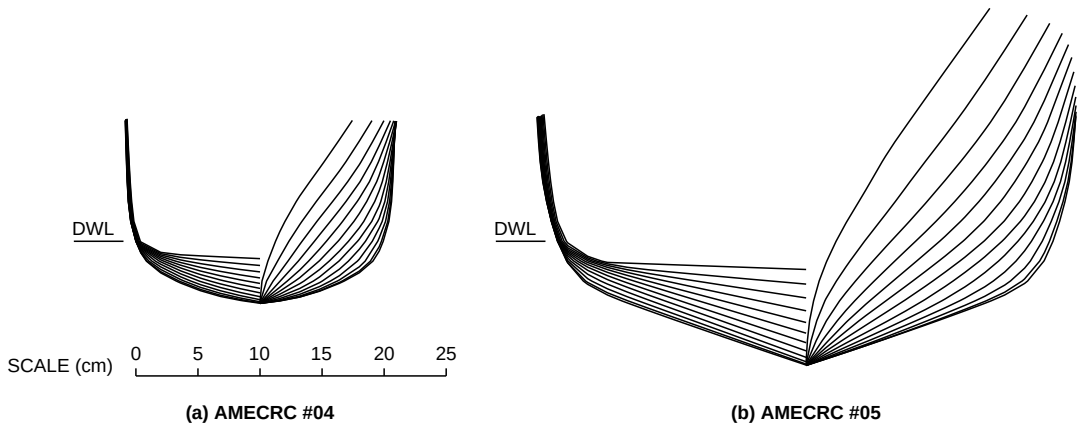

Figure 5-5: AMECRC systematic series models

5.4 Problems encountered in testing

The biggest problem during testing was the need to test at lower frequencies than initially envisaged. This was for two main reasons. The SWATH configuration, as already discussed, has inherently low natural frequencies in the heave and pitch modes. These natural frequencies are an encounter frequency phenomenon, and the high speeds at which the model was tested mean that there is a large Doppler shift between the wave frequency and the encounter frequency, making the wave frequencies required to excite resonance at these speeds even lower. The model could have been made smaller, although to remove the difficulties altogether would have required reducing the model size to the extent that accuracy of the results would have come into question.

Some consequences of low frequencies include finite depth effects due to the long wavelengths, the inability of the wave maker to generate accurate waves at these frequencies, and high wave speeds causing contamination of data from wave reflections.

5.4.1 Finite depth effects

It is not possible to quantify precisely how the presence of a channel bottom will affect the results without either comparing with deep water results or repeating the numerical analysis including bottom effects, neither of which was possible within the time constraints of this project. Some guidance is given by the results of Børresen and Faltinsen [11], and by Kashiwagi and Ohkusu [52], and will be discussed in the next chapter. Obviously though the change in wave speed for a given frequency means that the encounter frequency for a given wave frequency and boat speed will differ, or alternatively the same pair of wave and encounter frequencies at two depths will correspond to different boat speeds. Looking at the conventional strip theory equations, the resonance effects (particularly where there is little damping present), encapsulated in the left hand side of the equations, depend on the encounter frequency, while the exciting force, represented by the right hand side of the equations, are primarily wavelength dependent[4]. This will be discussed in detail in the next chapter, and illustrated very clearly in the actual towing tank results, also presented in the next chapter. Thus by plotting motions against both encounter and wave frequencies it should be possible to identify which features are dependent on which variable and therefore make inferences about the behaviour of the hull in deep water. However the results at lower frequencies should be regarded as potentially distorted due to depth effects.

Wave frequency and wave number for regular waves at arbitrary depth are related through the the equation

$$\omega = \sqrt{gk \tanh(kd)}, \tag{5.1}$$

and in deep water the $\tanh(kd)$ term reduces to 1, giving $\omega = \sqrt{gk}$. The main effect therefore that finite depth has is to modify the relationship between wavelength and wave frequency,

[4]The strip theory equations suggest a wave *frequency* dependence, but for a given depth this is equivalent to a wave *length* dependence. It will be argued in the next chapter that (if the water depth is not fixed) it is the length of the wave that is most important in determining the wave force.

which in turn modifies the wave speed. Figure 5-6 shows the ratio of wavelength, λ, wave phase velocity, c, and wave group velocity, c_g, to their deep water equivalents (λ_∞, c_∞, $c_{g\infty}$) as a function of frequency, for a water depth of 1.5m (the depth at which all the models were tested). If it is assumed that a boat's response in waves is primarily a function of wavelength and encounter frequency (as will be proposed in section 6.1.2), then the set of conditions giving rise to a particular response could be represented as a point in the k, ω_e-plane. We note also that the encounter frequency relation

$$\omega_e = \omega_0 + kU$$

may also be represented as lines in this plane corresponding to particular speeds. Thus, in dimensionless terms,

$$\omega_e \sqrt{\frac{L}{g}} = \sqrt{(kL)\tanh(kd)} + (kL)\,Fr. \tag{5.2}$$

(Note that in deep water $kL = \omega_0 \sqrt{\frac{L}{g}}$.)

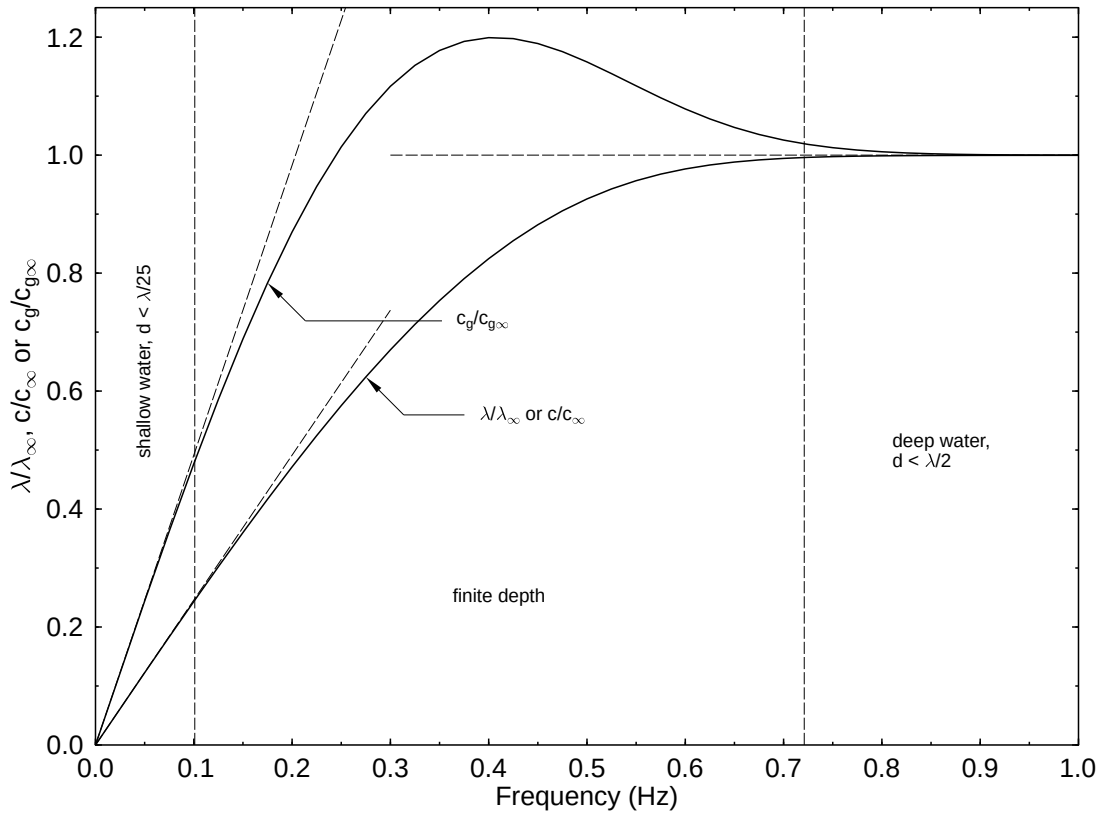

Figure 5-6: Finite depth and shallow water effects at low frequency (water depth 1.5m).

Contours of Froude number (Fr) in the k, ω_e-plane, defined by equation 5.2, have been plotted in figure 5-7 for both deep water and finite depth water. We see that, by considering a single point in the plane (which, according to the above assumptions, uniquely defines response) a given encounter frequency and boat speed in finite depth water may be considered equivalent

to the same encounter frequency but modified boat speed in deep water. For example, the point $\left(kL, \omega_e\sqrt{\frac{L}{g}}\right) = (1.0, 1.5)$ is consistent with approximately $Fr = 0.5$ in deep water, or $Fr = 0.75$ in finite depth water (in which $\frac{d}{L} = 0.6$).

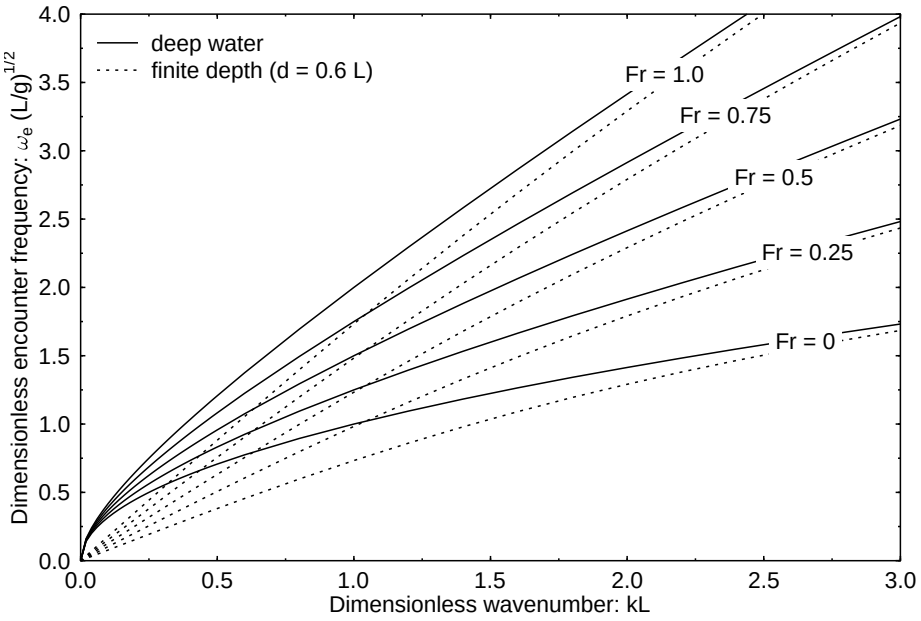

Figure 5-7: Showing the relationship between encounter frequency and wavenumber at various Froude numbers, for deep water and depth to model length ratio $\frac{d}{L} = 0.6$ (corresponding to the tests for SWATH #1 and #2)

The apparent speed shift due to finite depth can be shown to be

$$\begin{aligned} \Delta Fr &= Fr_{\text{finite}} - Fr_{\text{deep}} \\ &= \frac{1 - \sqrt{\tanh(kd)}}{\sqrt{kL}} \end{aligned} \tag{5.3}$$

and at $kL = 2.15$ is about 0.05, or at $kL = 3.33$ is about 0.01. In relation to the results presented in the next chapter, and in particular in figure 6-8, the apparent speed shift in waves of higher frequency than the former (equivalent to $\omega_0\sqrt{\frac{L}{g}} \geq 1.4$ in 1.5m deep water) represents less than half the increment in the Froude number between sets of results, which is significant but not large, while in the latter case (equivalent to $\omega_0\sqrt{\frac{L}{g}} \geq 1.8$) it represents less than $\frac{1}{10}$th of the increment, and is not significant[5].

5.4.2 Wave reflection

Wave reflection becomes a problem in towing tank testing at low frequencies because the associated high wave group speeds may be faster than the model speed, and reflected waves can catch

[5]The corresponding dimensionless wave frequency in the latter case for the AMECRC models, which were only 1.6m long, is $\omega\sqrt{\frac{L}{g}} = 1.5$. With the exception of the lowest data point in each case these models were not tested below this frequency, and there is therefore no problem with the interpretation of their results.

up with and overtake the model. Between the testing of SWATH #1 and SWATH #2 at the Australian Maritime College Towing Tank significant improvements were made to the beach, but for accurate results no reflections at all can be tolerated. Figure 5-6 shows also that, unlike wave velocity, wave group velocity at frequencies used in the present tests (above about 0.4Hz) are higher in finite depth than in deep water, making the problem worse. In 1.5m deep water at a wave frequency of 0.4Hz the wave group velocity is about 2.34m/s, so for the three higher model speeds (see table 5.2), which all exceed 2.34m/s, it was possible to avoid the problem at low frequencies by anticipating the arrival of the wave and starting the carriage a little early, so that the model reached the waves at about the same time the carriage had accelerated to its required speed. This was sufficient at the higher carriage speeds, but for the lower speeds it was necessary to start the carriage half way down the tank, giving the model a head start on the waves. The slower carriage speed meant that there was still sufficient time to obtain a reasonable number of data samples. At the very slow speeds it was not necessary to test at such low frequencies in order to obtain the shape of the transfer function curve because resonance occurred at higher wave frequencies, and thus the margin of safety against reflection was able to be maintained.

Other aspects of these problems that relate to the data analysis rather than to the conduct of testing are discussed in section 5.5.

5.4.3 Random waves

Initially testing in irregular as well as regular waves was envisaged, but numerous problems were encountered and only regular waves were used. The most significant problem with the irregular wave tests was the short sample length combined with the low natural frequency of the model. The sampling rate was 100Hz, and it was only feasible at the higher speeds to take 1024 samples[6], giving a frequency resolution after applying a fast Fourier transform (FFT) to the data of $\frac{100}{1024} = 0.098$ Hz. Given that the pitch resonance of SWATH #1 is at about 0.8Hz, and the corresponding wave frequency is about 0.4Hz at a model speed of 3.5m/s, this was not considered to be an acceptable resolution.

Even if one were to obtain results in these conditions, they would be highly dubious because the higher frequency components of the wave would travel slowly and either these would not be encountered until near the end of the run, or, if the carriage were started late enough for these to have reached the model, the model would be travelling through the reflected low frequency components as well newly generated waves. This is in particular a problem because the tank was not set up for the waves and model motions to be measured simultaneously or even at the same place (although it would have been possible to mount a moving wave probe on the carriage).

Other difficulties with the random wave testing related to generation of the waveforms. The software driving the wave maker was designed mainly for wedge or piston type paddles, and

[6] This corresponds to 36m of travel at 3.5m/s, and the *total* tank length is only 60m.

calibration for a hinged paddle had to be done manually (the software documentation and user instructions booklet gave the theoretical equations relevant to hinged paddles, which in fact gave results quite close to the manual calibration, but these equations did not appear to be implemented in the software as available and could not therefore be used for random waves). With regular waves one could easily adjust the wave height if it was not the desired value, but inevitably an irregular wave based on a predefined spectrum would not produce the same spectrum on output, and to do so would have required manual generation of the input file.

5.5 Post processing of tank data

Analysis of the towing tank data involved converting LVDT readings into heave and pitch (a simple geometry exercise), assessing the quality of the signals and, if necessary, rejection of part or all of the data, and then extraction of amplitude and frequency of the heave, pitch and wave signals (from which any other required data could be easily derived). Most of this was done using a computer program written by staff at the towing tank, although some significant modifications were made and these will be discussed below. Assessment of the data quality included manual checking of each data run however, and this will also be described below.

The most significant change made to the analysis program was the inclusion of finite depth effects. Figure 5-6 shows that for the depth of 1.5m (used throughout the tests) deep water wave equations can only be used with validity for wave frequencies down to about 0.7Hz, while actual frequencies used (because of the high speed and low natural frequency of the hulls tested) were often as low as 0.4Hz. Use of deep water equations in particular gave spurious wavelengths, which were required in the normalisation of pitch by division by the wave slope (wave height/length). An additional advantage of correcting the wavenumber calculation in the analysis program was that given the boat heave or pitch frequency, the wave frequency, and an accurate wavelength, (all obtainable from the raw data), it was possible to calculate an accurate estimate of the carriage speed, which could be compared with that recorded on the carriage speed control display as a cross check on the analysis.

The only other significant change was the way in which frequencies and amplitudes were calculated. The original program searched for peaks and troughs by looking for a data value that was a local maximum or minimum within 10 data samples either side of it, and frequencies were calculated from the period between successive peaks or troughs. This worked satisfactorily at high frequencies where peaks were sharp and a reasonably large number of them meant that errors were reduced by averaging. At the low frequencies typical of the present tests, coupled with inevitable noise in the data, the accuracy was not good, particularly for the frequency calculation, and occasionally the calculated results from good raw data were completely erroneous. By basing frequency calculations on distance between zero crossings instead of distance between peaks the spurious frequencies were totally eliminated and general accuracy was significantly improved. A

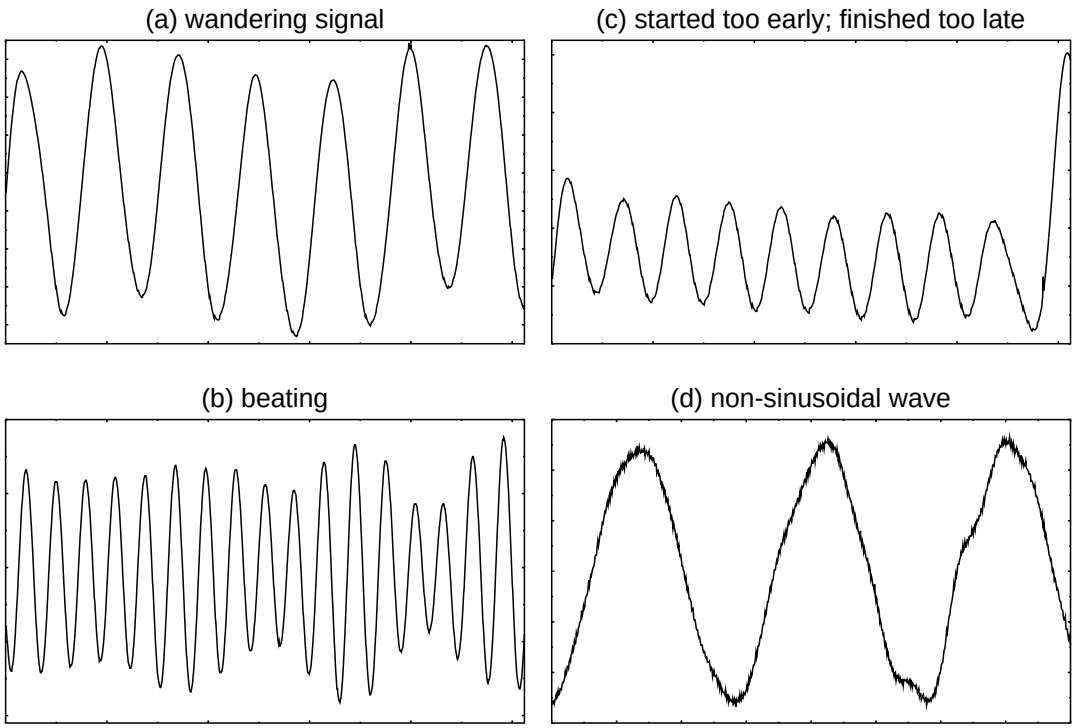

Figure 5-8: Showing examples of typical problems

very small amount of additional smoothing was required to avoid multiple zero crossings where there should have been one, but since the zero crossing is at (or near) a point of inflection the loss of accuracy is negligible. The overall improved accuracy from this method was evident from substantially better predictions of carriage speed using the method described in the previous paragraph, better correlation of results in cases where more than one run was done for a given set of conditions, and generally smoother transfer function curves.

Data could be less than ideal for many reasons, and it would be extremely difficult to produce a reliable computer program that could distinguish between data that should be rejected and data that should be accepted. It was considered simpler to inspect each signal manually using a graphing program, although this inevitably introduced some subjectivity into the process. After inspection of the data one of several actions could be taken:

1. analysis of the complete data for that run,
2. analysis of a window of data because of poor quality of part of the run,
3. either of the above, but with acceptance of the result subject to later checks,
4. manual modification of the data before applying one of the above,
5. complete rejection of the entire run.

Quality of data was an important issue, and only a small proportion of the runs (about 20%)

came under the first category. On the other hand with some care it was also only necessary to completely reject very few runs. Excluding problems attributed to equipment, and runs conducted for setting up purposes, slightly over 5% would fall into the latter category.

The only situation where the fourth of the above options was taken was where there was an obvious spike due to some sort of electrical interference, in which case the offending samples were replaced with interpolated values. Unless the spike occurred exactly on a peak or trough of the heave, pitch or wave signals the final result could not be affected.

The second category was common, mainly due to contamination of the beginning or end of the run. This could be because data acquisition was started too early (steady state not quite reached) or too late (the carriage starts to slow down at the end of the run before the set number of samples have been recorded), as illustrated in figure 5-8(c)[7]. At high speeds it was typical for both problems to occur because of the short run time, and unnecessary later work could be avoided by reducing the number of samples to avoid the problem. Contamination could also result at a combination of low speeds and low wave frequencies because of waves partly reflected by the beach overtaking the model. After recognising this problem it was largely overcome by starting the model from half way down the tank, and, because of the low speed in these cases, a good length of run was still easily obtained.

There were some unexplained phenomena that occurred consistently at certain encounter frequencies, which caused minor problems in the interpretation of results. These are illustrated in figures 5-8(a) and (b). The first of these was a slow sinusoidal drift of the mean model position, above which the expected oscillations at the wave encounter frequency were superimposed. The second was a slow periodic variation of the motion amplitude, similar to the beating pattern that occurs with the mixing of two wave signals of almost the same frequency and similar amplitudes. The amplitude of the beating was always small to begin with, quickly increasing as time progressed, as can clearly be seen in figure 5-8(b), although the tank was too short to find out what happened after a long time. Both these phenomena occurred always at particular encounter frequencies, and this frequency appeared to be independent of the model speed. The second is believed to be some sort of interference with a natural frequency of the system, although it is nowhere near the heave or pitch resonance frequencies and there is no discernable peak in the transfer function graph at this frequency.

When analysing the data the wandering signal problem generally came under the third category above. Because the distance between consecutive peaks and troughs and the period of oscillation were approximately constant there was no justification for immediate rejection of the data. Generally the problem was identified at the time of testing, and the run was repeated. If, as was generally the case, the repeated data were in agreement, the point produced a smooth transfer function curve, and the carriage speed estimate from the analysis program agreed with

[7]This is a good example of the effect of finishing data recording too late, but not a particularly clear one of starting too early.

the set speed, then the point was accepted, otherwise appropriate discretion was used. The beating problem was not in this category however because the motion amplitude was not a constant. Often, because the beating was initially minor and then growing, it was possible to discard the end of the run as in the second category above. However, depending on the extent of the problem, it could also fall into either of the third or last categories.

So far only the LVDT signal problems have been considered. The wave signal, apart from greater noise because of the different method of recording, was generally of much better quality. This was because it was taken at the beginning of each run before starting the carriage, reducing the possibility of timing problems, and recorded near the wave maker, eliminating reflection problems. The main problem was that at very low frequencies the wave maker was incapable of producing sinusoidal waves, probably because the hinged type paddle was inadequate in setting up the required wave particle velocities for long wavelength waves where the motions near the bottom of the tank are significant. Figure 5-8(d) shows an example. This was generally treated under the third category above unless the distortion was particularly bad. This was justified on several grounds. First, these frequencies were generally below any resonant frequencies, and the transfer function value is close to one, so if the results are not good it is usually quite obvious. Second, the actual model motions at these frequencies were sinusoidal, indicating little adverse influence, and third, if the explanation given above for the phenomenon is correct then it is likely that as the wave travels down the tank its shape improves as the wave energy becomes redistributed throughout the tank depth.

Chapter 6

Results and discussion

6.1 SWATH investigation

6.1.1 Introduction

The design of hulls for seakeeping is often regarded as an extremely complex problem, involving too many inter-related variables to be able to make meaningful qualitative statements about the effects of varying any of the design parameters. The results of this chapter will show on the contrary that, while it may not always be possible to make accurate qualitative predictions, even with quite sophisticated design tools, it is generally possible to make some meaningful predictions using very simple analogies. The motion of a ship in waves is no more than a forced vibration system, and there are many qualitative aspects that can be predicted at least in part by comparison with the familiar and well understood idealised spring-mass system.

Recall from section 5.1.1 that the purpose of investigating a family of semi-SWATH models was to make a significant departure from the conventional, for the purpose of highlighting and understanding some SWATH design issues, so that more rapid progress could be made through intelligent interpretation of results, as opposed to the trial and error approach of systematic series testing. We seek answers to the questions of the effect of water-plane area reduction (or 'SWATHness'), and of speed.

In order to extrapolate information a mathematical model simple enough to interpret intuitively needs to be developed. The alternative is extensive testing of systematic series (either physical or computational), and this does not necessarily give any guidance based on a physical understanding to estimation of performance of a projected and radically different type of vessel. The simple model should form the basis for explaining qualitatively observations, as well as giving approximate predictions. It provides the *general direction* for design. It should give a physical understanding and insight into the problem, and identify the important parameters.

On the other hand the sophisticated theories are still extremely important for quantifying and refining design. They should be good enough to provide *accurate answers* for designs. However

one must be cautious about accepting results of such theories, not only for the usual numerical modelling reasons, but because what might appear to be a favourable hull form by some criterion probably relies on fortuitous cancellations. A small change to operating conditions (such as to the speed, loading, or shape of the hull, the sea direction or spectral mix), or even simply the difference between the mathematical model and reality, is likely to remove such cancellations, causing the hull to perform little or no better than other similar forms.

Unfortunately existing strip theories are too complicated to provide the basis for simple physical assessment of directions, and are limited at present in their ability to provide accurate answers in particular at high speeds. A simple model that will be suggested below will be shown to be capable of producing nearly as good results (and certainly qualitatively similar), suggesting that there is nothing remarkable about the ability of complicated strip theories to provide predictions of the seakeeping of conventional vessels.

6.1.2 A simplified model

There is an obvious parallel between an oscillating boat and the classical dynamic problem of the forced oscillation of a simple damped spring mass system. The latter may be extended to two or more degrees of freedom, just as a boat is. But if we make the initial assumption that coupling effects do not dominate the motion (or even that the essential qualitative features of the motion are exhibited by the equivalent single degree of freedom system) we can keep the model as simple as possible, and therefore gain maximum insight, by investigating the single spring mass analogy. The following discussion will therefore be restricted initially to heave motion.

Even with such a simple analogy the correspondence is evident. Typical graphs in any vibration textbook show strong similarities with seakeeping results. Graphs of amplitude ratio for a spring mass system are analogous to the response of a vessel to a unit wave force. (It will be argued below that variation with frequency of added mass and damping does not significantly affect the response function.) However the seakeeping problem differs significantly from the simple spring mass system in that the wave forcing is a strong function of frequency, and simple equations can also be derived to represent approximately this aspect of the behaviour. Net response is then obtained as the product of the *wave force* and the *response to a unit force*.

Other differences include the speed dependence of the coefficients that describe the force and response, multiple degrees of freedom, and non-linearities. In terms of the objective of developing a simple model these vary in importance, and each will be discussed below in light of this objective. The main governing parameters will then be identified, typical values determined, and some results will be presented to highlight the implications for the preliminary design of unconventional ships and extrapolation of existing designs.

A total assessment of seakeeping must also include consideration of the seaway in which the vessel is intended to operate, and the criteria for judging performance. In terms of human comfort the latter may be expressed in terms of MSI (discussed briefly in the previous chapter),

but more generally many factors must be considered, as outlined for example by Mandel [65].

It should be stressed that the following discussion of the simplified model aims only at the broadest assessment of only motion response of the vessel. It is intended to shed light on the main trends and is not intended to provide a detailed prediction of motions.

Response to a unit force

The response of the simple spring mass system can be expressed (as derived for example by Rao [81]) as

$$\frac{H/2}{\delta_{st}} = \frac{1}{\sqrt{(1-r^2)^2 + (2\zeta r)^2}} \tag{6.1}$$

where, in terms of the vessel's hydrodynamic coefficients for a simplified representation of heave response,

$$\begin{aligned}
r &= \frac{\omega_e}{\omega_n} = \text{frequency ratio} \\
\omega_n &= \sqrt{\frac{C_{33}}{M\left(1+\frac{A_{33}}{M}\right)}} = \text{undamped natural frequency} \\
c_c &= 2\sqrt{M\left(1+\frac{A_{33}}{M}\right)C_{33}} = \text{critical damping coefficient} \\
\zeta &= \frac{B_{33}}{c_c} = \text{damping ratio} \\
\delta_{st} &= \frac{1}{C_{33}} = \text{static deflection (heave for a unit force of zero frequency)} \\
H &= \text{peak to peak heave}
\end{aligned} \tag{6.2}$$

Application of equation (6.1) requires only the specification of the natural frequency, ω_n, and the damping ratio, ζ. These depend in turn on added mass, damping and hydrostatic stiffness. Most of the difficulty in estimating values is associated with the first two of these, and these will be discussed briefly before estimating typical values for ω_n and ζ.

Added mass Typically the added mass is of similar magnitude to the actual mass ($\frac{A_{33}}{M} \simeq 1$). In the absence of free surface waves (i.e. in the high frequency limit) the heave added mass for a semi-circular section is identical to the actual mass, and figure 3-12 shows that, except at very low frequencies, it does not vary considerably from this value when free surface effects are modelled. For deep narrow sections it is expected to be lower, and for wide shallow sections higher, but, purely for practical purposes, one would not expect typical ship sections to vary too considerably from the aspect ratio of the semi-circle. Added mass affects mainly the natural frequency of the system. Even if it varies considerably, the influence on the natural frequency is approximately halved by dilution by the actual mass in the term $\left(1+\frac{A_{33}}{M}\right)$, and halved again by the square root. Thus for example a $\pm 50\%$ variation from $A_{33} = M$ would give approximately a $\pm 12.5\%$ variation of the natural frequency.

Damping The damping ratio influences the magnitude of the resonant peak in the motion response spectrum. This peak varies considerably from one set of experimental results to another, and it would be natural to assume that this variation is mainly due to variation in the damping ratio. As such it would be difficult to propose a simple model that would be universally applicable without considerable allowance for variation of empirical coefficients.

On the other hand if the added mass does not vary considerably from one hull form to another it is also reasonable to postulate that damping does not either. An exception perhaps is as a result of submergence, in which reduced proximity to the free surface would result in smaller free surface waves, hence a reduced mechanism for the energy dissipation that must be associated with damping. It will be shown that in fact a damping ratio that does not vary much from one boat to another could be entirely consistent with the observed considerable variation of the resonant peak magnitude, the effect being able to be explained in terms of a variation in the forcing function.

Frequency dependence Suppose that good estimates are known of the added mass and damping at the resonant frequency. We note that added mass and damping are generally weak functions of frequency, so motion should be reasonably well predicted anywhere in the vicinity of the resonant frequency. But at frequencies significantly differing from resonance we also note that the motion response is only weakly affected by the choice of resonant frequency or damping ratio, particularly where the latter is small and resonance effects are confined to a narrow frequency band. This is because the normalised response will always tend to unity in the zero frequency limit, and to zero in the high frequency limit, although the manner in which these limits are approached may vary (for example some of the low frequency pitch responses of SWATH forms presented later in this chapter (section 6.2.1) pass through a zone of low amplitude due to cancellation effects from heave coupling). Therefore, even if the estimates applicable for the resonant frequency are not the appropriate ones at other frequencies, the effect on motion predictions will be small. In other words, treating added mass and damping as constants for a given vessel (invariant with frequency) is quite adequate for the purposes of a broad simplified model.

Speed dependence With the exception of coupling (due to hydrodynamic asymmetry, as suggested by Gerritsma [32], and described in section 4.3), forward speed effects are not as dramatic as generally thought, are difficult to quantify, and recalling from section 4.3 that Newman [74] questions the use of forward speed corrections altogether in conventional strip theory, it is debatable whether they are accurately predicted by standard strip theories. The simple model gives reasonable predictions without allowing for speed effects on ω_n and ζ. Certainly the effect is expected to be of a higher order than those that are predicted by the proposed simplified model.

Note that speed has a major influence on the forcing function, and this accounts for most of

the observed speed dependent effects. This will be discussed below.

Typical coefficients In terms of length, L, beam, B, and draught, T, block coefficient, C_B, and water-plane area coefficient, C_{WP}, the hull stiffness in heave can be expressed as $\rho g C_{WP} LB$, and the total effective mass as $\rho C_B LBT\left(1+\frac{A_{33}}{M}\right)$. Thus the dimensionless natural frequency in heave (assuming one degree of freedom) is approximately

$$\omega_n^* = \omega_n \sqrt{\frac{L}{g}} = \alpha \sqrt{\frac{L}{T}} \tag{6.3}$$

where α is given by

$$\alpha = \sqrt{\frac{C_{WP}}{C_B\left(1+\frac{A_{33}}{M}\right)}}$$

and is a characteristic dimensionless parameter of a particular hull form, varying only slightly with speed through the A_{33} term. For a given hull shape C_{WP} and C_B can be quite precisely quantified, and as was shown above the exact value of A_{33} was not extremely critical.

For a general hull, if we assume $0.4 < C_B < 0.7$, $0.6 < C_{WP} < 0.8$, and $0.5 < \frac{A_{33}}{M} < 1.5$, then we obtain $0.6 < \alpha < 1.2$. Even this is not a considerable variation given the possible range of hulls represented by the chosen coefficient ranges.

The main point to make here is that the dimensionless natural frequency of a boat is primarily a function of its $\frac{L}{T}$ ratio, or, almost equivalently, the water-plane area to displacement ratio[1]. The latter ratio is the more relevant one for the description of SWATHs since these can have values of C_B (or C_{WP} depending on the definition of B used) significantly outside the ranges suggested. However one could refer to a notional effective draught, T_e, as a measure of 'SWATHness', chosen to give the correct natural frequency using the same value of α as for an equivalent conventional hull[2]. In the discussion of the wave force it will be shown that it is both convenient and appropriate to do this.

An $\frac{L}{T}$ ratio of 20 is fairly typical of a conventional boat,and values as low as $\frac{L}{T}=4$ have been chosen to represent a notional semi-SWATH in the following discussion. This corresponds to an 80% reduction in water-plane area compared to the conventional hull. A value of $\alpha = 1$ has also been used.

The damping ratio is probably most easily estimated empirically. All boats are significantly underdamped ($\zeta \ll 1$). This is not necessarily evident from typical response curves, and the reason will be made apparent below. However one only needs to visualise the free oscillation of a hull that has been given an initial heave displacement to verify this. In all the simulations illustrated below the value $\zeta = 0.18$ has been used, giving realistic results for the extremes of hull form and speed considered. It is reasonable to assume that a value in this vicinity is generally applicable for a simplified model of ship motions.

[1] The absolute natural frequency is mainly a function of draught.

[2] Perhaps the actual draught multiplied by the ratio of the maximum beam to the waterline beam.

A consequence of the low damping ratio ($\zeta \ll 1$) is that the damped natural frequency, $\omega_d = \omega_n\sqrt{1-\zeta^2}$, and the frequency of maximum response, $\omega_n\sqrt{1-2\zeta^2}$, will be for the present purposes almost the same as the natural frequency, ω_n.

Wave force

The incident wave is generally defined in terms of the surface elevation. Thus two aspects of the wave force need consideration.

First is the question of the actual incident wave definition, generally in terms of one of several standard spectra. This is highly dependent on the proposed route for which a boat is designed, and (when presenting results in terms of dimensionless quantities) also dependent on the boat length. This deals with the application of the hull, which is beyond the scope of the present work (being mainly concerned with inherent hydrodynamic properties of the hull itself). Since the towing tank results that follow are nondimensionalised to represent a constant wave height that is what will be assumed here.

The second aspect, and the one that will be presently considered, is the question of wave force for a unit wave height, as a function of frequency (or equivalently wavelength).

Total wave force is made up of the hydrostatic and Froude-Krylov forces, which are easily obtained by integrating the incident wave pressure field over the hull surface, and the diffraction force, which is far more difficult to evaluate. Both are functions primarily of wave frequency (as opposed to encounter frequency, the primary variable influencing response). Fortunately the diffraction force is small compared with the hydrostatic and Froude-Krylov forces, as is shown consistently in the many sets of results contained in Magee and Beck [64]. Therefore for our simplified model it is sufficient to ignore it.

An approximate expression for the hydrostatic and Froude-Krylov force can be obtained by assuming the hull to be a rectangular prism. Given that the pressure field underneath a wave in head seas can be expressed in the form $\frac{p}{\rho g} = \frac{H_w}{2}e^{ky+i(kx-\omega_0 t)}$, the magnitude of the total heave force on such a hull would be

$$|F| = \frac{\rho g B H_w}{2}\left|\int_0^L e^{-kT+ikx}dx\right|.$$

If we take $\rho g B L\frac{H_w}{2}$ as the unit force (the heave force at zero frequency), then, after integrating, the dimensionless force magnitude, F^*, would be

$$\begin{aligned} F^* &= e^{-kT}\sqrt{2\frac{|1-\cos(kL)|}{(kL)^2}} \\ &= \frac{e^{-kT}}{\left(\frac{kL}{2}\right)}\left|\sin\left(\frac{kL}{2}\right)\right|. \end{aligned} \tag{6.4}$$

This is a function of wave frequency since (for deep water) $k = \frac{\omega_0^2}{g}$. It should further be noted that, in the notation of equation (6.1), with the above definition of a unit force, $\delta_{st} = \frac{H_w}{2}$, the wave amplitude.

The force on a real hull can be estimated in terms of the force on a rectangular prism by considering an effective length and draught. (We note that in dimensionless terms the force is independent of beam.) The effective length and draught will both be slightly less than the actual ones.

Examples of equation (6.4) can be seen in figures 6-4, 6-5, and 6-6. The e^{-kT} term represents the Froude-Krylov correction resulting from the decay with depth of the non-hydrostatic component of pressure, while the remaining term accounts for the cancellation of force along the hull due to the changing phase in the longitudinal direction. At long wavelengths (low frequency) the force is hydrostatic ($F^* = 1$), and reduces to zero when the wavelength and boat length are equal ($\omega_0^* = \sqrt{2\pi}$) because of exact cancellation of phase along the hull. (The discontinuity in slope represents a phase reversal; the sign, and not the magnitude, of the slope changes because the absolute value is taken.) At higher frequencies the force is generally small, and is also zero when the ratio of boat length to wavelength is an integer.

These results show remarkable similarity to results given in Magee and Beck [64] for real hull forms (particularly if the former are plotted as a function of kL, as Magee and Beck do, instead of $\omega_0\sqrt{\frac{L}{g}}$). As an illustrative example, a typical figure of Magee and Beck's heave exciting force results has been reproduced below in figure 6-1, and this can be compared with figure 6-6. The main difference is the frequencies at which exact cancellation of the forces occurs, being slightly higher for the real hulls, confirming that the effective length is slightly less than the actual length.

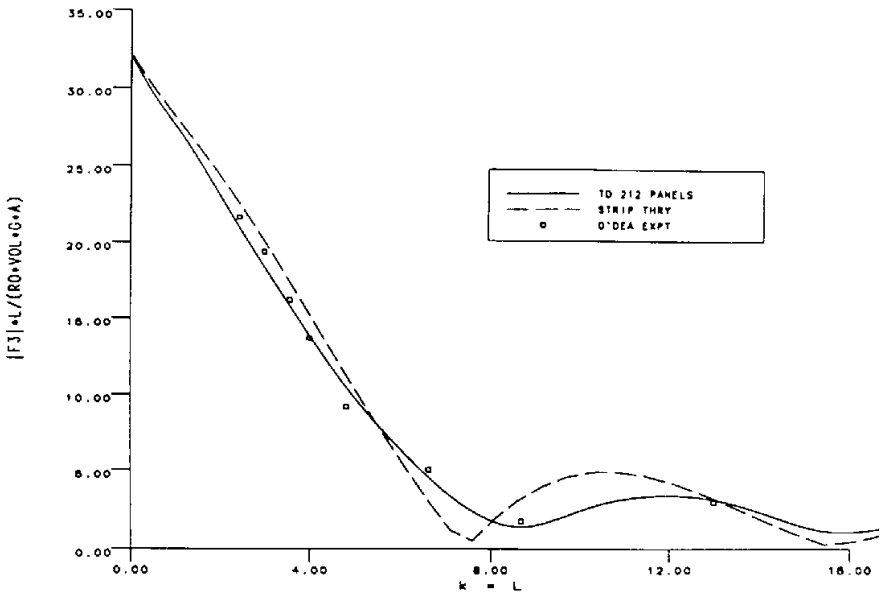

Figure 6-1: Reproduction of Magee and Beck [64] figure 310: Magnitude of heave exciting force as a function of kL for SL-7 containership, $Fr = 0.3$. (3D panel method, strip theory and experiment.)

Net response

Net response for a unit wave height is obtained as the product of response for a unit force (equation (6.1)) and force for a unit wave height (equation (6.4)), taking care to recognise that the former is a function of encounter frequency and the latter of wave frequency. The result is summarised as

$$\frac{H}{H_w} = \frac{\frac{2e^{-kT}}{kL}\left|\sin\left(\frac{kL}{2}\right)\right|}{\sqrt{\left(1-r^2\right)^2 + \left(2\zeta r\right)^2}} \tag{6.5}$$

where in deep water $r = \left(\omega_0^* + \left(\omega_0^*\right)^2 Fr\right)\frac{\sqrt{T/L}}{\alpha}$ in head seas, which embodies the Doppler shift between encounter and wave frequency, and $k = \frac{\omega_0^2}{g}$ (or $kL = \left(\omega_0^*\right)^2$).

Examples are given in figures 6-4, 6-5, and 6-6 illustrating the effects of both SWATHness and speed on total response, and these will be discussed below. Each of these figures shows the forcing for a unit wave height, the response for a unit force, and the net response for a unit wave height, illustrating the importance of both forcing and resonance effects. Also the dimensionless acceleration for a unit wave height is given as a means of evaluating options, as this in the primary stimulus to seasickness. The forcing is based on the rectangular prism analogy, and α and ζ are taken respectively as 1.0 and 0.18.

An investigation of the effect of speed Figures 6-4 and 6-5 show the effect of speed respectively for a notional conventional hull ($\frac{L}{T} = 20$) and a notional SWATH ($\frac{L}{T_e} = 4$, corresponding to an 80% water-plane area reduction on the notional conventional hull for the same displacement and length), as predicted by the simple model just described.

The only effect of speed is to change the wavelength at which the resonant frequency is encountered, shown by a left shift in the resonant peak when plotted against the wave frequency. The actual magnitude of the peak of the *dimensionless heave amplitude for unit force* graph does not change. The result is that this resonant peak is brought into coincidence with significant forcing, and the net response (*dimensionless heave for unit wave height*) is significantly increased. At low speeds the forcing is so small that the resonant peak is not even evident (which could be mistaken for supercritical damping). Because the forcing is asymptotic to the hydrostatic value at infinite wavelength (zero frequency) the net response approaches a maximum value as speed increases.

The SWATH, because of a lower natural frequency, reaches the maximum net response sooner as speed is increased (compare the *dimensionless heave for unit wave height* in figures 6-4 and 6-5). However again because of a lower natural frequency, the accelerations at high speed are significantly smaller for the SWATH. This must always be the case in the high speed limit because of the ceiling on the response. The maximum possible response will be $\left(\frac{H/2}{\delta_{st}}\right)_{\max} = \frac{1}{2\zeta\sqrt{1-\zeta^2}}$ ([81], equation (3.33)), or, given that $\zeta \ll 1$, $\left(\frac{H/2}{\delta_{st}}\right)_{\max} \simeq \frac{1}{2\zeta}$. If the assumption that ζ does not vary significantly is correct, and the further assumption made that the simplified model still holds at high speeds, then the conclusion to be made is that for high speed (at which $F^* = 1$,

i.e. $\delta_{st} = \frac{H_w}{2}$) the only significant change the hull shape can make is to decrease the natural frequency, and with it maximum accelerations.

An investigation of the effect of water-plane area reduction ('SWATHness') SWATHness, as suggested above, can be expressed in terms of the ratio $\frac{L}{T_e}$. The effect is twofold. First, there is a reduction of the resonant frequency, embodied in equation (6.3). Second, the force is reduced because of the Froude-Krylov term in equation (6.4).

One could argue that if the water-line beam is reduced while the maximum beam is maintained, as would be typical of a SWATH, then the draught would not actually increase significantly. Hence the use of an effective draught, T_e (which will be greater than the actual draught), as a measure of SWATHness would over predict the Froude-Krylov correction. On the contrary, the bulbous shape that would result means that the downward pressure above the point of maximum beam would be acting at a shallower average depth than the upward pressure force on the bottom part of the section, and in some extreme cases the Froude-Krylov correction could actually be under predicted. The issue was therefore dismissed as being of secondary relevance.

Figures 6-6 (a) and (b) illustrate the effect of SWATHness at low and high speeds respectively. At low speed (figure 6-6 (a)) both motions and accelerations increase with SWATHness, suggesting that a conventional hull form is preferable[3]. However at high speed (figure 6-6 (b)) the ceiling on the response combined with a lower natural frequency results in SWATHs having a considerable advantage over conventional hulls for accelerations.

Some comments relating to pitch motion

Response While pitch motion has been ignored in the preceding discussion for the sake of simplicity, it is worth making a few points.

- Pitch motion with constant wave height is characterised by low absolute forcing at low frequency. This is because the wave slope ($\frac{kH_w}{2}$) approaches zero. The heave force on the other hand does not vanish (the leading terms in equations (6.7) and (6.8) differ by the factor $\frac{x}{6} \equiv \frac{L}{12g}\omega^2$), and coupling with heave becomes very significant. Where the direct pitch moment and that due to heave coupling are of comparable magnitude one must therefore also consider the phase of the forces.

- One can derive equivalent expression for ω_n for pitch in a manner similar to that used for heave above. In doing so one finds that for conventional boats with typical radii of gyration the natural frequencies in heave and pitch are very similar. (This is not generally

[3]The results for long wavelength ($\omega\sqrt{\frac{L}{g}} < \sqrt{2\pi} \simeq 2.5$) are probably a realistic indication of expected typical motions, but at the higher frequencies the force is quite small and effects that have been ignored are likely to be significant. It is suspected that these effects would tend to cancel with the hydrostatic and Froude-Krylov forces since typical results do not generally show motions as large as observed for the small values of $\frac{T}{L}$ in figure 6-6(a). The large values are exaggerated in the accelerations graph because of the ω^2 factor present.

true when the waterline length and overall length differ substantially, as for example in the semi-SWATH models discussed in this chapter, because of their extended submerged bows.)

- Measured and computed responses frequently do not show two identifiable resonant peaks, as one would expect for a two degree of freedom system. This is because of the similarity between the two natural frequencies mentioned in the previous point, in combination with general 'smearing' effect of damping, and the attenuation due to low wave forcing at the low Froude numbers typical of most studies.

- If the theory were to be extended to two degrees of freedom then the heave analysis should be repeated taking into account phase.

Moment Following the derivation of equation (6.4), the equivalent expression for the pitch moment on a rectangular prism hull is

$$\begin{aligned} |M| &= \left| \int_{\frac{-L}{2}}^{\frac{L}{2}} \frac{\partial F}{\partial x} x \, dx \right| \\ &= \frac{\rho g B \frac{H_w}{2} e^{-kT}}{k^2} 2 \left| \sin\left(\frac{kL}{2}\right) - \left(\frac{kL}{2}\right) \cos\left(\frac{kL}{2}\right) \right|. \end{aligned}$$

If this is nondimensionalised in terms of the moment for an infinitely long wave of unit wave height one obtains

$$M^* = \frac{e^{-kT}}{2\left(\frac{kL}{2}\right)^2} \left| \sin\left(\frac{kL}{2}\right) - \left(\frac{kL}{2}\right) \cos\left(\frac{kL}{2}\right) \right|. \tag{6.6}$$

Although equations (6.4) and (6.6) appear quite different in form, it can be shown using Taylor series that

$$F^* = e^{-kT} \left| 1 - \frac{1}{6}x^2 + \frac{1}{120}x^4 - \frac{1}{5040}x^6 + \ldots \right| \tag{6.7}$$

$$M^* = e^{-kT} \frac{x}{6} \left| 1 - \frac{1}{10}x^2 + \frac{1}{280}x^4 - \frac{1}{15120}x^6 + \ldots \right|, \tag{6.8}$$

where $x = \left(\frac{kL}{2}\right)$, with errors in the absolute value term smaller than -0.024 and -0.007 respectively for $x \leq \pi$ ($\omega\sqrt{\frac{L}{g}} \leq 2.5$). If the second of these expressions (M^*) is multiplied by $\frac{6}{x}$ one obtains the moment normalised in terms of the moment for an infinitely long wave of unit slope, and the similarity of form of the two expressions becomes obvious.

Summary of findings

- The simple model described above gives significant insight into qualitative aspects of seakeeping.

- As speed is increased motions also increase, primarily due to the increased forcing resulting from encountering resonance in longer waves, but only to the point where the resonant frequency is encountered in wavelengths significantly longer than the boat length, in which

case the motions are asymptotic to their maximum value. Basically this means that at high speeds poor seakeeping is inevitable for all hull types (excluding the effect of appendages).

- For the same reason increasing SWATHness also increases motions. However the lower natural frequency of SWATHs at the same time reduces accelerations, and this to some extent cancels the effects of the increased motions. The increased motion effect dominates at low speeds where the rate of change of forcing with frequency at the natural frequency is high, but at high speeds where it is asymptotic (and therefore changes only slowly with frequency) the lower acceleration effect dominates.

- Therefore, at low speeds conventional hulls have better seakeeping, whereas at high speeds SWATHs are better.

- A complete comparison should consider actual vessel size and route, so that consideration is also given to both the incident sea wave spectrum and human response (MSI) factors.

These broad findings will be shown below to be confirmed by experimental and computational results.

Sources of additional damping It was stated above that the damping ratio does not vary much from one hull to another. This of course refers to the bare hull, and damping can be significantly increased with the use of fins, and even more by using controllable surfaces. Active ride control is probably of most benefit for slower vessels. If the speed is increased sufficiently for a fixed fin to provide high (perhaps even near critical) damping then the additional benefit of making the fin controllable becomes small.

6.2 Experimental results

6.2.1 SWATH models

Broad description of response features

Generally, all results for SWATH #2 and heave results for SWATH #1 are good in the sense that the behaviour over the whole frequency spectrum is clearly evident. As expected, the dimensionless responses all approach unity at low frequencies and zero at high frequencies. The response curves are quite smooth, both as a function of frequency (either wave or encounter) and as a function of speed. The pitch results for SWATH #1 on the other hand are a little inconclusive at the lower frequencies, particularly at the higher speeds (Froude number of 0.4 and above). The resonant peak is not fully defined, and the exact behaviour between zero frequency and the lowest frequencies tested can not be inferred. As explained in the previous chapter, this is basically because of the very low resonant frequency in pitch for SWATH #1, combined with the limitations of the towing tank.

It should also be repeated that for SWATH #2 wave frequencies well below the deep water limit were used in order to obtain some more conclusive data about the response near the pitch resonant frequency, and that therefore the low frequency results should be regarded as indicative only. Assuming, as suggested by the simplified model of section 6.1.2, that response is a function primarily of encounter frequency and wavelength, it was shown in section 5.4.1 that the main effect of a finite depth channel is to cause an apparent speed shift at the low frequencies (below about $\omega_0\sqrt{\frac{L}{g}} = 1.4$–$1.8$ for the SWATH models). Since figure 6-8 shows response to be a well behaved function of speed there should be no problem in making qualitative inferences from the experimental results about the response at low frequencies in deep water.

Relation to simplified model of section 6.1.2

As predicted in section 6.1.2, there are two distinct resonant frequencies, corresponding to predominantly heave and predominantly pitch mode shapes. These are very clear for these semi-SWATH models because of the large magnitude of the peaks and because the natural frequencies for heave and pitch differed significantly[4]. The pitch results also show obvious coupling from the heave motions, indicating that the heave resonance mode shape also contains significant pitch motion. The heave results on the other hand show little evidence of coupling, indicating that some insight may be gained from a single degree of freedom model. Following some initial general comments, the broad features of the heave results will be discussed in terms of the single degree of freedom simplified model of section 6.1.2. Then pitch and coupling effects will be discussed in terms of the qualitative predictions made in the same section.

Response plotted against *encounter* frequency clearly shows the resonance effect of equation (6.1). That is, figure 6-7 shows that, although they may vary in magnitude, all the resonance peaks for both heave and pitch line up. (The only deviation from this general rule is pitch at high speed for SWATH #1, particularly at the 25.72kg displacement, which will be discussed separately below.) This confirms the assumption that the added mass effects do not change substantially with increased speed. Also, SWATH #1, which has less hydrostatic stiffness for the same mass, has, as expected, a lower natural frequency. In pitch, because of the shortened waterline length, the natural frequency is lower again.

Heave response The actual magnitude of the heave peaks seems to be approaching a maximum of about 3.0 as speed is increased (the asymptotic manner in which it approaches this limit is perhaps most clearly evident in figure 6-8). This confirms the prediction of a ceiling on

[4]The "SWATHness" was achieved by a reduction of both waterline beam and length, meaning that, compared with the conventional reference hull, the hydrostatic stiffness in pitch (proportional to waterline length cubed) was reduced considerably more than was the heave stiffness (linearly dependent on waterline length), while the mass and moment of inertia (because of an extended submerged bow) were not changed. Given that the reference hull had similar natural frequencies in heave and pitch this causes the pitch resonant frequency for the SWATH models to be significantly lower than that for heave.

the net response. Furthermore, because this maximum appears to differ little between the two models, it supports the assumption of an approximately constant damping ratio (ζ) for different boats.

If response is plotted against *wave* frequency then the effect of a reduction of wave force at shorter wavelength, embodied in equation (6.4), becomes evident. This is illustrated particularly clearly in the SWATH #2 heave results of figure 6-8(b). In this example the peaks are a resonance effect, and as such are not directly relevant to the wave force. However the line to which the high frequency asymptote of the curve for each speed collapses is very similar in form to that described by equation (6.4) (see figure 6-6). The resonant peaks themselves also show the predicted reduction as wave frequency increases (i.e. as speed decreases), confirming the notion of net response being the product of wave force with an essentially constant peak response for unit wave force. This is evident in both the SWATH #1 and SWATH #2 results. In particular those of SWATH #1, which has a lower natural frequency, shows the asymptotic nature of the net response at high speed predicted by the simplified model.

Pitch response Pitch results do not show all these effects as clearly as heave, but, as pointed out above (section 6.1.2), this is due to the very small absolute pitch motions corresponding to a unit dimensionless pitch, and hence, especially at low frequency, behaviour may be dominated by coupling from heave motions. This effect is more marked in SWATH #1, in which (unlike SWATH #2) the centre of flotation and centre of buoyancy were significantly separated, and in which the resonant frequency for pitch was low. Figure 6-7(a), (the 25.72kg displacement results in particular) shows that at the higher Froude number the pitch resonance is almost completely cancelled by heave coupling. This phenomenon is also observed in many of the computational results (for example figure 6-15(a)). For SWATH #2 the longitudinal centres of flotation and buoyancy were almost coincident, and the same coupling effects at low frequency are therefore not as strong.

Coupling effects There is no noticeable coupling of pitch motions evident in the heave response (there is only the local drop in response evident in figure 6-7 for SWATH #2 at lower speeds, apparently coinciding with the pitch resonance, but figure 6-8 clearly confirms that this is a wave frequency effect, and as discussed above is due to the reduction of wave forcing associated with shorter wavelengths). This suggests that a single degree of freedom analogy is sufficient to capture the essential features of the heave motion response.

Pitch response on the other hand is more influenced by coupling from heave motions, as already noted for low wave frequencies. This coupling effect varies considerably, with the SWATH #2 at low Froude number showing least influence (best shown in figure 6-7). There are at least four possible reasons that this particular example shows least coupling: (i) the heave motion itself is less because of the reduced wave forcing at shorter wavelengths (there is a strong correlation between the magnitude of this secondary pitch peak and the heave resonant peak

at the different speeds, suggesting at least in the present case that this is the dominant of the four listed effects), (ii) the higher wave frequency, as described above, causes the coupling effects to be dimensionlessly less significant for pitch, (iii) SWATH #2 in general shows less coupling than SWATH #1 because its longitudinal centres of buoyancy and flotation are closer together, and (iv) effects due to the dependence of hydrodynamic coefficients on forward speed may be present, it being suggested in section 4.3.2 that the hydrodynamic components of the coupling coefficients arise partly due to the hydrodynamic asymmetry caused by forward speed.

The trend with the pitch peaks, which decrease as speed increases, accompanied by a slight decrease in the resonant frequency, appears to run contrary to the simple model predictions (see in particular figure 6-8(b)). This however is most likely due to the heave coupling effect, being a transition to the low frequency situation where it was seen that the peak was almost cancelled altogether. Evidence in support of this explanation is given in the two lowest Froude number results of figure 6-8(b) (22.0kg displacement), in which the pitch peak is observed to increase initially with speed (as they should according to the simple model) before the coupling effects start to take over. Increased damping is also a possible explanation, although in light of the above discussion, as well as due to the lack of any evidence of increased damping in the case of heave, it seems unlikely that this is the cause.

This discussion has concentrated on qualitative effects that are explainable in terms of a very simple model. More specific quantitative predictions require a more sophisticated model. Nevertheless these qualitative aspects are extremely important in the initial concept stage of design, and are not always well understood by many designers of high speed vessels.

H_w effects

Some investigation of the effect of wave height on motions was carried out. As shown in table 5.2 this was done for SWATH #1 at 3.5m/s and SWATH #2 at 2.0m/s and 3.0 m/s. Results are presented in figure 6-9(a). (Corresponding computational results in figure 6-9(b) will be discussed in section 6.4.2.)

The tests show that at the wave heights considered the non-linear component of motion was quite small, particularly for SWATH #2 at 2.0m/s (which was the lower of the three speeds). This result is probably due to the generally steep sides of the hull forms, but is still quite surprising considering that at times a significant length of the hull (from visual observations during testing it was estimated to be as much as 30% at times) emerged completely from the water during part of its cyclic motion. It is of particular relevance in consideration of neglected non-linear effects in the numerical motion predictions, and will be referred to again in section 6.5.4.

Resistance

Although SWATHs will in general offer improved passenger comfort at high speeds, there are many other aspects that must be considered in vessel design. Some, such as safety in extreme events, may be dealt with to some extent by appropriate design of the hull above the nominal waterline, and therefore will not be dealt with in this thesis. However resistance is an issue high on the list of priorities of boat builders and operators that, although not the primary focus of this thesis, must be considered when assessing different hull forms.

The resistance results for the two SWATH models have been discussed in section 5.3.1.

Possible improvements to the hull form

Some thoughts on improving the resistance characteristics of the SWATH hull forms have already been mentioned in section 5.3.1.

In terms of seakeeping, the SWATH hulls were successful in reducing the natural frequencies of response, which is probably the easiest of the objectives to achieve. The other main defining characteristic, the damping ratio, is a much more difficult problem to address, and is equally important as it defines the size of the resonant peak in response. Given that damping is associated with wave generation, and that SWATHs will in general have deeper sections and steeper sides than conventional hulls (the proximity of a disturbance to the surface has a major influence on the size of the waves that it generates, and vertical sides alone will in theory produce no waves in heave or pitch motion), there appears to be very little that can be done in terms of hull form about wave induced damping for this type of vessel. The bow shape chosen no doubt gave little benefit in this regard, but one would have to consider with a broader bow form the additional structural weight required to resist much higher slamming loads and associated global fatigue effects, as well as the effect of the slam induced accelerations on passenger comfort and noise.

To improve damping one must therefore rely on the use of other features such as lifting surfaces, either fixed or active, the former having more advantage as speed is increased. Whether these take the form of bow and stern fins or are more distributed (as for example bilge keels), what the optimum location and size should be, etc., would have to be the subject of further research. Their impact on resistance would also have to be taken into account.

Perhaps an ideal would be something that produces close to critical damping at cruise speed, in which case as the speed of vessels increases less might then be required. Also the lower natural frequencies of SWATHs means not only lower accelerations (through the ω^2 factor), but also smaller force requirements for such control surfaces. These all contribute to a reduced drag penalty.

6.2.2 Conventional hull: AMECRC systematic series towing tank tests

Models AMECRC #04 and AMECRC #05, as described in the previous chapter, are from a systematic series of models designed by Bojovic and Goetz [10], and tested for seakeeping by Macfarlane, Shaw and Lees [63]. The full set of seakeeping data is presented in Macfarlane et al. [63], and data for models #04 and #05 at the two highest Froude numbers are reproduced in figure 6-23[5].

These models have fairly shallow draughts compared with the SWATH models ($\frac{T}{L} = 0.031$ and 0.062 for AMECRC #4 and #05 respectively), and exhibit similar features (heave resonant peaks and resonant frequency) to those predicted by the simplified model of section 6.1.2 and shown in figure 6-4. As expected, AMECRC #05, because of its deeper draught, has a lower natural frequency and higher response.

Figure 6-23(b) shows that for AMECRC #05 the resonant frequency in heave is about $\omega_e\sqrt{\frac{L}{g}} = 3.2$, evident from the $Fr = 0.57$ results, which is lower than the lowest frequency tested at the higher Froude number ($Fr = 0.86$). This was presumably for reasons similar to those outlined in section 5.4 (finite depth effects, wave reflection, and limitations of the wave maker). The higher Froude number results for this model do not extend to sufficiently low frequencies to define the resonant peak, and are therefore of limited use.

Relation to simplified model

As for the SWATH results, the simple model gives mostly good qualitative predictions of the general response characteristics, except for pitch at low frequency. They do however suggest a higher damping ratio (ζ) than the SWATH models, but given their quite different hull shape this is not surprising. In particular, AMECRC #05 had a much wider beam and draught than the SWATHs, which could account for its higher observed damping. For the AMECRC models #04 and #05 $\frac{L}{B} = 8$ and 4 respectively, while for SWATH #1 and #2 $\frac{L}{B} = 29.2$ and 18.3 respectively at the waterline or 16.1 and 14.3 based on the maximum underwater beam. The displacements, scaled to a common length of 2.5m, are 22.0kg, 22.0kg, 27.3kg and 96.7kg respectively for SWATH #1 and #2, and AMECRC #04 and #05. This represents a considerable variation, and one would expect in particular AMECRC #05 not to be very comparable to the other three models. These results are therefore mainly of use in the validation of the present fixed reference frame time domain strip theory.

It would have been of interest to compare the SWATH results with their reference hull (which had $\frac{L}{B} = 14.0$), but the latter results were not made available for the exact reference

[5]The two presentations however differ slightly. The former normalises pitch using $\frac{\omega_0^2}{g}H_w$, while in figure 6-23 kH_w has been used. The result is identical at high frequencies, but at the lower frequencies of figure 6-23 finite depth effects cause a small difference, as illustrated in figure 5-6. The present work uses kH_w because this gives unit dimensionless pitch in the zero frequency limit, and it is also consistent with the presentation of the semi-SWATH tank results.

hull. However a set of response curves has been published in Watson et al. [96] for a more recent Incat boat with a similar (but larger) hull. These show a dimensionless heave of 2.2 and a dimensionless pitch of 1.7. Speed (or Froude number) has not been indicated on these results, but if one assumes that they correspond to cruise conditions (moderate to high speed) then these values, which exhibit significant response resonances, are certainly closer to typical heave and pitch peak values of the SWATH models than those of the AMECRC models are.

6.3 Preliminary validation of numerical methods

Three sets of numerical results were computed.

First was the program *BESTSEA* (*B*oundary *E*lement *S*trip theory *T*ime domain *SEA*keeping), based on the time domain high Froude number strip theory presented in this thesis.

The second set of numerical results was a set produced by the program *HYDROS* [22], a conventional (frequency domain) strip theory program based on the theory of Salvesen, Tuck and Faltinsen [84], written and generously made available by Prof. L. J. Doctors of the University of New South Wales. The purpose of the comparison was for further validation of *BESTSEA*, and a comparison of the strengths and weakness of the two theories.

Third, as *HYDROS* was applied only to the two SWATH models, and only for a fairly coarsely spaced selection of frequencies, I developed my own equivalent implementation of the Salvesen, Tuck and Faltinsen theory (head seas only) to allow greater flexibility of investigation, as it was a relatively minor extension of work already done on periodic Green function solutions (chapter 4) and forward speed sectional added mass and damping calculations (below). This program was called *STF*. Particular care was taken to ensure that the implementation was theoretically equivalent to *HYDROS*, such as in the inclusion of forward speed and end terms, and in the calculation of Froude-Krylov and diffraction forces. *STF* and *HYDROS* should therefore approach each other exactly as the numerical discretisation of the hull is refined.

Validation of *BESTSEA* and *STF* are discussed below.

6.3.1 *BESTSEA* tests

Steady wave pattern for parabolic strut

This test case was chosen because of the availability of published results for a solution by a similar method ([29] and [28]). The problem is very similar to Roberts' wavemaker problem [83] described in chapter 3; differences include satisfying the boundary condition on the exact hull location (as opposed to thin-ship), and application of the boundary condition on hull bottom (which was irrelevant for a thin ship approximation).

In order to maximise the validation potential (i.e. testing not just the theory but safeguarding against related bugs in *BESTSEA*) the problem was solved by modifying *BESTSEA* (by adding free surface elevation calculation, which consisted of copy and paste of hull pressure

with appropriate modifications) rather by modifying the program used to solve the wavemaker problem (which was aimed at validation the time domain Green function method).

At this point it is relevant to describe some of the structure of *BESTSEA*. *BESTSEA* makes use of the time domain Green function solution described in chapter 3. The latter was written as an independent program unit that required as input from some calling program information about geometry, boundary conditions and past history, and produced as output hydrodynamic body forces, and updated the source strength history with the current time step. The validation cases described in chapter 3, as well as *BESTSEA*, all used exactly the same core program unit just described, differing only in the calling program. The calling program in each case was responsible for evaluating geometry and boundary conditions, and keeping track of their history. The calling program in *BESTSEA* further divided the three dimensional hull into two dimensional sections, passed these one at a time to the core Green function program unit, re-arranged memory associated with the history of these sections as the hull moved forwards, and was responsible for integration of the equations of motion. This represented a significant increase in complexity over the purely two dimensional problems solved in chapter 3. Therefore by using *BESTSEA* as the starting point for the program used to solve the steady wave pattern for a parabolic strut many elements in the calling program were tested in addition to the Green function solution. All modifications were by *additions* to the program. Nothing was deleted, although some features (such as the wave input and the hull motions) were disabled.

Faltinsen and Zhao [29] present a comparison of results for both linear and non-linear forward speed strip theories and for thin ship (three dimensional) theory. It is their linear forward speed strip theory that is most equivalent to *BESTSEA* (exact body boundary condition, linearised free surface including all forward speed effects, two dimensional Laplace's equation), and agreement with this theory is very good. A comparison is shown in figure 6-10.

The only problem encountered was evaluation of the free surface within the region behind the point of maximum hull beam between the hull and a line extending directly backwards from the point of maximum beam. The problem is the $\frac{1}{z-\bar{c}}$ term in the convolution integral. The effective integration path in the Green function goes to infinity and back as $\bar{c}$ (representing the geometry history of the hull waterline forward of the current point) crosses over z (the free surface point). Although the net result is zero, the integrand contains an infinite number of oscillations, and if the combination of time step, hull geometry and speed are such that one does not return to the same part of the cycle after the time step that crosses this singularity (as in general it will not be) then an error results. Furthermore, ignoring the problem region, this does not detract from the validation value of the results because calculation of wave elevation at any point is independent of all other wave elevation calculations (although the errors will have affected immediately adjacent regions during the contouring process).

This is not a problem at all for ship motion problems, although the same Green function is used for the hull pressure calculation ($\frac{\partial \phi}{\partial t}$), because in that case z (a panel mid-point) is always

below the free surface, whereas $\bar{c}$ (the reflections of a panel end-point) is always *on or above* it. (In the free surface calculation z was always on the free surface.) It was therefore unnecessary to seek a solution to the problem.

Added mass and damping distribution with forward speed

Although traditional strip theory and *BESTSEA* differ considerably, they are both intended to represent the same physical process, but under differing assumptions. Provided they are both to some extent valid theories there must be some commonality in their predictions. Therefore as well as comparing global motions (section 6.4), which represent "average" effects for the hull and can therefore mask some internal errors, there is some benefit in comparing more detailed elements of the two theories. This section compares sectional hydrodynamic radiation forces distributions, and discusses their similarities and differences in terms of expectations based on similarities and differences between the two theories. These sectional forces will be represented in terms of forward speed sectional added mass and damping coefficients, and it will first be necessary to precisely define these for global heave and pitch motions.

The traditional strip theory representation of sectional forces, in terms of zero speed two dimensional added mass and damping coefficients is as follows.

In the notation of section 4.2, if we define $\Delta F = \frac{dF_3}{dx}$ = time-complex amplitude of sectional force per unit length of hull, then differentiating equation (4.14) one obtains $\Delta F = -\rho\left(p - U\frac{\partial P}{\partial x}\right)$ where p and P are defined in equation (4.20). But it was shown that $P = \frac{e^{i\omega t}}{\rho}\left(\xi_3 - \xi_5\left(x - \frac{U}{i\omega}\right)\right) i\omega Z$ and $p = i\omega P$ (equations (4.28) and (4.29)), hence

$$\Delta F = e^{i\omega t}\left\{\left(\xi_3 - \xi_5\left(x - \frac{U}{i\omega}\right)\right)\omega^2 Z + U\left[\left(\xi_3 - \xi_5\left(x - \frac{U}{i\omega}\right)\right) i\omega\frac{\partial Z}{\partial x} - i\omega\xi_5 Z\right]\right\}.$$

The complex sectional force amplitudes for unit heave and pitch motions are therefore, putting $Z = a + \frac{b}{i\omega}$,

$$\frac{\frac{\partial \Delta F}{\partial \xi_3}}{e^{i\omega t}} = \left(\omega^2 a + U\frac{\partial b}{\partial x}\right) - i\omega\left(b - U\frac{\partial a}{\partial x}\right), \tag{6.9}$$

$$\frac{\frac{\partial \Delta F}{\partial \xi_5}}{e^{i\omega t}} = \left(-\omega^2 ax - 2Ub + U^2\frac{\partial a}{\partial x} - Ux\frac{\partial b}{\partial x}\right) - i\omega\left(2Ua - bx + Ux\frac{\partial a}{\partial x} + \frac{U^2}{\omega^2}\frac{\partial b}{\partial x}\right). \tag{6.10}$$

We could define forward speed sectional added mass and damping coefficients for heave and pitch motion as $a_{FH} = \frac{\partial A_{33}}{\partial x}$, $a_{FP} = \frac{\partial A_{35}}{\partial x}$, $b_{FH} = \frac{\partial B_{33}}{\partial x}$ and $b_{FP} = \frac{\partial B_{35}}{\partial x}$. Note that, to avoid infinite values at the centre of pitch, a_{FP} and b_{FP} are the forces for a unit global pitch acceleration and velocity rather than the usual unit local heave acceleration and velocity. The total vessel added mass and damping coefficients in terms of total hydrodynamic forces are given in equation (4.32), from which $\frac{\partial A_{3j}}{\partial x} = \mathrm{Re}\left\{\frac{\frac{\partial \Delta F}{\partial \xi_j}}{\omega^2 e^{i\omega t}}\right\}$ and $\frac{\partial B_{3j}}{\partial x} = -\mathrm{Re}\left\{\frac{\frac{\partial \Delta F}{\partial \xi_j}}{i\omega e^{i\omega t}}\right\}$ (and obviously

$\frac{\partial A_{5j}}{\partial x} = -x\frac{\partial A_{3j}}{\partial x}$, $\frac{\partial B_{5j}}{\partial x} = -x\frac{\partial B_{3j}}{\partial x}$). Substituting (6.9) and (6.10) into these expressions gives

$$a_{FH} = a + \frac{U}{\omega^2}\frac{\partial b}{\partial x} \tag{6.11}$$

$$a_{FP} = -ax - \frac{2Ub}{\omega^2} + \frac{U^2}{\omega^2}\frac{\partial a}{\partial x} - \frac{Ux}{\omega^2}\frac{\partial b}{\partial x} \tag{6.12}$$

$$b_{FH} = b - U\frac{\partial a}{\partial x} \tag{6.13}$$

$$b_{FP} = -bx + 2Ua + \frac{U^2}{\omega^2}\frac{\partial b}{\partial x} + Ux\frac{\partial a}{\partial x}. \tag{6.14}$$

One can easily verify that $\int \frac{\partial A_{ij}}{\partial x}dx$ and $\int \frac{\partial B_{ij}}{\partial x}dx$ recover the usual expressions for A_{ij} and B_{ij} given in equations (4.33)–(4.37). Note that $a_{FP} \neq -xa_{FH}$ and $b_{FP} \neq -xb_{FH}$, meaning that even for identical local motions of a cross section the forces depend on whether global motion is heave or pitch. This does not violate the Timman-Newman symmetry relations [89].

Coefficients for combined heave and pitch may also be derived as follows. Suppose the boat oscillates with a particular combination of heave and pitch. The local heave at a point x forward of the origin will be $h_x = \xi_3 - x\xi_5$, noting that the quantities h_x, ξ_3 and ξ_5 are all complex. If we define $a_F(\xi_3, \xi_5) + \frac{b_F(\xi_3,\xi_5)}{i\omega} = \frac{\frac{d\Delta F}{dh_x}}{\omega^2 e^{i\omega t}}$, then from $\Delta F = \frac{d\Delta F}{dh_x}h_x = \frac{\partial \Delta F}{\partial \xi_3}\xi_3 + \frac{\partial \Delta F}{\partial \xi_5}\xi_5$ we obtain $Z_F(\xi_3 - x\xi_5) = Z_{FH}\xi_3 + Z_{FP}\xi_5$ (where $Z_* = a_* + \frac{b_*}{i\omega}$ for $_* = _F$, $_{FP}$, or $_{FH}$.). Letting $\xi_5 = \frac{|\xi_5|}{|\xi_3|}\xi_3 e^{-i\theta_{53}}$, in which θ_{53} represents the phase lag of pitch relative to heave, gives

$$Z_F = \frac{Z_{FH}|\xi_3| + Z_{FP}|\xi_5|e^{-i\theta_{53}}}{|\xi_3| - x|\xi_5|e^{-i\theta_{53}}}. \tag{6.15}$$

The right hand side of (6.15) may be evaluated from zero speed sectional coefficients using equations (6.11)–(6.14) and values of $|\xi_3|$, $|\xi_5|$ and θ_{53} obtained from full strip theory response calculations.

In order to compare with *BESTSEA* the left hand sides of (6.11)–(6.14) must be evaluated in terms of $\frac{\partial \Delta F}{\partial \xi_j} \simeq \frac{1}{\varepsilon}\left([\Delta F]_{\xi_j=\varepsilon} - [\Delta F]_{\xi_j=0}\right)$, using the above definitions of $\frac{\partial A_{ij}}{\partial x}$ and $\frac{\partial B_{ij}}{\partial x}$ ($\omega^2 e^{i\omega t}\frac{\partial}{\partial x}\left(A_{3j} + \frac{B_{3j}}{i\omega}\right) = \frac{\partial \Delta F}{\partial \xi_j}$). Similarly, the left hand side of (6.15) is obtained from $\omega^2 e^{i\omega t}Z_F = \frac{d\Delta F}{dh_x} = \frac{\Delta F(\xi_3,\xi_5) - \Delta F(0,0)}{(\xi_3 - x\xi_5)}$. Note that $[\Delta F]_{\xi_j=0}$ is not necessarily zero if steady flow terms are included in the time domain strip theory. Again, as for the parabolic strut comparison above, a minimum number of modifications were made to *BESTSEA* in order to provide maximum validation benefit.

Sectional added mass and damping distributions were calculated for SWATH #1 at two different speeds and a conventional hull form at a single speed. The frequency and relative heave and pitch amplitude and phase used were those corresponding to peak heave response as calculated by *BESTSEA*, and are indicated on figure 6-11.

A comparison of the two theories (figure 6-11) shows differences attributable to the differences in the theories. One would expect the hull boundary condition to strongly influence added mass and the free surface boundary condition to influence damping, and this accounts for the greater differences in the results in the latter case. In particular the SWATH model shows a smoother distribution of damping forces around the transition from its submerged bow to the surface

piercing sections aft (around section 8). The sharp changes in the two-dimensional theory are because, unlike in *BESTSEA*, the potential problem is solved for individual sections in total isolation, and forward speed effects are only included afterwards in combining coefficients.

An interesting observation is that in plotting damping against frequency, conventional sections (and fully submerged sections, as for example the bows of the SWATH models) show one peak, while SWATH sections show two peaks with an intermediate frequency of zero damping (due to cancellation of the waves produced by the keel and by the shoulders). This zero damping phenomenon is clearly shown in figure 6-2 between section 50 (the stern) and section 9 (just behind the stem) at a frequency of about 7r/s. The frequency chosen for figure 6-11 (i.e. the heave resonant frequecy) by chance almost coincided with the frequency of zero damping for a significant part of the hull length, consequently the damping in the 2D theory results is dominated by the $-U\frac{\partial a}{\partial x}$ and $2Ua + Ux\frac{\partial a}{\partial x} + \frac{U^2}{\omega^2}\frac{\partial b}{\partial x}$ terms of equations (6.13) and (6.14). The strong dependence of damping on the derivatives $\frac{\partial a}{\partial x}$ and $\frac{\partial b}{\partial x}$ contributes to the sharp changes near section 8, while *BESTSEA*, as expected, gives a smoother distribution. This phenomenon also accounts for the large predicted dimensionless heave values for the SWATH models, discussed in section 6.4.

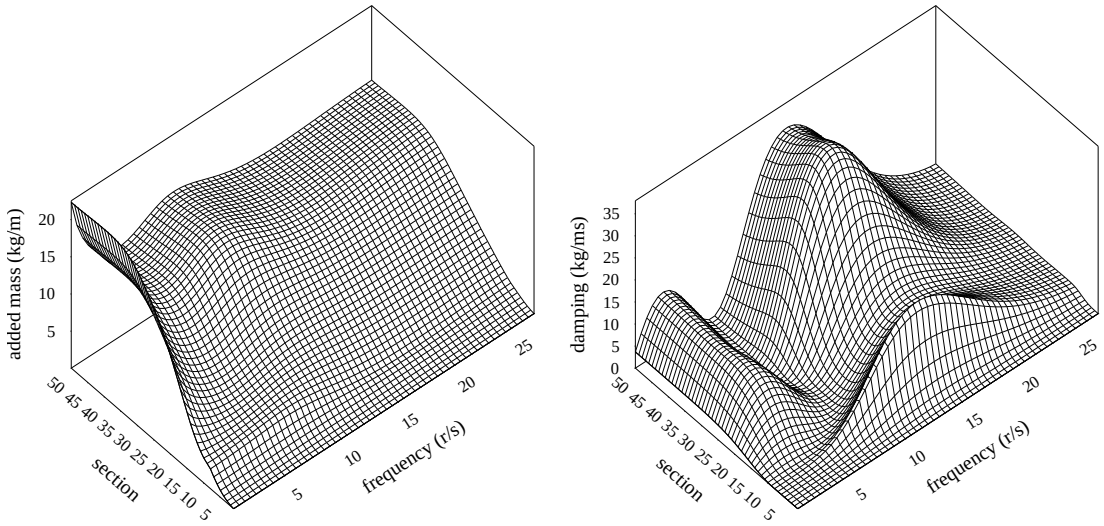

Figure 6-2: Zero speed sectional added mass and damping distribution as a function of frequency for SWATH #1

One can observe some numerical "noise" in the *BESTSEA* results of figure 6-11. Several factors contribute, including the presence of chines and non-sinusoidal forces. These effects diminished as the number of panels per section and the number of sections were increased.

To conclude, in comparing the two theories it must be emphasised that they are not mathematically equivalent except at zero speed. Significant differences are therefore inevitable, but assuming that the theories are not applied outside their range of validity one would also expect strong similarities between the results. These expectations are clearly borne out by the results.

Published results by similar theory: Faltinsen and Zhao's calculations for MARIN HSDSSS hull form

Motion computations by theories similar to *BESTSEA* have been published by Faltinsen and Zhao for the parent hull of the MARIN High Speed Displacement Ship Systematic Series (HSDSSS) Hull Form project ([29], [28], [25]) and for other hull forms ([105], [106]). The MARIN parent hull ([53] and [9]) is notionally identical to the AMECRC systematic series parent hull [10] (the only deliberate difference is the freeboard, but this is only of consequence for large motions), hence hull data were available for comparison with Faltinsen and Zhao's computations.

The theory used by Faltinsen and Zhao is described in [26] and [29]. Most significantly this theory uses the same free surface boundary condition and the same two dimensional form of Laplace's equation as *BESTSEA*. Differences fall into three categories:

1. Differences that theoretically should not affect the final result except due to numerical errors. These include the use of frequency rather than time domain, the use of simple sources and hence panels on the free surface, and the use of a reference frame moving with the boat (hence the introduction of spatial derivatives).

2. Differences that could easily be incorporated into *BESTSEA*. These include linearisation of pressures (including, in addition to the $\frac{1}{2}\rho V^2$ term, omission of the $\frac{\partial c}{\partial t}$ and $\frac{\partial \beta}{\partial t}$ terms of $\frac{\partial \phi}{\partial t}$ in equation 3.12), and restraint of the hull to its mean position.

3. Differences that could not be accommodated into *BESTSEA* without significant restructuring of the program to the extent that its validation value is compromised. Faltinsen and Zhao [29] present two forms of their expression for hull pressure. It is not totally clear which form was used for the motion predictions they published for the HSDSSS hull, but it appears they used the form that included interaction between the steady potential and oscillatory potential. However the body and free surface boundary conditions that they used did not include interaction terms. Also, very few details are given about their calculation of the diffraction potential. It was possible for them to make this distinction as the steady, forced motion and diffraction problems were solved separately, but in *BESTSEA* the three problems are solved simultaneously, and the exactly equivalent approximation would have required substantial changes to the present structure.

Motions predicted by *BESTSEA* are compared in figure 6-12 with numerical and experimental data scaled from Faltinsen's [28] figure 5. In view of the third category of differences between the two theories no attempt was made to modify *BESTSEA* to make it theoretically equivalent to the theory used in the results of Faltinsen and Zhao. For an infinitely slender hull these differences should not matter, but a moderate effect was expected as the HSDSSS hull had a $\frac{L}{B}$ of 8.

The heave response predicted by *BESTSEA* is about 10% greater than Faltinsen and Zhao's. Pitch also differs: *BESTSEA* predicts a response greater than the experimental results by a

similar amount to which Faltinsen and Zhao's is below, but *BESTSEA* identifies a small hump in the pitch response absent in Faltinsen and Zhao's results. Also Faltinsen and Zhao's pitch appears to be heading towards infinity at zero frequency, whereas *BESTSEA* appears to be heading towards zero. Neither of these is actually expected. The vast majority of both Faltinsen and Zhao's other published results and *BESTSEA* results approach unity as expected. This behaviour is also not unknown in traditional strip theory, similar behaviour being cited by Blok and Beukelman [9] (same model, same speed, Salvesen *et al.* theory [84]) and Lahtiharju *et al.* [56].

These differences are not outside the range observed for other comparisons between nominally similar but not exactly equivalent strip theories. For example Doctors [23] gives many examples of comparisons of the theories of Salvesen, Tuck and Faltinsen [84] and Korvin-Kroukovsky and Jacobs [54], with and without end terms, and with other more subtle variations such as the use of Lewis forms and panel methods. The results show substantial differences (greater than a factor of 2) in some cases with and without the inclusion of end terms, and significant differences for most other comparisons.

6.3.2 *BESTSEA*: hull discretisation and method of calculating forces

Some examples of investigations of the effects of panel refinement and methods of calculating forces are shown in figure 6-13, and these will be discussed below.

Panel refinement in particular was an important initial consideration because *BESTSEA* is computationally very time intensive. Computational time varied with the square of the number of panels, and (assuming a fixed total simulation time, rather than a fixed number of time steps) with the cube of the number of sections[6]. Therefore any unnecessary over-refinement very quickly pushed computational time (with the available resources) beyond reasonable limits.

Figure 6-13(a) shows calculations using 14 and 28 panels[7] on each cross section (50 sections) for SWATH #2 at two different Froude numbers. The difference for heave motion is negligible, but for pitch a small difference can be observed. 14 panels was therefore considered sufficient, and this was used for all subsequent calculations. It should be noted that hull forms with chines may require more panels for accurate results, for reasons discussed in section 4.5.1. The AMECRC hulls are both round hull forms, and the SWATH hulls only have chines over a short length near the stern, so this should not cause any problem in the present work.

The number of sections, in the present form of *BESTSEA*, affects not only the longitudinal spatial discretisation of quantities along the hull, but also the size of the time step. For simplicity

[6] Virtually all of the computational time involves evaluation of the convolution integrals in the Green functions, which each require one evaluation of the integrand for each section ahead of the given section (i.e. for each prior time step for that section). If the total number of sections is n, then the number of evaluations of the convolution integrand is proportional to $\sum_{i=1}^{n} i$, or approximately proportional to n^2. Another factor n appears due to the number of time steps per cycle, giving n^3 in total.

[7] This refers to the number of panels between the waterline and the keel, as symmetry was used.

the fixed strips of water were made to coincide always with particular cross sections of the hull, thus the time step was always $\frac{\Delta x}{U} = \frac{L}{n_s U}$, where Δx is the longitudinal spacing of the hull cross sections, n_s is the number of sections, and L is the hull length. Therefore at higher speeds, when the time step would be smaller (as shown by the $Fr = 0.7$ lines in figure 6-13(b)) both the spatial and temporal resolution were adequate with 25 sections. From this it can be inferred that the difference between the computations with 25 and 50 sections at $Fr = 0.4$ (shown in the same graph) is primarily due to coarse time steps, and not to the spatial resolution. This conclusion is confirmed by the degradation of results as frequency increases, indicating that the time step to motion period ratio is an important consideration. It can be shown that $\frac{T}{\Delta t} = \frac{2\pi Fr\, n_s}{\omega\sqrt{L/g}}$, thus with $Fr = 0.4$, $n_s = 25$, and $\omega\sqrt{\frac{L}{g}} = 5$, there would only be about 12 time steps per period. 50 sections were used for subsequent calculations, but the lower limit of Froude number was restricted to 0.4. Results at or near this Froude number may therefore be a little approximate, with figure 6-13(b) suggesting that the heave resonant peak is exaggerated by about 15% and pitch by about 5%, while the error at $Fr = 0.7$ is not significant.

As a possible future improvement to *BESTSEA*, by interpolating between given sections it should be possible without major difficulty to decouple the time step size from the longitudinal section spacing.

The choice of 14 panels and 50 sections was seen as a reasonable compromise between accuracy and computational time, and, with the exception of the sensitivity tests described above, was used throughout all other computations. At this level of refinement each time step required about 6 seconds of CPU time on a Silicon Graphics Origin 200 workstation with 180MHz IP27 MIPS R10000 processor. Given that typically a smooth RAO curve requires say 25–30 frequencies, each requiring about 500 time steps (in some cases more, especially at low frequencies or high speeds, but fewer at low speeds), this represents about 24 hours of CPU time per complete RAO curve, excluding any initial test runs. If quicker results are required use of 25 sections (hence also 250 time steps) would be cut this to 3 hours. Memory requirements by comparison are extremely modest, and are unlikely to be an issue.

Figure 6-13(c) shows the difference between calculation of pressure using $p = -\rho\left(\frac{\partial\phi}{\partial t} + \frac{1}{2}\nabla\phi\cdot\nabla\phi\right)$, labelled "exact", and $p = -\rho\frac{\partial\phi}{\partial t}$, labelled "linear", for SWATH #2 at $Fr = 0.4$, $H_w = \frac{L}{250}$. At the wave height shown, which, unless otherwise stated, was used throughout the computations, the difference is small but not negligible, and is generally one of slight damping of motions. Figure 6-9(b) shows the related effect of varying the wave height[8]. The validity or otherwise of using the exact form of the body pressure, or of using a particular linearised form, is discussed in section 2.5, as well as some related issues in section 4.4.1. Throughout the subsequent computations the "exact" form of the body pressure was used.

[8]This is not an exactly equivalent phenomenon because the non-linear effect of using a dynamic waterline was always used.

6.3.3 Implementation of Salvesen, Tuck and Faltinsen [84] theory

As mentioned in the beginning of section 6.3, motions were calculated using the University of New South Wales standard strip theory program *HYDROS* [22], but only for the SWATH models, and only for a fairly coarsely spaced selection of frequencies, and that an equivalent program *STF* was written to allow greater flexibility of investigation. Figure 6-14 shows comparisons of the latter implementation of the Salvesen, Tuck and Faltinsen [84] theory with *HYDROS*. The agreement is excellent, and suggest that *STF* can be used with confidence as representing traditional strip theory in the following comparison between *BESTSEA* and the experimental results. Agreement of calculations for the SWATH models at greater displacements was equally good.

The only significant differences in figure 6-14 are SWATH #1 heave at $Fr = 0.4$ and pitch at $Fr = 0.2$. These difference are small enough to be attributed to minor differences in the numerical implementations, which may include the following:

- *HYDROS* uses a Galerkin panel method, in which the velocity used in the hull boundary condition was averaged over each panel, rather than the simpler collocation method used by *STF* in which the velocity at the mid-point of the panel was taken. A full description of the difference is given in [21].

- There will naturally be small differences in the manner in which the two programs interpolate hull sections and panels from the given geometry data, even given the same resolution.

- Both programs made use of "lid panels" to avoid the problem of irregular frequencies (described in [21]). The number used by *HYDROS* is not known, but appears to be such as to give an approximately equal panel lengths on both the lid and the submerged part of the section, while the number in *STF* is specified explicitly.

- The *STF* results presented in figure 6-14 used 50 sections, and 24 panels (including 4 lid panels) over *half* the section (making use of symmetry). Further refinement produced no visible change in figure 6-14. The *HYDROS* results as supplied were calculated for a fixed number of sections (20) and panels per section (approximately 20 over the *whole* cross section, including the lid, but apparently able to be adjusted slightly by the program). It is not known to what tolerances the results had converged at this level of discretisation, but it is expected on the basis of *STF* results that small but visible differences might be observable in figure 6-14 on refinement from these levels. It is noted that the displacement calculated by *HYDROS* differed from the actual displacement by up to 1.1%, while *STF* was within 0.4% at the above resolution.

6.4 Numerical results

6.4.1 General comments

BESTSEA

The responses computed using *BESTSEA* are shown in figures 6-15, 6-16, and 6-19–6-23. *BESTSEA* predicts the general form of the response curves very well. All the main features of the experimental results are present, as well as many more subtle ones. The pitch calculations are excellent, and the natural frequencies are well predicted, but the magnitude of the peak heave response tends to be a little high. In general the predictions improve at higher speed, as should be expected for such a theory.

Prediction of the influence of speed on responses is good for the conventional hulls, and generally agrees with expectations based on the simplified model of section 6.1.2. It becomes progressively worse however for the SWATH models, but this is due to the zero damping phenomenon of two dimensional SWATH sections described in section 6.3.1, and is therefore a fault common to all strip theories at low speed.

The significant improvement over conventional strip theory of predictions of both coupling (discussed in more detail below in section 6.4.2) and pitch indicate more accurate representation of the variation of forces along the hull length. This is particularly pleasing since it mirrors the findings of Yeung and Kim [102] that in their similar *forward speed theory* "the improvement over strip-theory results in the hydrodynamic coupling coefficients of heave and pitch were particularly striking for a number of realistic hull forms". It is also compatible with the explanation of Gerritsma's [32] discussed in section 4.3.2 that coupling effects are introduced as a result of the hydrodynamic asymmetry caused by forward speed. The latter could equally apply to pitch.

One area of uncertainty in the comparison is the effect of non-linearity. *BESTSEA* in its present form sometimes starts to become unstable when a significant proportion of the hull emerges completely from the water. To avoid this problem with the AMECRC models the wave height in the numerical simulations was restricted to 10mm, while the tank tests for these hulls ware done in waves of height 30mm. This is particularly likely to affect the results for AMECRC #04, which, at 50mm, has half the draught of AMECRC #05. The experimental dimensionless heave in places approaches 1.5, which equates to a heave *amplitude* of $\frac{1.5\times 30\text{mm}}{2} =$ 22.5mm, a substantial proportion of the total draught and in fact greater than the draught at the stern ($\simeq$15mm). Support for this hypothesis is given by the fact that the numerical results for AMECRC #05 appear better than for AMECRC #04 (figure 6-23). Unfortunately no tests have been done to date on the AMECRC models to determine the effect of wave height and significance of non-linearities on the motions.

It should also be recalled that, as shown in section 6.3.2, the heave results at the lower speeds may in part be over predicted because of coarse time steps size in the numerical solution (see figure 6-13(b)). In order to achieve a sufficiently small time step it was necessary in the

present formulation of *BESTSEA* to have a larger number of cross sections than would have been necessary for a traditional frequency domain solution.

STF

The responses computed using *STF* are shown in figures 6-17–6-23. These show generally satisfactory prediction of the form of the heave response curves, although some of the subtleties present in the *BESTSEA* predictions are absent (details will be given in section 6.4.2). Pitch, however, is poorly predicted by *STF*, especially as speed increases, and in some cases lacks any resemblance to the experimental results. The natural frequencies are predicted well for the SWATH models in heave motion, but not for pitch, and not consistently well for the AMECRC models in either heave or pitch.

Heave peak responses predictions are generally satisfactory, but vary from too high for the SWATH models to too low for the conventional hulls. In general they are not better than the *BESTSEA* predictions, although the comparison is more favourable at the lower speeds. Predictions improve significantly as speed decreases, as one would expect, given the assumptions on which the theory is based, except SWATH #1 for reasons already noted. The pitch peak response is only well predicted for SWATH #1, and is particularly poorly predicted for SWATH #2. Again, predictions are improved as speed is decreased.

6.4.2 Comparison with experimental results

SWATH #1

Figure 6-19 gives a direct comparisons between experimental results and the two theories for SWATH #1 at its nominal displacement of 22.0kg.

Agreement between *BESTSEA* and the experimental results is mostly good, and generally better than *STF*. However the influence of speed on heave is opposite to both the simplified model and experimental results, and this feature is predicted by both theories. This is explained in terms of the zero damping frequency for SWATHs discussed in section 6.3.1. Figure 6-2 shows this zero damping frequency to be just above 1Hz ($\omega_e\sqrt{\frac{L}{g}} = 3.2$) for most of the vessel length, which unfortunately closely coincides with the vessel heave resonance, thus this explanation is entirely consistent with the observations. In reality significant hydrodynamic damping would be present due to three dimensional wave effects.

Experimental data is insufficient at low frequency, due to towing tank limitations and model size. In particular the pitch resonant peak is not shown in the experimental results, thus limited conclusions can be drawn about the quality of pitch predictions from the comparison.

A point of interest is the very low trough in the pitch response at around $\omega_e\sqrt{\frac{L}{g}} \simeq 2.5$ (most evident at the lowest Froude number). This must be due to a cancellation effect from coupling, rather than to reduced forcing (which is a minimum around $\frac{kL}{2} \simeq 4.5$, or $\omega_e\sqrt{\frac{L}{g}} \simeq 6.6$

at $Fr = 0.4$, as suggested by equation (6.6) putting $\left(\frac{2}{kL}\right)^2 \left(\sin\frac{kL}{2} - \frac{kL}{2}\cos\frac{kL}{2}\right) = 0$, and in any case is not a function of encounter frequency) or to very high damping (which might cause a dip below unity, but not by that much). The effect on pitch of coupling from the heave motions in this case is to increase pitch to the right of the heave natural frequency and decrease it to the left. The reason is that near resonance (especially with subcritical damping) there is a rapid change of phase of response from being in phase with forcing on the low frequency side of the peak to π out of phase on the high frequency side. Associated coupling (when the heave natural frequency is higher than the pitch natural frequency) causes a shift from a cancellation of pitch to a reinforcement of pitch as one progresses upwards in frequency. Hence (as expected due to the overprediction of heave for reasons already cited) pitch is too low at the trough ($\omega_e\sqrt{\frac{L}{g}} \simeq 2.5$) and too high at the peak ($\omega_e\sqrt{\frac{L}{g}} \simeq 3.0$).

The results of the SWATH #1 model at 25.72kg displacement (figure 6-20) reinforce the findings of the previous figure, that *BESTSEA* gives predictions as good as or better than *STF* at all speeds and all frequencies, and for both heave and pitch. (Experimental results are only available at this displacement for $Fr = 0.4$ and 0.6.) It was recognised in the tank tests that in spite of potential finite depth effects it was necessary to extend the lower frequency limit as far as practical in order at least qualitatively to investigate pitch behaviour more thoroughly. The low frequency experimental pitch results are therefore a little more conclusive then in the previous figure, and confirm very well the computed results.

The deeper draught caused the model to have less damping, hence the predictions are generally better than the previous figure. In particular the coupling effects discussed above are very good.

SWATH #2

Comparisons for SWATH #2 at its nominal displacement (22.0kg) are shown in figure 6-21.

The experimental data for this model in general is much more conclusive than for SWATH #1 at low frequency, mainly due to its higher natural frequencies, a consequence of its larger waterplane area. Tests were also conducted at longer wavelengths, which would affect the lowest frequency results. However the effects (as suggested by equation (5.3)) should be negligible at the heave resonance and at the pitch resonance at low speed, but equivalent to an apparent speed reduction at the pitch resonance of about 10% at the highest Froude number. While there would be an observable effect on the results it is not great enough to alter any of the conclusions drawn from them.

There is still an overprediction of heave due to the "SWATH phenomenon" described above, and (as above) through coupling this causes a slight overprediction of pitch just above the heave natural frequency and a slight underprediction just below. The form of the traditional frequency domain strip theory vessel added mass and damping coefficients suggests that coupling increases with speed, and this is certainly suggested by the numerical results. Apart from this pitch is

extremely well predicted by *BESTSEA*, and certainly much better than traditional strip theory (*STF* doesn't even predict the correct pitch natural frequency).

Heave is well predicted by *BESTSEA* at high speed, and (as one would expect) improving as speed increases. On the other hand *STF* improves in its predictions as speed is decreased (also as one would expect).

It is worth also noting some more subtle features in the experimental heave results predicted by *BESTSEA* but absent in the *STF* results. Most evident at the lowest speed, as one approaches the heave peak from low frequency, there is a dip below unity, followed by a slight hump half way up the left side of the main heave peak. The hump can also clearly be seen in the *BESTSEA* and experimental results for SWATH #1 at $Fr = 0.4$ (figure 6-19). This is attributed to coupling from the pitch resonant peak, in the same manner that the equivalent feature in the pitch results was explained above in terms of coupling form the heave resonant peak. The effect is more pronounced at lower speeds because the *absolute* pitch is greater (both the dimensionless pitch at resonance and the unit pitch kH_w for a given encounter frequency are larger at lower speeds).

The 28.50kg displacement results (figure 6-22) reinforce the 22.00kg displacement results and the conclusions drawn from them.

H_w effects

Figure 6-9(b) shows the effect of mild non-linearities in response as predicted by *BESTSEA*. Unfortunately the heave peaks for SWATH#2 at the highest wave height resulted in unstable numerical behaviour in *BESTSEA*, and a reason for this is suggested in section 6.5.3. However there is enough of the response for the 3.0m/s case to suggest that the heave resonant peak and the corresponding coupling peak in pitch are both reduced at $H_w = 40$mm, while the pitch resonant peak is not significantly affected. This is in agreement with the experimental results in figure 6-9(a).

The result for SWATH #1 is particularly good, with the heave peak at $H_w = 40$mm, both experimentally and numerically, showing an increase in frequency and a slight increase in magnitude, while the corresponding pitch peak shows also an increase in frequency but with a significant reduction in magnitude.

AMECRC #04 and AMECRC #05 results

Figure 6-23 shows comparisons for the conventional hulls. Again limited experimental data exists at low frequency and high speed. The behaviour of AMECRC #04 in pitch, and of AMECRC #05 for both heave and pitch, at $Fr = 0.86$ are in particular unclear.

As for all the other results, *BESTSEA* approaches the tank results as speed increases, while *STF* diverges from the experimental results. Pitch in all cases is better in *BESTSEA* than in *STF*.

Both theories give a similar quality of heave prediction, but *BESTSEA* tends to overpredict while *STF* tends to underpredict. The overprediction can be explained in terms of additional damping terms, for example the transverse wave system, friction, and transom related flow circulation effects, which will be discussed in detail in the section 6.5, but the underprediction can not be adequately explained.

Particular features in the heave response (the dip to the left of the main peak) are again present in the *BESTSEA* results but not in *STF* (for example AMECRC #04, $Fr = 0.57$). Also the frequency of maximum peak responses for both models and in both heave and pitch is predicted better by *BESTSEA*. At the higher speed in particular they are predicted poorly by *STF*.

Note that AMECRC #05 is a severe test case for *any* strip theory, with a beam to length ratio of only 4. Also AMECRC #04, as stated above, is likely to be subject to significant non-linearities. Therefore the comparisons are not displeasing.

6.5 Discussion of approximations made in *BESTSEA*

To summarise, the agreement between *BESTSEA* and the experimental results is generally good (and in places excellent) by the standards of typical expectations for seakeeping computations, particularly at higher speeds (for which the theory was intended). This is demonstrated by the general improvement over the conventional strip theory results. However by the standards of computational predictions in many other engineering applications, where errors consistently of the order of say 1–2% are sought, the comparison is not favourable. Obviously achievement of this order of accuracy in seakeeping problems (particularly high speed) is well beyond the present state of the art. Nevertheless a discussion of the approximations involved, and an assessment of their importance, is relevant in prioritising future research, and may also suggest ways to significantly improve predictions in the shorter term through approximate treatment of phenomena.

Discussion of the various approximations must be in the context of the nature of the disagreement between the numerical and experimental results. The most significant difference was the magnitude of the heave peaks (and related phenomena such as the associated effect on pitch due to coupling), suggesting an underprediction of damping forces. The resonant frequencies were well predicted (suggesting at least reasonable added mass predictions), and the general form of the response curves predicted by *BESTSEA* (apart from the magnitude of the heave peak) is in general excellent, suggesting both appropriate prediction of coupling forces and variations of coefficients with frequency. In fact, regarding the general form of the curves, *BESTSEA* gave generally a far better prediction of pitch than *STF*, and in several cases predicted subtleties of the heave response curves absent altogether in the *STF* results.

Much discussion in earlier chapters has already focused on approximations to the potential

flow solution, in particular the neglect of the longitudinal derivative in Laplace's equation, and forward speed and non-linear terms in the free surface boundary condition. We recall that *BESTSEA* generally overpredicts peak responses, while *STF* in many cases underpredicts. It is difficult to reconcile a potential flow based method underpredicting response peaks, as it implies an additional source of input energy. Overprediction of peaks on the other hand, provided the margin of overprediction is reasonable, fits comfortably with the notion of neglect of mechanisms for energy loss present in real flows. This observation in itself therefore suggests that the treatment of the hydrodynamics by *BESTSEA* is a significant improvement over traditional strip theory.

In view of the previous paragraph, and that it appears that *BESTSEA*'s main shortcoming is its underprediction of damping, the role of viscous related phenomena seems important. The following discussion therefore, while also commenting on some of the potential flow approximations, will focus in particular on viscous related phenomena.

The purpose of this section is not to predict accurate magnitudes of various neglected effects, but merely to assess whether they are likely contributors to the differences between the experimental and the numerical results. For this purpose an order of magnitude only is sought for the various effects. Each source of damping will be assessed as likely, possible, or unlikely to account for differences in the results, either alone or in combination with others. If the net effect is positive, then the numerical results can be considered entirely consistent with the assumptions made.

We will return for the moment to the simplified model of section 6.1.2 as a means of assessing likely contributions of the various sources of damping. Although this is approximate, and only represents a single degree of freedom, it is sufficiently accurate for our stated purpose. SWATH #2 will be used as an illustrative discussion case.

The total heave damping coefficient, B_{33}, may be written as $B_{33} = B_{33,w} + B_{33,o}$, where the subscript $_w$ denotes the component due to wave generation (i.e. damping calculated by *BESTSEA*), and the subscript $_o$ denotes the damping due to all other effects. $B_{33,o}$, representing the force on the hull for a unit heave velocity, needs to be identified for each proposed source of damping.

The total damping coefficient corresponding to the model tests can be estimated by recalling from section 6.1.2 (and using the notation of that section) that $\zeta = \frac{B_{33}}{2(M+A_{33})\omega_n}$, and at resonance if $\zeta \ll 1$ then $\left(\frac{H}{\delta_{st}}\right)_{\max} \simeq \frac{1}{2\zeta}$. Putting (for SWATH #2 at $U = 3.5$m/s) $\left(\frac{H}{\delta_{st}}\right)_{\max} = 3$ (from the experimental results), $M = 22$kg, $\frac{\omega_n}{2\pi} = 1.3$Hz, and assuming $A_{33} \simeq M$, we find

$$\begin{aligned} B_{33} &= \frac{2\left(M + A_{33}\right)\omega_n}{2\left(\frac{H}{\delta_{st}}\right)_{\max}} \\ &= 120 \text{ kg/s.} \end{aligned} \tag{6.16}$$

Repeating with $\left(\frac{H}{\delta_{st}}\right)_{\max} = 3.8$ (from the numerical results) gives $B_{33,w} = 95$ kg/s, hence we

require

$$B_{33,o} \simeq 25 \text{ kg/s}, \quad \text{or} \quad \zeta = 0.035, \tag{6.17}$$

representing a required 26% increase on present damping. (Other results require more or less, but this is a good starting point for an order of magnitude assessment.) Proposed individual contributions to $B_{33,o}$ will be denoted below as $B_{33,i}$.

6.5.1 Flow circulation

Lifting forces exist on all transom stern vessels due to the flow circulation required to enforce a Kutta condition on a trailing edge (in this case the transom stern, where tangential flow detachment occurs but is not automatically implied by the free surface boundary condition).The importance of introducing vorticity to account for the Kutta condition on the transom stern is also referred to in connection with the steady flow problem by Nakos and Sclavounos [71] and Cole [17]. The unsteady component of this force on heaving or pitching planing hulls contributes to the added mass and damping of the vessel. This effect occurs for all transom stern hulls operating at speeds high enough to completely ventilate the stern, whether actually planing or not, but non-planing hulls differ mainly in that the wetted length does not change significantly during unsteady motions. Other differences will be discussed below after estimating the possible magnitude of this effect.

Strip theories can and do take into account tangential flow separation at the transom stern, but in the absence of vorticity this must be done at the sacrifice of specifying atmospheric pressures at the stern. Faltinsen [28] shows that specification of zero pressure at the transom does affect motions, although, as stated by the author, this was done in an arbitrary manner with no justification other than to demonstrate possible significance of such an effect. The dependence of the lift force on flow circulation suggests that the influence on pressure may not be so localised to the stern. Also the following discussion suggests the net effect is one of damping, contrary to the *increase* in motions shown in [28].

The unsteady lifting problem has been studied by Ulstein and Faltinsen [91]. This is a two dimensional analysis, applicable to high aspect ratio lifting surfaces, but nevertheless can provide a useful estimate of the importance of the effect. It will be shown that order of magnitude estimates indicate damping effects may be substantial, while added mass effects are insignificant.

Ulstein and Faltinsen [91] (figures 5 and 6) show results of calculations for a heaving flat plate at an angle of attack, both with and without consideration of the change in wetted length. For the present estimates, the case without changing wetted length will be considered. As well as being more realistic for non-planing transom stern hulls this gives a more conservative estimate of damping (approximately half the value of the case with consideration of changing wetted length, except at combinations of low frequency and high speed) while not changing the conclusion that the added mass effect is insignificant.

Ulstein and Faltinsen present added mass and damping per unit width of plate. Actual values for a ship may be estimated by multiplying by $\frac{A_{wp}}{L}$ (waterplane area to length ratio). (This ignores three-dimensional effects, which tend to reduce lift due to the low aspect ratio of the hull as a lifting surface, and the fact that the longitudinal force distribution should be multiplied by the local beam rather than the average beam.) In terms of Ulstein and Faltinsen's dimensionless added mass and damping, $A^* = \frac{A}{\rho L^2}$ and $B^* = \frac{B}{\rho L^2 \omega}$, and their reduced frequency, $k = \frac{\omega_e L}{2U} = \frac{\omega_e \sqrt{L/g}}{2Fr}$, we have $\frac{A_{33}}{M} = A^* \frac{A_{wp} L}{\nabla}$ and (noting that $C_{33} = \rho g A_{wp}$) $B_{33} = 2kB^* \frac{C_{33} U}{g}$. We note also that the range of k values of interest is around the resonant frequency (say $\omega_e \sqrt{\frac{L}{g}} = 2$–$6$) and speed of say $Fr = 0.5$–1.0, thus $k \simeq 1$–6.

In the above range of k $A^* < \frac{\pi}{8} \simeq 0.39$ according to all theories presented in [91], and for slender ships $\frac{A_{wp} L}{\nabla} \ll 1$, hence we conclude the contribution to total effective mass is negligible.

In the same range of k the damping with no change in wetted length (scaled from Ulstein and Faltinsen's figure 6) appears to approximate $B^* = \frac{1}{2k}$. (This is slightly greater than half the given asymptotic value of damping for the changing wetted length case of $B^* \sim \frac{\pi}{4k}$.) Combining with the above expression for B_{33}, and expressions for the damping ratio $\zeta = \frac{B_{33}}{2(M+A_{33})\omega_n}$ and undamped natural frequency in pure heave motion $\omega_n = \sqrt{\frac{C_{33}}{M+A_{33}}}$, gives

$$\zeta \simeq \frac{\tau_n}{2} \tag{6.18}$$

where τ_n is the value of $\tau = \frac{\omega_e U}{g}$ corresponding to the undamped natural frequency. (Where the wetted length changes due to unsteady motions in the manner of a planing flat plate Ulstein and Faltinsen's results indicate damping could be up to almost twice this value.)

Considering a typical case of $\omega_n^* = 4$ and $Fr = 0.5$ gives $\tau = 2$ hence $\zeta \simeq 1$. Although this estimate is obviously high (it implies no resonant peak at all) it is an order of magnitude larger than any other source of damping to be proposed below. It clearly indicates that damping effects due to unsteady lifting forces produced by ventilation of a transom stern may be substantial.

This two-dimensional analysis assumes a large beam to length ratio. Smaller ratios, as would be typical, would result in smaller forces due to the ability of fluid to 'escape' laterally (equivalent to the tip vortices at the ends of an aerofoil). Perhaps effective length is limited by the beam; multiplication of ζ by $\frac{B}{L}$ gives the right order of magnitude. In fact Cole shows a dependence on beam for the three dimensional steady case; her [17] expression for the vortical and spray drag for a low aspect ratio flat ship ($T \ll B \ll L$) is a function of $K^2 = Fr^2 \frac{B}{L}$. A dependence of ζ on beam (as opposed to a dependence of only $B_{33,i}$ on beam, which would be partly cancelled due to corresponding increases in other coefficients) also explains the varying requirements of the models, SWATH #1 requiring the least damping and the conventional hulls the most.

Cole [17] also shows (under certain conditions) that energy in the vortical flow is equivalent far behind the boat to the steady wave energy. Thus if a similar relationship holds for the unsteady component of flow, and given that the radiated energy accounts for the damping force, it is reasonable to expect the "planing damping" to be of the same order as the wave damping

for typical high speed transom ship forms. This again confirms the likely importance of this effect on high speed ship motions.

6.5.2 Direct viscous effects

Viscous effects are usually ignored in numerical seakeeping studies, except in the case of roll damping for monohulls, on the basis that they are negligible. However, viscous forces are likely to be significantly larger for high speed vessels than for conventional vessels, as will be apparent from the derivation of equation (6.20).

We seek to determine therefore whether viscous effects could account for the observed differences between experimental and numerical results. The discussion will treat separately skin friction and form drag effects.

Skin friction

The viscous shear stress, τ, is assumed to be of the form

$$\tau = \frac{1}{2}\rho \left|\vec{v}\right|^2 c_F \tag{6.19}$$

where c_F is a friction coefficient to be determined and $\vec{v}$ is the local velocity of the water relative to the hull. Furthermore the direction of the shear stress acting on the hull is the same as that of $\vec{v}$.

The shear stress and relative velocity will both be locally in a plane tangential to the hull, and, assuming a slender hull, this will be approximately the plane parallel to both the longitudinal (x) axis and the local tangent to the cross section, which we will call the xt plane. Assume that the boat is travelling at speed U in the $+x$ direction, and that $\vec{v}$ makes an angle θ with the $-x$ axis. Let also the component of $\vec{v}$ tangential to the hull section (the t component), obtained from the strip theory solution, be denoted v_t. Thus $\tan\theta = \frac{v_t}{U}$, since $-U$ will be the x component of $\vec{v}$. We note that, except at very slow speeds or conditions of extreme motion, $U \gg v_t$, and therefore $\left|\vec{v}\right|^2 \simeq U^2$ and $\sin\theta \simeq \frac{v_t}{U}$.

Finally, it is only the tangential component of τ that is of interest in motion prediction. The longitudinal component contributes to drag, but not to heave and pitch damping. Thus we obtain $\tau_t = \tau \sin\theta \simeq \frac{1}{2}\rho U^2 c_F \sin\theta$, which simplifies to

$$\tau_t \simeq \frac{1}{2}\rho U v_t c_F. \tag{6.20}$$

(We note that this gives linear damping in as far as v_t is a linear function of heave and pitch.)

The vertical component of shear force is obtained by integration over the projection of the hull area onto a vertical plane. As a first approximation for heave motion we could take v_t to be the heave velocity[9], and apply this stress over an area $2LT$ (length $\times$ draught of vessel, both

[9]Given that at resonance the heave velocities lag the wave velocities by a phase difference of $\frac{\pi}{2}$, and the dimensionless heave $\gg 1$, it is sufficient for the present purposes to assume that the relative motion between boat and water is approximately equal to the absolute boat motion.

sides). This gives a contribution to $B_{33,o}$ as

$$B_{33,i} = c_F \times \rho LTU. \tag{6.21}$$

Using an expression for c_F given by Lloyd [61] (equations 12.21 and 12.22) applicable to roll damping, $c_F = 0.0004 + [3.36 \log_{10}(\mathbf{R}) - 5.6]^{-2}$ (where the Reynolds number ($\mathbf{R} = \frac{\rho UL}{\mu}$) is based on the hull length and forward speed), with a model Reynolds number of 7.3×10^6 ($L = 2.5$m, $U = 3.5$m/s), gives a friction coefficient of 0.0067. Substitution of values for SWATH #2 ($T \simeq 0.085$m) into equation (6.21) gives $B_{33,i} \simeq 5.0$kg/s

It is to be noted that Lloyd's expression for shear stress differs from equation (6.20) in that he does not take into account the forward speed of the boat, giving (in the present notation) $\tau = \frac{1}{2}\rho v_t^2 c_F$. This is quite appropriate for typical monohulls, for which the roll amplitudes are large and the forward speed is slow, but it is inadequate for the heave and pitch motions of high speed catamarans. In the latter case the expression (6.20) actually gives a much higher estimate of friction (by a factor of $\frac{U}{v_t}$).

In spite of probably overestimating $B_{33,i}$ (due to use of LT as the effective area, and to the $\frac{U}{v_t}$ factor mentioned in the previous paragraph) the above estimate of 5.0kg/s falls well short of the required value given in equation (6.17)[10]. Thus, simple skin friction effects may be ruled out as the primary cause of difference because their inclusion gives negligible improvement, while some results (e.g. SWATH #1) show no need at all for increased damping. There is therefore no strong argument, either a physical or an empirical, for the systematic inclusion of viscous friction terms.

Form drag of the heaving cross section

A bluff body with a cross sectional area A exposed to a steady flow stream of velocity U experience a form drag force D typically represented as

$$D = C_D \frac{1}{2} \rho U^2 A. \tag{6.22}$$

Application of this to unsteady flow with a substantial cross-flow component (the longitudinal relative velocity due to the forward motion of the boat) is questionable, and the discussion under the heading of "flow circulation" is probably more relevant. However if we accept this approximation for obtaining an order of magnitude estimate, replace U^2 with Uv as we did for skin friction (v in this case being the heave velocity), and assume the force to apply only during upward motion this gives an average damping coefficient over each cycle of $B_{33,i} = \frac{D}{v} = \frac{1}{4} C_D \rho U A$.

Using the maximum underwater plan area of SWATH #2 of 0.306m^2 and the required damping given in equation (6.17) gives a drag coefficient of 0.093 required to explain the differences

[10]The value estimated here is consistent with calculations in which equation (6.20) was used in *BESTSEA*. Those results are not shown here because an error existed in *BESTSEA* at the time (which has since been corrected), and the accuracy required for this discussion does not warrant repeating the calculations.

between numerical and experimental results at $U = 3.5$m/s. This is lower than typical for most bluff bodies, suggesting that form drag more than adequately accounts for the required heave damping. However considering the questionable applicability of equation (6.22) it is difficult to draw any conclusion other than that this is possibly a plausible explanation.

6.5.3 Hull entry effects

A possible additional source of damping is through the energy loss associated with the spray produced by the entry into the free surface of wedge shaped hull forms, particularly bow sections. Some features of the flow are described by Cointe [16], and Johnstone and Mackie [50], while Hughes [48], Dobrovol'skaya [20], and Zhao and Faltinsen [104] give results of the total force calculation for the cases of a 90° wedge, small wedge angles, and large wedge angles respectively. The analysis generally involves the assumptions of irrotational flow and (for large impact velocity or small time, i.e. $\frac{gT}{U} \ll 1$) negligible gravitational effects, the latter being a consequence of the large inertial forces at impact. (Inertia suggests added mass effects, but it is the rate of change of these inertial forces due to the quadratic variation with depth of displaced volume of the wedge as it penetrates at constant speed that results in a damping force.) The neglect of gravity causes the flow to be "geometrically self similar", i.e. at any point of time all quantities scale with the depth of penetration, and the potential may be written in the form $\phi(x, y, t) = U^2 t \varphi\left(\frac{x}{Vt}, \frac{y}{Vt}\right)$. The force may be written as

$$F = C_F \rho U^2 D, \tag{6.23}$$

where $D = Ut$ is the depth of penetration, and Hughes [48] found for the 90° wedge $C_F = 3.40$. Hughes also cites an expression by Wagner [95]

$$C_F = \pi \left(\frac{\pi}{2\sigma} - 1\right)^2, \tag{6.24}$$

(where σ is the deadrise angle) adopted by the U.S. National Bureau of Standards to represent experimental results for intermediate nose angles (i.e. wedge angles around 90°), which agrees well with his result.

The potential flow solution used to model the flow in each 'strip' in the present time domain strip theory does take this into account to some extent, but the free surface is linearised about the undisturbed free surface, and, while it would exhibit some of the features of the hull entry problem, it is inappropriate for representing accurately such a highly non-linear problem. On the other hand, considering the approximations involved it turns out to be surprisingly good at predicting wedge entry forces, suggesting that the spray jet contribution is only a significant proportion of the total force at large wedge angles.

Figure 6-3 compares predictions from the time domain panel method used in *BESTSEA* with equation (6.24) (from Wagner [95]), and results of Dobrovol'skaya [20], Zhao and Faltinsen [104], and Hughes [48]. It is not claimed that *BESTSEA* correctly represents the physics of bow entry, but it does give good predictions of the force for small wedge angles. Even for a 90° wedge

($\alpha = \frac{\pi}{4}$) it differs from Hughes' results by only 21%, which is significant but not as substantial as one might expect. That the panel method underpredicts is also consistent with the neglect of the spray jets, noting that this is a source of energy loss, and recalling that the force on the wedge, being velocity dependent, is essentially a damping force. It is unsurprising to find the worst agreement for large wedge angles.

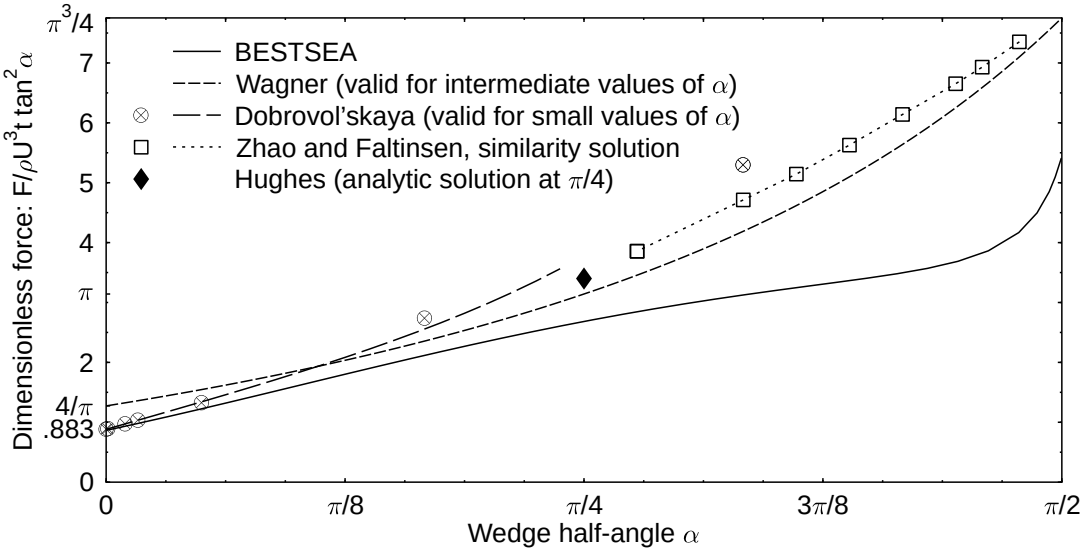

Figure 6-3: Limiting value as $\frac{gt}{U} \to 0$ of vertical force on wedge entering free surface at constant speed

In terms of the effect on the ship motion predictions of *BESTSEA* one might also question the role of three dimensionality of the *bow* entry problem (as opposed to *wedge* entry). However leaving such questions aside, if one assumes that the force for a conventional hull acts for half of an oscillation cycle (i.e. during entry only) for perhaps only the forward most 20% of the hull, this additional local 21% damping force[11] translates to only 2.1% globally averaged over a cycle. It does not therefore appear particularly significant in this context. The SWATH models on the other hand, having fine bow lines, would experience only small hull entry forces in moderate sized waves, and figure 6-3 indicates the error for smaller wedge angle to be proportionally less. This is in addition to the much reduced time the normally submerged bows spend entering the water, and the net effect is that the error is negligible. Also, hull entry forces are likely to increase pitch damping more than heave, and therefore do not explain well the differences between the computational and experimental results in figures 6-19–6-23.

As an observation possibly pertinent to the discussion of wave height effects in section 6.4.2, it was noted in preparing figure 6-3 that for larger wedge angles the predictions from the time

[11] The AMECRC models have a fine bow angle, but it rapidly opens out to 90° by about 20-25% of its length (and eventually 180° at the stern). The 90° wedge entry result is quite appropriate then since the hull entry effects can generally be assumed to be confined to at most the forward 20-25% of the hull during normal tank tests.

domain panel method was poorly behaved beyond very small values of $\frac{gt}{U}$, and required use of very small time steps to stabilise, which may account for why a satisfactory solution for the SWATH models at large wave heights was elusive near the heave resonance (see discussion of figure 6-9). Although the bow is very fine, the keel angle of SWATH #2 reaches 90° at only 12% of the length from the bow, and flattens out completely at 36%. In the tank tests at the larger wave height it is estimated that about $\frac{1}{3}$ of the hull emerged from the water at some frequencies.

Since the hull entry problem occurs on a very different time scale to the general ship motion problem it would be difficult to combine the two solutions, particularly where the geometrical self similarity assumption can not be applied (for example with most real bow forms, including in particular flared or wave piercing bows). Other difficulties would include how to incorporate the hull entry effects into the Green function convolution integrals for the present strip solutions, and when to make the transition. It may be simpler in the end to seek a single solution with a non-linear free surface boundary condition.

In respect of there being significant damping due to hull entry forces, it must be remembered that several factors contribute to the apparent wedge entry velocity, including heave and pitch velocities, and pitch angle of attack and keel angle combined with the forward speed.

6.5.4 Unspecified non-linear effects

As an order of magnitude assessment of non-linear effects one could assume them to be purely quadratic (i.e. that cubic and higher order non-linear effects are small). Figure 6-9(a) shows that for SWATH #2 at 3.0m/s the dimensionless heaves were 3.1 and 2.8 respectively for wave heights of 20 and 40mm. Since ζ is directly proportional to B_{33} at the resonant frequency, one could write say $\zeta = \zeta_q + \zeta_l$, where the subscripts $_q$ and $_l$ refer to quadratic and linear terms, proportional to the square of the heave velocity. This implies that $\left(\frac{\zeta_q}{H_w}\right)$ is a constant, and one obtains from $\left(\frac{H}{\delta_{st}}\right)_{\max} \simeq \frac{1}{2\zeta}$ that $\zeta_l + H_w\left(\frac{\zeta_q}{H_w}\right) = \frac{1}{2(H/\delta_{st})_{\max}}$. Substituting the dimensionless heave values of 3.1 and 2.8 cited above corresponding to wave heights of 20 and 40mm gives,

$$\begin{array}{rcl} \zeta_l + 0.02\left(\frac{\zeta_q}{H_w}\right) & = & \frac{1}{2\times 3.1} \\ \zeta_l + 0.04\left(\frac{\zeta_q}{H_w}\right) & = & \frac{1}{2\times 2.8} \end{array} .$$

Solving gives $\zeta_l = 0.144$ and $\zeta_q = 0.864 H_w$, which suggests that an accurate theory should predict a dimensionless heave of 3.28 at $H_w = 10$mm, an increase of 6% on the $H_w = 20$mm results.

While this is significant, it is insufficient to alone account for differences between the numerical and experimental SWATH results. The AMECRC hulls on the other hand are likely to experience stronger non-linearities due to their shallow draughts.

6.5.5 Three-dimensional wave effects

The neglect of three dimensional effects in the wave patterns (in particular the transverse wave system — the divergent waves, although present in the form of a strip-like solution, are also modified by the presence of three dimensional effects) arises through the approximation of Laplace's equation with a two-dimensional equivalent, justified on the basis that for a slender hull form the longitudinal derivative term is of higher order than the other two. This is of course not true in the far field of the hull. There are also three dimensional terms in the non-linear free surface boundary condition, but these are not the primary source of three dimensionality of the wave pattern. (This is apparent from noting that the linear form need not contain three-dimensional terms; they can be eliminated by formulating the problem in a fixed reference frame, as in the present theory, or equivalently by the use of the *pseudo-time* variable of Yeung and Kim [100], [102].)[12]

We note that the main qualitative difference between a three dimensional solution and a strip theory one (which is essentially two-dimensional) is the presence of a transverse wave pattern (as described for example by Yeung and Kim [102]). This is a neglected mechanism for energy dissipation, and hence a potential source of additional damping. Furthermore it is predominantly a far field effect, and would therefore affect heave (in which a far field observer sees essentially a point source, since motions of all parts of the hull reinforce) rather than pitch (in which a far field observer sees cancellation of effects of motions at the bow and stern).

Damping is strongly influenced by wave and free surface effects, which in turn are the primary areas of influence of three-dimensionality. An excellent example of the consequence of ignoring the three-dimensionality of Laplace's equation is the low damping at low speed due to the zero damping frequency of two-dimensional SWATH sections described in section 6.3.1. These results also support the hypothesis that three-dimensionality becomes less important at high speeds.

The magnitude of free surface effects is strongly dependent on the proximity of the disturbance caused by the hull to the free surface. Therefore this explanation is consistent with the fact that the deepest hull, SWATH #1, shows the best results (at high speeds), followed by SWATH #2 and then the conventional hulls.

Finally, although the explanation seems to explain observations qualitatively, it is impossible to quantify the effects, and hence validate the explanation, without actually undertaking a fully three-dimensional solution.

[12] At this point it is worth noting the relevant equivalences between the theories of Faltinsen and Zhao [26], Yeung and Kim [100], and the present theory. All use a fully three dimensional free surface boundary condition, but Faltinsen and Zhao use a non-linear form while the other two use a linear form. All use a two-dimensional form of Laplace's equation (although the later comprehensive theory of Yeung and Kim [102] uses a three-dimensional form for the far field part of its solution). Faltinsen and Zhao and the present theory both include steady terms in the body boundary condition in unsteady problems, while Yeung and Kim do not. Hence only the comprehensive theory of Yeung and Kim can claim to have three-dimensional wave effects, while only Faltinsen and Zhao and the present theory can claim to have steady-unsteady interaction. None of the theories have both.

6.5.6 Side wall and bottom effects

As shown numerically by Kashiwagi and Ohkusu [52], towing tank side walls can have a significant effect on the hydrodynamic forces acting on a translating oscillating body under certain conditions. Hearn [45] also alerts to the possibility of such an effect, in particular at low frequency (and presumably also low speed). However Kashiwagi and Ohkusu's results tend to indicate that for values of $\tau = \frac{U\omega_e}{g} \gg \frac{1}{4}$ the side wall effects are not significant. This is to be expected on consideration of the wave pattern in unrestricted waters for the case $\tau \gg \frac{1}{4}$, in which waves are confined to a narrow wedge behind the oscillating body, as opposed to the $\tau < \frac{1}{4}$ case where a ship confined by side walls could experience interactions with reflections of the part of the wave system ahead of the hull. As the values of τ in the vicinity of the heave resonance for SWATH #2 are within the range 1.5–3.0 (depending mainly on Froude number), and since none of the typical interference behaviour observed by Kashiwagi and Ohkusu is present in the experimental results presented in this chapter, it is reasonable to conclude that side wall effects are not the primary source of difference between numerical and experimental results.

Bottom effects were discussed briefly in the previous chapter (section 5.4.1). The issue is that they are inevitably present in the experimental results but have been ignored in the numerical calculations (all three of HYDROS [22], *STF* and *BESTSEA*). While they no doubt have an effect it seems unlikely that this effect would be of a magnitude sufficient to account for the observed differences between numerical and experimental results. Furthermore the effects would become more predominant as the frequency gets lower, and therefore would not explain why the results for SWATH #1, which has a lower natural frequency, are significantly better than those for SWATH #2, or similarly why pitch results are generally better than heave.

6.5.7 Summary

The most likely explanations of the difference between the *BESTSEA* results and experimental results seem to be circulation effects and flow three dimensionality, the former becoming more important as speed increases, and the latter becoming less important. However the fact that *BESTSEA* gave better predictions at higher speeds tends to give support to the argument that three-dimensional effects are more important. (Perhaps if the speeds were further increased the situation would reverse.) It was also argued that three-dimensionality was seen to qualitatively account for lack of sufficient heave damping (through the absence of a transverse wave system) while still accounting for the good pitch results. On the other hand the dependence of ζ due to circulation effects on beam (as opposed to just $B_{33,o}$) favourably explained the differences required from one hull to another.

Both of these effects could be incorporated into a strip theory. Cole [17] presents a method for calculating circulation for a flat ship in steady motion in which the problem is solved in cross-sectional strips and integrated from the bow to the stern. It may be possible to intro-

duce a comparable technique for unsteady motion into a program such as BESTSEA. Three dimensionality has been introduced using asymptotic matching in the theory of Yeung and Kim [102].

The two viscous related effects discussed were negligible on the one hand (skin friction), and possibly important but questionable on the other (form drag). However they both suffer however from two major problems: that viscous effects increase with speed, contrary to the observed improvement in predictions, and that these effects would increase both heave and pitch damping, therefore would not explain the currently excellent pitch predictions. Also, they do not adequately account for the variety of required additional damping from one model to another.

Bow entry effects proved to be an unsatisfactory explanation, as they were argued to be insignificant, and to affect mainly pitch.

Further, as described in section 6.4.1, some of the test data (especially AMECRC #04, which has a shallow draught relative to the test wave height) might be subject to strong non-linearities at the resonant peaks that were not modelled by the present version of BESTSEA. Required is a review of model tests with regard to wave amplitude effects at resonant peaks, particularly for the AMECRC models, and improvement of the facility in BESTSEA to properly handle flat bottomed hull sections entering the water.

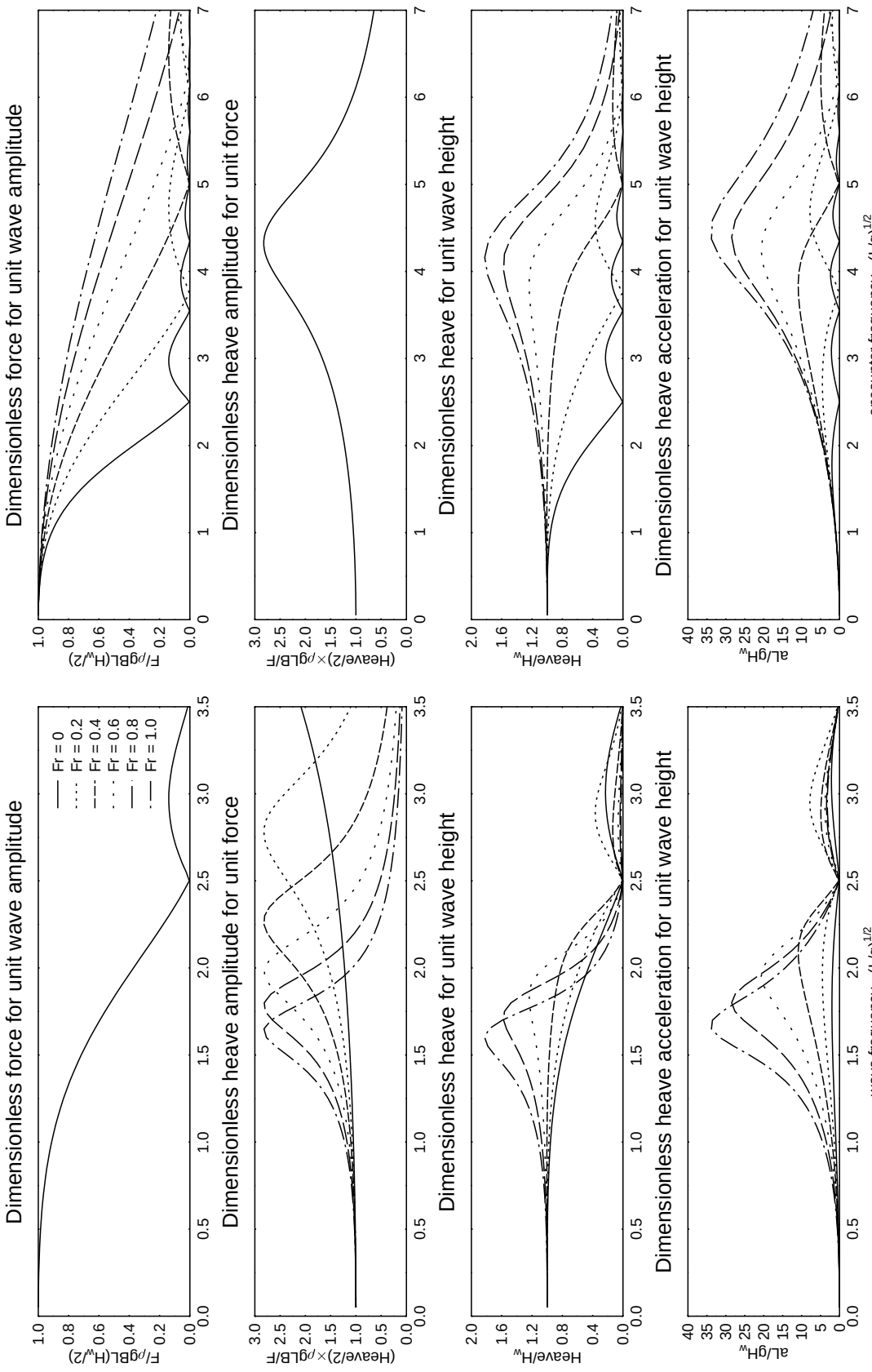

Figure 6-4: Effect of variation of speed on motion response for conventional boat based on simplified model ($\frac{T}{L} = 0.05$, $\zeta = 0.18$)

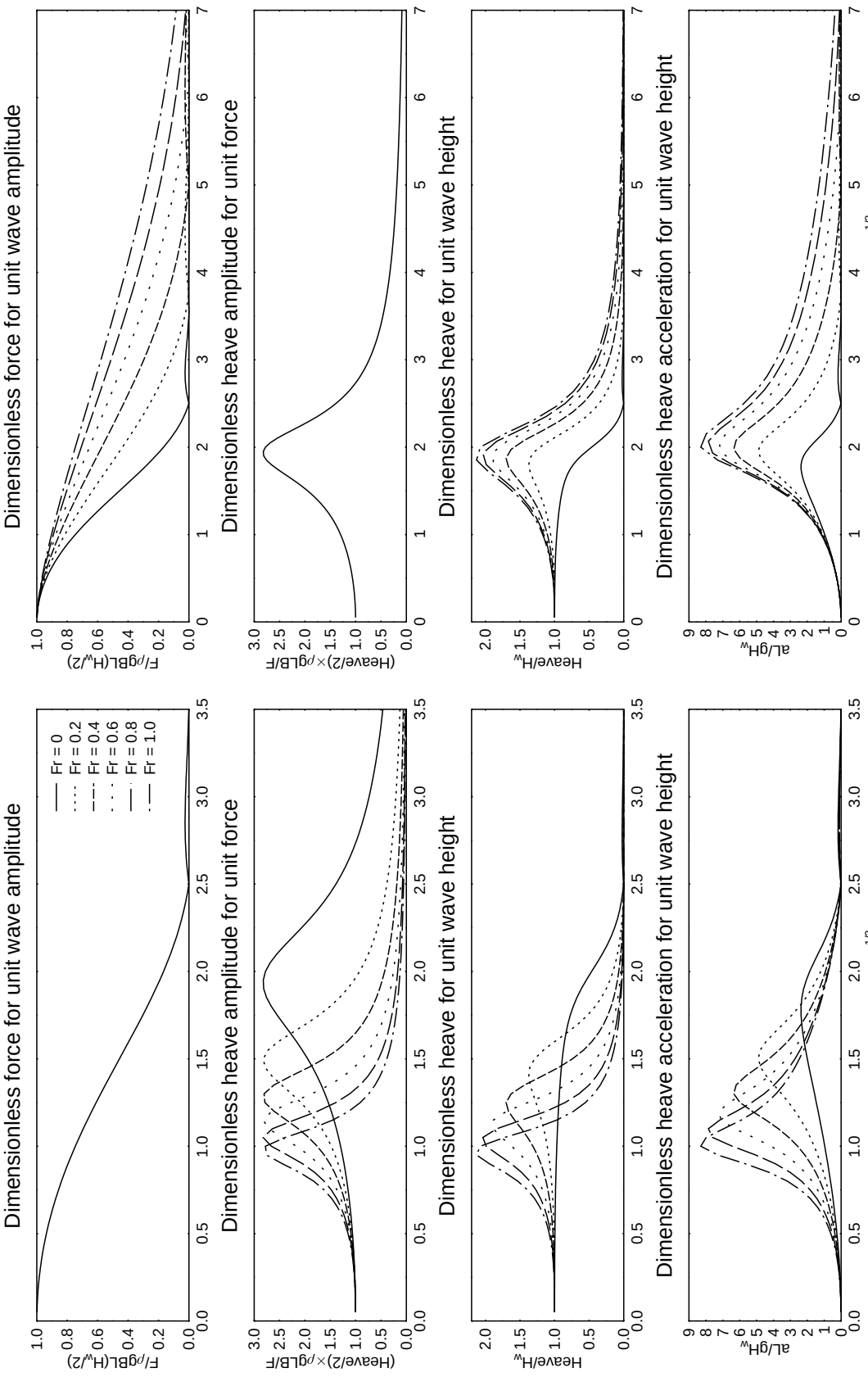

Figure 6-5: Effect of variation of speed on motion response for SWATH based on simplified model ($\frac{T}{L} = 0.25$, $\zeta = 0.18$)

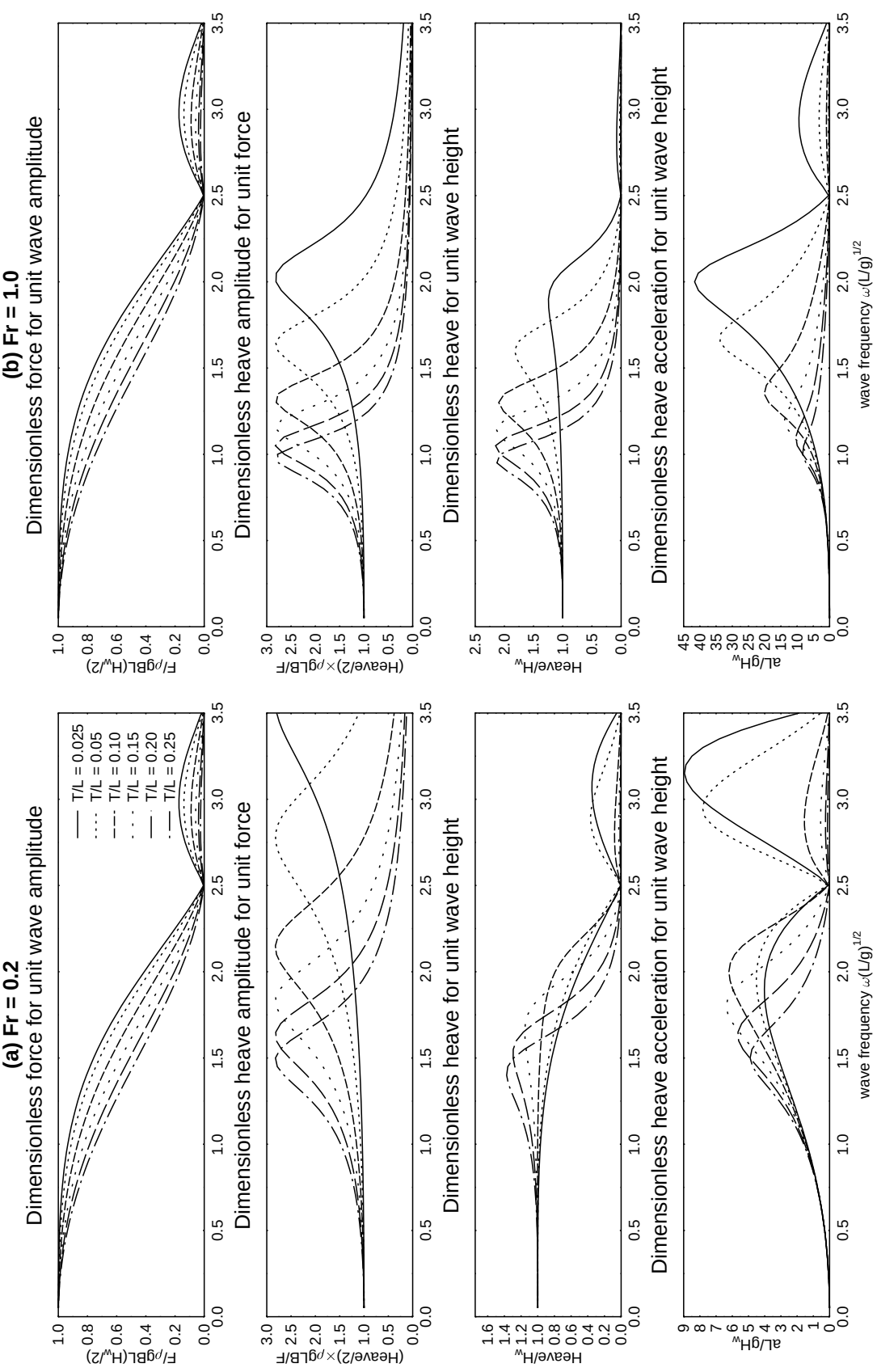

Figure 6-6: Effect of variation of SWATHness on motion response at low and high Froude numbers based on simplified model ($\zeta = 0.18$)

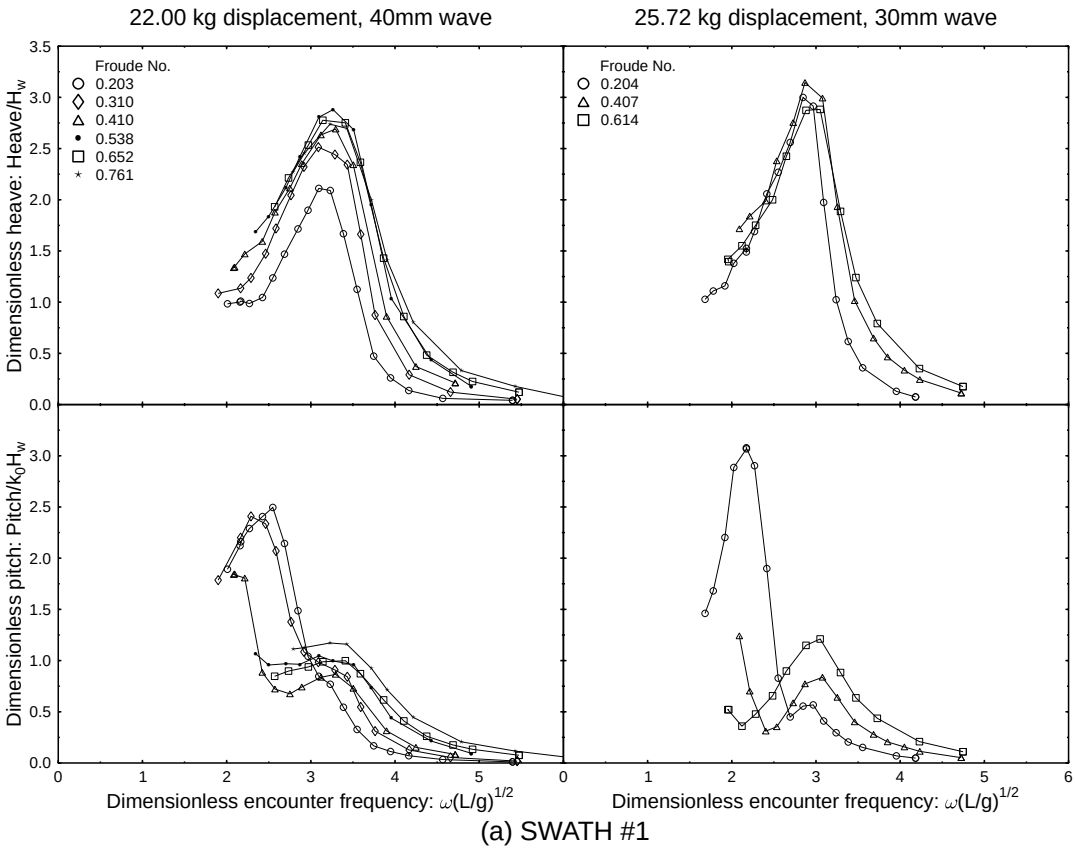

(a) SWATH #1

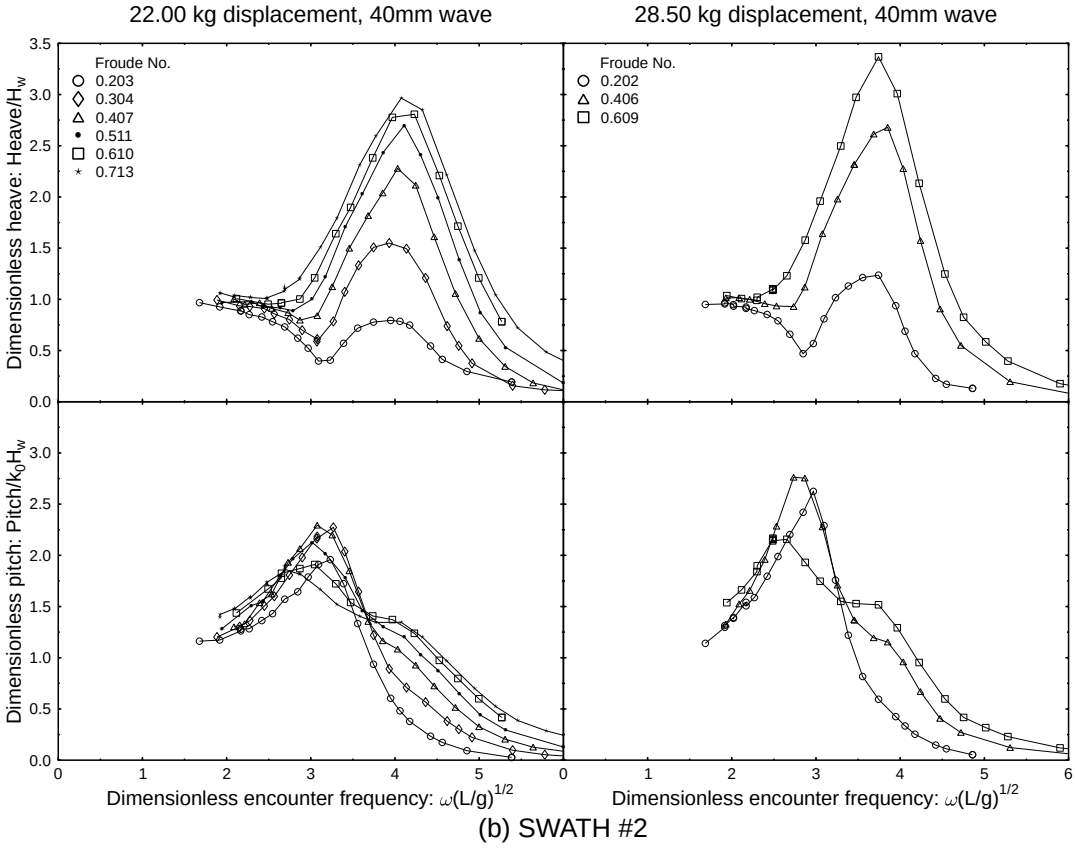

(b) SWATH #2

Figure 6-7: Towing tank seakeeping results for semi-SWATH models in regular head seas as a function of encounter frequency.

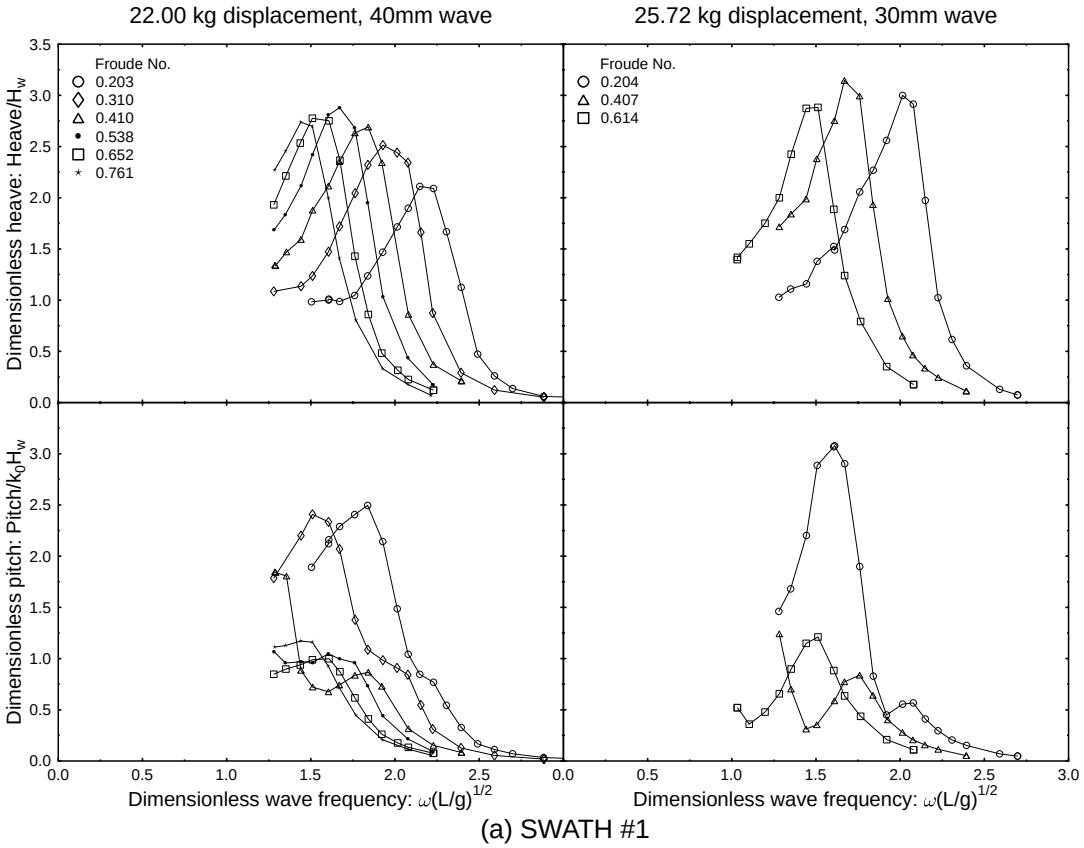

(a) SWATH #1

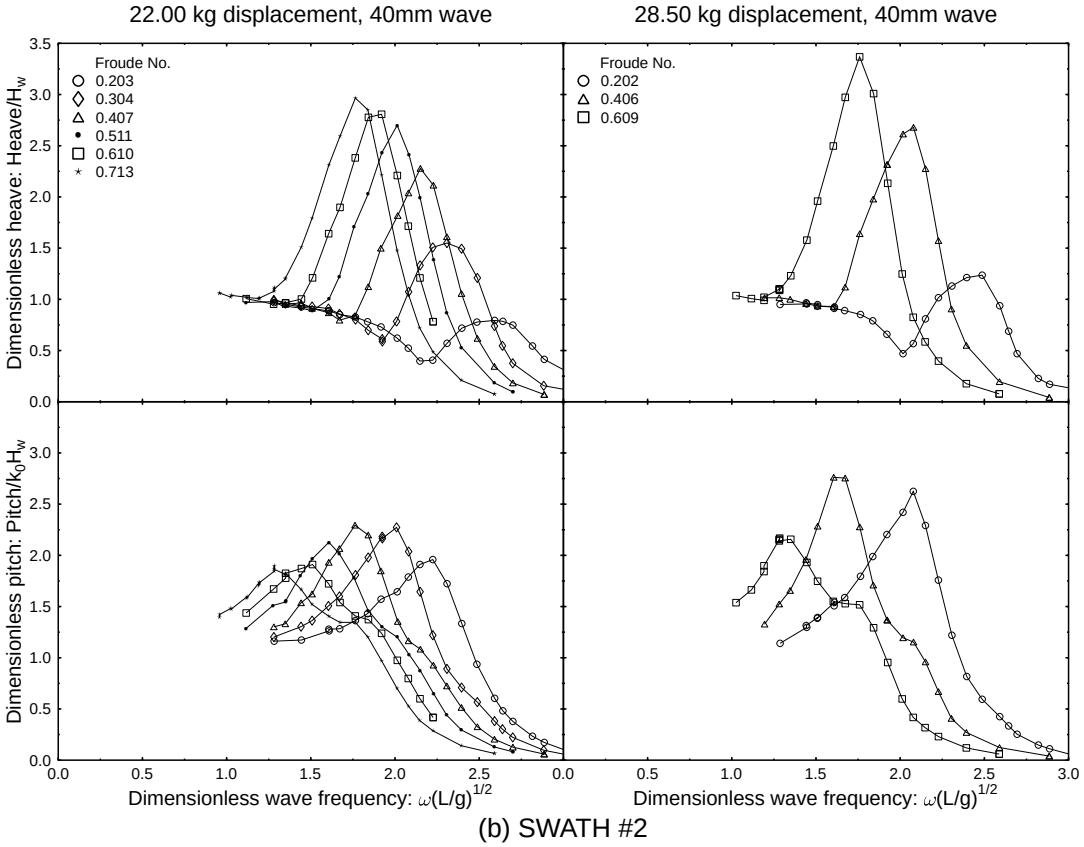

(b) SWATH #2

Figure 6-8: Towing tank seakeeping results for semi-SWATH models in regular head seas as a function of wave frequency.

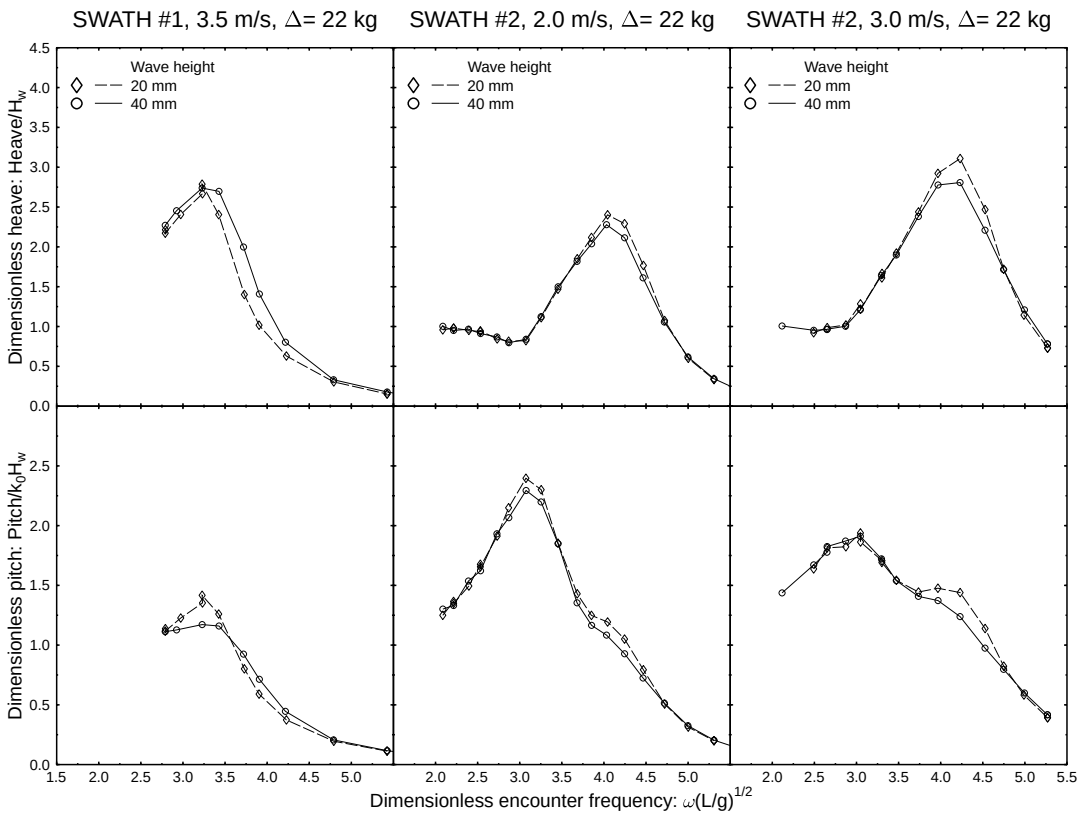

(a) Tank tests

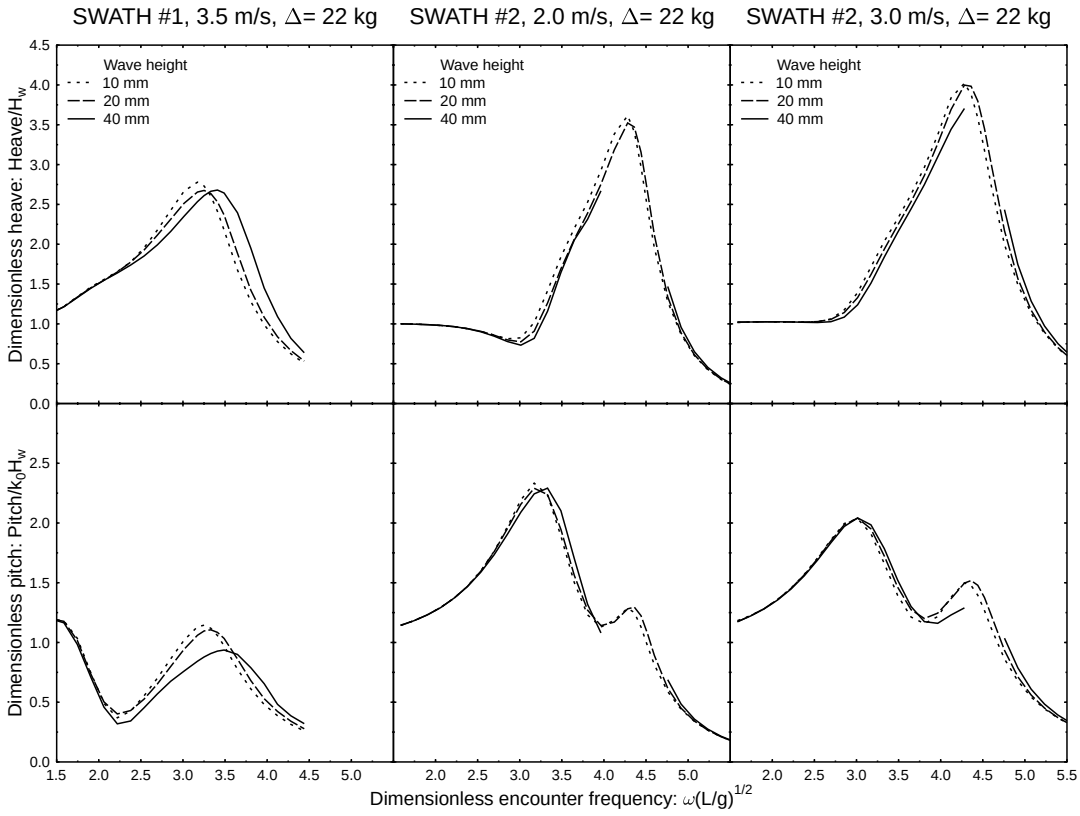

(b) BESTSEA

Figure 6-9: Effect of wave height on semi-SWATH model response for selected conditions: experimental and computed results

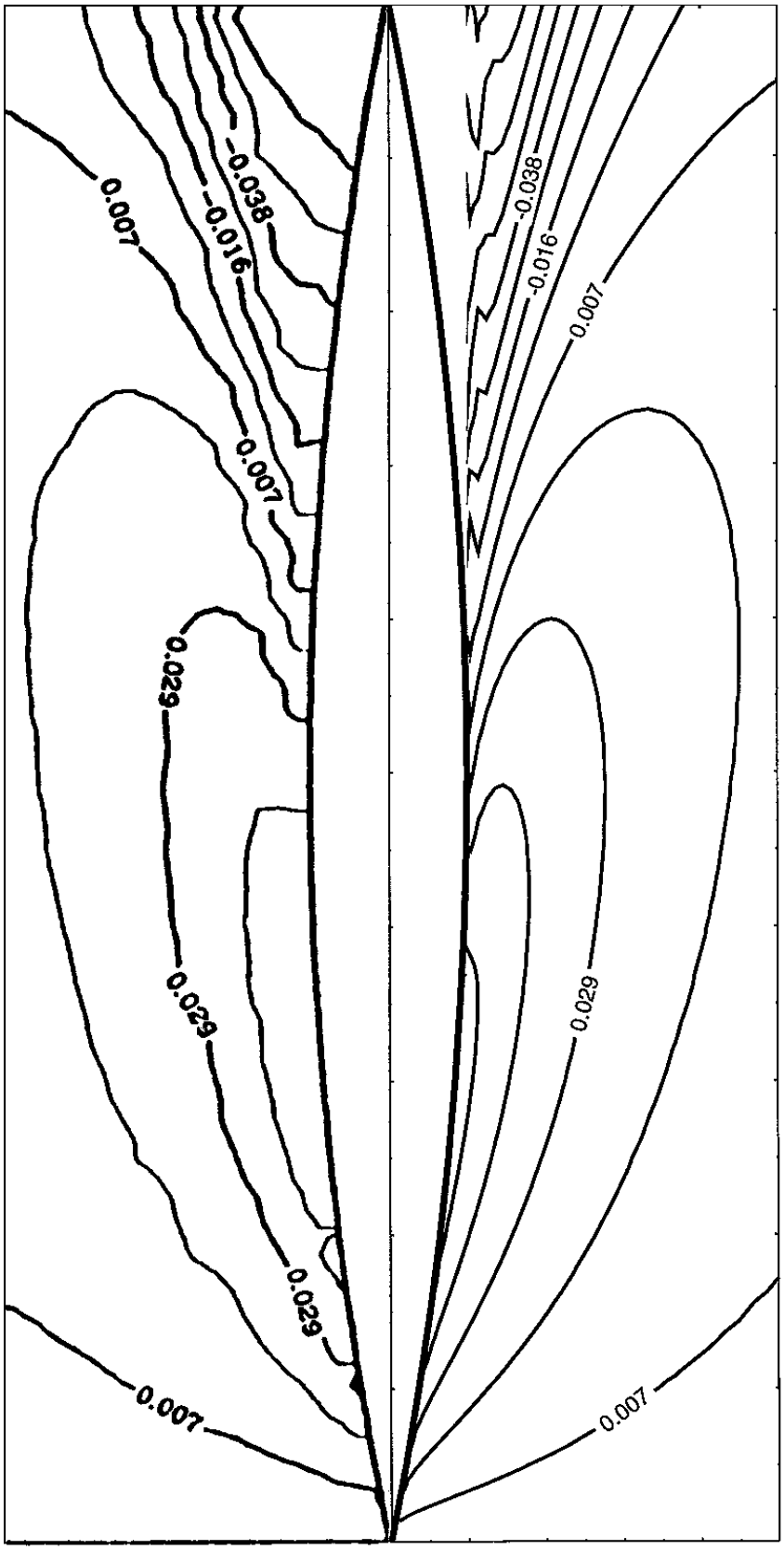

Figure 6-10: Wave elevation around parabolic strut with vertical sides ($Fr = 1.0$, $\frac{B}{L} = 0.1$, $\frac{T}{L} = 0.25$), normalised by strut length. Left: equivalent theory of Faltinsen and Zhao [29]. Right: modified *BESTSEA*.

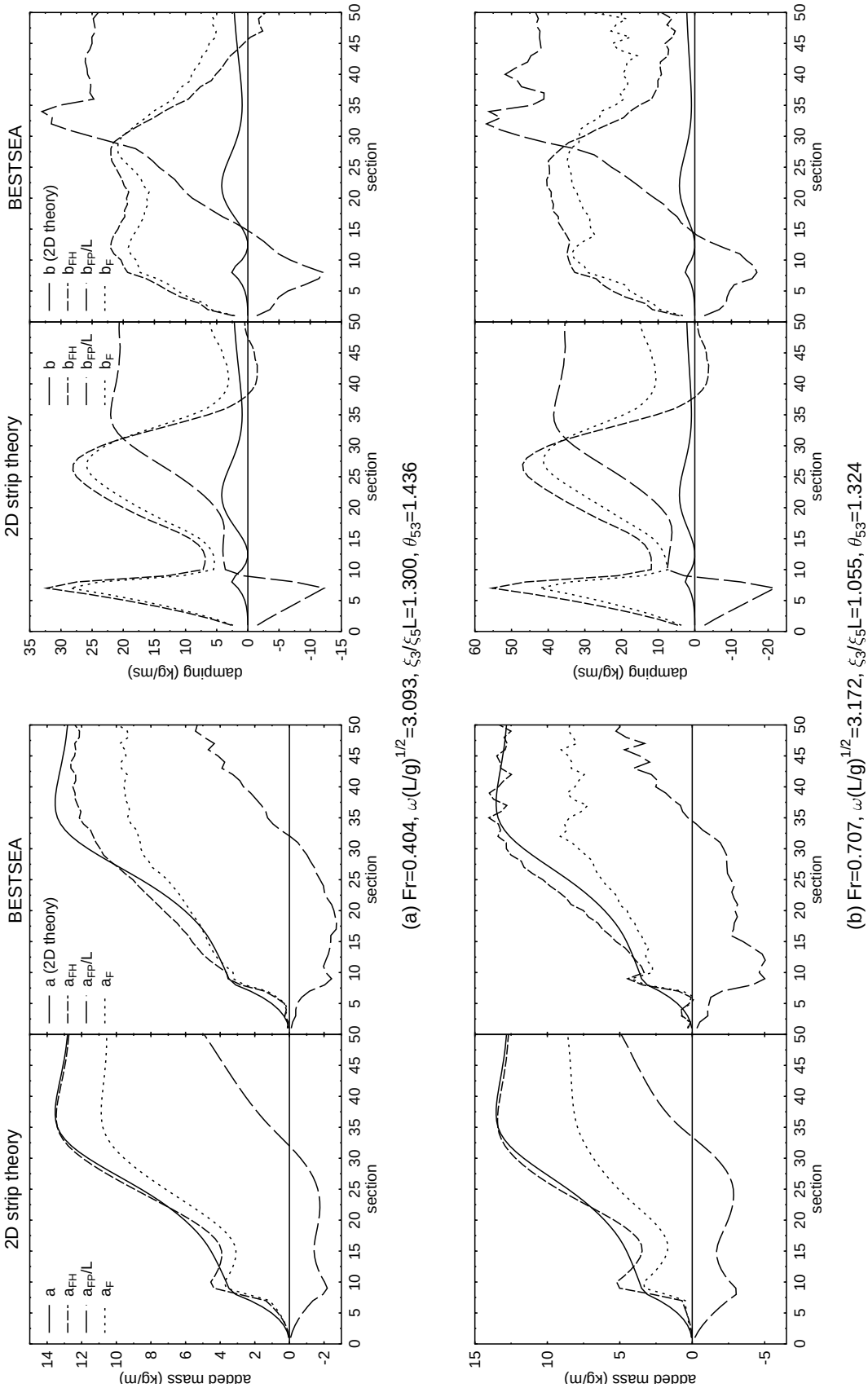

Figure 6-11: Sectional added mass and damping distribution at forward speed: comparison of conventional strip theory and *BESTSEA*

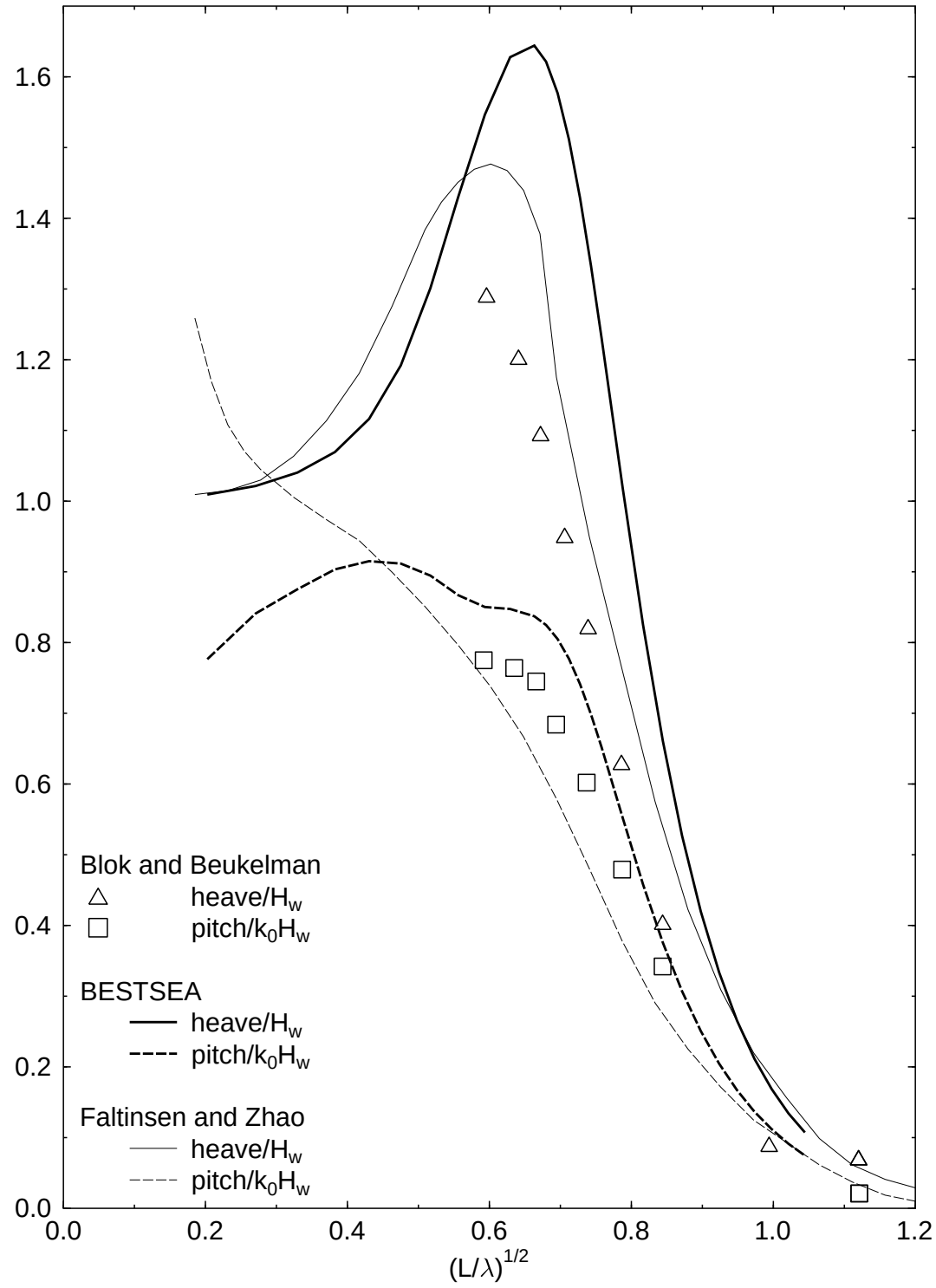

Figure 6-12: Comparison of *BESTSEA* motion predictions for MARIN HSDSSS parent hull at $Fr = 1.14$ with similar theory of Faltinsen and Zhao [29] and experiments of Blok and Beukelman [9]

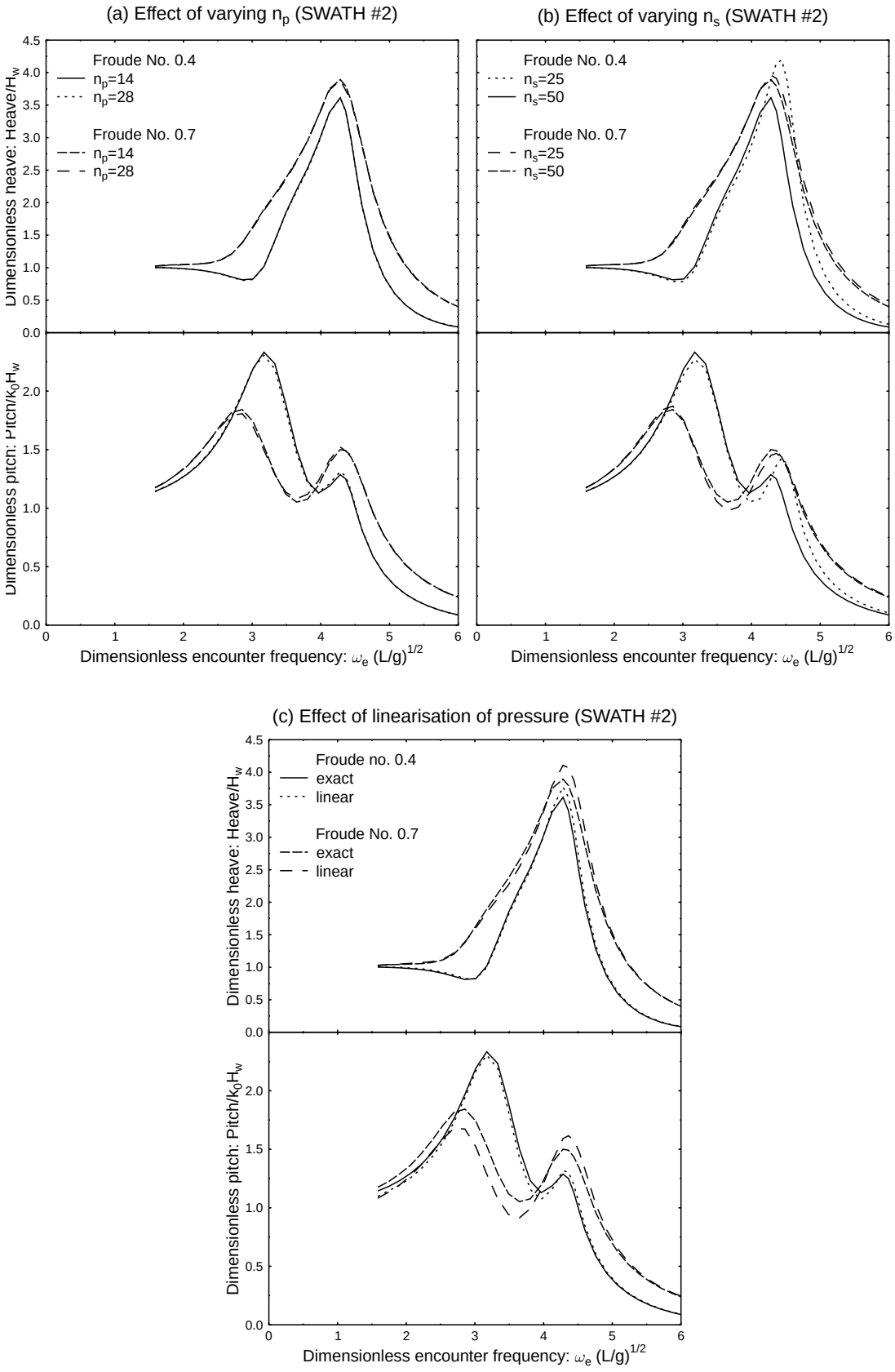

Figure 6-13: BESTSEA validation runs: effect of number of panels and sections, and of method of calculating force

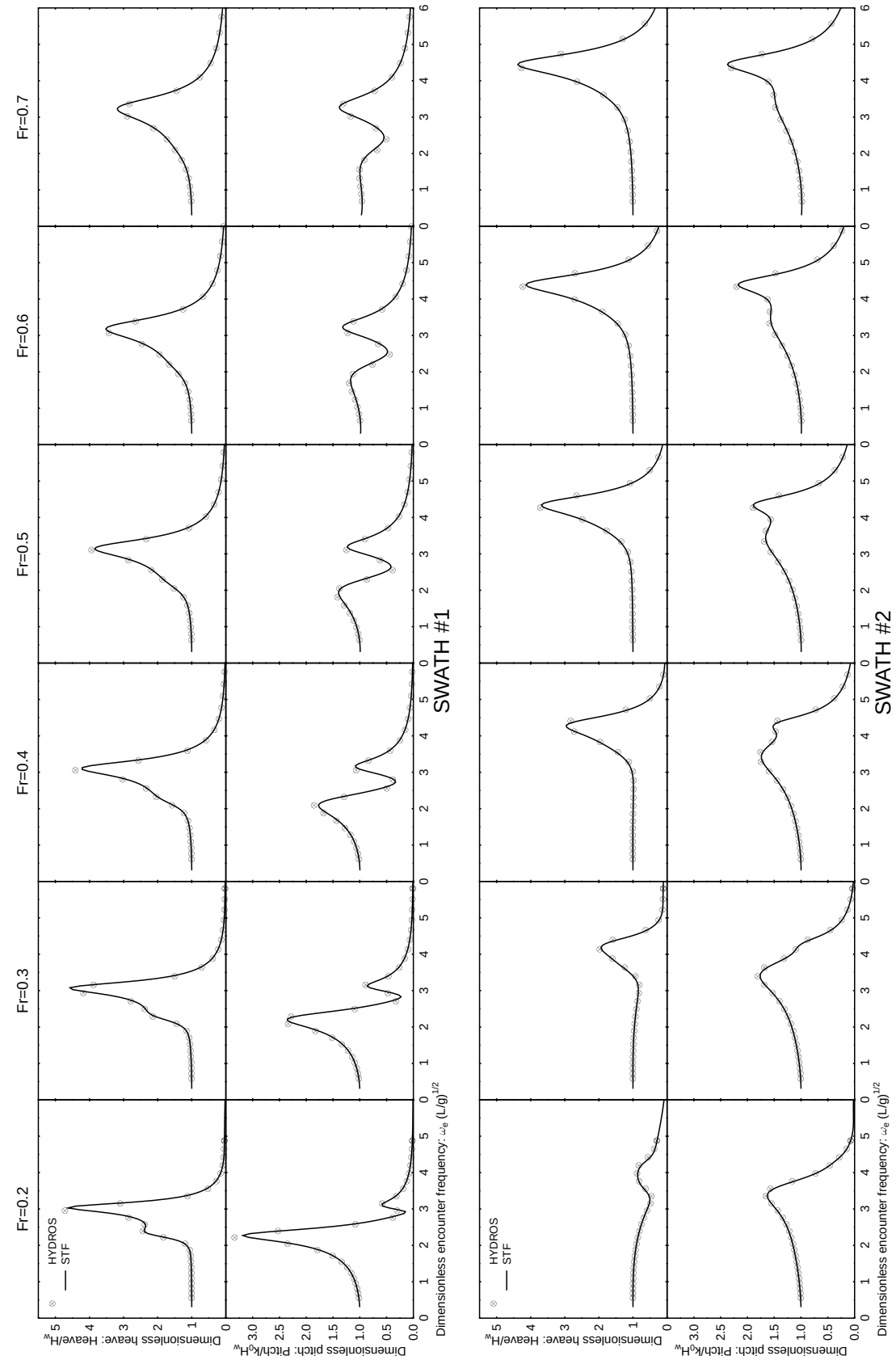

Figure 6-14: Comparison of motion predictions for SWATH models using *HYDROS* [22] and *STF*

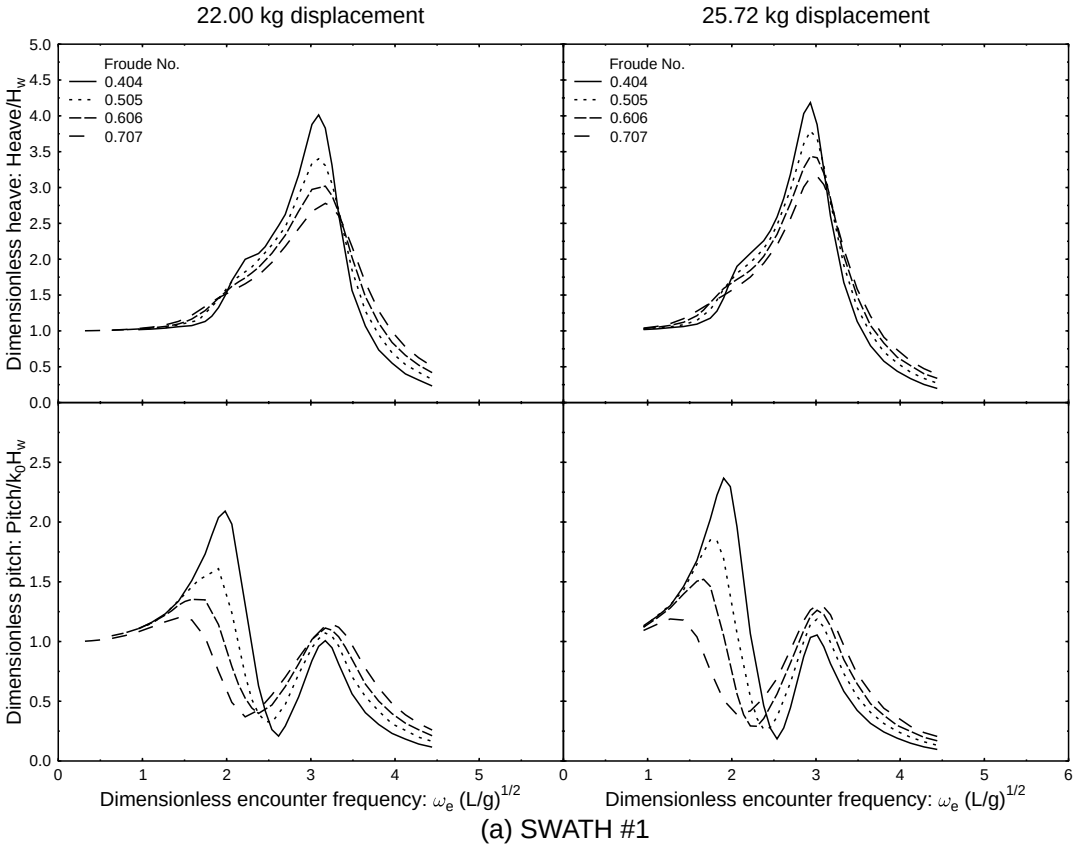

(a) SWATH #1

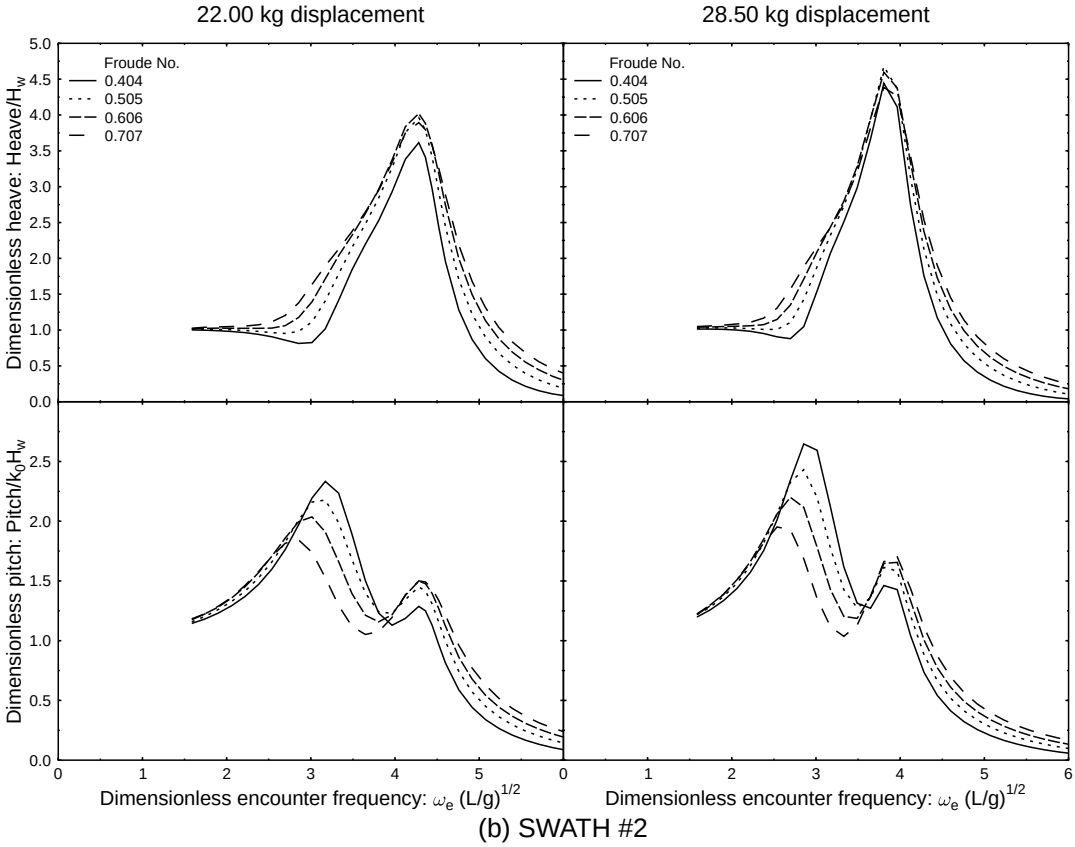

(b) SWATH #2

Figure 6-15: Response of semi-SWATH models in head seas calculated using BESTSEA, plotted as a function of encounter frequency

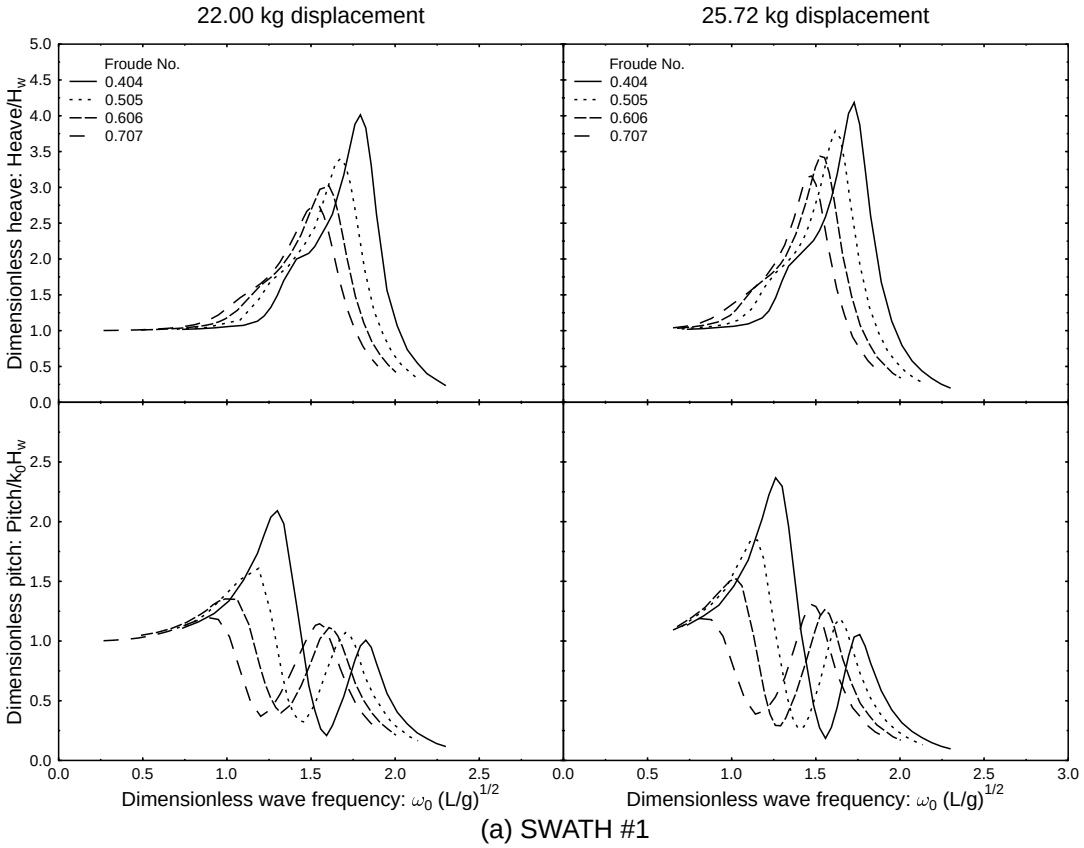

(a) SWATH #1

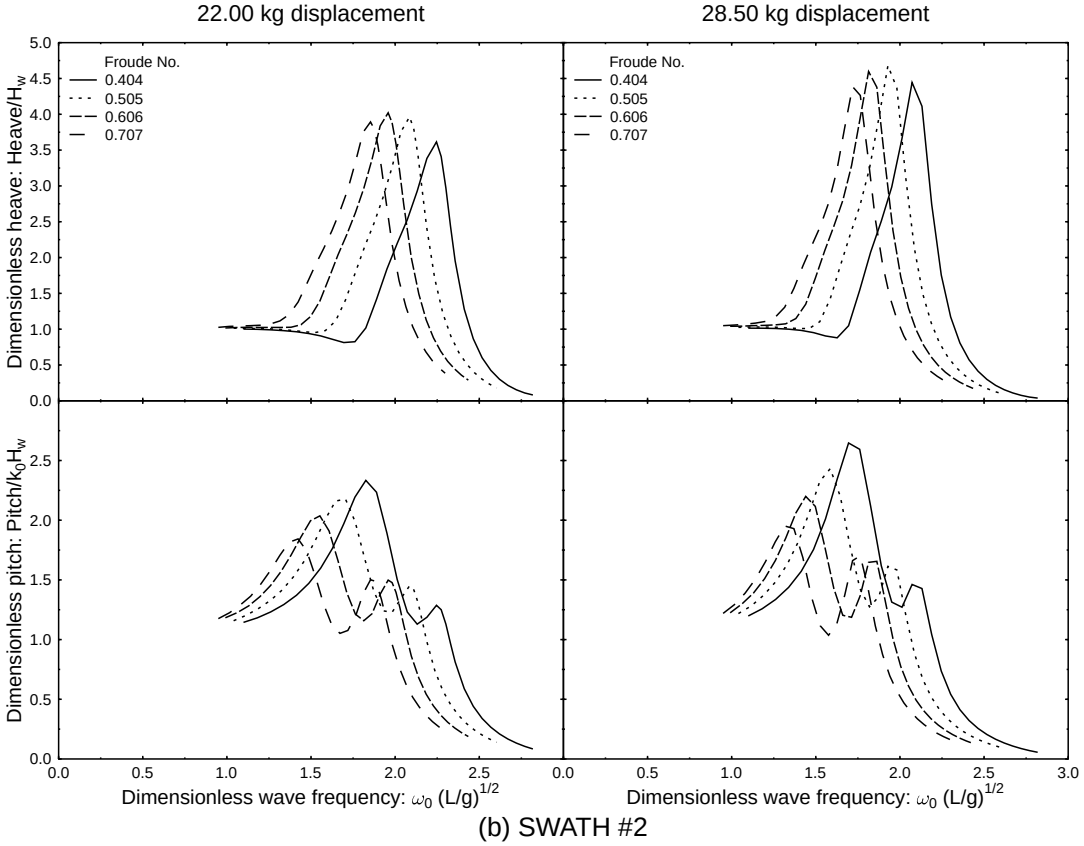

(b) SWATH #2

Figure 6-16: Response of semi-SWATH models in head seas calculated using BESTSEA, plotted as a function of wave frequency

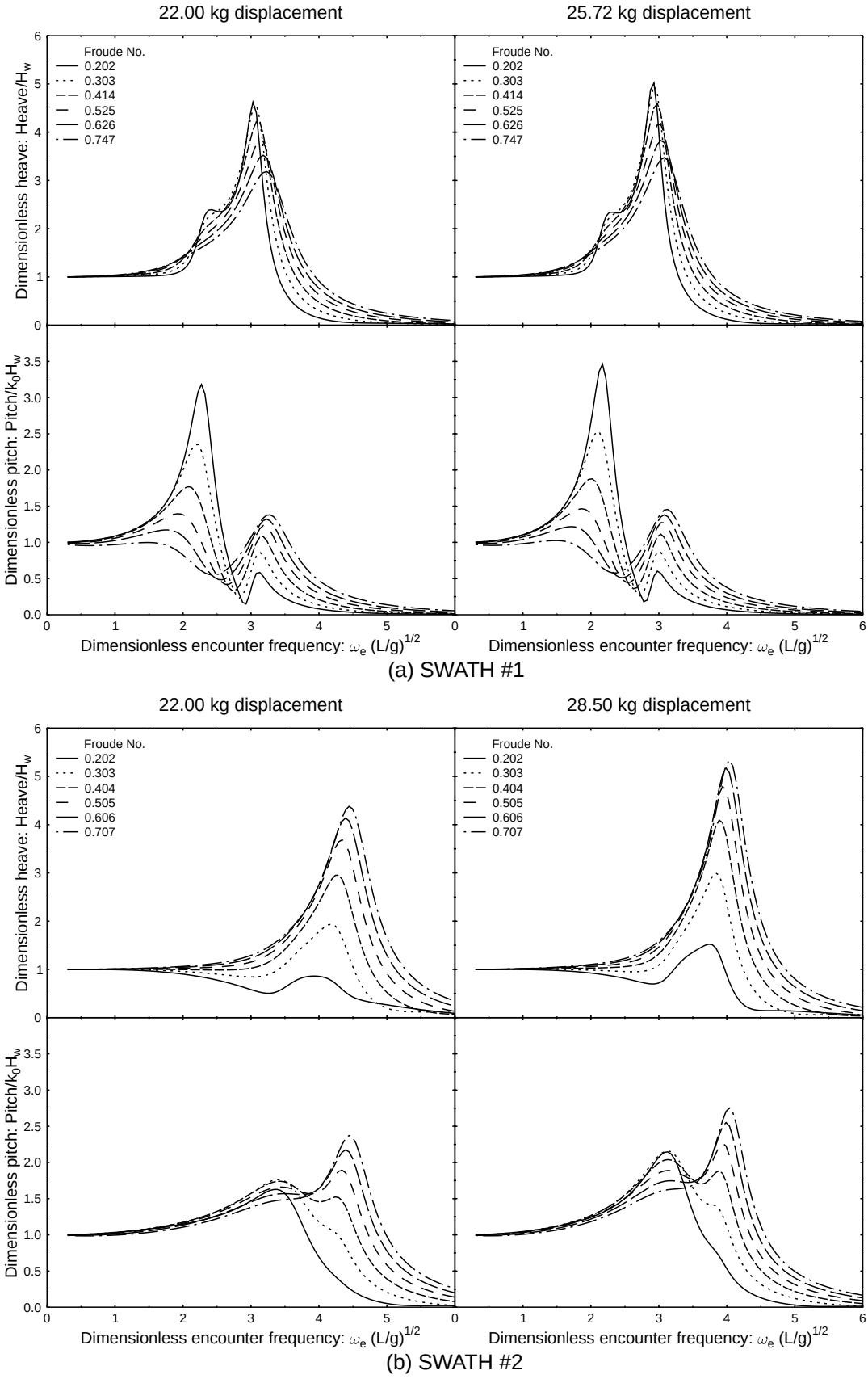

Figure 6-17: Response of semi-SWATH models in head seas calculated using STF, plotted as a function of encounter frequency.

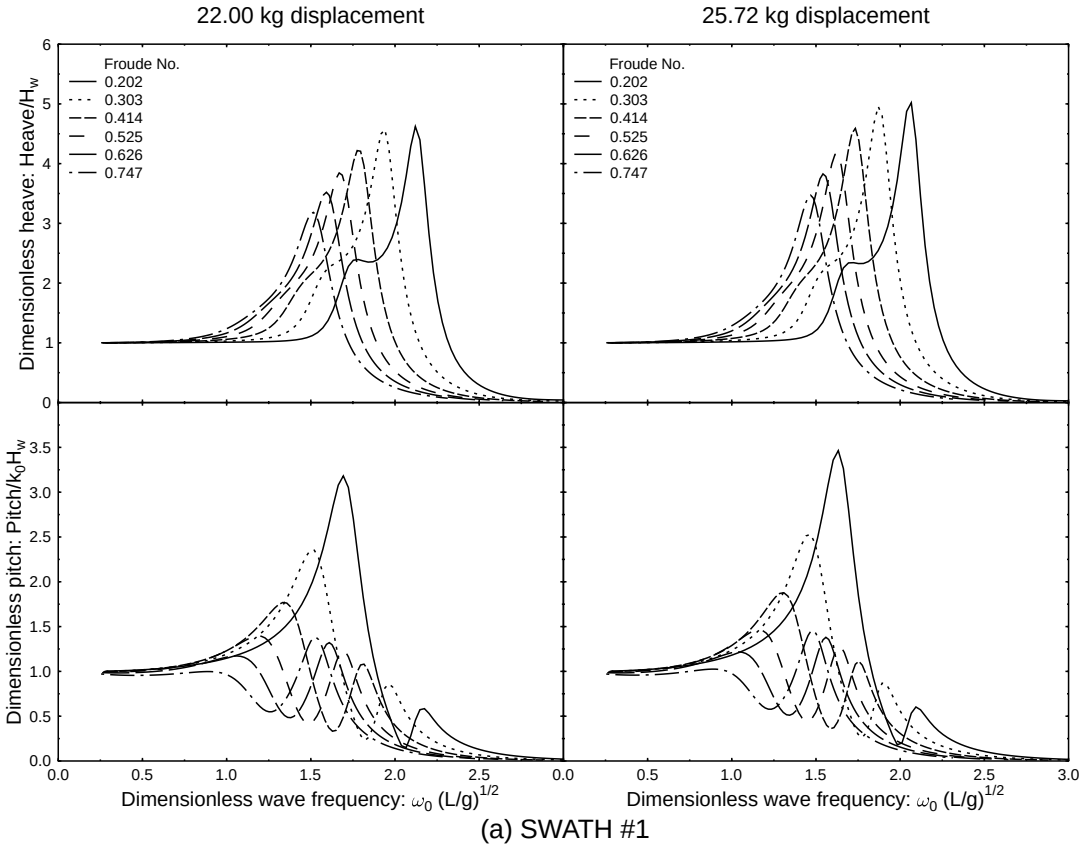

(a) SWATH #1

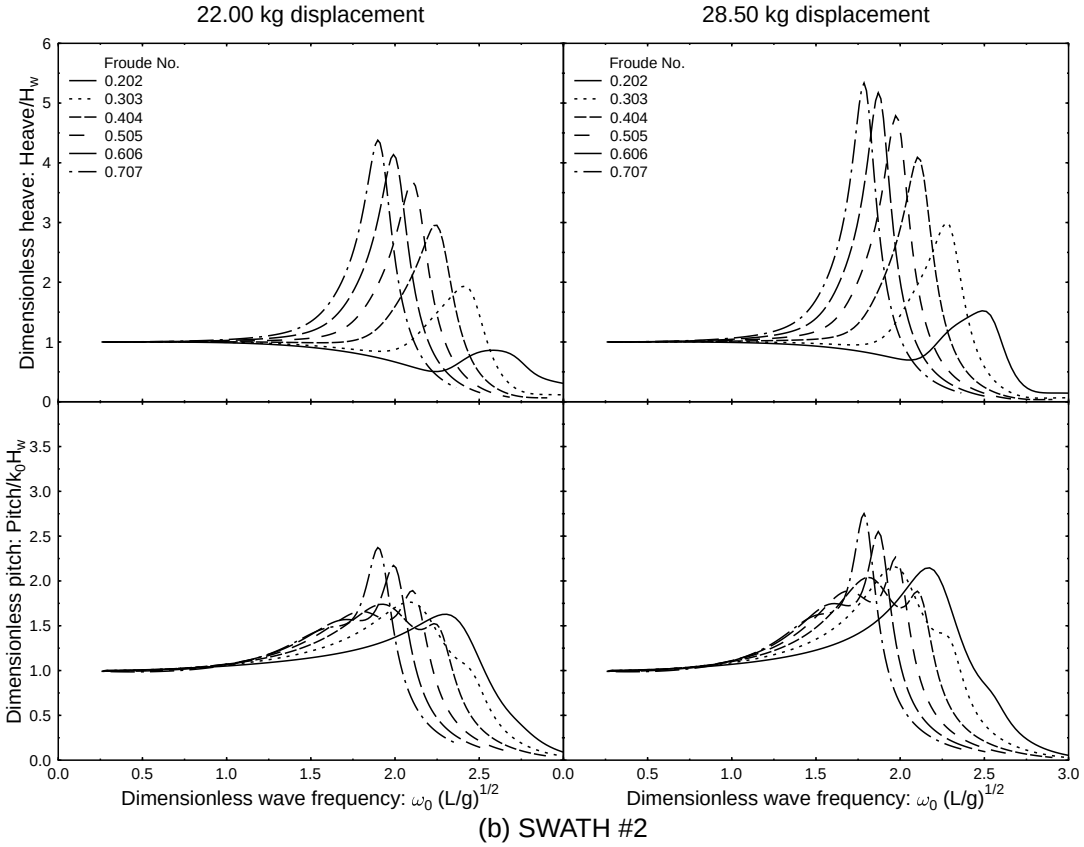

(b) SWATH #2

Figure 6-18: Response of semi-SWATH models in head seas calculated using STF, plotted as a function of wave frequency.

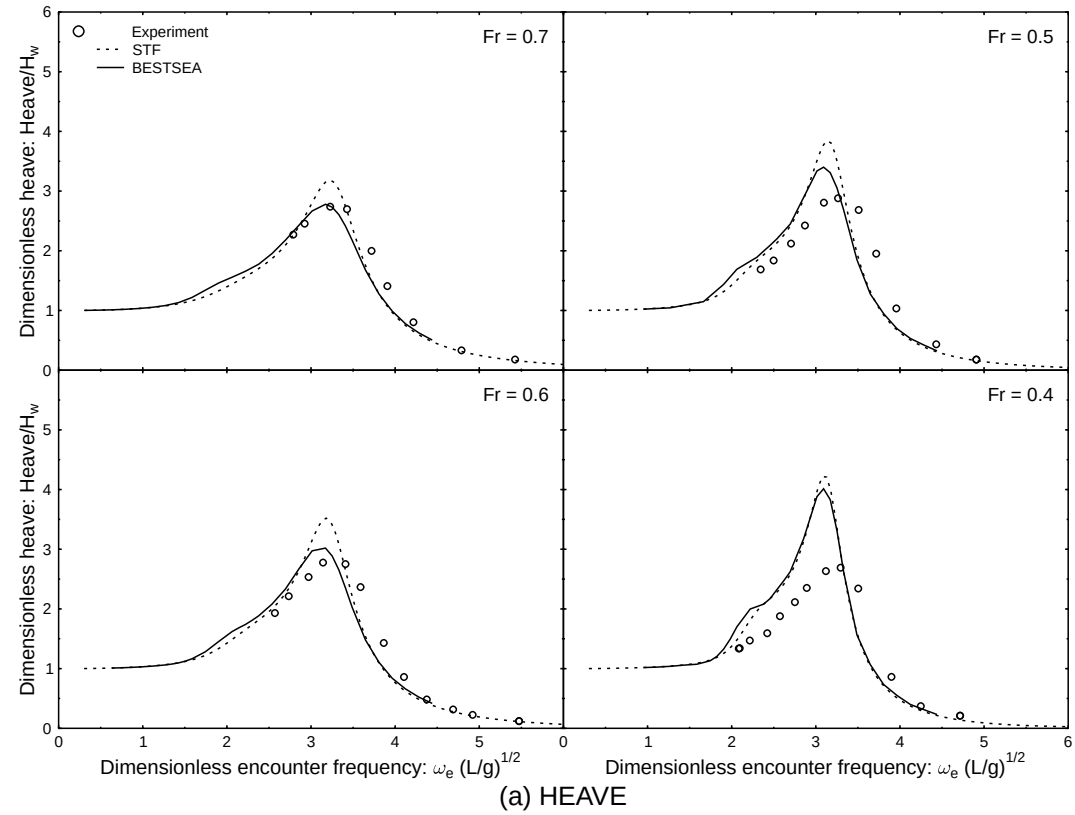

(a) HEAVE

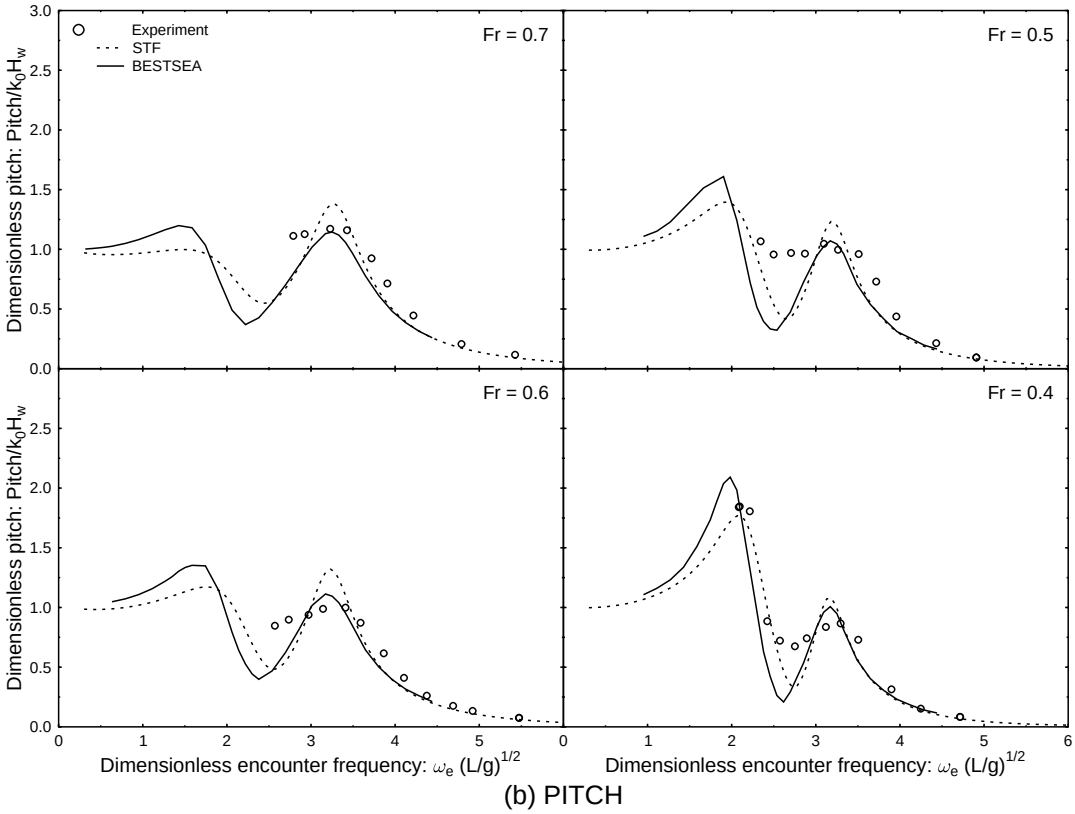

(b) PITCH

Figure 6-19: SWATH #1, $\Delta = 22.0$kg: comparison between towing tank, BESTSEA and STF

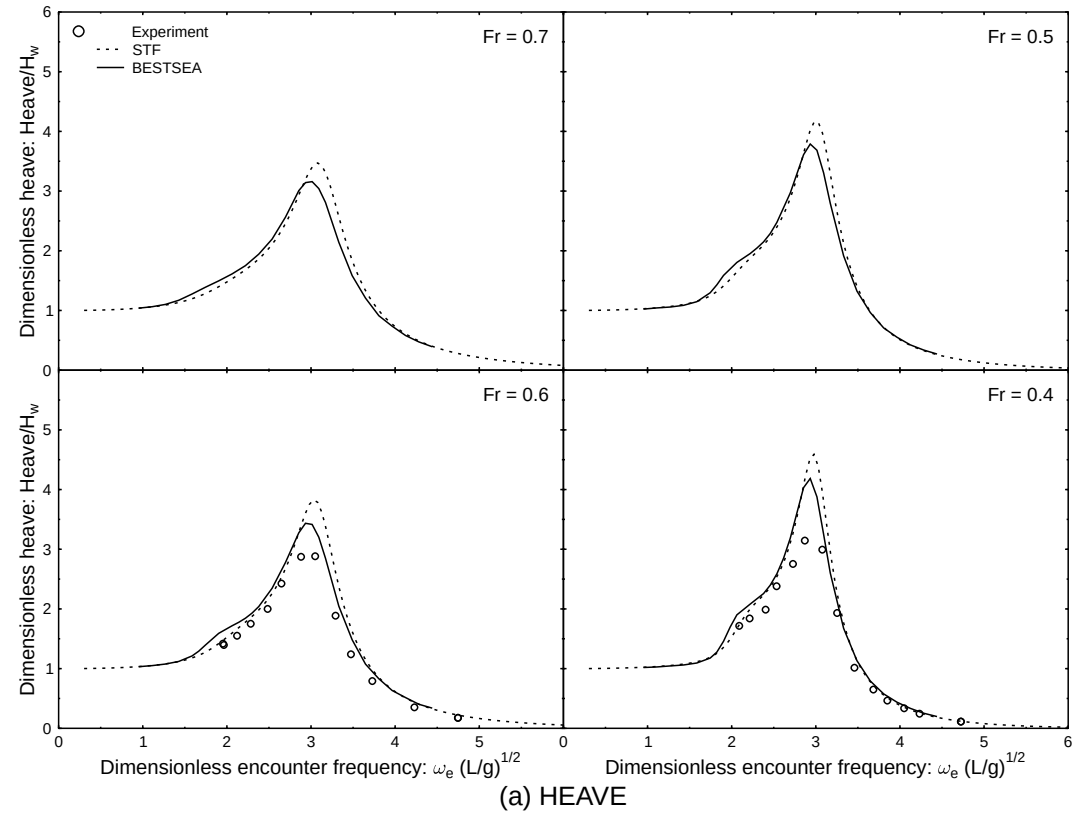

Figure 6-20: SWATH #1, $\Delta = 25.72$kg: comparison between towing tank, BESTSEA and STF

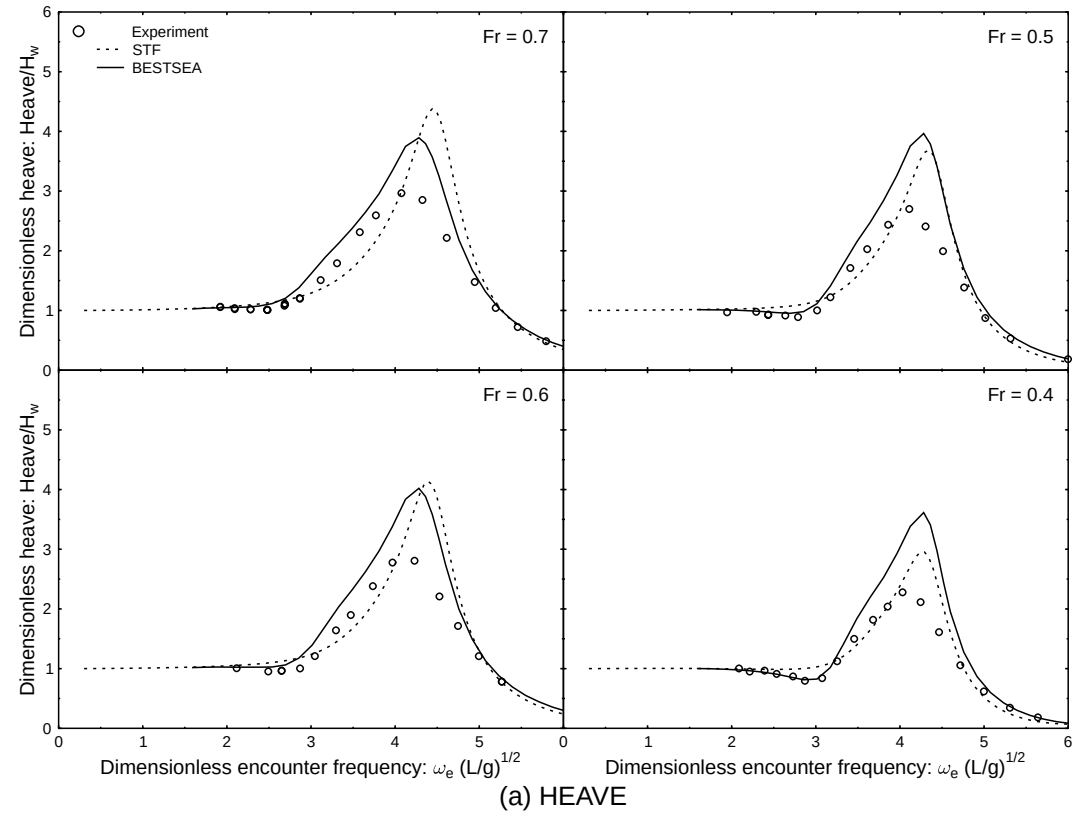

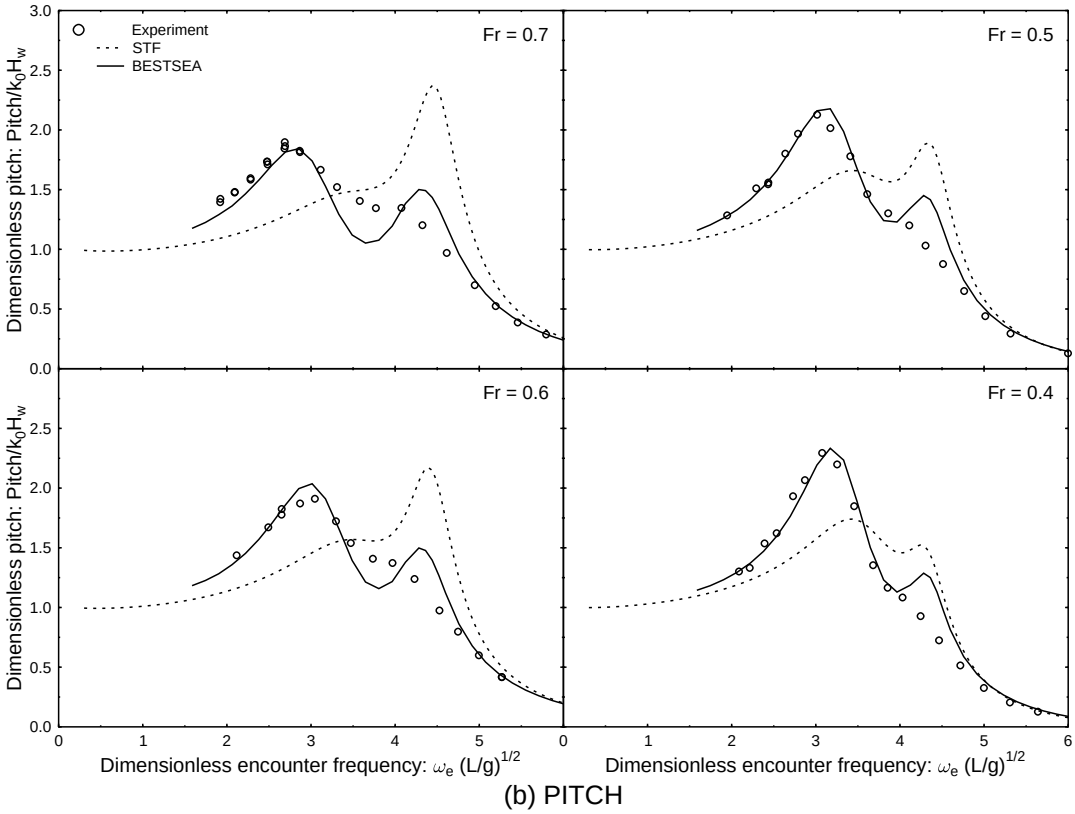

Figure 6-21: SWATH #2, $\Delta = 22.0$kg: comparison between towing tank, BESTSEA and STF

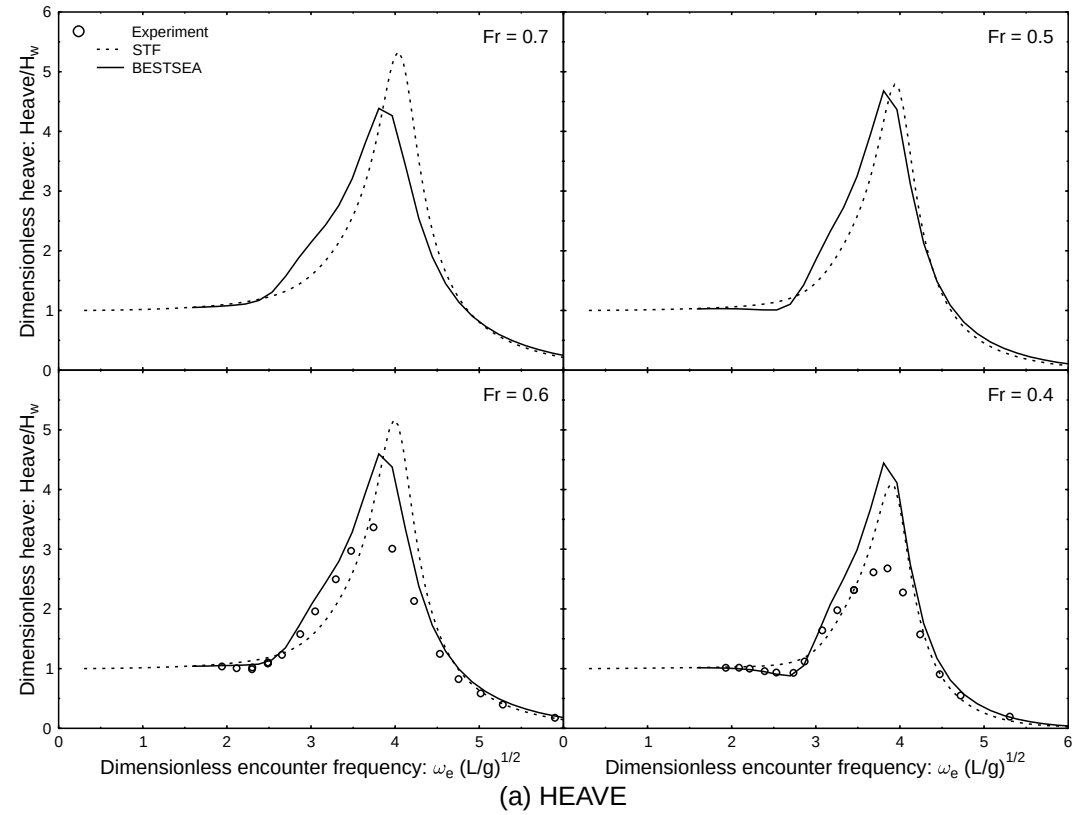

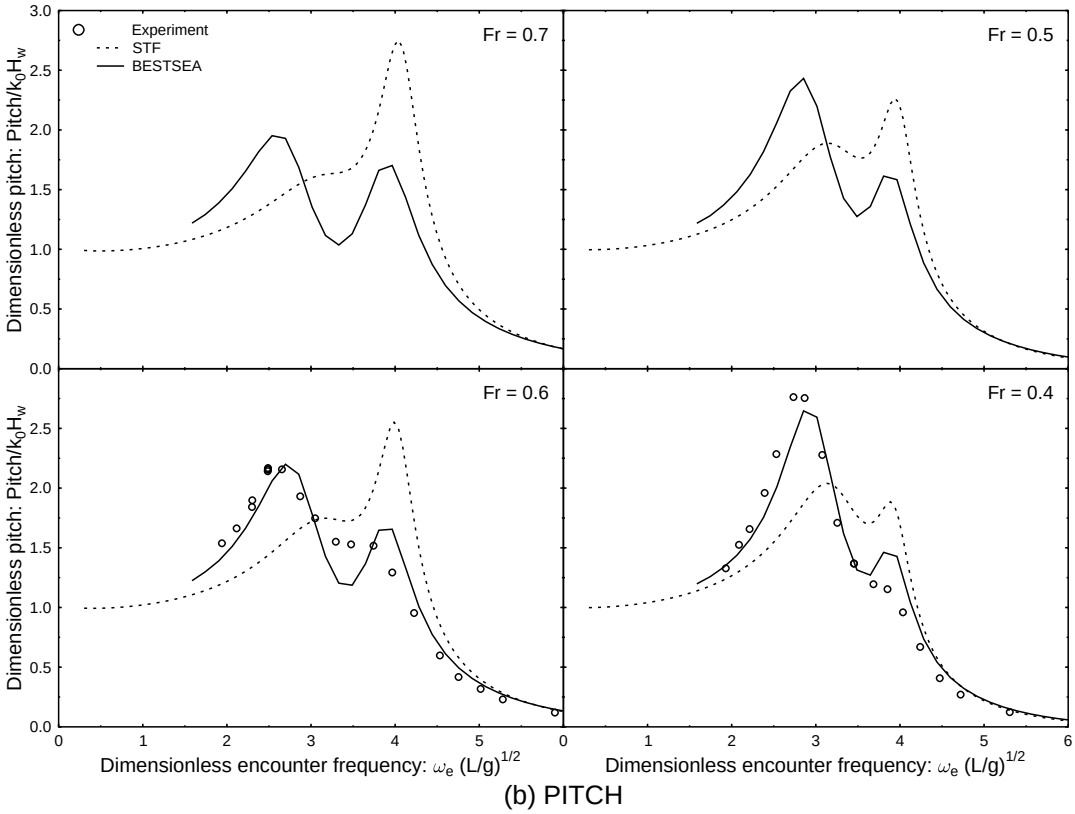

Figure 6-22: SWATH #2, $\Delta = 28.50$kg: comparison between towing tank, BESTSEA and STF

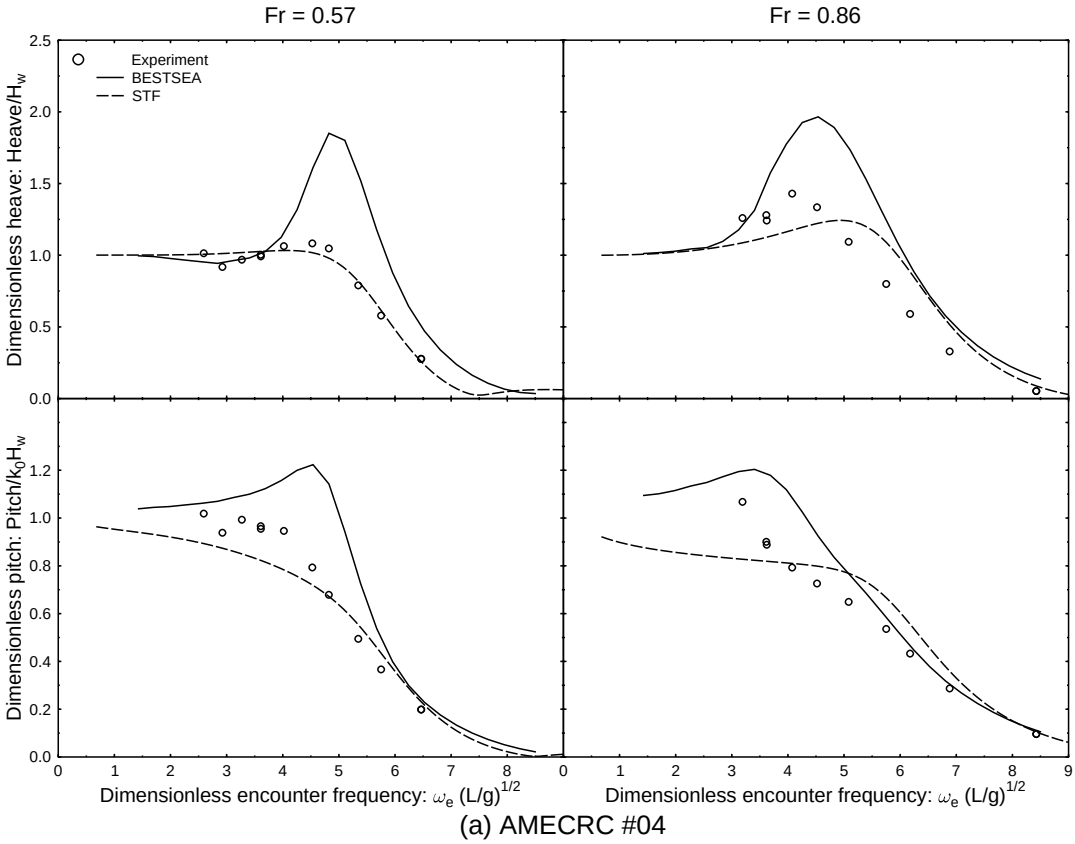

(a) AMECRC #04

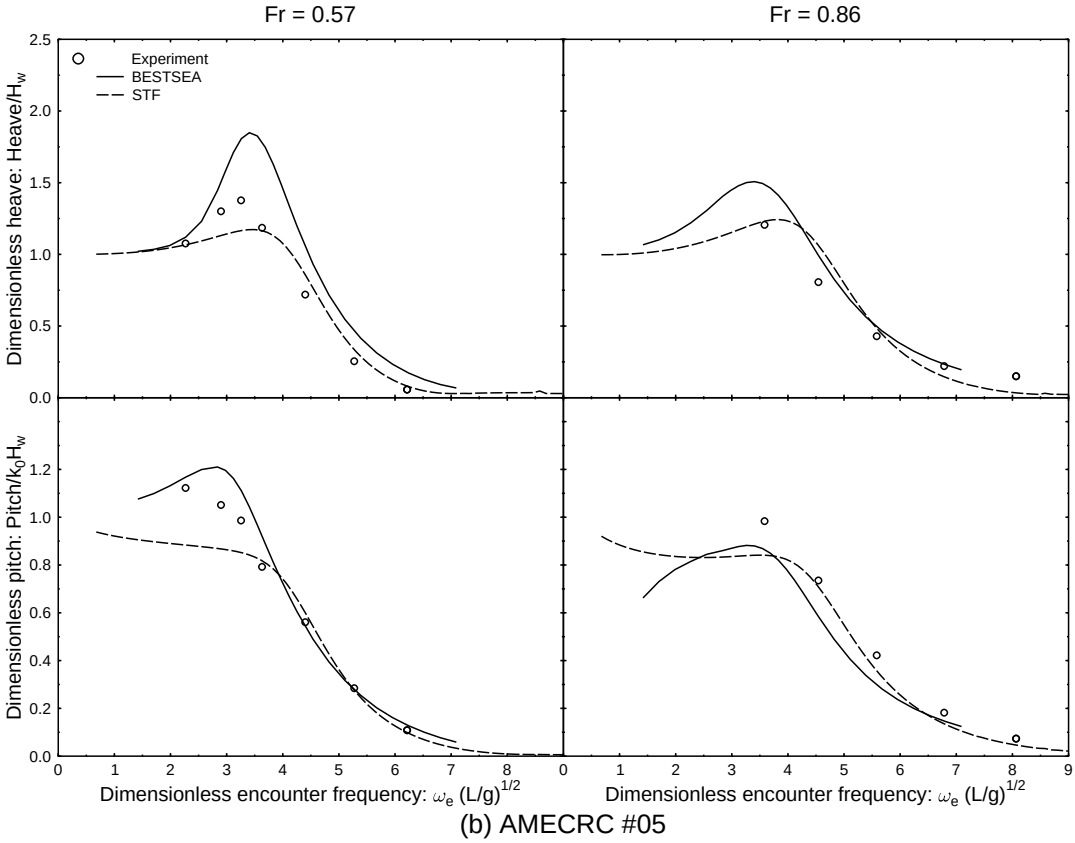

(b) AMECRC #05

Figure 6-23: Comparison of towing tank results, BESTSEA and STF for models AMECRC #04 and #05

Chapter 7

Conclusions

This chapter will summarise the main findings of this thesis, as well as suggest related research that has been identified for possible future work.

7.1 SWATHs

It was shown that the most obvious difference between the seakeeping of a SWATH (or semi-SWATH) and a conventional hull is the lower natural frequencies of the former. Furthermore it is possible to tune the heave and pitch natural frequencies independently by the use of extended bulbous bows. (No doubt a similar effect could be achieved by extending the stern, but the bulbous bow has the advantage of moving the centre of flotation aft, reducing the tendency of large bow motions.) The other main response characteristic, damping ratio, is far less strongly influenced by 'SWATHness'. These observations were made mainly from the model tests. A simplified model of motions was proposed in section 6.1.2, mainly for the purposes of understanding physically what was behind the broad trends, which assisted considerably in the interpretation of these results.

A lower natural frequency was shown to become more advantageous as speed is increased. Therefore it is recommended that for slow ships a conventional (shallow draught) hull form be used, but for very high speeds a SWATH form is clearly better. (Figure 6-6 suggests that "high speed" would generally mean a Froude number of $O(1)$ or greater.) At intermediate speeds a SWATH will probably have significantly larger motions but lower accelerations than a conventional hull, which makes it desirable from a passenger comfort point of view, but less desirable for general operational and safety reasons. A lower natural frequency also assists active ride control systems, allowing greater response time and requiring smaller forces.

Although damping ratio is less affected than natural frequency by SWATHness there is a slight tendency towards less damping for SWATHs, but this only slightly offsets their advantages. Damping was found to be more dependent on details of the geometry. The higher damping of the AMECRC models compared with the SWATH models was attributed mainly to a greater

beam (they were originally intended as monohulls) and (a related property) less steeply sloped sides. Additionally it was noted that damping could be increased by the use of appendages.

One problem was access to the seakeeping data for the reference hull on which the SWATH models were based. The solution adopted was to use some of the AMECRC systematic series data. This was not entirely satisfactory because the hull forms were quite different, and it is suspected that many of the differences in seakeeping properties could be attributed to differences in the hull form other than those that were intended to be systematically varied in the current project. Future work could therefore include testing of the reference hull, or at least an equivalent conventional hull designed to the same constraints as the two SWATH models, so that a more comprehensive comparison can be made. This could be followed up with testing of other SWATH forms designed with the benefit of the insights gained so far from this project.

Apart from slightly less damping, the main drawback of SWATHs, is their resistance. It was shown that for hulls that were in no way optimised this amounted to an additional 5% approximately, although further investigation would be required before accepting this as an accurate indication. One must remember that the passengers are paying the fuel bill, and this seems a small penalty considering the seakeeping advantages at high speed. Probably the most important finding was that both motions and accelerations will inevitably increase with speed, regardless of the type of hull, and therefore as higher speeds are demanded designers of high speed ferries *must* place greater importance on the seakeeping properties of their designs.

7.2 *BESTSEA*

7.2.1 Present status

Not surprisingly *BESTSEA* was generally but not universally better than traditional strip theory. It gave much better predictions of pitch motions and coupling effects, and was particularly good for high speed vessels, while it tended to over predict heave motions (more so at lower speeds) and it required considerably more CPU time. It also offers considerable flexibility and potential for future incorporation of additional features not possible in a frequency domain theory, some of which are listed below in section 7.2.2. Other aspects, such as local unsteady pressure prediction, were not addressed in this thesis, but are currently being investigated in a related research project conducted by AMECRC involving measurements on an 8m catamaran. There is a possibility that *BESTSEA* could produce good results here, but this has not been demonstrated yet.

If *BESTSEA* were to gain the status of a useful design or analysis tool it would need to show a net gain in terms of costs and benefits over both traditional strip theory and three-dimensional theories. In order to achieve this it is felt that some further optimisation for computational speed would be required. This is quite easily achievable, but would require a significant investment of time.

In terms of further improvements to the motion predictions, as pointed out in chapter 1,

a "well judged assessment of which of the simplifying assumptions of traditional strip theory must be abandoned" is required, and that this may vary depending on the application. In chapter 6 it was concluded that as a minimum for high speed vessels a more accurate (probably three-dimensional) representation of the steady and unsteady wave fields would be required, although this seems to be less essential as speed increases. Unsteady lifting forces due to the flow circulation that results from the zero pressure condition on the transom is also likely to be very important, and more so as speed increases. Viscous and slamming effects, while important (especially for large amplitude motions) are likely to be individually of higher order, but their combined effect may be significant. Modelling of these effects could be incorporated in future versions. The whole point of a time domain solution after all is to allow non-linear effects to be modelled.

Three-dimensionality could be introduced by applying unification techniques in the manner of Newman [73] or Yeung and Kim [102]. The process will no doubt differ from either of the cited examples since *BESTSEA* is a time domain theory. The result will also differ significantly in its simultaneous treatment of the steady flow problem. A possible problem is the containment of free surface history effects (the convolution integral in the Green function). The three-dimensional solution could be represented with either translating or stationary sources, and these source functions would involve ever-expanding convolution integrals requiring numerical evaluation. It might appear at first that the use of stationary sources could prevent the growth of the convolution integral in the same way they do by the use of a fixed reference frame for the two-dimensional strip solutions, if they only need to be distributed within the length of the hull. But Yeung and Kim [102] found that "for a body moving in or near a free surface with a mean forward speed, the line distribution of singularities representing its far-field behaviour generally extends beyond the actual length of the body itself. The distribution reduces to the length of the body if the forward speed vanishes." With all this apparent complexity one must then question whether it would not be easier to opt for a simple three-dimensional solution rather than seeking to incorporate three-dimensional effects in the present two-dimensional time domain method.

7.2.2 Future development of *BESTSEA*

In addition to improvements to heave predictions and optimisation for computing speed the list below suggests some future possibilities for *BESTSEA* (not in any particular order). Some could be achieved quite simply, while others may require considerable effort.

1. A greater range of output options could be included, including local pressures, shear forces and bending moments.

2. Being in the time domain, it would be possible to include the effects of hull flexibility on motions and loads.

3. As it is obviously aimed at the analysis of high speed ships, the ability to define multi-hulls would be an advantage (including tri-hulls and catamarans with centre bows).

4. This thesis has concentrated on heave and pitch motions. While it is important to first get these right it would be essential to expand capabilities to oblique seas, and surge, sway, yaw and roll motions, and the present method is capable of such expansion.

5. Being a time domain method, periodic sea input should be expanded to arbitrary random sea input.

6. Investigation of effects that may become important at very high speeds, for example the zero pressure condition at a transom stern.

7. More precise treatment of slamming loads (which should be tied in with hull flexibility).

8. Additional forces, such as from appendages or ride control systems.

There are also some problems that were incompletely solved for the present, namely emerging sections and chines, which would eventually need more satisfactory resolution.

The improvement in accuracy with increasing Froude number and SWATHness (in contrast to traditional strip theory) indicates that the method may be particularly relevant to the design of very high speed vessels operating at Froude numbers greater than unity, for which low response SWATH type forms may become an essential rather than an optional design feature.

7.3 Innovations in computational methods

7.3.1 Time domain panel method

This thesis presented in chapter 3 a two-dimensional time domain panel method based on free surface Green functions, in which the motion of a body may be specified completely arbitrarily, with no restriction on amplitude, and including the possibility of deformation. The author is not aware of the existence of a comparable method.

Also included in chapters 2 and 3 is a fairly comprehensive summary and comparison of two-dimensional free surface panel methods, including a solution to every major category of linear problem. This was a vital element in the validation of the time domain panel method that formed the core of *BESTSEA*. Such a summary and comparison has not previously been seen in a single work.

7.3.2 Stability of integration of the equations of motions

It was found that the presence of implicit added mass terms in the time dependent force on a freely floating body caused instability in the integration of the equations of motion. This problem is absent in the frequency domain due to the ability to separate radiation and diffraction forces.

Traditional methods of overcoming instability in numerical integration of initial value differential equations were found unable to overcome the problem. A solution was found in Beck et al. [5], in which both ϕ and $\frac{\partial \phi}{\partial t}$ were solved for explicitly, but this was found to be inefficient for the present problem due to the necessity of iteration.

In section 4.6 an extremely simple and robust method of stabilisation was presented, which could be adapted to any method of solution of the differential equation of motion. It involved at each time step combining the calculated force with an extrapolated one, in which the two had error propagation in opposite directions. Provided the ratio of the combination was within a certain range stability was assured, and the solution was independent of the chosen ratio. This range did not need to be known beforehand as it could safely be determined by trial and error as computation proceeded.

7.3.3 Simplified model for visualisation of seakeeping properties

As already mentioned in section 7.1, a simplified model of ship motions was introduced in section 6.1.2, which was extremely useful in interpreting the physical significance of the broad features of the experimental results. It was not intended as a design or analysis tool, but rather to assist in the understanding of which of the major hull features influence its seakeeping so that designers can make informed decisions in the preliminary design stage. The main findings are presented at the end of section 6.1.2, and implications for designers summarised in section 7.1. The model was not extended fully to two degrees of freedom, as it was felt that this would have detracted from its simplicity. It was argued however, and confirmed by experimental results, that at low frequencies pitch motion becomes dominated by coupling with heave.

Bibliography

[1] Milton Abramowitz and Irene A. Stegun. *Handbook of Mathematical Functions*, volume 55 of *Applied Mathematics*. National Bureau of Standards, 1964.

[2] J. G. Beaumont and D. W. Robinson. Classification aspects of ship flexibility. *Philosophical Transactions of the Royal Society of London Series A*, 334:371–389, 1991.

[3] Robert F. Beck. Time-domain computations for floating bodies. *Applied Ocean Research*, 16:267–282, 1994.

[4] Robert F. Beck, Yusong Cao, and Tzung-Hang Lee. Fully nonlinear water wave computations using the desingularised method. In *Sixth International Conference on Numerical Ship Hydrodynamics*, 1993.

[5] Robert F. Beck, Yusong Cao, Stephen M. Scorpio, and William W. Schultz. Nonlinear ship motion computations using the desingularised method. In *Twentieth Symposium on Naval Hydrodynamics*, 1994.

[6] Robert F. Beck and Stephen M. Scorpio. A desingularised boundary integral method for nonlinear water wave problems. In *Twelfth Australasian Fluid Mechanics Conference*, pages 255–258, 1995.

[7] E. Becker. Das Wellenbild einer unter der Oberfläche eines Stromes schwerer Flüssigkeit pulsierenden Quelle. *Zeitschrift für angewandte Mathematik und Mechanik*, 38:391–399, 1958.

[8] P. L. Betts and T. T. Mohamad. Water waves: a time-varying unlinearized boundary element approach. In T. Kawai, editor, *Finite Element Analysis*, pages 923–929. University of Tokyo Press, 1982.

[9] Jan J. Blok and Wim Beukelman. The high-speed displacement ship systematic series hull forms — seakeeping characteristics. *Transactions of Society of Naval Architects and Marine Engineers*, 92:125–150, 1984.

[10] P. Bojovic and G. Goetz. Geometry of AMECRC systematic series. Technical Report IR 96/6, Australian Maritime Engineering CRC Limited, 1996.

[11] R. Børresen and O. M. Faltinsen. Ship motions in shallow water by unified theory. In *Fifteenth Symposium Naval Hydrodynamics*, pages 51–65, 1984.

[12] J. C. Brown, J. D. Clarke, R. S. Dow, G. L. Jones, and C. S. Smith. Measurement of wave-induced loads in ships at sea. *Philosophical Transactions of the Royal Society of London Series A*, 334:293–306, 1991.

[13] Yusong Cao, Robert F. Beck, and William W. Schultz. An absorbing beach for numerical simulations of nonlinear waves in a wave tank. In *Eighth International Workshop on Water Waves and Floating Bodies*, St. Johns, Newfoundland, May 1993.

[14] Yusong Cao, William W. Schultz, and Robert F. Beck. Three-dimensional desingularised boundary integral methods for potential problems. *International Journal for Numerical Methods in Fluids*, 12:785–803, 1991.

[15] R. B. Chapman. Free-surface effects for yawed surface-piercing plate. *Journal of Ship Research*, 20:125–136, 1976.

[16] Raymond Cointe. Free-surface flows close to a surface-piercing body. In Touria Miloh, editor, *Mathematical Approaches in Hydrodynamics*, chapter 22, pages 319–334. Society for Industrial and Applied Mathematics, Philadelphia, 1991.

[17] Susan Cole. A simple example from flat-ship theory. *Journal of Fluid Mechanics*, 189:301–310, 1988.

[18] P.R. Couser, A.F. Molland, N.A. Armstrong, and I.K.A.P. Utama. Calm water powering predictions for high-speed catamarans. In *Fourth International Conference on Fast Sea Transportation*, pages 765–773, 1997.

[19] C. W. Dawson. A practical computer method for solving ship-wave problems. In *Proceedings International Conference on Numerical Ship Hydrodynamics*, pages 30–38, 1977.

[20] Z. N. Dobrovol'skaya. On some problems of similarity flow of fluid with a free surface. *Journal of Fluid Mechanics*, 36:805–829, 1969.

[21] Lawrence J. Doctors. Application of the boundary-element method to bodies oscillating near a free surface. In *International Symposium on Computational Fluid Dynamics*, pages 1–10, 1987.

[22] Lawrence J. Doctors. The HYDROS/3 programs: Description and documentation. Technical Report 15968-03, Unisearch, University of New South Wales, 1993.

[23] Lawrence J. Doctors. Course notes presented at the workshop on seakeeping design analysis of high-speed marine vehicles, volume 2: Procedures for calculation of ship motions,

August 1994. Held at the Sydney node of the Australian Maritime Engineering Cooperative research Centre, School of Mechanical and Manufacturing Engineering, The University of New South Wales.

[24] Lawrence J. Doctors. The influence of a proboscidean bow on ship motions. In *Twelfth Australasian Fluid Mechanics Conference*, pages 263–266, 1995.

[25] O. Faltinsen. Hydrodynamics of high speed vehicles. In M. Ohkusu, editor, *Advances in Marine Hydrodynamics*, chapter 3, pages 133–175. Computational Mechanics Publications, Southampton, 1996.

[26] O. Faltinsen and R. Zhao. Numerical predictions of ship motions at high forward speed. *Philosophical Transactions of the Royal Society of London Series A*, 334:241–252, 1991.

[27] O. M. Faltinsen. *Sea Loads on Ships and Offshore Strucrures*. Cambridge University Press, 1990.

[28] Odd M. Faltinsen. On seakeeping of conventional and high-speed vessels. *Journal of Ship Research*, 37(2):87–101, June 1993.

[29] O.M. Faltinsen and R. Zhao. Flow predictions around high-speed ships in waves. In Touvia Miloh, editor, *Mathematical Approaches in Hydrodynamics*, chapter 19, pages 265–288. Society for Industrial and Applied Mathematics, Philadelphia, 1991.

[30] E. Fontaine and O.M. Faltinsen. Steady flow near a wedge shaped bow. In B. Molin, editor, *Twelfth International Workshop on Water Waves and Floating Bodies*, pages 75–79, 1997.

[31] C. William Gear. *Numerical Initial Value Problems in Ordinary Differential Equations*. Prentice-Hall, 1971.

[32] J. Gerritsma. Forced oscillation experiments. *Philosophical Transactions of the Royal Society of London Series A*, 334:199–211, 1991.

[33] Joseph P. Giesing and A. M. O. Smith. Potential flow about two-dimensional hydrofoils. *Journal of Fluid Mechanics*, 28:113–129, 1967.

[34] R. W. Hamming. *Numerical Methods for Scientists and Engineers*. McGraw-Hill, 2nd edition, 1973.

[35] T. H. Havelock. *The Collected Papers of Sir Thomas Havelock on Hydrodynamics*. Office of Naval Research, 1963.

[36] T. H. Havelock. The displacement of the particles in a case of fluid mition. In C. Wigley, editor, *The Collected Papers of Sir Thomas Havelock on Hydrodynamics*, pages 81–93. Office of Naval Research, 1963.

[37] T. H. Havelock. The effect of speed of advance upon the damping of heave and pitch. In C. Wigley, editor, *The Collected Papers of Sir Thomas Havelock on Hydrodynamics*, pages 617–620. Office of Naval Research, 1963.

[38] T. H. Havelock. The forces on a circular cylinder submerged in a uniform stream. In C. Wigley, editor, *The Collected Papers of Sir Thomas Havelock on Hydrodynamics*, pages 420–428. Office of Naval Research, 1963.

[39] T. H. Havelock. The method of images in some problems of surface waves. In C. Wigley, editor, *The Collected Papers of Sir Thomas Havelock on Hydrodynamics*, pages 265–277. Office of Naval Research, 1963.

[40] T. H. Havelock. Periodic irrotational waves of finite height. In C. Wigley, editor, *The Collected Papers of Sir Thomas Havelock on Hydrodynamics*, pages 132–145. Office of Naval Research, 1963.

[41] T. H. Havelock. The resistance of a submerged cylinder in accelerated motion. In C. Wigley, editor, *The Collected Papers of Sir Thomas Havelock on Hydrodynamics*, pages 545–553. Office of Naval Research, 1963.

[42] T. H. Havelock. Some cases of water motion due to a submerged obstacle. In C. Wigley, editor, *The Collected Papers of Sir Thomas Havelock on Hydrodynamics*, pages 119–131. Office of Naval Research, 1963.

[43] T. H. Havelock. The vertical forces on a cylinder submerged in a uniform stream. In C. Wigley, editor, *The Collected Papers of Sir Thomas Havelock on Hydrodynamics*, pages 297–303. Office of Naval Research, 1963.

[44] T. H. Havelock. The wave resistance of a cylinder started from rest. In C. Wigley, editor, *The Collected Papers of Sir Thomas Havelock on Hydrodynamics*, pages 536–544. Office of Naval Research, 1963.

[45] Grant E. Hearn. Low frequency damping: the development of its theoretical prediction. In W. G. Price, P. Temarel, and A. J. Keane, editors, *Dynamics of Marine Vehicles and Structures in Waves*, pages 237–252. Elsevier Science Publishers, 1991.

[46] J. L. Hess. Panel methods in computational fluid dynamics. *Annual Review of Fluid Mechanics*, 22:255–274, 1990.

[47] J. L. Hess and A. M. O. Smith. Calculation of potential flow about arbitrary bodies. *Progress in Aeronautical Sciences*, 8:1–137, 1967.

[48] O. F. Hughes. Solution of the wedge entry problem by numerical conformal mapping. *Journal of Fluid Mechanics*, 56:173–192, 1972.

[49] Bruce L. Hutchison. Seakeeping studies: a status report. *Transactions of Society of Naval Architects and Marine Engineers*, 98:263–317, 1990.

[50] Eveline A. Johnstone and A. G. Mackie. The use of Lagrangian coordinates in the water entry and related problems. *Proceedings of the Cambridge Philosophical Society*, 74:529–538, 1973.

[51] S. W. Joo, W. W. Schultz, and A. F. Messiter. An analysis of the initial-value wavemaker problem. *Journal of Fluid Mechanics*, 214:161–183, 1990.

[52] M. Kashiwagi and M. Ohkusu. Side-wall effects on hydrodynamic forces acting on a ship with forward and oscillatory motions. In *Fifth International Conference on Numerical Ship Hydrodynamics*, pages 499–511, 1990.

[53] J. A. Keuning. Distribution of added mass and damping over the length of a model at high forward speed. Technical Report 774, Delft University of Technology, January 1988.

[54] B. V. Korvin-Kroukovsky and Winnifred R. Jacobs. Pitching and heaving motions of a ship in regular seas. *Transactions of Society of Naval Architects and Marine Engineers*, 65:590–632, 1957.

[55] D. C. Kring, D. A. Mantzaris, G. B. Tcheou, and P. D. Sclavounos. A time-domain seakeeping simulation for fast ships. In *Fourth International Conference on Fast Sea Transportation*, pages 455–461, 1997.

[56] Erkki Lahtiharju, Tuomo Karppinen, Matti Hellevaara, and Timo Aitta. Resistance and seakeeping characteristics of fast transom stern hulls with systematically varied form. *Transactions of Society of Naval Architects and Marine Engineers*, 99:85–118, 1991.

[57] Sir Horace Lamb. *Hydrodynamics*. Dover, 6th edition, 1945. Republication of 6th (1932) edition of the work originally published in 1879 by Cambridge University Press.

[58] Jaw-Fang Lee, Jonq-Ren Kuo, and Chung-Pan Lee. Transient wavemaker theory. *Journal of Hydraulic Research*, 27(5):651–663, 1989.

[59] James A. Liggett. *Fluid Mechanics*. McGraw Hill, 1994.

[60] Yuming Liu and Dick K. P. Yue. On the solution near the critical frequency for an oscillating and translating body in or near a free surface. *Journal of Fluid Mechanics*, 254:251–266, 1993.

[61] A. R. J. M. Lloyd. *Seakeeping: Ship Behaviour in Rough Weather*. Ellis Horwood, 1989.

[62] Yudell L. Luke. *The Special Functions and their Approximations*, volume 1. Academic Press, 1969.

[63] G. Macfarlane, M. Shaw, and M. Lees. Presentation of the AMECRC systematic series regular wave testing results. Technical Report IR 95/25, Australian Maritime Engineering CRC Limited, 1995.

[64] Allan Magee and Robert F. Beck. Compendium of ship motion calculations using linear time-domain analysis. Technical Report 310, Department of Naval Architecture and Marine Engineering, University of Michigan, October 1988.

[65] Philip Mandel. Seagoing box scores and seakeeping criteria for monohull, SWATH, planing, hydrofoil, surface effect ships, and air cushion vehicles. Technical Report DTNSRDC/SDD-79/1, David W. Taylor Naval Ship Research and Development Center, 1979.

[66] Philip Mandel. Assessing ship seaway performance. In Edward V. Lewis, editor, *Principles of Naval Architecture*, volume 3, chapter 8 section 7, pages 137–60. SNAME, 2nd edition, 1989.

[67] S. J. Maskell and F. Ursell. The transient motion of a floating body. *Journal of Fluid Mechanics*, 44(2):303–313, 1970.

[68] J. H. Michell. The highest waves in water. *The London, Edinburgh, and Dublin Philosophical Magazine and Journal of Science. Fifth Series*, 36:430–437, 1893.

[69] Alfred H. Morris Jr. NSWC library of mathematics subroutines. Technical report, Naval Surface Warfare Center, Dahlgren Division, 1993.

[70] D. Nakos and P. Sclavounos. Ship motions by a three-dimensional Rankine panel method. In *Eighteenth Symposium on Naval Hydrodynamics*, pages 21–40, 1991.

[71] D. E. Nakos and P. D. Sclavounos. Kelvin wakes and wave resistance of cruiser and transom stern ships. *Journal of Ship Research*, 38(1):9–29, March 1994.

[72] J. N. Newman. *Marine Hydrodynamics*. MIT Press, 1977.

[73] J. N. Newman. The theory of ship motions. *Advances in Applied Mechanics*, 18:221–283, 1978.

[74] J. N. Newman. The quest for a three-dimensional theory of ship-wave interactions. *Philosophical Transactions of The Royal Society of London Series A*, 334:213–227, 1991.

[75] J. N. Newman. The approximation of free-surface green functions. In P. A. Martin and G. R. Wickham, editors, *Wave Asymptotics*, chapter 7, pages 107–135. Cambridge University Press, 1992.

[76] J. Nicholas Newman. Panel methods in marine hydrodynamics. In *Eleventh Australasian Fluid Mechanics Conference*, pages 123–130, 1992.

[77] T. Francis Ogilvie and E. O. Tuck. A rational strip theory of ship motions: Part 1. Technical Report 013, University of Michigan, Department of Naval Architecture and Marine Engineering, 1969.

[78] J. F. O'Hanlon and M. E. McCauley. Motion sickness incidence as a function of the frequency and acceleration of vertical sinusoidal motion. Technical Report memorandum 1973-1, Human Factors Research Inc., 1973.

[79] William H. Press, Saul A. Teukolsky, William T. Vetterling, and Brian P. Flannery. *Numerical Recipes in FORTRAN: The Art of Scientific Computing*. Cambridge University Press, 2nd edition, 1992.

[80] A. P. Prudnikov, Yu. A. Brychkov, and O. I. Marichev. *Integrals and Series*. Gordon and Breach, 1986.

[81] Singiresu S. Rao. *Mechanical Vibrations*. Addison-Wesley, 1986.

[82] Hoyte C. Raven. A practical nonlinear method for calculating ship wavemaking and wave resistance. In *Proceedings 19th Symposium on Naval Hydrodynamics*, 1992.

[83] A. J. Roberts. Transient free-surface flows generated by a moving vertical plate. *Quarterly Journal of Mechanics and Applied Mathematics*, 40(1):129–158, 1987.

[84] Nils Salvesen, E. O. Tuck, and Odd Faltinsen. Ship motions and sea loads. *Transactions of Society of Naval Architects and Marine Engineers*, 78:250–287, 1970.

[85] Christian Schack. Research on semi-SWATH hull forms. In *Proceedings of the Third International Conference on Fast Sea Transportation*, pages 527–538, 1995.

[86] Paul D. Sclavounos. The unified slender-body theory: Ship motions in waves. In *Fifteenth Symposium Naval Hydrodynamics*, pages 177–193, 1985.

[87] Paul D. Sclavounos, David C. Kring, Yifeng Huang, Demetrios A. Mantzaris, Sungeun Kim, and Yonghwan Kim. A computational method as an advanced tool of hydrodynamic design. *Transactions of Society of Naval Architects and Marine Engineers*, 105, 1997.

[88] S. Scorpio, R. Beck, and F. Korsmeyer. Nonlinear water wave computations using a multipole accelerated, desingularized method. In *Twenty First Symposium on Naval Hydrodynamics*, pages 64–74, 1996.

[89] R. Timman and J. N. Newman. The coupled damping coefficients of a symmetric ship. *Journal of Ship Research*, 5(4):1–7, 1962.

[90] E. O. Tuck. The effect of non-linearity at the free surface on flow past a submerged cylinder. *Journal of Fluid Mechanics*, 22:401–414, 1965.

[91] Tore Ulstein and Odd M Faltinsen. Two-dimensional unsteady planing. *Journal of Ship Research*, 40(3):200–210, 1996.

[92] F. Ursell. On the heaving motion of a circular cylinder in the surface of a fluid. *Quarterly Journal of Mechanics and Applied Mathematics*, 2:218–231, 1949.

[93] F. Ursell. The decay of the free motion of a floating body. *Journal of Fluid Mechanics*, 19(2):305–319, 1964.

[94] F. Ursell. Some unsolved and unfinished problems in the theory of waves. In P. A. Martin and G. R. Wickham, editors, *Wave Asymptotics*, chapter 12, pages 220–244. Cambridge University Press, 1992.

[95] H. Wagner. Über Stoß- und Gleitvorgänge an der Oberfläche von Flüssigkeiten. *Zeitschrift für Angewandte Mathematik und Mechanik*, 12:193–215, 1932.

[96] N. L. Watson, M. R. Davis, and T. J. Roberts. Shipborne measurements of sea conditions and seakeeping response of high speed ferries. In *Fourth International Conference on Fast Sea Transportation*, pages 713–718, 1997.

[97] John V. Wehausen. The wave resistance of ships. *Advances in Applied Mechanics*, 13:93–244, 1973.

[98] John Vrooman Wehausen and Edmund V. Laitone. Surface waves. In S. Flügge, editor, *Handbuch der Physik*, volume 9, pages 445–814. Springer-Verlag, 1960.

[99] R. W. Yeung. The transient heaving motion of floating cylinders. *Journal of Engineering Mathematics*, 16:97–119, 1982.

[100] R. W. Yeung and S. H. Kim. Radiation forces on ships with forward speed. In *Proceedings Third International Conference on Numerical Ship Hydrodynamics*, pages 499–515, 1981.

[101] Ronald W. Yeung. Numerical methods in free-surface flows. *Annual Review of Fluid Mechanics*, 14:395–442, 1982.

[102] Ronald W. Yeung and Sea H. Kim. A new development in the theory of oscillating and translating slender ships. In *Fifteenth Symposium Naval Hydrodynamics*, pages 195–218, 1985.

[103] Y. S. Yu and F. Ursell. Surface waves generated by an oscillating circular cylinder in water of finite depth: Theory and experiment. *Journal of Fluid Mechanics*, 11:529–551, 1961.

[104] R. Zhao and O. Faltinsen. Water entry of two-dimensional bodies. *Journal of Fluid Mechanics*, 246:593–612, 1993.

[105] Rong Zhao. A complete linear time-domain analysis for predicting ship motions at high froude number. *International Shipbuilding Progress*, 44(440):341–361, December 1997.

[106] Rong Zhao and Jan V. Aarsnes. Numerical and experimental studies of nonlinear motions and loads of a high-speed catamaran. In *Proceedings of the Third International Conference on Fast Sea Transportation*, pages 1017–1030, 1995.

[107] D. X. Zhu and M. Katory. 3-D time domain numerical model for the prediction of ship motions in random seas. *International Journal of Offshore and Polar Engineering*, 5(2):120–126, June 1995.